Synthesis and Catalytic Application of Complexes with Pyridylidene Amide Ligands in Transfer Hydrogenation

Inaugural dissertation

of the Faculty of Science,

University of Bern

presented by

Alicia Beaufils

from France

Supervisor of the doctoral thesis:

Prof. Dr. Martin Albrecht

Department of Chemistry, Biochemistry and

Pharmaceutical Sciences

Synthesis and Catalytic Application of Complexes with Pyridylidene Amide Ligands in Transfer Hydrogenation

Inaugural dissertation

of the Faculty of Science,

University of Bern

presented by

Alicia Beaufils

from France

Supervisor of the doctoral thesis:

Prof. Dr. Martin Albrecht

Accepted by the Faculty of Science.

Bern, March 27, 2025 The Dean

Prof. Dr. Jean-Louis Reymond

Experience is a great teacher.

– John Legend –

Acknowledgments

In this page, I would like to acknowledge the numerous persons that took part in my PhD journey - mostly through support, guidance, and kindness.

First, I would like to thank Martin. I am extremely grateful for the opportunity you gave me to work in your group and for the experiences I gained throughout this journey. I deeply appreciate the lessons learned through your passion of chemistry, but also to develop as a more proficient and critical-thinking scientist. You were always helpful, patient, and available to guide me through the years, thus I would like to thank you for your time and dedication. It was a pleasure to work under your supervision.

I express my sincere gratitude to Prof. Dr. Eva Hevia and Prof. Dr. Walter Baratta for taking the time to review this doctoral dissertation and being part of my PhD defence committee.

I would like to thank all former and current members of the Albrecht Research Group, particularly: Nicolas – je me dois de commencer par mon compatriote, un grand merci pour tes conseils à l'intérieur et en dehors du labo; Laura and Claire – I am grateful to have met both of you and will always smile at some of our "secret" stories; Kevin, Pamela, Albert, Alex, Natalie, Pascal, Wowa, Esaïe, Giacomo, Luke, Taj, Fabienne, Sabela, and Lars, with whom I shared some great moments during my stay in Bern.

Of course, I want to thank the people outside of the group, that were nice and helpful along the way: die Materialausgabe, Hausdienst und Werkstatt, namentlich Michel, Marco, Daniel, und Simon; the other staff members of the DCBP, particularly Ilche and Dib for their confidence and support; the members of the Broekmann and Hevia group, especially for the latter for the fruitful discussions during our yearly group meetings.

Je tiens à remercier mes deux françaises (ou presque) préférées de Bern, Sophia et Aline, pour tous nos moments partagés.

My special thanks go to my dear friend Ivo, that I know since my first days in Bern (Bolligen to be precise). I will always be grateful for your support until now, and I thank you for showing me the way through this PhD. We shared a lot, either at the DCBP or elsewhere, and I am looking forward for the next to come!

Pour finir, je remercie infiniment ma famille, particulièrement mes parents, Fabienne et Jean-Marc, et mon frère, Michael, pour leur présence et leurs encouragements à travers toutes ces années. Sans eux, je ne serais ni là ni la personne que je suis aujourd'hui. Merci à vous.

Contributions from other sources

Chapter I

ChatGPT	*Phrasing of some paragraphs*

Chapter II

Dr. Philipp Melle	*First synthesis of complexes 3 and 5*
Dr. Nicolas Lentz	*General supervision and fruitful discussions*

Chapter IV

Dr. Philipp Melle	*Electrochemical measurements of complex 3a*
Nicole Elia	*Synthesis of 1f and 2g*

Table of Contents

Chapter I

Pyridylidene amide ligands for stabilization of coordinatively unsaturated complexes

I.1. Abstract

This chapter describes the importance of transition-metal catalysis, as a more sustainable alternative to the use of stoichiometric reagents. Illustrated by different examples, we will discuss the crucial influence of the design of complex and ligand to achieve tailored catalytic reactions. The main focus of this chapter will be on coordinatively unsaturated complexes, usually described as entry-points or intermediates in numerous catalytic cycles, to better understand the formation and isolation of these generally highly reactive and unstable species. The crucial role of steric effect and π-donation of the ligands for stabilization will be covered in detail, including examples of phosphine and non-phosphine containing complexes. Especially, structural aspects including the pyramidalization angle α will be discussed, as this parameter directly correlates with the saturation of the metal center. Furthermore, the use of donor-flexible ligands for the stabilization of coordinatively unsaturated complexes will be highlighted, with a particular focus on pyridylidene amines and amides (PYEs/PYAs). The combination of known systems for careful complex design and the evidenced flexibility of PYAs establish the aim of this thesis: the development of N,N'-PYA ruthenium complexes and further application in transfer hydrogenation using ethanol as hydrogen source.

I.2. Catalysis and sustainable chemistry

Introduction. For centuries, chemistry has played an essential role in human advancement by improving our quality of life. From the development of medicines, as the recent discovery of Sofosbuvir,[1,2] a prodrug that revolutionized the treatment of Hepatitis C with better recovery rates and shorter treatment duration compared to previously available, to the creation of materials that we use in our everyday life as polyethylene (PE), the most common plastic material used primarily for packaging,[3,4] chemistry has for many years operated with minimal restrictions, allowing for immense innovation and progress. This freedom was accompanied by the widespread use of various chemicals and processes that contributed significantly to industrial growth and prosperity. This implies that today, the majority of manufacturing products are derived from petroleum feedstocks or natural gas.[5]

However, this approach to chemical manufacturing, far less controlled at the time, has not come without drawbacks either. The consequences of chemical production, distribution, and use emerged over time and impacted both the environment and human health. Even though some problems were resolved locally, exemplified by the innovation in the oil refining industry starting in the 1950s with the development of catalytic processes leading to less pollution,[6] several concerns have grown into global crises such as green-house gas emission[7] or plastic pollution.[8] A re-evaluation of traditional chemical processes appeared to be needed to mitigate the impact of pollution,[9] toxic waste,[10] and the depletion of natural resources.[11] This shift in perspective led to the creation and development of green chemistry, a field devoted to the design of chemical products and processes that minimize the generation and use of toxic and hazardous substances.

The concept of green chemistry was first described by Paul Anastas and John Warner, and defined as "*the design of chemical products and processes that reduce or eliminate the use and generation of hazardous substances*."[12] This definition highlights that green chemistry is not just aiming at managing chemical hazards, but also at preventing them at the source. Early on, the chemical industry has also embraced the broader definition of sustainable technology, as outlined in the Brundtland Report, "Our Common Future."[13] This definition describes sustainable technology as meeting "*the needs of the present without compromising the ability of future generations to meet their own needs*," reflecting a commitment to long-term environmental goals.

The 12 Principles of Green Chemistry. The relationship between green chemistry and sustainability is symbiotic. While sustainability is the overall goal, a vision of a future where human activities does not compromise environmental health or resource availability, green chemistry provides the tools and principles necessary to achieve this vision and serves as the means to achieve it. Since their formulation in the 1990s, the Twelve Principles of Green Chemistry (Figure I.1) have remained unchanged, demonstrating their relevance and applicability in guiding toward more sustainable practices.[5] As the chemical industry continues to evolve, integrating green chemistry principles is becoming increasingly vital. By shifting focus from yield maximization to

sustainability and safety, the industry can continue to innovate while minimizing its ecological footprint, ultimately contributing to a more sustainable planet for future generations.

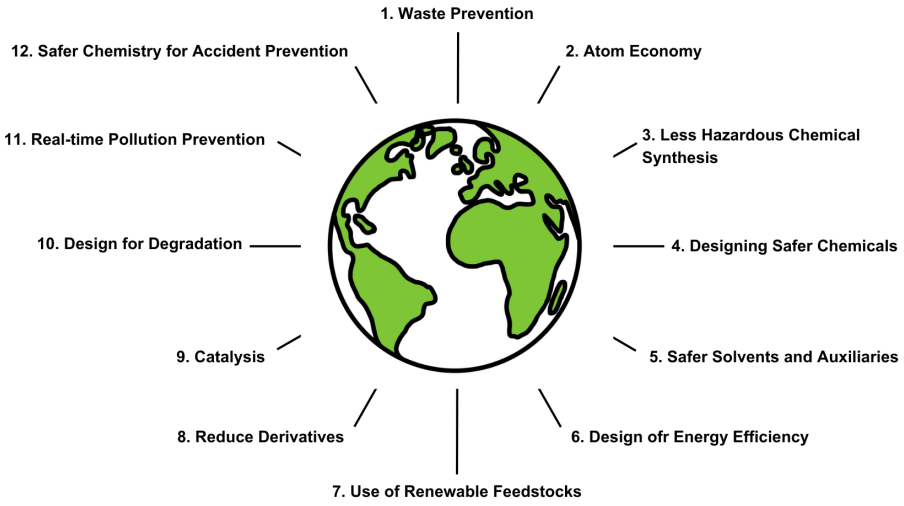

Figure I.1. The Twelve Principles of Green Chemistry, summarized into the acronym PRODUCTIVELY.[14]

The importance of catalysis. The majority of waste in the fine chemical and pharmaceutical industry segments is composed of inorganic salts, a direct consequence of the use of traditional stoichiometric inorganic reagents. This is highlighted by a higher E factor (representing the amount of waste produced per kilogram of product) compared to the other chemical industry sectors (Table I.1).[5] One of the reasons for this discrepancy can be attributed to the smaller quantities of product produced in these sectors, leading to a smaller effort for waste reduction.

Table I.1. E-factors for chemical industry sectors.[5]

Industry segment	Product tonnage	E factor (kg waste per kg product)
Oil refining	10^6–10^8	< 0.1
Bulk chemicals	10^4–10^6	< 1 to 5
Fine chemicals	10^2–10^4	5 to > 50
Pharmaceuticals	10–10^2	25 to > 100

One way to circumvent, or at least decrease, the amount of waste generated during a chemical process is to use catalytic reagents. In contrast to stoichiometric reagents, which very often generate stoichiometric amounts of waste,[15] a catalyst, defined as a "*substance that increases the rate of a reaction without modifying the overall standard Gibbs energy change in the reaction,*"[16] is not consumed during a reaction. This implies less energy, feedstock, and waste – directly linked to the first two principles of green chemistry. Since the 20th century, many examples of innovative catalytic processes have been developed, leading to a decrease in the amount of waste and an increase in the amount and quality of products in the oil industry: catalytic reforming processes based on metal-containing catalysts, for the conversion of low-octane alkanes and napthenes into high-octane

branched alkanes and aromatics is one of many examples. Today, catalysts are involved in the production of over 80 % of all manufactured products (valued at 10^{12} $).[17]

Because large-scale industrial processes prioritize efficiency, sustainability, and safety while ensuring economic viability, industrially applied catalysts have now expanded and played a vital role in modern processes. Maybe the most significant example of such applications is the Haber Bosch process, primarily used for the synthesis of ammonia from nitrogen and dihydrogen with an iron catalyst. About 1% of the world's total energy production is used for ammonia synthesis, primarily for the manufacturing of ammonia fertilizer (between 75 and 90% of ammonia is used to make fertilizer).[18] While the reaction is thermodynamically favored at room temperature, the kinetic is very slow (equation 1).

$$N_2 + 3\ H_2 \rightleftarrows 2\ NH_3 \qquad \Delta H_{298K} = -92.28\ kJ/mol \tag{1}$$

High temperatures (400–500°C) and high pressures (>100 bar) are necessary to drive the reaction forward, resulting in approximately 2% of the global CO_2 emissions.[19] Traditional Haber Bosch plants largely contribute to these CO_2 emissions, as they use natural gas (50%), oil (31%), and coal (19%) as feedstocks.[20] New approaches aim to decouple ammonia synthesis from conventionally used fossil fuels (*via* methane reforming), using renewable energy sources instead.[21] Switching from methane-based to electrical energy has increased energy efficiency by 50% and decreased the CO_2 emissions. Further system enhancements, using high-efficiency motors, alternative ammonia separation techniques, or modular scalability of the process, further enhance energy use and economic viability and highlight the importance of continuous research improvement of known chemical processes.

Selectivity is a parameter intrinsically influencing efficiency and environmental impact in catalytic processes by reducing the amount of waste (including by-products) and the production cost. The main advantage of selective chemical reactions is to reduce the need for protecting groups, thus increasing the overall efficiency and speed of the desired synthesis. Numerous examples of enantioselective,[22] diastereoselective,[23] regioselective,[24] or chemoselective[25] chemical reactions have expanded over the years and are nowadays applied in industry, as shape-selective zeolites catalysts like ZSM-5 for the selective alkylation of toluene with ethylene to form *para*-ethyltoluene,[26] or vanadium-based catalysts for the selective catalytic reduction of Nitrogen Oxide (NOx), an air pollutant emitted at high concentrations in power plants or automobiles.[27]

I.3. Catalyst design

Heterogeneous and homogeneous catalysis. Catalysis is usually classified into two main categories: heterogeneous catalysis, in which the catalyst on solid, porous material or impregnated in such material is in a different phase than the reactants, and homogeneous catalysis, in which the catalyst is in the same phase as the reactants.[17]

Approximately 80% of catalytic processes in the industry are catalyzed heterogeneously, largely due to their operational advantages. Catalyst recycling is very simple, usually through filtration or sedimentation, minimizing downstream processing steps, which is particularly interesting in large-scale synthesis, even more considering their general reusability, making heterogeneous catalysts cost-effective.[28] Fixed bed or fluidized bed reactors, used for many industrially important reactions such as ammonia synthesis or Fluid Catalytic Cracking (FCC) process, operate in continuous processes, with the catalyst remaining in the reactor and allowing the concomitant introduction of new reactants while withdrawing the products (Table I.2).[29] In contrast to batch processes, this process is highly efficient and significantly enhances production rates. Heterogeneous catalysts are also known to be thermally and chemically stable. For instance, a general setup for the FCC process involves catalyst temperature cycling between 500 and 760 °C.[30] While it is clear that the catalyst can be exposed to harsh reaction conditions, this results in catalyst deactivation with an average lifetime of about one month.

Table I.2. Selected examples of heterogeneous catalysts of industrial importance.[29]

Catalyst (support/promoter)	Reactor type	Reaction
Fe (promoter)	Fixed bed	Ammonia synthesis
Ni (support)	Fixed bed	Steam reforming
Fe or Co (support)	Fixed bed or entrained bed	Fischer-Tropsch synthesis
Clays, zeolites	Fluidized bed	Fluid catalytic cracking process

Although heterogeneous catalysis has numerous advantages, homogeneous catalysis remains essential, particularly for reactions requiring high selectivity and mild reaction conditions (Table I.3). The often-cited comment by D. Parker in 1998, stating that, "... *at the molecular level, there is little to distinguish between homogeneous and heterogeneous catalysis, but there are clear distinctions at the industrial level*" is more than doubtful.[17] Indeed, compared to heterogeneous catalysts, the active site of homogeneous catalysts is generally well-defined and leads to a better mechanistic understanding of its micro "processes", *i.e.* catalytic cycles, with the possibility of modulating the steric and electronic properties of these molecularly defined catalysts enabling a greater control over the reaction outcome.[31] Common techniques such as spectroscopic methods (NMR, IR, UV-Vis) and single crystal X-ray diffraction are useful for kinetics and identifying intermediate states of the catalyst, enabling a better understanding of the reaction at a molecular level.

Table I.3. Comparison of homogeneous and heterogeneous catalytic systems.[31]

	Homogeneous	Heterogeneous
Phase	Liquid	**Liquid/gas/solid**
Temperature	**Low**	High
Diffusivity	**High**	Can be an issue
Heat transfer	**Easy**	Can be an issue
Catalyst separation	Difficult	**Easy**
Recycling	Expensive	**Simple**
Active site	**Well-defined**	Poorly defined
Catalyst modification	**Easy**	Difficult
Reaction mechanism	**Well understood**	Poorly understood
Selectivity	**High**	Variable
Activity (relative to metal content)	**High**	Variable

This distinction can be easily exemplified by comparing two catalytic reactions involving carbon monoxide: the Fischer-Tropsch reaction[32] (Scheme I.1) and the hydroformylation[33] (Scheme I.2). The Fischer-Tropsch reaction implies heterogeneous catalysts of structures that are not precisely known, complicating any straightforward interpretation of structure-catalytic performance relationships. The surface enol mechanism (Scheme I.1) is one of the main reaction pathways proposed for this reaction, but even after more than 90 years of research on iron-based Fischer-Tropsch catalysis, the molecular mechanism is not yet clearly elucidated.

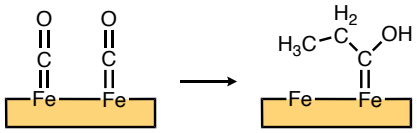

Scheme I.1. Representation of the metal surface structure for one of the proposed mechanisms of the Fischer-Tropsch reaction.[32]

In contrast, the molecular structure of the homogeneous catalyst implied in the hydroformylation of alkenes is known as a trigonal-bipyramidal Rh(I)-d^8 (Scheme I.2). In solution, $RhH(CO)(PPh_3)_3$ dissociates to $RhH(CO)(PPh_3)_2$, proposed as the active catalytic species.

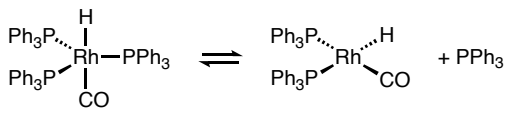

Scheme I.2. Well-defined Rh-catalyst involved in the hydroformylation of alkenes.[33]

An example that showcases the importance of understanding the reaction mechanism using well-defined catalysts is the first industrially applied synthesis of a chiral pharmaceutical, L-Dopa, a drug for the treatment of Parkinson's disease, using a chiral metal catalyst, developed by Knowles and Monsanto (Scheme I.3.a).[34]

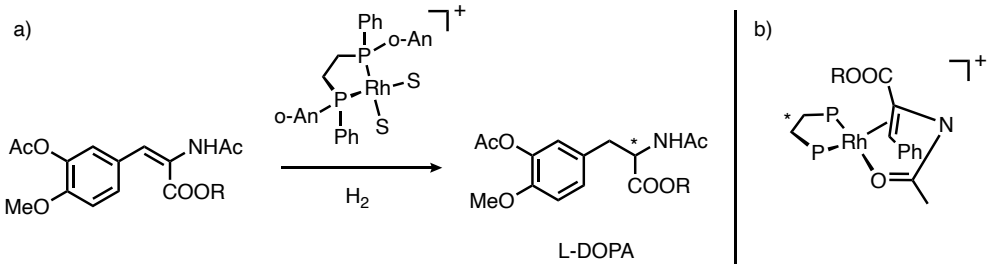

Scheme I.3. a) Synthesis of L-Dopa using a Rh-DIPAMP catalyst;[34] b) one diastereomer of the alkene-rhodium intermediate.[35]

The synthesis of L-Dopa is catalyzed by a well-defined cationic rhodium-bisphosphine complex. The enantioselectivity derivates from the chiral catalyst, as shown in the alkene-rhodium intermediate (Scheme I.3.b).[35] During the first step, the prochiral alkene coordinates to the rhodium center with either of the enantiotopic faces, forming two possible structures. The presence of a polar substituent, in this case, the acetamido group, is crucial as it functions as a secondary complexation function in addition to the alkene functionality. In the absence of amide oxygen coordination, the formation of a less rigid structure would result in a lower enantiomeric excess of the product.

Further studies by Halpern[36] and Brown[37] revealed that the most stable alkene intermediate observed by NMR spectroscopy does not lead to the major enantiomeric product. The least stable intermediate reacts faster in the following irreversible oxidative addition of dihydrogen, determining the enantioselectivity of the alkene hydrogenation (Scheme I.4).

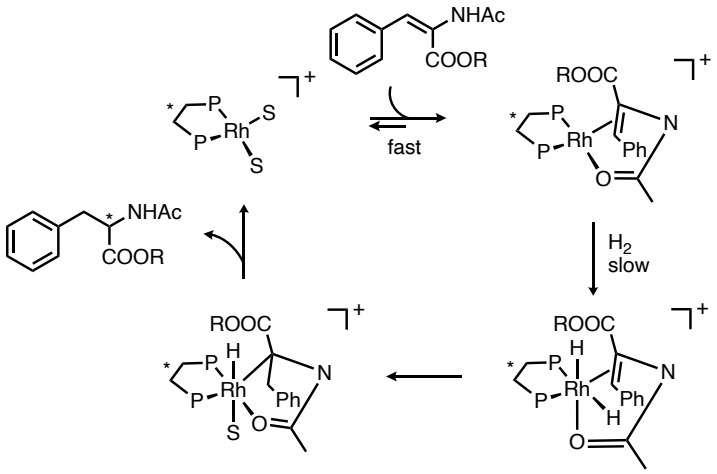

Scheme I.4. Mechanism of asymmetric hydrogenation of cinnamic acid (for one diastereomer) using Rh-DIPAMP catalyst.[36,37]

This example illustrates the importance of understanding reaction mechanism, as these findings have been applied to other enantioselective reactions with nearly 100 % enantiomeric excess. By converting ketones first to acyl hydrazones, with the addition of a temporary auxiliary donor atom to increase the rigidity of the intermediate structure via secondary complexation of the hydrazide oxygen, the Dupont team[38] obtained very high enantiomeric excess for the catalytic reductive amination (Scheme I.5).

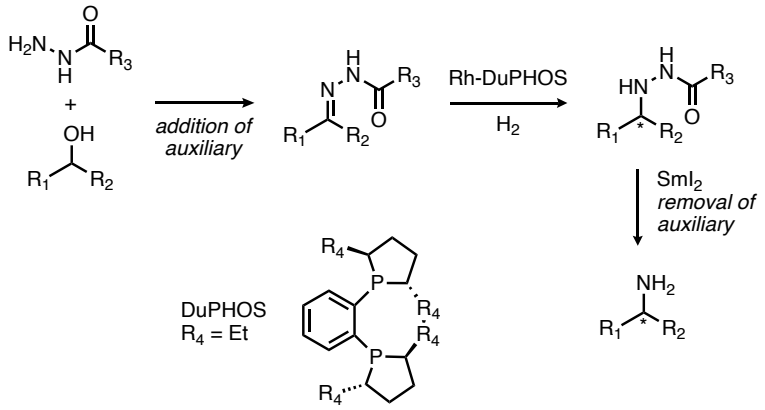

Scheme I.5. Mechanism of asymmetric catalytic reductive amination using Rh-DuPHOS catalyst.[38]

Numerous examples of industrially-applied homogeneous catalysis are present, including the Monsanto and Cativa processes,[39] using respectively rhodium and iridium catalysts for the production of acetic acid by catalytic carbonylation of methanol; in olefin metathesis with the Grubbs catalyst,[40] a Ru-alkylidene complex used for the production of pharmaceuticals and polymers; the Wacker process,[41] using a Pd(II) complex for the oxidation of olefins to carbonyls; or the Ziegler-Natta processes,[42] for the polymerization of ethylene and propylene to polyethylene and polypropylene.

In conclusion, the choice between homogeneous and heterogeneous catalytic processes largely depends on the application, as each offers distinct advantages and limitations. While homogeneous catalysis usually provides higher selectivity and control over the reaction, heterogeneous catalysis allows harsher reaction conditions and catalyst recycling. The question is not whether in general homogeneous catalysis is better than heterogeneous catalysis or the reverse, as the optimal choice is highly dependent on each application. Factors such as reaction conditions, stability of the catalyst, and environmental and economic considerations all play a role when considering the most suitable catalytic approach. Nevertheless, we can agree that research in catalysis is crucial, as it offers more efficient, cost-effective, and environmentally friendly chemical processes. Thus, developing new or improving existing catalytic routes is of great interest.

Design of transition-metal homogeneous catalysts. In homogeneous catalysis, the design of complex and ligands is crucial for achieving tailored catalytic reactions. Transition metal complexes are highly competent as catalysts and can be tuned either directly at the metal center (choice of the metal, oxidation state, or coordination number) or with a careful choice of ligands that can influence the catalytic process in various ways through electronic and steric effects.

The choice of metal in homogeneous catalysis is crucial as different transition metals (metals with partly filled *d* or *f* shells) exhibit unique properties and can facilitate a variety of reactions depending on their oxidation states, coordination abilities, and affinity for substrates. The industrial synthesis of acetic acid *via* carbonylation of methanol is a good example of the influence of metal choice on catalytic performance.[43] The first industrial approach to acetic acid production was the BASF

process commercialized in 1960 using a cobalt iodide catalyst.[44] While effective, the carbonylation process requires high pressure and high temperature (700 bar, 250°C) and depends strongly on these conditions to obtain acetic acid yields of 90% based on methanol and 70% based on carbon monoxide. Monsanto achieved a breakthrough in the 1970s by switching from cobalt- to rhodium-iodide catalyst, enabling much milder reaction conditions (30-60 bar, 180°C) with a selectivity of more than 99% and 90% for methanol and carbon monoxide, respectively.[45] The system is not sensitive to hydrogen, consequently, the by-products observed in the BASF process, as methane or propionic acid, are much less reduced.

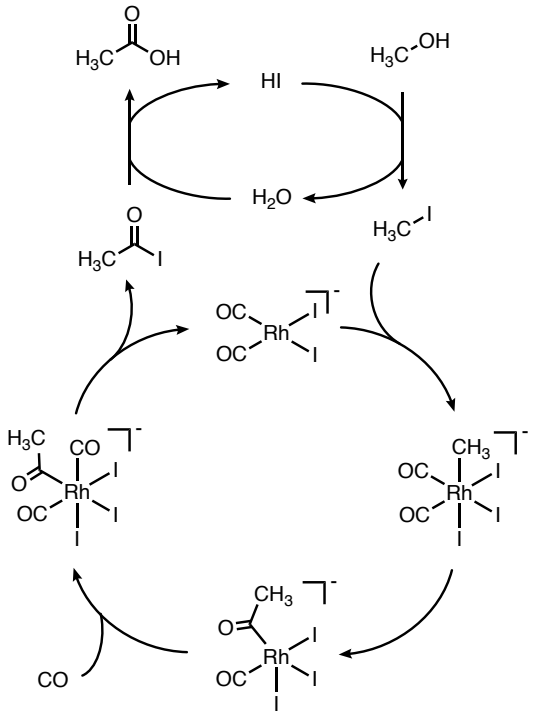

Scheme I.6. Mechanism of rhodium-catalyzed methanol carbonylation for the synthesis of acetic acid developed by Monsanto.[46]

The oxidative addition of methyl iodide to the active species $[Rh(CO)_2I_2]^-$, formed from hydrogen iodide and methanol, is followed by migratory insertion of the methyl group to form the pentacoordinate acyl intermediate (Scheme I.6).[46] In the case of the BASF process, CH_3I reacts with a coordinatively saturated d10 complex, $[Co(CO)_4]^-$, which is the preferred electron configuration of Co(I). The methyl migration to form the corresponding acyl cobalt carbonyl complex is therefore less favored than using a Rh(III) species. Further coordination of CO allows the elimination of acetyl iodide together with the regeneration of the starting active species. In a second catalytic cycle, acetyl iodide reacts with water to release the desired acetic acid and hydrogen iodide, that subsequently reacts with methanol to regenerate the methyl iodide promoter.

Monsanto studied both rhodium- and iridium-catalyzed methanol carbonylation reactions. Based on these results and knowledge on iridium chemistry, BP developed in the 1990s what is now known as the Cativa process, further improving the commercial synthesis of acetic acid.[39] The reaction

pathway, using $[Ir(CO)_2I_2]^-$ as active species, is very similar to the rhodium-catalyzed process described in Scheme I.6. This catalyst change firstly originates from the desire to reduce the water content in the reaction mixture, but several other advantages as higher catalyst stability and reduced liquid by-products are obtained. The evolution of the process over the years highlights the importance of the metal choice to impact key factors in the reaction, as milder reaction conditions and higher selectivity in the Monsanto process, and improved stability, efficiency, and economic viability in the Cativa process.

The coordination number is another pivotal parameter in homogeneous transition-metal complexes applied in catalysis that expanded from simple and low coordination metal salts to more carefully designed complexes bearing advanced ligand scaffold, exemplified by the different ruthenium complexes presented in Figure I.2. Simple $RuCl_2$ was applied in 1966 in the catalytic hydrogenation of maleic and fumaric acids to succinic acid in aqueous solution, involving the formation of Ru(II)-olefin complex which reacts with hydrogen to form succinic acid.[47] $RuCl_3$ was applied recently in the alkylation of methylazaarenes using alkyl- or aryl-alcohols as alkylation agents.[48] Mechanistic studies revealed a stepwise transfer hydrogenation, aldol condensation, and hydrogenation reaction pathway. The Grubbs catalysts are metal carbenes complexes used in olefin metathesis. The first-generation Grubbs catalyst represented here, synthesized from $RuCl_2(PPh_3)_3$, phenyldiazomethane and tricyclohexylphosphine in a one-pot synthesis,[49] is an important precursor to the multiple generations that followed.[40] Ru-MACHO is a commercially available pincer complex applied in hydrogenation reactions, mainly of esters.[50] However, due to its proven efficiency in hydrogenation of a wider range of carbonyl functionalities, Ru-MACHO in the presence of polyamine was used as the first example of homogeneous catalyst for CO_2 capture from air and direct conversion to methanol, with up to 79% of CO_2 captured converted to methanol.[51]

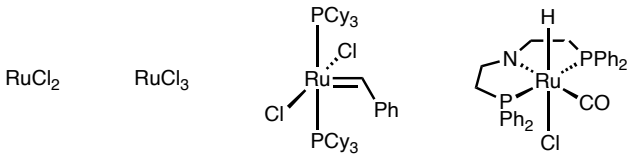

Figure I.2. Series of ruthenium complexes applied in catalysis.[47-51]

The research on developing ligands in homogeneous catalysis has expanded over the years, as participative and non-participative ligands are modulating the electronic and steric properties of transition-metal complexes, thus influencing their catalytic activity, selectivity, or stability. A well-established method to quantify the electronic effects of various ligands is by observing the difference in the CO stretching frequencies of metal complexes, as *trans*-[Rh(CO)Cl(L)].[52] Being easily identifiable, the CO stretching frequency is a useful probe to understand the electronic properties, particularly of tertiary phosphine ligands, and enables the report of large ligand electronic databases. Electron-donating ligands can increase electron density at the metal, facilitating oxidative addition processes, while electron-withdrawing ligands may enhance reductive elimination steps. For example, the rate of addition of MeI to the square-planar coordinatively unsaturated $[Ir(CO)Cl(L)_2]$, where L = $P(4\text{-}X\text{-}C_6H_4)_3$, increases significantly as X becomes more electron-donating.[53] Giering

group disclosed that this electronic effect is more significant for the oxidation addition of MeI compared to H_2 and proposed that a second electronic parameter relative to the number of aryl substituents present in the phosphine ligand impacts the overall reaction. This investigation shows the importance of understanding and exploiting the ligand electronic effects that can vary depending on the system studied. The steric properties of ligands can control the coordination environment around the metal center, thus affecting substrate coordination, activation, and reaction pathways.[54] For instance, in palladium-catalyzed Suzuki-Miyaura cross-coupling, there is a clear correlation between ligand sterics and the C2:C4 selectivity (Figure I.3).[55] Two competing mechanisms for oxidative addition explain the different site preference: sterically hindered strong σ-donor ligands, as PCy_3 and SIPr, favor the C4 selectivity by promoting oxidative addition through a low-coordinate 12 e^- palladium species, while smaller ligands or better π-acceptor, as PPh_3 and SIMes, favor coordination of a second ligand.

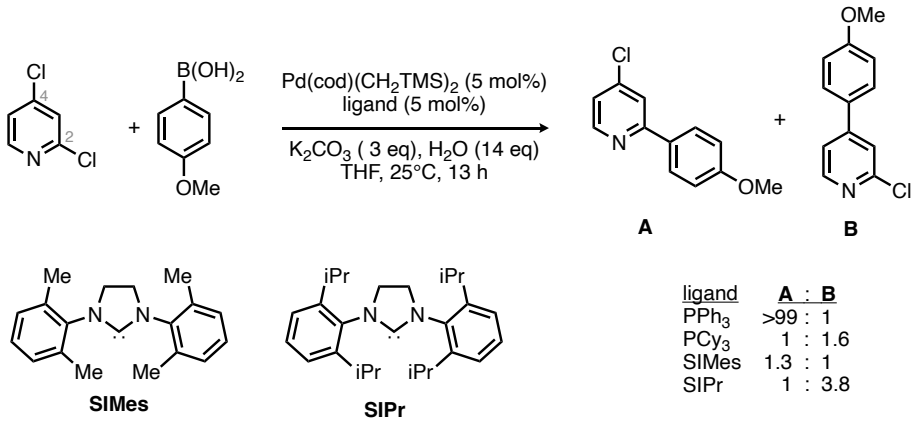

Figure I.3. Influence on C2:C4 selectivity of palladium-catalyzed Suzuki-Miyaura cross-coupling using different phosphines and NHCs ligands.[55]

Other ligand parameters also impact the reactivity and selectivity in transition metal homogeneous catalysis. Introducing a confined space as a second coordination sphere, through the encapsulation of transition metal complexes, is a recently developed method to induce selectivity and activity.[56] For example, encapsulated cobalt(II)-porphyrin catalyst preferentially cyclopropanates styrene over larger substrates, while the non-encapsulated catalyst gives equal distribution of the products, showcasing that the second coordination sphere controls the size selectivity.[57] Ligand flexibility also plays a crucial role in controlled reactivity, with the ligand adapting throughout the catalytic cycle. In rhodium-catalyzed asymmetric hydroboration, the TADDOL-derived ligands display two different conformations during hydride migration and C-B reductive elimination, promoting high levels of regio- and enantioselectivities.[58] In manganese-based superoxide dismutase mimics, the ligand flexibility is more crucial than the metal center redox potential when the reaction occurs through an inner-sphere electron-transfer mechanism.[59] N,O-chelating ligands, inspired by α-chiral amino acids in metalloproteins, exhibit diverse coordination modes and are an example of cooperative ligands, highly valuable in catalysis.[60]

I.4. Underligated complexes

Introduction. Since the discovery of metallocenes by Wilkinson and Fischer, the field of organotransition metal chemistry has been predominantly dominated by complexes following the 18-electron rule. Also referred to as the effective atomic number, it describes the tendency of a metal center to reach the noble gas configuration in its valence shell and form a thermodynamically stable complex containing 18 valence electrons, including the metal d electrons and the electrons conventionally considered as being supplied by the surrounding ligands. Organometallic complexes that do not follow this rule and possess fewer ligands that exist in the coordinatively saturated complexes are known as coordinatively unsaturated complexes and are often described in-between Werner-type and 18-electron complexes.[61,62] Sometimes called low-valent or underligated complexes, the isolation and characterization of such compounds remained relatively scarce in comparison, as they are usually highly reactive and unstable towards air, moisture, or thermal conditions. However, the interest in exploring and understanding the reactivity of coordinatively unsaturated complexes is high due to their potential involvement as entry points or intermediates in numerous catalytic processes, as the 16-electron Grubb's complexes $[RuCl_2(=CHR)(PR'_3)_2]$ in olefin metathesis.[63]

The stability of coordinative unsaturated complexes mainly arises from the presence of bulky and π-donor ligands. On the one hand, ligands with lone pairs available, such as halide or isoelectronic analogs, stabilize the electronically unsaturated configuration through π-bonding. For instance, the corresponding unsaturated 16-electron dihydrogen derivative of $[RuH_2(H_2)_2(PCy_3)_2]$, $[RuH(H_2)I(PCy_3)_2]$, is relatively stable due to the π-donation of the iodo ligand, showcasing that electron saturation is not necessary for stabilization of coordinated H_2.[64] On the other hand, complexes with low coordination numbers have been stabilized by the introduction of highly bulky ligands, as in the case of the two-coordinate $[Mn(C(SiMe_3)_3)_2]$.[65] The coordination at the Mn center is strictly linear and the $C(SiMe_3)_3$ ligands are staggered around the C–Mn–C direction. The $C(SiMe_3)_3$ groups are interlocked and effectively fill the space around the Mn center, thus providing steric shielding against the coordination of additional ligands to the metal center.

Although these two parameters, steric effect and π-donation of the ligands, are generally accepted, they cannot always alone rationalize the reactivity of coordinatively unsaturated complexes. For instance, coordination of another PMe_3 to the 15-electron $[CpVCl(PMe_3)_2]$ is not observed (Figure I.4).[61] The same occurs with the chromium analog $[CpCrCl_2(PMe_3)]$, inducing also that the size of the metal and the metal-ligand bond strength are not an important factor here. However, $[CpVCl_2(PMe_3)_2]$ is stable,[66] even with bulkier phosphine as $[CpVCl_2(PEt_3)_2]$, suggesting that coordination of an additional ligand is possible. $[CpVCl_2(PMe_3)_2]$ can be converted to the alkyl analog $[CpVR_2(PMe_3)_2]$ (R = Me, Ph),[67] indicating that neither π-donation is a key parameter in the stabilization of these species. In this case, the influence of the pairing energy has been discussed to explain these complex reactivities,[68] but in the majority of the coordinatively unsaturated

complexes that we will discuss, particularly half-sandwich 16-electron complexes, bulky and π-donor ligands are important factors for the stabilization.

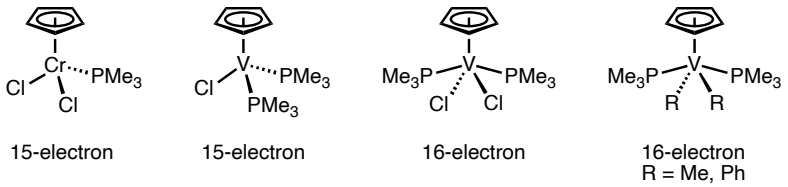

Figure I.4. Series of unsaturated chromium- and vanadium-complexes, representing the limits of theoretical stabilization by bulky and π-donor ligands.[61, 66-68]

Preparation of phosphine-based underligated complexes. Complexes of the type $[(C_5R_5)MXL]$ (X = monoanionic ligand, L = neutral ligand) are one of the most studied classes of 16-electron complexes, using (C_5R_5) but especially bulky phosphine ligands for stabilization of $[(C_5R_5)MX(PR_3)]$ species. In general, phosphines are widely used as ligands because they are stable, and their electronic and steric factors can be conveniently modulated. In 1988, Tilley and coworkers exploited the lability of tetrameric $[(Cp^*RuCl)_4]$ to prepare $[Cp^*RuClL]$ (with L = P*i*Pr$_3$, PCy$_3$) from the reaction with the corresponding phosphine.[69] The same complexes are obtained from the reduction of $[Cp^*RuCl_2L]$ with zinc.[70] These synthetic methods were used in the early days of the discovery of underligated phosphine-based complexes for the synthesis of various unsaturated $[Cp^*RuCl(PR_3)]$ complexes (Scheme I.7.a). Noteworthy, Onate and coworkers reported in 2011 the synthesis of 16-electron tetrasubstituted cyclopentadienyl $[(C_5HR^1R^2R^3R^4)RuCl(P{i}Pr_3)_2]$ (with R^1 = (C(CH$_3$)=CH$_2$, R^2 = Et, R^3 = *n*Pr, R^4 = Me) by reacting $[RuH_2Cl_2(P{i}Pr_3)_2]$ and 2-methyl-1-hexen-3-yne in toluene, via the formation of an alkenylcarbene intermediate with a maximum yield of 60% (Scheme I.7.b).[71]

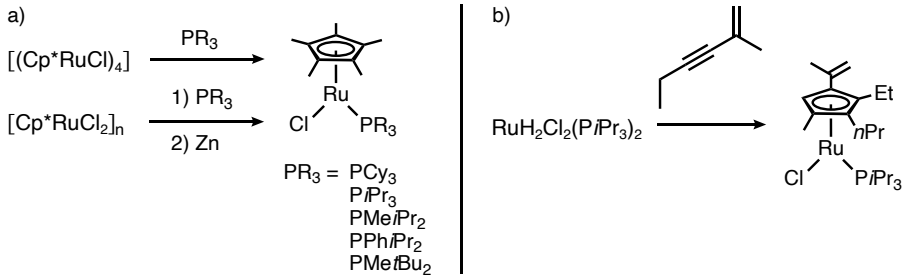

Scheme I.7. a) General synthetic method for the formation of $[Cp^*RuCl(PR_3)]$ complexes;[69,70] b) Unusual synthesis of tetrasubstituted cyclopentadienyl Ru complex.[71]

There is a direct correlation between the cone angle of the phosphine ligands and the formation of either the unsaturated 16-electron $[Cp^*RuCl(PR_3)]$ species or the 18-electron $[Cp^*RuCl(PR_3)_2]$ species (Table I.4). Phosphines with the smaller cone angle, PMe$_3$, PEt$_3$, PPh$_2$Me, and even PPh$_3$, favor the formation of the corresponding 18-electron complexes (entries 1–4). PMe*i*Pr$_2$, with a cone angle of 146°, defines the steric limits for the stabilization of 16-electron complexes as both $[Cp^*RuCl(PMe{i}Pr_2)_2]$ and $[Cp^*RuCl(PMe{i}Pr_2)]$ complexes are accessible depending on the amount of phosphine added during the synthesis (entry 5).[72] As presented before, bulky phosphines with a larger cone angle permit the isolation of 16-electron complexes (entries 6–7). Thermodynamic

investigations using a relative bond enthalpy scale established that the two sterically demanding phosphine ligands exhibit the weakest Ru–PR_3 bond (see relative BDE, Table I.4).[73] In order to determine whether sterics or electronics in the phosphine system was predominant, the relative Ru–PR_3 bond enthalpies were plotted against the Tolman's electronic parameter and the phosphine cone angles, revealing a good linear relationship ($R^2 = 0.98$) for the latter and emphasizing the major role of phosphine steric effects. Addition of less bulky ligands (CO, pyridine, or C_2H_4) to complexes [Cp*RuCl(P*i*Pr$_3$)] and [Cp*RuCl(PCy$_3$)] yielded the corresponding 18-electron complexes, highlighting that saturation is feasible but highly dependent on the incoming ligand added.[69] In addition, reaction of [Cp*RuCl$_4$] with more sterically demanding PPh*t*Bu$_2$ (cone angle 170°) was unsuccessful and gave the unreacted starting material.[74] Excessive steric bulk of the ligand limits the phosphine attack on the tetramer, resulting in inefficient Ru–PR_3 interaction for effective stabilization of 16-electron species.

Table I.4. List of phosphine ligands, cone angles, and relative Bond Disruption Enthalpies (BDE).[73,75]

entry	phosphine	cone angle (°)	complex	relative BDE (kcal/mol)[a]
1	PMe$_3$	118	[Cp*RuCl(PMe$_3$)$_2$]	21.1
2	PEt$_3$	132	[Cp*RuCl(PEt$_3$)$_2$]	18.4
3	PPh$_2$Me	136	[Cp*RuCl(PPh$_2$Me)$_2$]	19.7
4	PPh$_3$	145	[Cp*RuCl(PPh$_3$)$_2$]	14.0
5	PMe*i*Pr$_2$	146	[Cp*RuCl(PMe*i*Pr$_2$)$_2$] or [Cp*RuCl(PMe*i*Pr$_2$)]	-
6	P*i*Pr$_3$	160	[Cp*RuCl(P*i*Pr$_3$)]	9.4
7	PCy$_3$	170	[Cp*RuCl(PCy$_3$)]	10.5

[a]Relative BDE for the reaction Cp*RuCl + nL → Cp*Ru(L)$_n$Cl, with relative BDE values refer to the only, or the average of the two Ru—PR_3 bond energy values unless noted otherwise.

π-donation from the lone pairs of X ligand is another key parameter for the stabilization of [Cp*RuX(PR_3)]. Caulton and coworkers hypothesized that the degree of π-donation should be different depending on the X ligands.[74] They reported the synthesis of a series of potential π-donor X-containing [Cp*RuX(PR_3)] derivatives (PR_3 = P*i*Pr$_2$Ph, PCy$_3$; X = I, OCH_2CF_3, $OSiPH_3$, $OSiMe_2Ph$, NHPh) and their CO adducts [Cp*RuX(PR_3)CO] to understand the nature of the Ru–X bond. The [Cp*RuX(PR_3)] complexes were synthesized either through chloride ion metathesis (Scheme I.8) or according to the general method by reaction of the tetrametic [(Cp*RuI)$_4$] and the corresponding phosphine ligand (Scheme I.7). The [Cp*RuX(PR_3)] complexes rapidly reacted with CO (1 atm) at 25°C, with a color change from blue or purple to orange/yellow. The stretching frequencies ν_{CO} (cm^{-1}) of the carbonyl group in [Cp*RuX(PR_3)CO] adducts are ranked according to anionic ligand X here:

$$\text{I (1930)} > \text{Br (1928)} > \text{Cl (1925)} >> OCH_2CF_3\ (1914) > OSiPh_3\ (1906) > \text{NHPh (1904)} > OSiMe_2Ph\ (1903)$$

Alkoxides and amide ligands are much better donors than the halides tested, as seen with the Ru–X bond lengthening upon CO binding, higher in the case of alkoxide X = OCH_2CF_3 than halides (X

= Cl or I).[69,76] These data are in accordance with ethylene binding experiments. When subjecting [Cp*RuX(PR_3)] species (X = OCH_2CF_3, Cl, I) to an atmosphere of $^{13}C_2H_4$ at 25°C, no change is observed for [Cp*Ru(OCH_2CF_3)(PR_3)], while 80% of chloride and 100% of iodide derivatives form a 1:1 adduct. Higher π-donation (*i.e.* lower ν_{CO} in [Cp*RuX(PR_3)CO]) is competing with the binding of ethylene, a weaker and thus more discriminating Lewis base than CO.

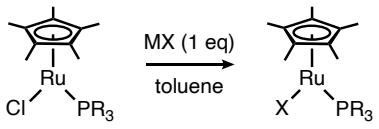

PR_3 = $PiPr_2Ph$, PCy_3
MX = $Tl(OCH_2CF_3)$, $K(OSiPh_3)$, $K(OSiMe_2Ph)$, Li(NHPh)

Scheme I.8. Chloride ion metathesis for the synthesis of 16-electron alkoxo-, siloxo-, and phenylimido-complexes.[74]

Cationic complexes of the type $[Cp^*RuP_2]^+$ are traditionally generated by halide abstraction from the corresponding [Cp*RuClP_2] complexes. However, $[Cp^*RuP_2]^+$ species are known to be reactive towards suitable donor molecules, thus primary reports of the isolation of these cationic complexes were using bulky, non-coordinating anion as $[BAr^F{}_4]^-$. For example, the isolation of [Cp*Ru(dippe)][$BAr^F{}_4$] (dippe = 1,2-bis(di*iso*propylphosphino)ethane, Ar^F = 3,5-$(CF_3)_2C_6H_3$) was achieved by chloride abstraction from the corresponding [Cp*RuCl(dippe)] in the presence of $NaBAr^F{}_4$ in fluorobenzene under argon.[77] Performing the reaction under nitrogen instead of an argon atmosphere yielded the cationic terminal dinitrogen complex [Cp*Ru(N_2)(dippe)][$BAr^F{}_4$].[78] Similar nitrogen coordination was observed upon attempts to crystallize the complex [RuH(DuPHOS-Me)$_2$][PF_6], producing instead crystals of terminal dinitrogen complex [Ru(N_2)H(DuPHOS-Me)$_2$][PF_6].[79] The choice of solvent is also critical, and sometimes even poorly coordinating solvents are not sufficient. [Cp*RuCl(PR_3)] (PR_3 = PCy_3, P*i*Pr_3, PMe_3) in the presence of NaBAr'$_4$ in fluorobenzene under argon resulted in the formation of [Cp*Ru(η^6-C_6H_5F)][$BAr^F{}_4$], with coordinated fluorobenzene.[77] The loss of PR_3 generated concomitantly the fragment $[Cp^*Ru]^+$, which is known for its high affinity towards aromatic systems.[80] The tendency of $[Cp^*RuP_2]^+$ species to react with donor molecules to fill their coordination sphere and form more stable 18-electron complexes led to other types of reactivity, such as the formation of halide bridges[78] or the coordination of phosphine aromatic substituents. For example, solid-state analysis of [CpRu(PMe*i*Pr_2)(PPh_3)][$BAr^F{}_4$][81] revealed the unusual η^3-coordination mode of PPh_3 through one C=C bond of the phenyl rings thus acting as a chelating four-electron donor ligand, which was also observed by crystallographic study using synchrotron radiation for [$CpMo(CO)_2(PPh_3)$][$BAr^F{}_4$][82] or in the presence of more bulky phosphine ligands as BINAP[83] and MeO-BIPHEP.[84]

In addition to the sterics and π-donation arising from the ligands, the capping ring (Cp, Cp*, arene) is also important and can profoundly affect the stability of these complexes. While pentamethylcyclopentadienyl permits the isolation of 16-electron species as [Cp*Ru$(P)_2$][$BAr^F{}_4$] (with $(P)_2$ = dippe or PMe*i*Pr_2) (*vide supra*), also attributed to the good σ-donor character of the ligands, the corresponding cyclopentadienyl analogs showcase different reactivity. Using the same

reaction conditions, *i.e.,* addition of $NaBAr^F_4$ to a solution of $[CpRuCl(P)_2]$ in fluorobenzene under argon, the corresponding $[CpRu(P)_2]^+$ species reacts further with traces of dinitrogen present in high-purity argon furnishing the dinitrogen-bridged complexes $[(Cp^*Ru(P)_2)_2(\mu\text{-}N_2)][BAr^F_4]$.[81] Noteworthy, if the reaction is performed directly under a nitrogen atmosphere, the terminal dinitrogen complexes $[Cp^*Ru(P)_2(N_2)][BAr^F_4]$ are isolated. The reactivity of 16-electron complex is also influenced by the nature of the capping ring. For instance, the coordinatively unsaturated [Cp*Ru(SDmp)] (Dmp = 2,6-(mesityl)$_2C_6H_3$) was found to mediate the trimerization of phenylacetylene to afford the cationic $[Cp^*Ru(\eta_6\text{-}C_6H_3Ph_3)][SDmp]$, with SDmp as counter-anion (Scheme I.9.a).[85] In order to retain the thiolate in the coordination sphere, the introduction of a tethered SDmp ligand, with an additional interaction between the ligand and the ruthenium center, was achieved.[86] Starting from $[Ru(p\text{-}cym)Cl_2]_2$ (*p*-cym = *p*-cymene) the synthesis was achieved via successive additions of LiSDmp, PR_3 (R = Et, Ph), and $NaBAr^F_4$ to yield the corresponding $[(SDmp)Ru(PR_3)][BAr^F_4]$ complex (Scheme I.9.b). The tethered SDmp ligand prevented the dissociation of the thiolate, with insertion of phenylacetylene into the Ru–S bond (Scheme I.9.c).

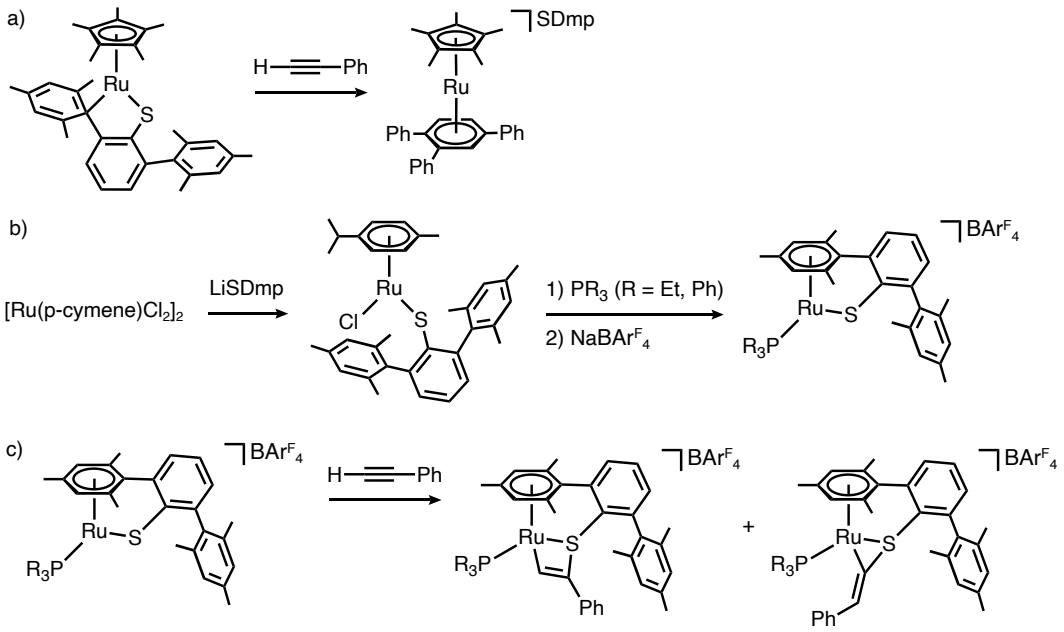

Scheme I.9. a) Trimerization of phenylacetylene yielding $[Cp^*Ru(\eta_6\text{-}C_6H_3Ph_3)][SDmp]$;[85] b) Synthesis of $[(SDmp)Ru(PR_3)][BAr^F_4]$ with tethered SDmp ligand; c) Insertion of phenylacetylene in the Ru-S bond.[86]

While considerable effort has been made to investigate both neutral $[(C_5R_5)MX(PR_3)]$ and cationic $[(C_5R_5)RuP_2]^+$, the examination of alternative phosphine-containing complexes, with incorporation of different heteroatoms, continues to grow in order to understand and expand the reactivity of coordinatively unsaturated complexes (Figure I.5). $[Cp^*Ru(\kappa^2\text{-}P,N)]$ complexes have been described as key intermediates in numerous catalytic transformations, including the hydrogenolysis of epoxides[87] or the hydrogenation of cyclic imides,[88] where the unique chemoselectivity originates from the bifunctional nature of Ru–NH moiety. The first 16-electron $[Cp^*Ru(\kappa^2\text{-}P,N)]$ complex was isolated by Tucurlet and coworkers using N-phosphinoamidinate ligand.[89] Net transfer of hydrogen from ammonia borane to the complex was achieved and the process is reversible, though requiring

5 days at 75°C. The first N-heterocyclic carbene-phosphinidenide ruthenium complex [(*p*-cym)RuCl{(IMes)P}] was applied in the hydroboration of nitriles, esters and amides in neat pinacolborane.[90] In contrast, the corresponding neutral (IMes)PH acted as a two-electron donor and yielded the corresponding 18-electron complex [(*p*-cym)$RuCl_2$\{(IMes)P}], with decreased catalytic activity. Phosphine-containing complexes with different coordinating heteroatoms were also described over the years, exemplified by the phosphoramidate iridium [(Cp*Ir(κ^2-O,N)][BAr^F_4] complex,[91] or the dichalcogenoimidodiphosphinate ruthenium [(C_6Me_6)Ru{N($Ph_2PMe)_2$}][OTf] complex.[92]

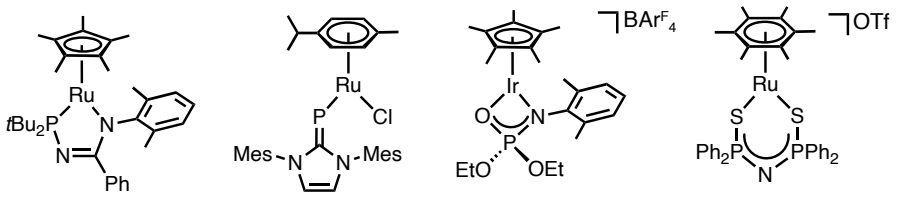

Tucurlet, 2014 Tamm, 2022 Weller, 2015 Leung, 2009

Figure I.5. Representative examples of other phosphine-containing unsaturated complexes.

Preparation of non-phosphine-based underligated complexes. In the meantime, the synthesis of complexes of the type [(C_5R_5)ML] and [(C_5R_5)ML]$^+$ with L ≠ PR_3 have been described. In comparison to phosphine-based unsaturated complexes, the majority of non-phosphine analogs bear bidentate ligands to increase their stability.

Heteroallyl ligands, and particularly amidinates [$R_1N{=}C(R_2)NR_3$], have been investigated since the 1990s to form a large number of transition metal complexes.[93,94] The particularity of these ligands is that they can coordinate to the metal center through various bonding modes, either η^1, η^2, or η^3-bonding modes (giving 2, 4, or 6 electrons to the metal center).[95] Access to [Cp*Ru(amidinate)] complexes is accomplished by the treatment of lithium amidinates with [Cp*RuCl]$_4$ or [Cp*Ru(OMe)]$_2$ as ruthenium precursors.[96] In this case, π-stabilization from the amidinate ligand is more relevant than the stabilization from strong σ-donation from the nitrogen atom as proposed by Kirchner.[94] Compared to their model complex, [CpRu(tmeda)][BAr^F_4] (tmeda = $Me_2NC_2H_4NMe_2$), conjugation in the amidinate moiety leads to a milder σ-donation from the nitrogen compared to tmeda. Noteworthy, [CpRu(tmeda)][BAr^F_4] was the first isolated coordinatively unsaturated cyclopentadienyl [CpRuL]$^+$ complex with a similar synthetic pathway as the [$CpRuP_2$]$^+$ complexes, *i.e.* formation of the 18-electron complex followed by halide abstraction.[97] Reaction of tmeda with the cationic [CpRu(MeCN)][PF_6] precursor yielded the coordinatively saturated [CpRu(tmeda)(MeCN)][PF_6] complex. Due to the lability of MeCN, it was readily replaced upon addition of NEt_4Cl, and further halide abstraction using $NaBAr^F_4$ gave the corresponding [CpRu(tmeda)][BAr^F_4] complex.

The alkoxy-ruthenium precursor [Cp*Ru(OMe)]$_2$, formed readily from the reaction of methanol with [Cp*$RuCl_2$]$_2$, was also used for the synthesis of [Cp*Ru(acac)] complex (acac = acetylacetone).[98] Firstly described as a coordinatively unsaturated species, re-interpretation of the X-ray crystal

structure revealed its dimer nature in the solid state.[99] Other bis(alkoxo)complexes have been reported, exemplified by the series of group 9 pinacolate complexes [Cp*M(pinacolate)] (M = Co, Rh, Ir, pinacolate = $OC(CH_2)_2C(CH_2)_2O$).[100] Interestingly, unlike other 16-electron species (*vide infra*), these complexes present no propensity to form stable 18-electron species upon addition of 2-electron donor ligand. However, both [Cp*Co(pinacolate)] and [Cp*Rh(pinacolate)] complexes produced acetone upon irradiation. Trapping of the [Cp*Co] fragments was possible using 2,3-dimethylbutadiene to form the corresponding [Cp*Co(2,3-dimethylbutadiene)] complexes (Scheme I.10).

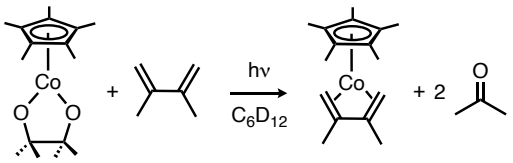

Scheme I.10. Trapping of [Cp*M] in the presence of 2,3-dimethylbutadiene under irradiation.[100]

N,N'-analogs of acac, the so-called diketiminates ligands $[R_1NC(R_2)CC(R_2)NR_3]$, have also been intensely studied for the stabilization of coordinatively unsaturated main group and transition-metal complexes.[101] In comparison to amidinates that usually form four-membered chelates upon coordination of the two nitrogen atoms to the metal center, resulting in a narrow N–M–N bite angle, diketiminates partially encapsulates the metal center with the N-substituents, generally aromatics, thus preventing dimerization. Synthesis of coordinatively unsaturated [Cp*Ru(diketiminates)] is achieved either directly,[102] or through the corresponding 18-electron species upon halide abstraction[103] depending on the substituents (Scheme I.11). Complexes bearing CF_3 substituents at the α-position present a large increase of β–CH ^{1}H chemical shifts, pointing toward a greater π-delocalization within the diketiminate ligand. This increased π-orbital overlap arises from a contraction of σ-bonding due to the electron-withdrawing substituents in the extended π-molecular orbitals orthogonal to the ligand plane. Introduction of CF_3-substituted aryls was similarly applied for the synthesis of the first stable iminoarsane, resulting in strengthened As=N π-bond.[104] Cationic arene complexes of the type $[(C_6H_6)Ru(diketiminates)]^+$ were also reported.[105] The treatment of $[(C_6H_6)RuCl_2]_2$ with lithiated diketiminate $[Li\{R_1NC(R_2)CC(R_2)NR_3\}]$ (with R_1, R_3 = 2,6-$(CH_3)_2C_6H_3$, R_2 = Me) in CH_2Cl_2 resulted in the clean formation of the 18-electron $[(C_6H_6)RuCl(diketiminate)]$. Chloride abstraction with Me_3SiOTf, or one-pot reaction using $[(C_6H_6)RuCl_2]_2$, NaOTf, and $[Li\{R^1NC(R^2)CC(R^2)NR^3\}]$ resulted in coordinatively unsaturated $[(C_6H_6)Ru(diketiminate)]$ complex, isolated as a less usual dark orange solid. This color is attributed to a strong metal-to-ligand charge transfer, characterized by UV-Vis spectroscopy with a broad absorption peak at 434 nm. Similar MLCT interactions are reported for $[(C_6H_6)Ru(diazobutadiene)]$.[106]

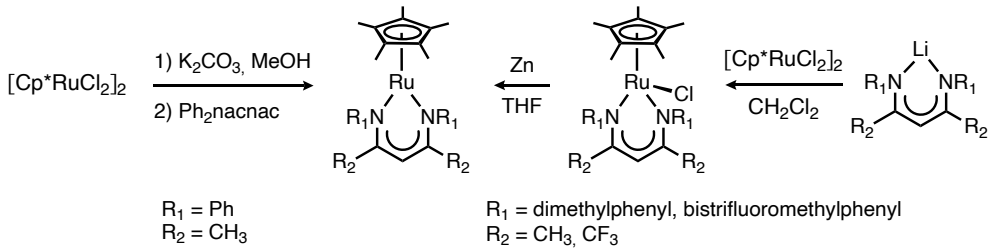

Scheme I.11. Synthetic pathways of neutral [Cp*Ru(diketiminate)] complexes.[102,103]

Bis(imidazoline-2-imine) BL^R ligands are another class of largely studied ancillary ligands, with proven applications in a variety of catalytic reactions. Due to the efficient stability of a positive charge, the basic and nucleophilic properties of the imidazolin-2-ylidenes are transferred to the exocyclic nitrogen.[107] This results in highly basic diimines with strong electron-donating capabilities, exemplified by the isolation of coordinatively unsaturated [Cp*Ru(BL^R)][Cl] (R = *i*Pr, Me).[108] The synthesis is straightforward, with direct addition of deprotonated BL^R ligands to the ruthenium precursor $[Cp^*RuCl]_4$. Easy counterion anion exchange from chloride to triflate can be performed using NaOTf, but more interestingly is the absence of coordination of the chloride counterion knowing the propensity of cationic 16-electron species to fill their coordination sphere. The resistance of the ruthenium center to bind π-basic ligand as chloride, whereas strong binding of σ-donor/π-acceptor ligands as CO is observed, is ascribed to the strong π-basic nature of the ligands.

The capping ligands in these half-sandwich complexes can be varied to C_6R_6 ring, yielding the cationic 16-electron complexes [(C_6R_6)Ru(BL^R)][Cl] (C_6R_6 = C_6H_6, *p*-cym, R = *i*Pr, Me),[109] or through less ordinary open ruthenocene starting material, yielding the pentadienyl- and cyclopentadienyl 16-electron complexes [(C_7R_{11})Ru(BL^R)][BF_4] and [CpRu(BL^R)][BF_4] (R = *i*Pr, Me).[110] In the latter, the protonated open ruthenocene, obtained upon treatment of the ruthenium precursor [(C_7H_{11})$_2$Ru], further reacts with cyclopentadiene to yield the corresponding Cp half-open ruthenocene complex. These two species can react with the deprotonated bis(imidazoline-2-imine) and give the desired complexes upon displacement of the diene ligand (Scheme I.12). The large dihedral angle between the imidazole and the N–Ru–N plane prevents any substantial π-interaction between the imidazole and the nitrogen atoms, indicating clear charge separation. These complexes were tested in the catalytic transfer hydrogenation of ketones using iPrOH as hydrogen source (1 mol% catalyst, 10 mol% KOH, 82°C) and compared to previously mentioned complexes bearing BL^R ligand scaffold.[110] While the cyclopentadienyl complexes present similar activities to Cp*Ru(BL^R)][Cl] and [(C_6R_6)Ru(BL^R)][Cl] complexes, the pentadienyl complex [(C_7R_{11})Ru(BL^{Me})][BF_4] displays the highest activity with full conversion of acetophenone within 30 min.

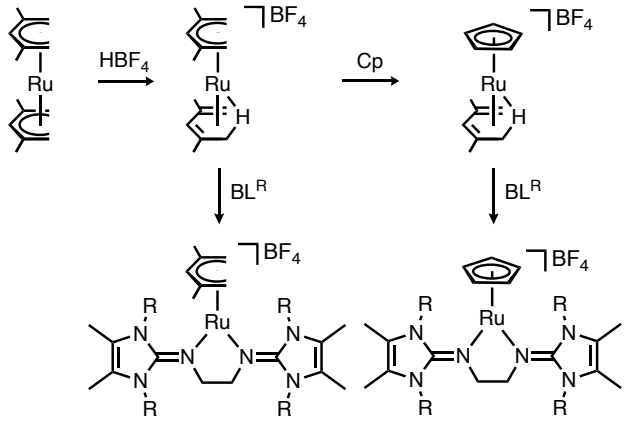

Scheme I.12. Synthetic pathways of cationic complexes $[(C_7R_{11})Ru(BL^R)][BF_4]$ and $[(C_5R_{11})Ru(BL^R)][BF_4]$ (R = *i*Pr, Me).[110]

Maybe the clearest illustration of the involvement of coordinatively unsaturated complexes in homogeneous catalysis is the Noyori-Ikariya complex, applied successfully in asymmetric transfer hydrogenation reactions.[111] In a communication in 1997, both the catalyst precursor [(*p*-cym)RuCl(S,S-TsDPEN)] (S,S-TsDPEN = (1S,2S)-*N*-*p*-toluenesulfonyl-1,2-diphenylethylenediamine), the coordinatively unsaturated catalyst [(*p*-cym)Ru(S,S-TsDPEN)], and the reactive intermediate [(*p*-cym)RuH(S,S-TsDPEN)] were isolated and characterized (Figure I.6).[112] The 18-electron catalyst precursor was obtained by reaction of $Ru(p\text{-cym})Cl_2]_2$ with (S,S)-TsDPEN in the presence of Et_3N. Easy HCl elimination upon treatment with KOH in a CH_2Cl_2-water system yielded the coordinatively unsaturated complex. While this reaction is reversible in the presence of Et_3NHCl, the 18-electron hydrido intermediate is obtained upon addition of H_2 (80 atm) in toluene. Solid state analysis of [(*p*-cym)Ru(S,S-TsDPEN)] complex revealed a HN–Ru bond of 1.897 Å comprised between the N–Ru bond in Ru-anilide complex (2.01-2.16 Å) and the Ru–N bond in Ru-imide complex (1.75 Å), suggesting the double bond character of the HN–Ru bond. Coordination of (S,S)-TsDPEN to other transition metals was achieved, resulting in the formation of [Cp*M(S,S-TsDPEN)] (M = Ir, Rh).[113] Interestingly, while the hydrido species [Cp*IrH(S,S-TsDPEN)] was formed quantitatively in *i*PrOH, no hydride derivative could be obtained under the same conditions suggesting that the rhodium center favors the stabilization of the coordinatively unsaturated complex in these reaction conditions.

Other coordinatively unsaturated complexes incorporating amido ligands are capable of N–M π-bonding, as complexes of the type $[Cp^*M(HNC_6H_4NH)]$ (M = Rh, Ir).[114,115] Interestingly, when one of the NH is tosylated, a marked asymmetry is observed between the M–N bonds. As observed in $[Cp^*Rh(HNC_6H_4NTs)]$ complex,[116] the Rh–NH bond is much shorter than the Rh–NTs bond (1.9372 vs. 2.0796 Å), due to the large electron-withdrawing effect of the tosyl group.

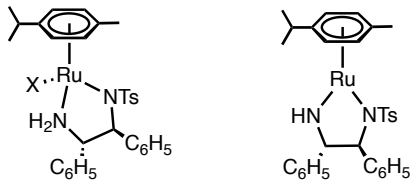

Catalyst precursor: X = Cl
Reactive intermediate: X = H

Catalyst

Figure I.6. The three different complexes involved in the asymmetric transfer hydrogenation of ketones.[112]

The isolation of complexes of the type $[(C_5R_5)ML]$ and $[(C_5R_5)ML]^+$ is of course not limited to bis-amido containing ligands. Complexes bearing pyridyl-amido ligands, as described by Liu[117] and Carmona,[118] are isolated as coordinatively unsaturated complexes due to concomitant steric bulk arising from the ligand and π-stabilization from the amido-nitrogen. Numerous coordinatively unsaturated carbene complexes [Cp*RuCl(1,3-R_2-imidazol-2-ylidene)][119] (R_2 = 4-methylphenyl (ITol), 4-chlorophenyl (IpCl), adamantyl (IAd) and 4,5-dichloro-1,3-bis(2,4,6-trimethylphenyl)-imidazol-2-ylidene (IMesCl)) are easily accessible upon treatment of $[Cp^*RuCl]_4$ with the corresponding free carbene. The tricationic bis-carbene complex $[Cp^*Ru(C_6H_{12}N_3)_2][CF_3SO_3]_3$ was also reported in the early 2000s.[120] Carbenes acting as 2-electron donors are in agreement with the relatively long C–Ru bonds (2.071 and 2.079 Å). Other carbon-coordinating complexes have been described, as in $[Cp^*RhAr_2]$ complexes (Ar = C_6F_6, $C_6F_3Cl_2$-3,5).[121] Fast aryl transmetalations were uncovered upon mixing these two complexes. This exchange was catalyzed by undetectable amounts of hydroxo-bridge $[(Cp^*RhAr)_2(\mu\text{-}OH)_2]$ species, potentially interesting for catalyzed water oxidation processes. As a note, numerous bi-metallic 16-electron complexes of the type $[(Cp^*M)_2(\mu\text{-}RX)_2]$ were reported as precursors for the synthesis of unsaturated complexes.[122–124]

Solid-state structure. Half-sandwich coordinatively unsaturated complexes are structurally characterized as two-legged piano-stool structures. The pyramidalization angle α is defined as the angle between the centroid of the L–Ru–X moiety, the metal center, and the centroid of the capping ring. The plane defined by the L–Ru–X atoms is nearly perpendicular to the capping ring (C_5R_5 or C_6R_6), resulting in a pyramidalization angle α equal or superior to 170° (Table I.5, entries 1–5). α is a good indicator of the coordinative unsaturation of complexes, as α inferior to 170° is associated with either the presence of agostic interactions between the ligands and the metal center, or a dimeric structure in the solid state. For instance, even though first reported as a 16-electron complex,[119] the correct structure of [Cp*RuCl(ICy)] was further confirmed as a chloride-bridged dimeric complex $[(Cp^*Ru(ICy))_2(\mu\text{-}Cl)_2]$, supported by a pyramidalization angle α = 143.1° (Table I.5, entry 6). The low α of 166.0° for [Cp*RuCl(IAd)] results from an agostic interaction between the ruthenium center and a hydrogen atom from one of the adamentyl ligand, with a Ru–H bond of 2.20 Å (entry 7).[119]

Table I.5. Pyramidalization angle α for neutral monomer [Cp*RuXL] complexes.[125]

entry	complex	α (°)
1	[Cp*RuCl(P*i*Pr$_3$)]	175.6
2	[Cp*RuCl(PPh*i*Pr$_2$)]	172.2
3	[Cp*RuCl(OSiPh$_2$)(PCy$_3$)]	174.1
4	[Cp*RuCl(IMes)]	170.3
5	[Cp*RuCl(ICy)]	143.1
6	[Cp*RuCl(IAd)]	166.0

As early as 1977, Hofmann analyzed the orbitals of coordinatively unsaturated [CpMn(CO)$_2$] and concluded on the preferred pyramidal structure of these species, with an empty coordination site at the manganese.[126] Based on an analysis of the variation in the structure of five-coordinated d^6 complexes,[127] in the presence of π-acceptor or more than one π-donor ligand, these complexes adopt a square pyramidal structure **A** (Figure I.7, left). In accordance with this, the occupancy of the Cp ring in three facial sites of the square pyramid results in a pyramidal metal center, as in [CpMn(CO)$_2$] complex with α = 160°. For ML$_4$X d^6 complexes, with one π-donor X ligand, a distorted trigonal bipyramidal structure **B** with a M–X multiple bond and no stereochemically active empty orbital is predicted. This is the case in [(C$_5$R$_5$)RuXL] complexes where a metal planar structure is observed (Figure I.7, right).

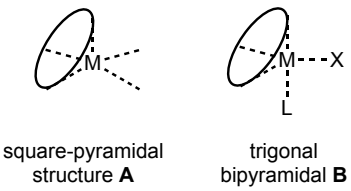

Figure I.7. Representation of the square-pyramidal and the trigonal bipyramidal structures **A** and **B** with a Cp ring (represented as the oval shape),[128] reproduced from ref 73.

Caulton and coworkers investigated the influence of ligand orbitals on the complex geometries of four different coordinatively unsaturated complexes [CpRuH$_2$]$^-$, [CpRuI(PH$_3$)], [CpRu(OH)(PH$_3$)], and [CpRu(CO)$_2$]$^+$.[74] Extended Hückel calculations showed a strong preference for [CpRuI(PH$_3$)] and [CpRu(OH)(PH$_3$)] to remain planar compared to [CpRuH$_2$]$^-$, highlighting that π-donor ligand increases the preference for a planar structure over σ-donor ligand. Based on the molecular orbitals (MOs) of the three occupied d orbitals d_{x2-y2}, d_{z2} and d_{yz}, and the LUMO (d_{xz}) in a C$_s$ symmetry (Figure I.8), the calculated orbital energies were plotted against the pyramidalization angle α in Walsh diagrams. As a note, the d_{x2-y2} energy is not dependent on the pyramidalization angle α. The complex geometry **A** or **B** is determined by the competition between the destabilization of d_{xz} (from increasing antibonding interactions with the ligand σ-donor orbitals when α decreases) and the stabilization of d_{z2}. If the energy difference between d_{z2} and the LUMO is small, the pyramidal structure is preferred. Due to the combination of the metal xz and the ligand π^*_{CO} orbitals, the LUMO is low in energy for

$[CpRu(CO)_2]^+$ and thus the pyramidal structure **A** is adopted. On the contrary, the absence of π^* stabilization from the σ-donor ligand in $[CpRuH_2]^-$ leads to a higher LUMO, and, thus, a smaller stabilization of d_{z2}. Because d_{z2} is not compensating enough for the destabilization of d_{xz}, the planar structure **B** is favored for $[CpRuH_2]^-$. The LUMO is even more destabilized in the case of $[CpRuI(PH_3)]$ and $[CpRu(OH)(PH_3)]$ due to the overlap with the ligand X p_z lone pair, confirming the planar structure **B** of complexes of the type [(Cp)MLX]. A comparison of the relative energies of optimized $[CpRu(H_2NCH_2CH_2NH_2)]^+$ and $[CpRu(H_2PCH_2CH_2PH_2)]^+$ depending on the pyramidalization angle α revealed that amine ligands participate much less in the LUMO than phosphine ligands.[77]

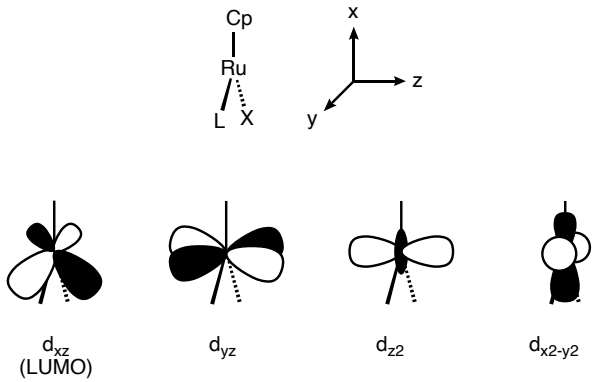

Figure I.8. Representation of the metal orbitals studied, reproduced from ref. 73.

Transition metal amidinate complexes usually adopt a planar structure, with the ligand bonding to the metal through the two nitrogen atoms. Interestingly, this is not the case for coordinatively unsaturated [Cp*Ru(amidinate)] and $[Cp^*Ru(amidinate)]^+$ complexes that present a folded structure, with the central carbon of the amidinate close to the ruthenium center.[94] Even though $[Cp^*Ru(tBuN{=}C(C_6H_5)NtBu)]$ shows an almost perfectly planar structure with a pyramidalization angle α of 179°, the N–C–N plan is folded with an angle of 48.9°.[96] DFT calculations support that the short distance between the ruthenium center and the central carbon of the ligand (Ru–C = 2.336 Å) is arising from the coordination of the π-electrons of the ligand. In contrast to the d^0-titanium amidinate complex[129] where the similar folded structure was attributed to crystal packing, the d-electrons of the ruthenium center can interact with both the π- and π^*-orbitals of the ligand. In comparison, analogous diketiminate complexes such as $[Cp^*Ru(R_1NC(R_2)CC(R_2)NR_1)]$ (R_1 = 3,5-Me-Ar, R_2 = Me) show a planar structure (α = 179°) with a much higher separation distance between the ruthenium center and the central carbon of 3.429 Å.

Masked coordinatively unsaturated complexes. "Masked" coordinatively unsaturated complexes, are acting as a source of coordinatively unsaturated complexes, thus reacting as such with the addition of two-electron donor ligands to form coordinatively saturated complexes. The use of hemilabile ligands, defined as having at least one substitutionally labile donor function with other firmly bound group(s) to the metal center,[130] is one of the common methods to access coordinatively unsaturated complexes. A recent review by Blacquiere[131] nicely describes the use of structurally

responsive ligands (SRLs), *i.e.* ligands that exhibit self-tuning denticity, hapticity, or versatile coordination.

The "indenyl hemilability"[132] is one example of such transformation, with the proposed interconversions of enantiomeric forms of [Cp*Ru(κ^3-P,C,C')] through reversible Ru–C(sp^3) bond cleavage generating the [Cp*Ru(κ^2-P,C)] intermediate complex (Scheme I.13). Even though this coordinatively unsaturated complex was not isolated, indirect support for its reversible formation was obtained through the addition of L ligands (L = CO, PPh_3, $PHPh_2$, 4-dimethylaminopyridine, piperidine, 2,6-dimethylaniline, and NH_3) yielding the corresponding 18-electron complexes, hence the term "masked" coordinatively unsaturated complex.

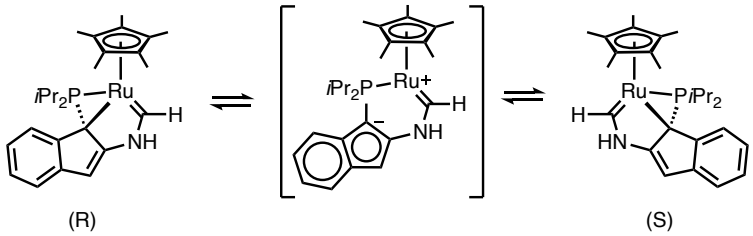

(R) (S)

Scheme I.13. Proposed interconversion of enantiomers through the [Cp*Ru(κ^2-P,C)] intermediate complex.

[Cp*Ru(η^2-H_3B-dppm)][PF_6] is also considered as a "masked" coordinatively unsaturated complex,[133] with change in the ligand hapticity upon coordination of L ligands forming the 18-electron complexes [Cp*Ru(L)(η^1-H_3B-dppm)][PF_6] (L = CO, PMe_3). Even though the H_3B scaffold binds the ruthenium center through a η^2-bonding mode (Ru–H = 1.61 and 1.70 Å), the Ru–B bond distance of 2.09 Å is quite short and suggests a Ru–B interaction. Interestingly, the solid-state structure of the complex is similar to coordinatively unsaturated complexes with a pyramidalization angle α of 174.1° (considering the P–Ru–B centroid). Other examples involved π-coordination of arenes in biphenyl monophosphine[83], or ruthenacyclopentatriene[134] complexes. Notably, using bisphosphinimo methanide ligands,[135] the η^3 to η^2-slippage upon coordination of CO was attributed to a transient stabilization of the intermediate through arene coordination of the ligand, and not directly to the $\eta^3 \rightleftharpoons \eta^2$ equilibrium allowing the formation of a 16-electron species.

Thus, the combination of suitable ligands can enable the isolation of reactive coordinatively unsaturated complexes through π-donation and steric bulks, or at least the synthesis of "masked" coordinatively unsaturated complexes using structurally responsive ligands.

I.5. Pyridylidene amine and amide ligands

Donor-flexible ligands. Unlike most ligands that have static properties, the use of ligands with flexible donor properties is encouraging for the stabilization of coordinately unsaturated complexes. Donor-flexible ligands can adapt their electronic character, either acting as a neutral L-type donor or as an anionic X-type ligand. This feature is particularly interesting as donor interaction from anionic X-type ligand with the metal center would stabilize the coordinatively unsaturated complex, and

further saturation at the metal center would be associated with modulation of the ligand electronics to more neutral L-type character.

NHCs were initially considered to be almost pure σ-donor.[136] However, filled and empty π, π* orbitals on the NHC ring can also contribute to the NHC–M bond. An example to illustrate this concept is $[Ir(I\mathit{t}Bu)_2][PF_6]$ (I*t*Bu = *N,N*-di(*tert*-butyl)imidazol-2-ylidene), isolated as a 14-electron complex.[137] Molecular orbital analysis revealed that the NHC ligand can donate electron density to the iridium center from the filled π orbital through π → d donation.[138] Thus, NHC ligands are much more electronically flexible than just acting as simple σ-donor, either as described for $[Ir(I\mathit{t}Bu)_2][PF_6]$ by stabilizing electron-poor metals, or by stabilizing electron-rich metals through d → π* backdonation.[139] Indeed in a systematic bonding analysis of a series of NHC complexes, the results indicated that it exists at least 10% of π-contribution.[140] Over the years, their ability to stabilize coordinatively unsaturated complexes has been widely studied.[141,142]

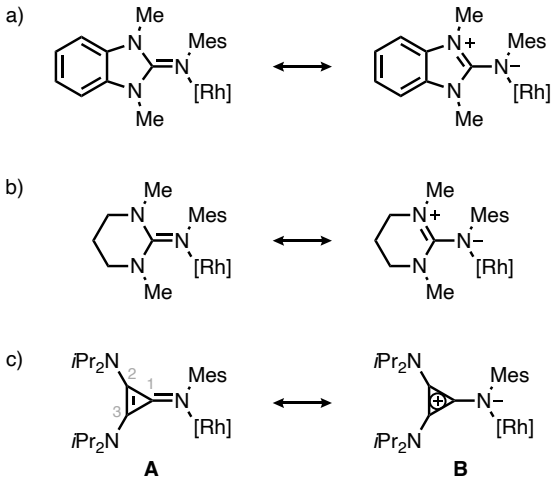

Scheme I.14. Representation of the two limiting resonance structures for $[RhCl(CO)_2L]$ with L = a) benzimidazolimine, b) guanidine and c) cyclopropenylimine scaffolds.

Alcarazo and coworkers extrapolated the coordination behavior of carbodicarbenes to isoelectronic systems in which the central carbon atom is replaced by a nitrogen atom.[143] In order to minimize backdonation from the central nitrogen to the carbene moiety, one of the carbene moieties is replaced by strong σ-donor and very poor π-acceptor such as benzimidazole, guanidine, and cyclopropenyl scaffolds (Scheme I.14). An analysis of the CO stretching frequencies of the resulting rhodium complexes $[RhCl(CO)_2L]$ highlighted the strong donor properties of these ligands.[143] Interestingly, comparison of the solid-state structures of the free cyclopropenyl ligand and upon rhodium coordination revealed the electronic flexibility of the ligand, with the cyclopropenyl moiety acting as an electron reservoir. In the free ligand, the loss of aromaticity in the cyclopropenyl ring (C1–C2 = 1.420 Å, C2–C3 = 1.371 Å) compensates the π-electron density arising from the imino nitrogen (C1–N = 1.295 Å), resulting in resonance structure **A**, while upon nitrogen coordination to the metal center the aromaticity is recovered with a resonance structure closer to **B** (C1–C2 = 1.398 Å, C2–C3 = 1.395 Å, C1–N = 1.326 Å). This π-conjugation, leading to two resonance structures **A**

and **B** possessing an overall neutral charge, was further expanded in other N-donor ligand systems, such as BL^R ligands presented earlier, and proved effective for the stabilization of coordinatively unsaturated complexes (Scheme I.15).[108,109,144]

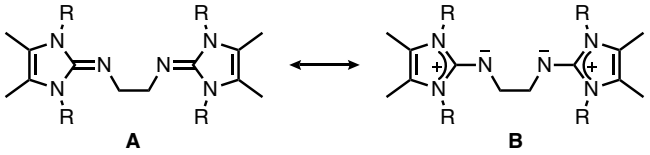

Scheme I.15. Limiting resonance structures of bis(imidazoline-2-imine) BL^R ligands.[108]

The same flexibility character in pyridinium-imine was reported as far as 1921[145,146] but it was only in 2009 that both the groups of Johnson[147] and Douthwaite[148] reported the first examples of transition metal complexes bearing these N-donor ligands. Always with this idea of mimicking the donor properties of NHCs, the general structure of these pyridylidene amides (PYEs) relies on an alkylated pyridine ring with an exocyclic nitrogen atom, either at the *ortho*, *meta*, or *para* position. This nitrogen atom can switch between an imine form **A** with minimized charge separation and a zwitterionic amido form **B** benefiting from aromatic stabilization (Scheme I.15.a). Pyridylidene amides (PYAs), firstly introduced by Wright,[149] possess the same donor-flexibility with an additional resonance structure **C** on the amide group, through a negative charge on the oxygen (Scheme I.15.b). Typical synthesis of PYEs involved N-alkylation of pyridine chloride with an alkyl halide followed by electrophilic substitution using an amine. PYAs are synthesized through the reaction of an aminopyridine with an acyl chloride and subsequent methylation of the pyridine ring. In both cases, easy modulation of the substituents R_1 and R_2 from usually cheap and commercially available starting materials, is possible.

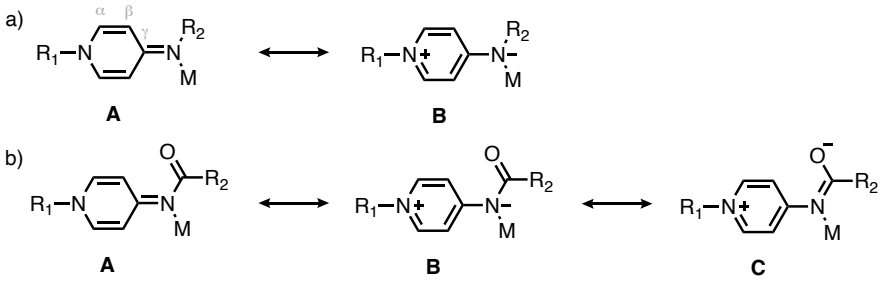

Scheme I.15. Limiting resonance structures of a) *para*-pyridylidene amine (PYE) and b) *para*-pyridylidene amide (PYA) complexes.

Noteworthy, while it is the case for *ortho*- and *para*-PYE/PYA ligands, no neutral resonance structure is accessible for *meta*-analogs, that are thus classified as mesoionic ligands.[150] As we would expect, since the negative charge is predominantly present at the exocyclic nitrogen atom, *meta*-PYE/PYAs can be considered at first glance more strongly donating than the *ortho*- and *para*-forms that have a more accessible neutral quinoidal form. A structural probe to decipher between the two resonance structures **A** and **B** is the difference between C_α–C_β and C_β–C_γ bond lengths. The smaller the difference is, the more pronounced the aromaticity and thus the zwitterionic form **B**. The more marked double-bond localization can also be observed using the C_γ–$N_{exocyclic}$ bond distance, which

is contracted and closer to an imine C=N double bond in the resonance structure **A**. This is also accompanied by a small dihedral angle (defined as the angle between the pyridyl ring and the exocyclic M–N–C(O) plane) due to π-conjugation from the exocyclic nitrogen to the pyridyl ring. For instance, the pincer platinum complex [PtH{pyr(*para*-PYA)$_2$}][BAr$^F{}_4$] exhibits an almost planar structure with an average dihedral angle of 3° and localized double-bond character within the pyridyl ring with average C_α–C_β and C_β–C_γ bond lengths of 1.349(8) and 1.413(6) Å respectively, illustrating a pronounced neutral quinoidal form.[151] Despite the fact that *meta*-PYE/PYA ligands are very good donors in numerous complexes, this fact cannot be generalized as there are other parameters to consider. In the case of *ortho*-PYE/PYAs, steric encumbrance arises from the alkylated pyridyl nitrogen and creates a dihedral strain, destabilizing the planar arrangement. This effect can be observed within the [AuCl{pyr(PYA)$_2$}][PF$_6$] series,[152] with a significantly higher dihedral angle of 68° for the *ortho*-PYA in comparison to 50 and 46° for the *meta*- and *para*-analogs respectively, suggesting an increased predominance of the zwitterionic form within the series. Although establishing trends in the donation of PYA/PYE ligands is difficult due to the number of factors that need to be considered (*i.e. ortho/meta/para*-analogs, steric encumbrance, ancillary substituents, etc), the donor flexibility of these ligands cannot be denied and is attractive for further stabilization of coordinatively unsaturated complexes.

Coordinatively unsaturated PYE complexes. The coordinatively unsaturated phenolate-PYE complex [Ir(O,N-*ortho*-PYE)][PF$_6$] was described in 2022 for its application in formic acid dehydrogenation (Figure I.9).[153] This iridium complex is particularly stable, as neither coordination of donor solvents as MeCN or DMSO, or ligand coordination as PPh$_3$ or CO was observed. Further evidence for the unfavored coordination of exogenous ligands to the iridium center was obtained upon synthesis of the analog complexes [Ir(O,N-*ortho*-PYE)][Cl] and [Ir(O,N-*ortho*-PYE)][F].[154] Solid state analysis of [Ir(O,N-*ortho*-PYE)][Cl] revealed a bond distance superior to 5.9 Å between the chloride and the closest iridium center, indicating that the chloride was not coordinated despite the formally positively charged iridium center. The stabilization of [Ir(O,N-*ortho*-PYE)][X] complexes through π-bonding from the nitrogen is highly plausible, and in accordance with the previously discussed coordinatively unsaturated complexes. Noteworthy, a two dimensional ^{19}F-^{1}H HOESY NMR experiment of [Ir(O,N-*ortho*-PYE)][F] disclosed a correlation between the pyridyl N–CH$_3$ and the fluoride anion. Such ion pairing is in accordance with a positive charge localized on the pyridyl N–CH$_3$ in the zwitterionic structure.

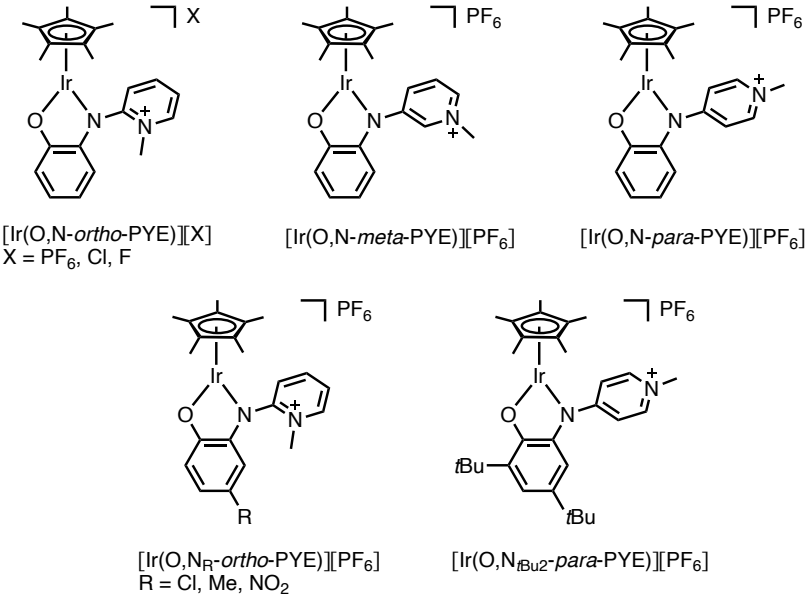

Figure I.9. Representations of the different phenolate-PYE iridium complexes.[153,154]

To further understand the ability of this phenolate-PYE to stabilize such coordinatively unsaturated iridium center, a series of related iridium complexes was synthesized (Figure I.9).[154] Interestingly, [Ir(O,N-*para*-PYE)][PF_6] crystallized as a three-legged piano-stool structure with bridging phenolate oxygen. The C_γ–$N_{exocyclic}$ bond of 1.320(4) Å (compared to 1.392(5) and 1.416(7) Å in [Ir(O,N-*ortho*-PYE)][PF_6] and [Ir(O,N-*meta*-PYE)][PF_6] respectively) suggests a higher contribution of the neutral quinoidal structure and coordination of the less π-basic imine. However, DOSY NMR spectroscopy indicates a monomeric structure in solution, with a diffusion parameter comparable to [Ir(O,N-*ortho*-PYE)][PF_6] (6.60 vs 6.83 × 10^{-10} m^2 s^{-1}) and the theoretical value of the monomeric cation in solution (6.77 × 10^{-10} m^2 s^{-1}).[155] Introduction of steric bulk on the phenolate with *t*Bu groups in *ortho*- and *para*-positions in [Ir(O,N_{tBu2}-*para*-PYE)][PF_6] restored the monomeric structure in the solid state, forcing the preponderance of the zwitterionic resonance structure. This form is further supported by a higher dihedral angle of 89.3° in comparison to 46.9° for the less bulky [Ir(O,N-*para*-PYE)][PF_6]. The increasing donor properties within the *para*- < *meta*- < *ortho*-PYE series is corroborating with the electron density at the iridium center probed by cyclic voltammetry (Table I.6, entries 1–3). Specifically, [Ir(O,N-*ortho*-PYE)][PF_6] imparts the lowest oxidation potential ($E_{1/2}$ = +0.17), followed by the [Ir(O,N-*meta*-PYE)][PF_6] complex ($E_{1/2}$ = +0.35 V), while [Ir(O,N-*para*-PYE)][PF_6] complex features the highest potential ($E_{1/2}$ = +0.48 V). Further substitution at the *para*-position of the phenolate with electron-withdrawing and electron-donating substituents revealed a direct correlation between the redox potential of the complexes and the Hammett parameters of the substituents (entries 4–6), indicating direct control of the iridium electron density through these O-donor substituents.

Table I.6. Selected electrochemical data for the series of [Ir(O,N-PYE)][PF_6] complexes.[a]

entry	complex	$E_{1/2}$ (V)
1	[Ir(O,N-*ortho*-PYE)][PF_6]	+0.17
2	[Ir(O,N-*meta*-PYE)][PF_6]	+0.35
3	[Ir(O,N-*para*-PYE)][PF_6]	+0.48
4	[Ir(O,N_{Me}-*ortho*-PYE)][PF_6][b]	+0.11
5	[Ir(O,N_{Cl}-*ortho*-PYE)][PF_6][b]	+0.22
6	[Ir(O,N_{NO2}-*ortho*-PYE)][PF_6][b]	+0.40

[a]1 mM complex, 100 mM (Bu_4N)PF_6 as supporting electrolyte, MeCN as solvent, scan rate 100 mV.s^{-1}. All potentials referenced to Fc^+/Fc; [b]Substitution at the *para*-position of the phenolate.

I.6. Aim and scope of the thesis

The design of complexes is crucial for achieving efficient catalytic reactions, particularly through the synthesis of coordinatively unsaturated complexes that are often described as entry points or reaction intermediates in numerous catalytic cycles. The aforementioned phenolate-PYE ligands have demonstrated the ability of such donor-flexible ligands to stabilize coordinatively unsaturated complexes.[153,154] Herein, we aim to expand the family of coordinatively unsaturated donor-flexible complexes to better comprehend the intrinsic stability of such species. Because N,N'-bidentate donor-flexible ligands have shown to be useful systems for this purpose,[102,109,112,143] we aim to develop N,N'-PYA ruthenium complexes in combination with the evidenced flexibility of pyridylidene amide.

We also aim to explore the activity of these complexes in catalytic transfer hydrogenation. Numerous examples of PYA ruthenium complexes have been successfully applied in transfer hydrogenation reactions,[156–160] particularly using isopropanol as hydrogen source. Here, we will disclose the ability of these N,N'-PYA ruthenium complexes to further push the renewability of this reaction using ethanol as hydrogen source and apply these complexes in the catalytic transfer hydrogenation of ketones and α,β-unsaturated carbonyls. Furthermore, fine-tuning of the ligand system will provide enhanced chemoselectivity in the catalytic olefin transfer hydrogenation of α,β-unsaturated ketones.

Chapter II presents the synthetic protocol to obtain the model coordinatively unsaturated N,N'-PYA ruthenium complex. Reactivity studies with a series of two-electron donor ligands demonstrate the flexibility of the ligand scaffold through the stabilization of both 16- and 18-electron species. The accessibility of the ruthenium center is further evidenced by the excellent performance of the complex in the catalytic transfer hydrogenation of ketones using ethanol.

Chapter III further investigates the catalytic application of this complex in transfer hydrogenation reactions. It presents the first example of chemoselective room-temperature transfer hydrogenation of C=C bond in α,β-unsaturated carbonyls using ethanol to yield a variety of functionalized products.

Preliminary mechanistic studies show some light on the potential implication of a ruthenium-alkoxide complex as an initially formed species.

Chapter IV focuses on further improvement of catalytic performances in transfer hydrogenation using the synthesis of a second generation of coordinatively unsaturated N,N'-PYA ruthenium complexes. Modulation of the ligand scaffold enhances the selectivity in C=C bond transfer hydrogenation of α,β-unsaturated ketones, with significantly less over-hydrogenation of the C=O bond over time.

I.7. References

[1] M. J. Sofia, D. Bao, W. Chang, J. Du, D. Nagarathnam, S. Rachakonda, P. G. Reddy, B. S. Ross, P. Wang, H.-R. Zhang, S. Bansal, C. Espiritu, M. Keilman, A. M. Lam, H. M. M. Steuer, C. Niu, M. J. Otto, P. A. Furman, *J. Med. Chem.* **2010**, *53*, 7202–7218.

[2] N. Afdhal, S. Zeuzem, P. Kwo, M. Chojkier, N. Gitlin, M. Puoti, M. Romero-Gomez, J.-P. Zarski, K. Agarwal, P. Buggisch, G. R. Foster, N. Bräu, M. Buti, I. M. Jacobson, G. M. Subramanian, X. Ding, H. Mo, J. C. Yang, P. S. Pang, W. T. Symonds, J. G. McHutchison, A. J. Muir, A. Mangia, P. Marcellin, *N. Engl. J. Med.* **2014**, *370*, 1889–1898.

[3] R. Geyer, J. R. Jambeck, K. L. Law, *Sci. Adv.* **2017**, *3*, e1700782.

[4] Eug. Bamberger, F. Tschirner, *Ber. Dtsch. Chem. Ges.* **1900**, *33*, 955–959.

[5] P. Anastas, N. Eghbali, *Chem. Soc. Rev.* **2010**, *39*, 301–312.

[6] M. A. Murphy, *Chem. Int.* **2021**, *43*, 21–25.

[7] M. Filonchyk, M. P. Peterson, L. Zhang, V. Hurynovich, Y. He, *Sci. Total Environ.* **2024**, *935*, 173359.

[8] W. C. Li, H. F. Tse, L. Fok, *Sci. Total Environ.* **2016**, *566–567*, 333–349.

[9] R. Naidu, B. Biswas, I. R. Willett, J. Cribb, B. Kumar Singh, C. Paul Nathanail, F. Coulon, K. T. Semple, K. C. Jones, A. Barclay, R. J. Aitken, *Environ. Int.* **2021**, *156*, 106616.

[10] A. Kumar, A. K. Thakur, G. K. Gaurav, J. J. Klemeš, V. K. Sandhwar, K. K. Pant, R. Kumar, *Environ. Sci. Pollut. Res.* **2023**, *30*, 105030–105055.

[11] M. Höök, X. Tang, *Energy Policy* **2013**, *52*, 797–809.

[12] P. T. Anastas, J. C. Warner, J. C. Warner, *Green Chemistry: Theory and Practice*, Oxford University Press, Oxford, **2000**.

[13] C. G. Brundtland, *The World Commission on Environmental Development* **1987**.

[14] S. L. Y. Tang, R. L. Smith, M. Poliakoff, *Green Chem.* **2005**, *7*, 761–762.

[15] G. Rothenberg, *Catalysis: Concepts and Green Applications*, Wiley-VCH, Weinheim, **2015**.

[16] A. D. MacNaught, A. Wilkinson, *Compendium of Chemical Terminology: IUPAC Recommendations*, Blackwell Science, Oxford, **1997**.

[17] B. Cornils, W. A. Herrmann, H. Zanthoff, C.-H. Wong, *Catalysis from A to Z: A Concise Encyclopedia*, Wiley, **2013**.

[18] L. K. Boerner, *Chemical & Engineering News* **2019**.

[19] S. Menegat, A. Ledo, R. Tirado, *Sci. Rep.* **2022**, *12*, 14490.

[20] R. Lan, J. T. S. Irvine, S. Tao, *Int. J. Hydrogen Energy* **2012**, *37*, 1482–1494.

[21] C. Smith, A. K. Hill, L. Torrente-Murciano, *Energy Environ. Sci.* **2020**, *13*, 331–344.

[22] A. Garg, D. Rendina, H. Bendale, T. Akiyama, I. Ojima, *Front. Chem.* **2024**, *12*, 1398397.

[23] B. Q. Li, Z.-W. Qiu, A.-J. Ma, J.-B. Peng, N. Feng, J.-Y. Du, H.-P. Pan, X.-Z. Zhang, X.-T. Xu, *Org. Lett.* **2020**, *22*, 1903–1907.

[24] L. C. R. Carvalho, E. Fernandes, M. M. B. Marques, *Chem. Eur. J.* **2011**, *17*, 12544–12555.

[25] N. A. Afagh, A. K. Yudin, *Angew. Chem. Int. Ed.* **2010**, *49*, 262–310.

[26] N. Y. Chen, W. E. Garwood, *Catal. Rev.* **1986**, *28*, 185–264.

[27] B. Ye, B. Jeong, M. Lee, T. H. Kim, S.-S. Park, J. Jung, S. Lee, H.-D. Kim, *Nano Converg.* **2022**, *9*, 51.

[28] M. Miceli, P. Frontera, A. Macario, A. Malara, *Catalysts* **2021**, *11*, 591.

[29] J. Hagen, *Industrial Catalysis: A Practical Approach*, Wiley, **2015**.

[30] E. T. C. Vogt, B. M. Weckhuysen, *Chem. Soc. Rev.* **2015**, *44*, 7342–7370.

[31] P. W. N. M. van Leeuwen, *Homogeneous Catalysis: Understanding the Art*, Kluwer Academic Publishers, Dordrecht, **2004**.

[32] E. De Smit, B. M. Weckhuysen, *Chem. Soc. Rev.* **2008**, *37*, 2758.

[33] D. Evans, J. A. Osborn, G. Wilkinson, *J. Chem. Soc. A* **1968**, 3133.

[34] W. S. Knowles, M. J. Sabacky, B. D. Vineyard, *Ann. N. Y. Acad. Sci.* **1973**, *214*, 119–124.

[35] J. A. Moulijn, P. W. N. M. van Leeuwen, R. A. van Santen, *Catalysis: An Integrated Approach to Homogeneous, Heterogeneous and Industrial Catalysis*, Elsevier, Amsterdam ; New York, **1993**.

[36] J. Halpern, *Science* **1982**, *217*, 401–407.

[37] J. M. Brown, P. A. Chaloner, *J. Am. Chem. Soc.* **1980**, *102*, 3040–3048.

[38] M. J. Burk, J. E. Feaster, *J. Am. Chem. Soc.* **1992**, *114*, 6266–6267.

[39] D. Forster, T. C. Singleton, *J. Mol. Catal.* **1982**, *17*, 299–314.

[40] R. H. Grubbs, *Handbook of Metathesis*, John Wiley, Chichester, England, **2003**.

[41] M. Eckert, G. Fleischmann, R. Jira, H. M. Bolt, K. Golka, in *Ullmann's Encyclopedia of Industrial Chemistry*, Wiley, **2006**.

[42] A. Vaughan, D. S. Davis, J. R. Hagadorn, M. S. Salwani, in *Reference Module in Materials Science and Materials Engineering*, Elsevier, **2017**.

[43] C. Le Berre, P. Serp, P. Kalck, G. P. Torrence, in *Ullmann's Encyclopedia of Industrial Chemistry*, Wiley, **2014**, pp. 1–34.

[44] G. J. Sunley, D. J. Watson, *Cat. Today* **2000**, *58*, 293–307.

[45] F. E. Paulik, J. F. Roth, *Chem. Commun.* **1968**, 1578a.

[46] T. W. Dekleva, D. Forster, in *Advances in Catalysis*, Elsevier, **1986**, pp. 81–130.

[47] J. Halpern, J. F. Harrod, B. R. James, *J. Am. Chem. Soc.* **1966**, *88*, 5150–5155.

[48] T.-Y. Feng, H.-X. Li, D. J. Young, J.-P. Lang, *J. Org. Chem.* **2017**, *82*, 4113–4120.

[49] P. Schwab, M. B. France, J. W. Ziller, R. H. Grubbs, *Angew. Chem. Int. Ed.* **1995**, *34*, 2039–2041.

[50] W. Kuriyama, T. Matsumoto, O. Ogata, Y. Ino, K. Aoki, S. Tanaka, K. Ishida, T. Kobayashi, N. Sayo, T. Saito, *Org. Process Res. Dev.* **2012**, *16*, 166–171.

[51] J. Kothandaraman, A. Goeppert, M. Czaun, G. A. Olah, G. K. S. Prakash, *J. Am. Chem.*

Soc. **2016**, *138*, 778–781.

[52] A. Roodt, S. Otto, G. Steyl, *Coord. Chem. Rev.* **2003**, *245*, 121–137.

[53] M. R. Wilson, H. Liu, A. Prock, W. P. Giering, *Organometallics* **1993**, *12*, 2044–2050.

[54] J. F. Hartwig, *Organotransition Metal Chemistry: From Bonding to Catalysis*, University Science Books, Sausalito, **2010**.

[55] J. P. Norman, N. G. Larson, S. R. Neufeldt, *ACS Catal.* **2022**, *12*, 8822–8828.

[56] S. H. A. M. Leenders, R. Gramage-Doria, B. De Bruin, J. N. H. Reek, *Chem. Soc. Rev.* **2015**, *44*, 433–448.

[57] M. Otte, P. F. Kuijpers, O. Troeppner, I. Ivanović-Burmazović, J. N. H. Reek, B. de Bruin, *Chem. Eur. J.* **2014**, *20*, 4880–4884.

[58] H. Shao, S. Chakrabarty, X. Qi, J. M. Takacs, P. Liu, *J. Am. Chem. Soc.* **2021**, *143*, 4801–4808.

[59] M. Richezzi, S. Signorella, C. Palopoli, N. Pellegri, C. Hureau, S. R. Signorella, *Inorganics* **2023**, *11*, 359.

[60] M. W. Drover, J. A. Love, L. L. Schafer, *Chem. Soc. Rev.* **2017**, *46*, 2913–2940.

[61] R. Poli, *Chem. Rev.* **1996**, *96*, 2135–2204.

[62] P. Muller, *Pure and Applied Chemistry* **1994**, *66*, 1077–1184.

[63] R. H. Grubbs, S. Chang, *Tetrahedron* **1998**, *54*, 4413–4450.

[64] B. Chaudret, G. Chung, O. Eisenstein, S. A. Jackson, F. J. Lahoz, J. A. Lopez, *J. Am. Chem. Soc.* **1991**, *113*, 2314–2316.

[65] N. H. Buttrus, C. Eaborn, P. B. Hitchcock, J. D. Smith, A. C. Sullivan, *J. Chem. Soc., Chem. Commun.* **1985**, 1380.

[66] J. Nieman, J. H. Teuben, J. C. Huffman, K. G. Caulton, *J. Organomet.* **1983**, *255*, 193–204.

[67] Bart. Hessen, J. H. Teuben, T. H. Lemmen, J. C. Huffman, K. G. Caulton, *Organometallics* **1985**, *4*, 946–948.

[68] R. Poli, *J. Organomet.* **2004**, *689*, 4291–4304.

[69] B. K. Campion, R. H. Heyn, T. D. Tilley, *J. Chem. Soc., Chem. Commun.* **1988**, 278–280.

[70] T. Arliguie, C. Border, B. Chaudret, J. Devillers, R. Poilblanc, *Organometallics* **1989**, *8*, 1308–1314.

[71] A. Collado, M. A. Esteruelas, E. Oñate, *Organometallics* **2011**, *30*, 1930–1941.

[72] M. J. Tenorio, K. Mereiter, M. C. Puerta, P. Valerga, *J. Am. Chem. Soc.* **2000**, *122*, 11230–11231.

[73] L. Luo, S. P. Nolan, *Organometallics* **1994**, *13*, 4781–4786.

[74] T. J. Johnson, K. Folting, W. E. Streib, J. D. Martin, J. C. Huffman, S. A. Jackson, O. Eisenstein, K. G. Caulton, *Inorg. Chem.* **1995**, *34*, 488–499.

[75] J. Jover, J. Cirera, *Dalton Trans.* **2019**, *48*, 15036–15048.

[76] E. Cesarotti, M. Angoletta, N. P. C. Walker, M. B. Hursthouse, R. Vefghi, P. A. Schofield, C. White, *J. Organomet.* **1985**, *286*, 343–360.

[77] H. Aneetha, M. Jiménez-Tenorio, M. C. Puerta, P. Valerga, V. N. Sapunov, R. Schmid, K. Kirchner, K. Mereiter, *Organometallics* **2002**, *21*, 5334–5346.

[78] H. Aneetha, M. Jiménez-Tenorio, M. C. Puerta, P. Valerga, K. Mereiter, *Organometallics*

2003, *22*, 1779–1782.

[79] M. Schlaf, A. J. Lough, R. H. Morris, *Organometallics* **1997**, *16*, 1253–1259.

[80] A. A. Dembek, P. J. Fagan, *Organometallics* **1995**, *14*, 3741–3745.

[81] H. Aneetha, M. Jiménez-Tenorio, M. C. Puerta, P. Valerga, K. Mereiter, *Organometallics* **2002**, *21*, 628–635.

[82] T.-Y. Cheng, D. J. Szalda, R. Morris Bullock, *Chem. Commun.* **1999**, 1629–1630.

[83] D. D. Pathak, H. Adams, N. A. Bailey, P. J. King, C. White, *Journal of Organometallic Chemistry* **1994**, *479*, 237–245.

[84] N. Feiken, P. S. Pregosin, G. Trabesinger, M. Scalone, *Organometallics* **1997**, *16*, 537–543.

[85] Y. Ohki, H. Sadohara, Y. Takikawa, K. Tatsumi, *Angew. Chem.* **2004**, *116*, 2340–2343.

[86] Y. Ohki, Y. Takikawa, H. Sadohara, C. Kesenheimer, B. Engendahl, E. Kapatina, K. Tatsumi, *Chem. Asian J.* **2008**, *3*, 1625–1635.

[87] M. Ito, M. Hirakawa, A. Osaku, T. Ikariya, *Organometallics* **2003**, *22*, 4190–4192.

[88] M. Ito, A. Sakaguchi, C. Kobayashi, T. Ikariya, *J. Am. Chem. Soc.* **2007**, *129*, 290–291.

[89] C. M. Kelly, A. J. Ruddy, C. A. Wheaton, O. L. Sydora, B. L. Small, M. Stradiotto, L. Turculet, *Can. J. Chem.* **2014**, *92*, 194–200.

[90] J. Bhattacharjee, D. Bockfeld, M. Tamm, *J. Org. Chem.* **2022**, *87*, 1098–1109.

[91] M. W. Drover, H. C. Johnson, L. L. Schafer, J. A. Love, A. S. Weller, *Organometallics* **2015**, *34*, 3849–3856.

[92] W. Cheung, W. Chiu, I. D. Williams, W. Leung, *Eur. J. Inorg. Chem.* **2009**, *2009*, 792–798.

[93] J. Barker, M. Kilner, *Coord. Chem. Rev.* **1994**, *133*, 219–300.

[94] H. Nagashima, H. Kondo, T. Hayashida, Y. Yamaguchi, M. Gondo, S. Masuda, K. Miyazaki, K. Matsubara, K. Kirchner, *Coord. Chem. Rev.* **2003**, *245*, 177–190.

[95] A. Lane, C. Barnes, M. Vollmer, J. Walensky, *Inorganics* **2014**, *2*, 540–551.

[96] Y. Yamaguchi, H. Nagashima, *Organometallics* **2000**, *19*, 725–727.

[97] C. Gemel, J. C. Huffman, K. G. Caulton, K. Mauthner, K. Kirchner, *J. Organomet. Chem.* **2000**, *593–594*, 342–353.

[98] U. Kölle, J. Kossakowski, G. Raabe, *Angew. Chem. Int. Ed. Engl.* **1990**, *29*, 773–774.

[99] U. Kölle, G. Raabe, *Angew. Chem. Int. Ed. Engl.* **1993**, *32*, 1294–1294.

[100] A. W. Holland, D. S. Glueck, R. G. Bergman, *Organometallics* **2001**, *20*, 2250–2261.

[101] L. Bourget-Merle, M. F. Lappert, J. R. Severn, *Chem. Rev.* **2002**, *102*, 3031–3066.

[102] H. Huang, R. P. Hughes, A. L. Rheingold, *Polyhedron* **2008**, *27*, 734–738.

[103] A. D. Phillips, K. Thommes, R. Scopelliti, C. Gandolfi, M. Albrecht, K. Severin, D. F. Schreiber, P. J. Dyson, *Organometallics* **2011**, *30*, 6119–6132.

[104] J.-T. Ahlemann, A. Künzel, H. W. Roesky, M. Noltemeyer, L. Markovskii, H.-G. Schmidt, *Inorg. Chem.* **1996**, *35*, 6644–6645.

[105] A. D. Phillips, G. Laurenczy, R. Scopelliti, P. J. Dyson, *Organometallics* **2007**, *26*, 1120–1122.

[106] H. Tom Dieck, W. Kollvitz, I. Kleinwaechter, *Organometallics* **1986**, *5*, 1449–1457.

[107] M. Tamm, D. Petrovic, S. Randoll, S. Beer, T. Bannenberg, P. G. Jones, J. Grunenberg,

Org. Biomol. Chem. **2007**, *5*, 523.

[108] D. Petrovic, T. Glöge, T. Bannenberg, C. G. Hrib, S. Randoll, P. G. Jones, M. Tamm, *Eur. J. Inorg. Chem.* **2007**, *2007*, 3472–3475.

[109] T. Glöge, D. Petrovic, C. Hrib, P. G. Jones, M. Tamm, *Eur. J. Inorg. Chem.* **2009**, *2009*, 4538–4546.

[110] T. Glöge, K. Jess, T. Bannenberg, P. G. Jones, N. Langenscheidt-Dabringhausen, A. Salzer, M. Tamm, *Dalton Trans.* **2015**, *44*, 11717–11724.

[111] R. Noyori, S. Hashiguchi, *Acc. Chem. Res.* **1997**, *30*, 97–102.

[112] K. Haack, S. Hashiguchi, A. Fujii, T. Ikariya, R. Noyori, *Angew. Chem. Int. Ed. Engl.* **1997**, *36*, 285–288.

[113] K. Mashima, T. Abe, K. Tani, *Chem. Let.* **1998**, *27*, 1201–1202.

[114] C.-K. Paek, J.-J. Ko, J.-K. Uhm, *Bull. Korean Chem. Soc.* **1994**, *15*, 980–984.

[115] P. Espinet, P. M. Bailey, P. M. Maitlis, *J. Chem. Soc., Dalton Trans.* **1979**, 1542.

[116] A. J. Blacker, E. Clot, S. B. Duckett, O. Eisenstein, J. Grace, A. Nova, R. N. Perutz, D. J. Taylor, A. C. Whitwood, *Chem. Commun.* **2009**, 6801.

[117] X. Hu, L. Guo, M. Liu, M. Sun, Q. Zhang, H. Peng, F. Zhang, Z. Liu, *Inorg. Chem.* **2022**, *61*, 10051–10065.

[118] A. Zamorano, N. Rendón, J. López-Serrano, J. E. V. Valpuesta, E. Álvarez, E. Carmona, *Chem. Eur. J.* **2015**, *21*, 2576–2587.

[119] J. Huang, H.-J. Schanz, E. D. Stevens, S. P. Nolan, *Organometallics* **1999**, *18*, 2370–2375.

[120] A. Chaumonnot, B. Donnadieu, S. Sabo-Etienne, B. Chaudret, C. Buron, G. Bertrand, P. Metivier, *Organometallics* **2001**, *20*, 5614–5618.

[121] M. N. Peñas-Defrutos, C. Bartolomé, M. García-Melchor, P. Espinet, *Chem. Commun.* **2018**, *54*, 984–987.

[122] U. Koelle, J. Kossakowski, *J. Chem. Soc., Chem. Commun.* **1988**, 549.

[123] K. Bücken, U. Koelle, R. Pasch, B. Ganter, *Organometallics* **1996**, *15*, 3095–3098.

[124] R. E. Blake, R. H. Heyn, T. D. Tilley, *Polyhedron* **1992**, *11*, 709–710.

[125] M. Jiménez-Tenorio, M. C. Puerta, P. Valerga, *Eur. J. Inorg. Chem.* **2004**, *2004*, 17–32.

[126] P. Hofmann, *Angew. Chem. Int. Ed. Engl.* **1977**, *16*, 536–537.

[127] J. F. Riehl, Y. Jean, O. Eisenstein, M. Pelissier, *Organometallics* **1992**, *11*, 729–737.

[128] The Cp ring binds to the metal in a η^5-binding mode. The three bonds in the structures **A** and **B** are a representation of the three facial sites occupied by the Cp ring.

[129] J. R. Babcock, C. Incarvito, A. L. Rheingold, J. C. Fettinger, L. R. Sita, *Organometallics* **1999**, *18*, 5729–5732.

[130] P. Braunstein, F. Naud, *Angew. Chem. Int. Ed.* **2001**, *40*, 680–699.

[131] J. M. Blacquiere, *ACS Catal.* **2021**, *11*, 5416–5437.

[132] M. A. Rankin, G. Schatte, R. McDonald, M. Stradiotto, *Organometallics* **2008**, *27*, 6286–6299.

[133] N. Merle, G. Koicok-Köhn, M. F. Mahon, C. G. Frost, G. D. Ruggerio, A. S. Weller, M. C. Willis, *Dalton Trans.* **2004**, 3883–3892.

[134] M. Jiménez-Tenorio, M. C. Puerta, P. Valerga, *Eur. J. Inorg. Chem.* **2005**, *2005*, 2631–2640.

[135] C. Bibal, Y. D. Smurnyy, M. Pink, K. G. Caulton, *J. Am. Chem. Soc.* **2005**, *127*, 8944–8945.

[136] W. A. Herrmann, C. Köcher, *Angew. Chem. Int. Ed. Engl.* **1997**, *36*, 2162–2187.

[137] N. M. Scott, R. Dorta, E. D. Stevens, A. Correa, L. Cavallo, S. P. Nolan, *J. Am. Chem. Soc.* **2005**, *127*, 3516–3526.

[138] L. Cavallo, A. Correa, C. Costabile, H. Jacobsen, *J. Organomet. Chem.* **2005**, *690*, 5407–5413.

[139] J. A. M. Lummiss, C. S. Higman, D. L. Fyson, R. McDonald, D. E. Fogg, *Chem. Sci.* **2015**, *6*, 6739–6746.

[140] H. Jacobsen, A. Correa, C. Costabile, L. Cavallo, *J. Organomet. Chem.* **2006**, *691*, 4350–4358.

[141] N. M. Scott, S. P. Nolan, *Eur. J. Inorg. Chem.* **2005**, *2005*, 1815–1828.

[142] W. Baratta, W. A. Herrmann, P. Rigo, J. Schwarz, *J. Organomet. Chem.* **2000**, *593–594*, 489–493.

[143] H. Bruns, M. Patil, J. Carreras, A. Vázquez, W. Thiel, R. Goddard, M. Alcarazo, *Angew. Chem. Int. Ed.* **2010**, *49*, 3680–3683.

[144] D. Petrovic, C. G. Hrib, S. Randoll, P. G. Jones, M. Tamm, *Organometallics* **2008**, *27*, 778–783.

[145] Roger. Adams, J. B. Campbell, *J. Am. Chem. Soc.* **1949**, *71*, 3539–3540.

[146] A. E. Tschitschibabin, R. A. Konowalowa, A. A. Konowalowa, *Ber. dtsch. Chem. Ges. A/B* **1921**, *54*, 814–822.

[147] M. E. Doster, S. A. Johnson, *Angew. Chem. Int. Ed.* **2009**, *48*, 2185–2187.

[148] Q. Shi, R. J. Thatcher, J. Slattery, P. S. Sauari, A. C. Whitwood, P. C. McGowan, R. E. Douthwaite, *Chem. Eur. J.* **2009**, *15*, 11346–11360.

[149] P. D. W. Boyd, L. J. Wright, M. N. Zafar, *Inorg. Chem.* **2011**, *50*, 10522–10524.

[150] M. Navarro, M. Li, S. Bernhard, M. Albrecht, *Dalton Trans.* **2018**, *47*, 659–662.

[151] A. J. Bukvic, V. Kesselring, M. Aeschlimann, M. Albrecht, *Inorg. Chem.* **2023**, *62*, 2905–2912.

[152] A. J. Bukvic, M. Albrecht, *Inorg. Chem.* **2022**, *61*, 14038–14045.

[153] N. Lentz, M. Albrecht, *ACS Catal.* **2022**, *12*, 12627–12631.

[154] N. Lentz, S. Reuge, A. Beaufils, M. Albrecht, *Organometallics* **2024**, *43*, 1536–1546.

[155] R. Evans, Z. Deng, A. K. Rogerson, A. S. McLachlan, J. J. Richards, M. Nilsson, G. A. Morris, *Angew. Chem.* **2013**, *125*, 3281–3284.

[156] M. Navarro, C. Segarra, T. Pfister, M. Albrecht, *Organometallics* **2020**, *39*, 2383–2391.

[157] P. Melle, Y. Manoharan, M. Albrecht, *Inorg. Chem.* **2018**, *57*, 11761–11774.

[158] P. Melle, M. Albrecht, *Chimia* **2019**, *73*, 299–303.

[159] P. Melle, J. Thiede, D. A. Hey, M. Albrecht, *Chem. Eur. J.* **2020**, *26*, 13226–13234.

[160] K. F. Donnelly, C. Segarra, L.-X. Shao, R. Suen, H. Müller-Bunz, M. Albrecht, *Organometallics* **2015**, *34*, 4076–4084.

Chapter II

Air-Stable Coordinatively Unsaturated Ruthenium(II) Complex for Ligand Binding and Catalytic Transfer Hydrogenation of Ketones from Ethanol

This chapter has been published and is reproduced from:

A. Beaufils, P. Melle, N. Lentz, M. Albrecht

Inorg.Chem. **2024**, *63*, 2072–2081

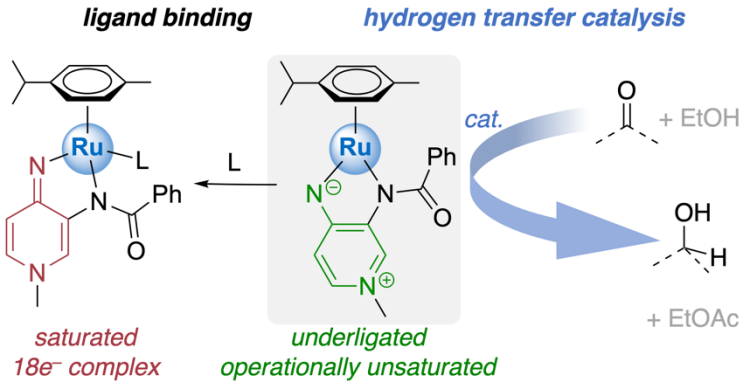

Link of the article: https://doi.org/10.1021/acs.inorgchem.3c03859

II.I. Abstract

Coordinatively unsaturated complexes are interesting from a fundamental level for their formally empty coordination site and, in particular, from a catalytic perspective as they provide opportunities for substrate binding and transformation. Here, we describe the synthesis of a novel underligated ruthenium complex [Ru(cym)(*N,N′*)]$^+$, **3**, featuring an amide-functionalized pyridylideneamide (PYA) as the *N,N′*-bidentate coordinating ligand. In contrast to previously investigated underligated complexes, complex **3** offers the potential for dynamic modifications, thanks to the flexible donor properties of the PYA ligand. Specifically, they allow both for stabilizing the formally underligated metal center in complex **3** through nitrogen π-donation and for facilitating through π-acidic bonding properties the coordination of a further ligand L to the ruthenium center to yield the formal 18e$^-$ complexes [Ru(cym)(*N,N′*)(L)]$^+$ (**4**: L = $P(OMe)_3$; **5**: L = PPh_3; **6**: L = N-methylimidazole; **7**: L = pyridine) and neutral complex [RuCl(cym)(*N,N′*)] **8**. Analysis by ^{1}H NMR and UV–vis spectroscopies reveals an increasing Ru–L bond strength along the sequence pyridine < 1-methylimidazole < PPh_3 < $P(OMe)_3$ with binding constants varying over 3 orders of magnitude with log(K_{eq}) values between 2.8 and 5.7. The flexibility of the Ru(PYA) unit and the ensuing accessibility of saturated and unsaturated species with one and the same ligand are attractive from a fundamental point of view and also for catalytic applications, as catalytic transformations rely on the availability of transiently vacant coordination sites. Thus, while complex **3** does not form stable adducts with O-donors such as ketones or alcohols, it transiently binds these species, as evidenced by the considerable catalytic activity in the transfer hydrogenation of ketones. Notably, and as one of only a few catalysts, complex **3** is compatible with EtOH as a hydrogen source. Complex **3** shows excellent performance in the transfer hydrogenation of pyridyl-containing substrates, in agreement with the poor coordination strength of this functional group to the ruthenium center in **3**.

II.2. Introduction

Coordinatively unsaturated complexes are considered as entry points for catalytic cycles, as they feature a vacant site available for substrate coordination and transformation. Such underligated species are usually obtained *in situ* either from dimer cleavage, as exemplified with Shvo' catalyst,[1] *via* halide abstraction,[2,3] through the release of a weekly coordinating ligand, often a solvent molecule,[4] or by steric congestion imparted by a bulky ligand.[5] In some cases, the underligated complex is sufficiently stable and can be used directly for catalytic transformations.[6–8] For example, several ruthenium arene complexes have been isolated and characterized that feature a two-legged rather than the typically observed three-legged piano-stool geometry.[9] These underligated complexes were described as "low-coordinate" or as "operationally unsaturated"[9–12] to emphasize the availability, in principle, of a further coordination site. A bonding analysis indicated that many of these operationally unsaturated ruthenium complexes feature either an L/X or L/L' ligand set in which one of the two ligands acts as a π-donor and may thus formally be considered as a 4e-donor, which then imparts coordinative saturation, *i.e.* 18 outer shell electrons at the ruthenium center.

A useful system that can modulate between π-donor and π-acidic interactions with the metal center is the so-called pyridylidene amide (PYA) ligand,[13,14] since these ligands feature a continuum between two limiting resonance structures **A** and **B** (Scheme II.1).[15] The π-basic zwitterionic limiting resonance structure **A** demonstrates the potential of PYA ligands to act as 4e-donor to stabilize an operationally unsaturated, underligated metal center, while the π-acidic quinoidal limiting resonance form **B** provides a 2e-ligation that may be more relevant upon substrate coordination. The electronic flexibility of PYA ligands to modulate their donor properties in response to the electronic situation at the metal center therefore offers great potential for catalytic application in accessing both the operationally unsaturated catalytically active species and the substrate-coordinated intermediate.

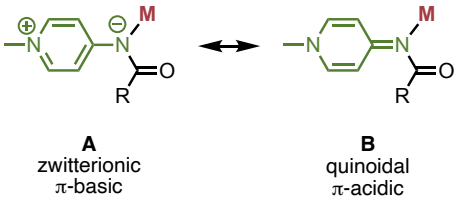

A
zwitterionic
π-basic

B
quinoidal
π-acidic

Scheme II.1. Limiting resonance structures **A** and **B** of *para*-PYA ligands.

We recently demonstrated the benefits of this concept with an underligated iridium Cp* complex containing a donor-flexible pyridylidene amine (PYE) ligand, which displays remarkable activity and longevity in formic acid dehydrogenation catalysis.[16] Here, we extended this concept to ruthenium(II) cymene complexes. Specifically, we report on the synthesis and the stability of an *N,N'*-bidentate underligated PYA ruthenium complex, its ability to coordinate exogenous ligands, and the exploitation of this reactivity to devise a catalytic transfer hydrogenation process using EtOH as an appealing hydrogen donor.

II.3. Results and discussion

Preparation and characterization of ruthenium complex 3. Ligand synthesis involved selective N-Boc protection of 3,4-diaminopyridine to form *tert*-butyl(3-aminopyridin-4-yl)carbamate according to published procedure (Scheme II.2).[17] Subsequent reaction with benzoyl chloride under basic conditions yielded compound **1**, which featured in ^{1}H NMR spectroscopy two broad singlets at δ_H = 8.81 and 8.86 ppm for the two distinct amide protons. Addition of an excess of MeOTf to **1** resulted in the selective methylation of the pyridine nitrogen and concomitant Boc-deprotection of the 4-amino site to form pyridinium triflate **2a**. Its formation was confirmed by the loss of the *t*-Bu proton resonances at 1.48 ppm and the appearance of a NH_2 proton resonance as a broad singlet at δ_H = 6.59 ppm. Quantitative anion substitution of OTf^- by PF_6^- was achieved by reacting the triflate salt with an excess of NH_4PF_6 in a H_2O/CH_3CN mixture. The ^{1}H NMR spectra of **2a** and **2b** were essentially identical, and successful anion metathesis was confirmed by ^{19}F NMR spectroscopy and elemental analysis. Ruthenation of salt **2b** was accomplished in the presence of the ruthenium precursor $[RuCl_2(cym)]_2$ (cym = *p*-cymene) and NaOAc in CH_2Cl_2 under reflux conditions to afford complex **3** as an air- and moisture-stable red solid in 66% yield. Ligand coordination was confirmed by the disappearance of the NH_2 and NH singlets, together with the appearance of a strongly deshielded NH singlet at δ_H = 9.98, integrating for one proton only. Coordination was further supported by the two distinct doublets for the aromatic C_{cym}–H resonances at 5.28 and 5.08 ppm. No signal for any coordinated solvent was detected, even when changing from coordinating solvents such as MeCN or DMSO to non-coordinating CD_2Cl_2.

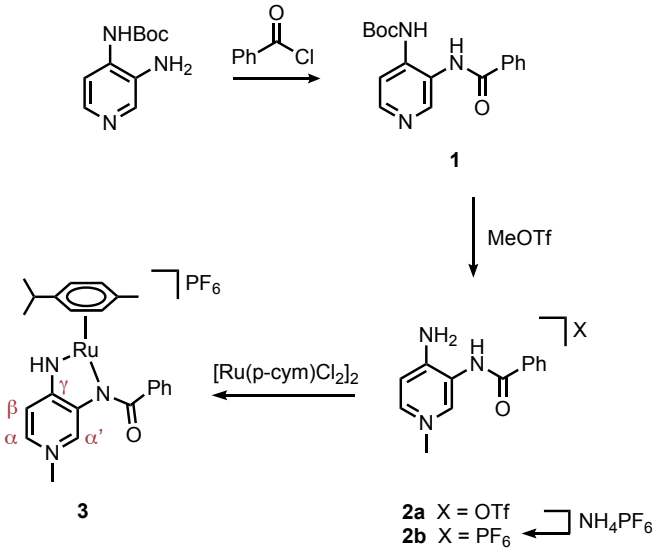

Scheme II.2. Synthesis of ligand precursor **2b** and ruthenium complex **3**.

Suitable crystals for X-ray diffraction analysis were obtained from a CH_2Cl_2/Et_2O mixture. The structure of complex **3** reveals an unusual two-legged piano-stool geometry in the solid state (Figure II.1 and Table II.2). The Ru–N2–C=O unit features a large dihedral angle of 45.9°, indicative of only limited π electron delocalization within the amide N–C=O functionality. This bonding mode is further supported by comparison of the bond length alteration within the amide group, with short Ru–N2

(2.043(2) Å) and C=O (1.216(3) Å) bonds and an elongated N2–C7 (1.398(3) Å) bond. These observations are similar to previously reported pincer PYA ruthenium complexes, depicting a predominantly anionic and π-basic amide nitrogen (form **A**, Scheme II.1).[18] The bond length alteration within the pyridylidene system was used as a tool for probing the electronic flexibility of the PYA ligand system. The shorter bond distances for C_α–C_β compared to C_β–C_γ (1.371(4) Å vs 1.415(3) Å, see Scheme II.2 for labelling) are indicative of a more pronounced neutral quinoidal structure (resonance structure **B**, Scheme II.1). This presence of structural elements of both resonance forms **A** and **B** demonstrates the flexibility of the ligand and the continuum that is often present between these forms, as opposed to the limiting extremes. Related underligated half-sandwich ruthenium complexes bearing L,L' or L,X–type ligands have been reported previously and were termed "operationally unsaturated".[9–12] The plane characterized by L–Ru–(X/L') is usually perpendicular to the Cp- or benzene-derived arene ligand. The underligation or unsaturation is typically enabled by a combination of π-donation of the L'/X-ligand and steric hindrance from the ligands. In complex **3**, the essentially sp^2-hybridized N1 amine may induce such π-stabilization, while the perpendicular orientation of the benzoyl unit imposes some steric congestion.

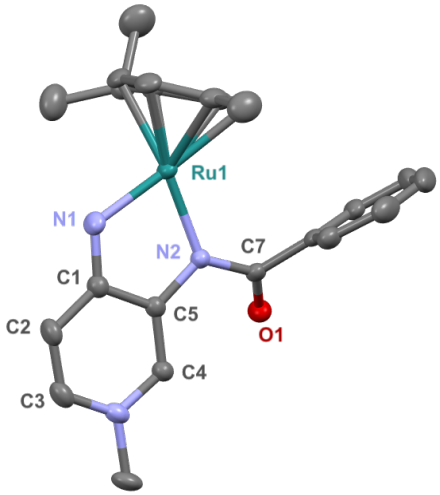

Figure II.1. Molecular structure of ruthenium complex **3** from X-ray diffraction (50% probability ellipsoids; hydrogen atoms and non-coordinating PF_6^- anion omitted for clarity).

Reaction of complex 3 with two-electron donor ligands. Understanding the coordination chemistry of operationally unsaturated complex **3** is crucial for exploiting the potentially available coordination site for catalysis. Therefore, complex **3** was exposed to a series of ligands to produce a formal 18 valence electron species, including pyridine (pyr) and *N*-methylimidazole (NMI) as N-donors, the P-donors PPh_3 and $P(OMe)_3$, as well as O-donors (ketone, alcohols) and CO and ethylene as C-donor ligands. While the N- and P-donors were binding to the ruthenium center of **3** instantaneously and produced complexes **4–7** (Scheme II.3), different amounts of each ligand were necessary to ensure complete binding. In contrast, the presence of CO resulted in rapid degradation of the complex to an unknown arene-free carbonyl complex through *p*-cymene dissociation, although the product was unstable and we were unable to isolate it. No coordination of ethylene was observed

by ^{1}H NMR spectroscopy upon exposure of complex **3** to an ethylene atmosphere. Likewise, addition of an excess of *i*PrOH or acetone did not lead to any detectable coordination, however at a very large excess (>5,000 eq) the red color of complex **3** became more faint, indicative of limited stability.

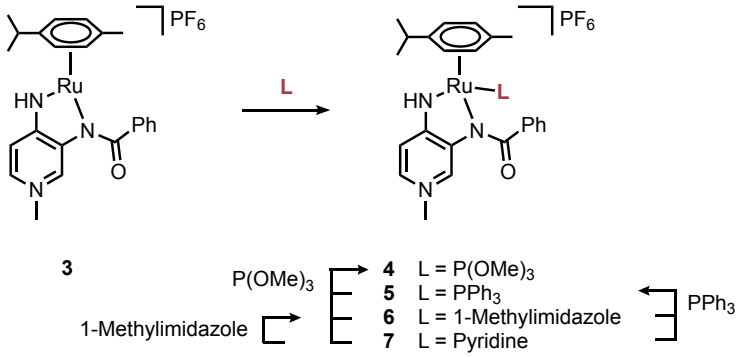

Scheme II.3. Synthesis of complexes **4–7**.

Macroscopically, binding of N- and P-donor ligands was accompanied by a change of color from dark red (complex **3**) to yellow/orange (complexes **4–7**). Microscopically, the bonding results in a hypsochromic shift of the absorption maximum from 409 nm to around 350 nm. Moreover, ^{1}H NMR spectroscopy revealed diagnostic changes in the aromatic region of the PYA unit upon the formation of the three-legged piano-stool complexes **4–7**. While substoichiometric additions of PPh_3, $P(OMe)_3$, or NMI ligands resulted in spectra showing two species, viz, residual **3** as well as the new complexes **4–6**, pyr addition resulted in the formation of a single set of signals that shifts upon changing the amounts of pyridine. Therefore, PPh_3, $P(OMe)_3$ or NMI qualify as strong binding and produce a slow exchange system on the ^{1}H NMR time scale, with the simultaneous observation of both the formal 16- and 18-electron complexes at a given concentration of ligand (Figure II.2.a). In contrast, a fast exchange limit is reached with pyridine, indicative of a rapid interconversion of **3** and **7** and hence the appearance of averaged signals by ^{1}H NMR spectroscopy (Figure II.2.b).

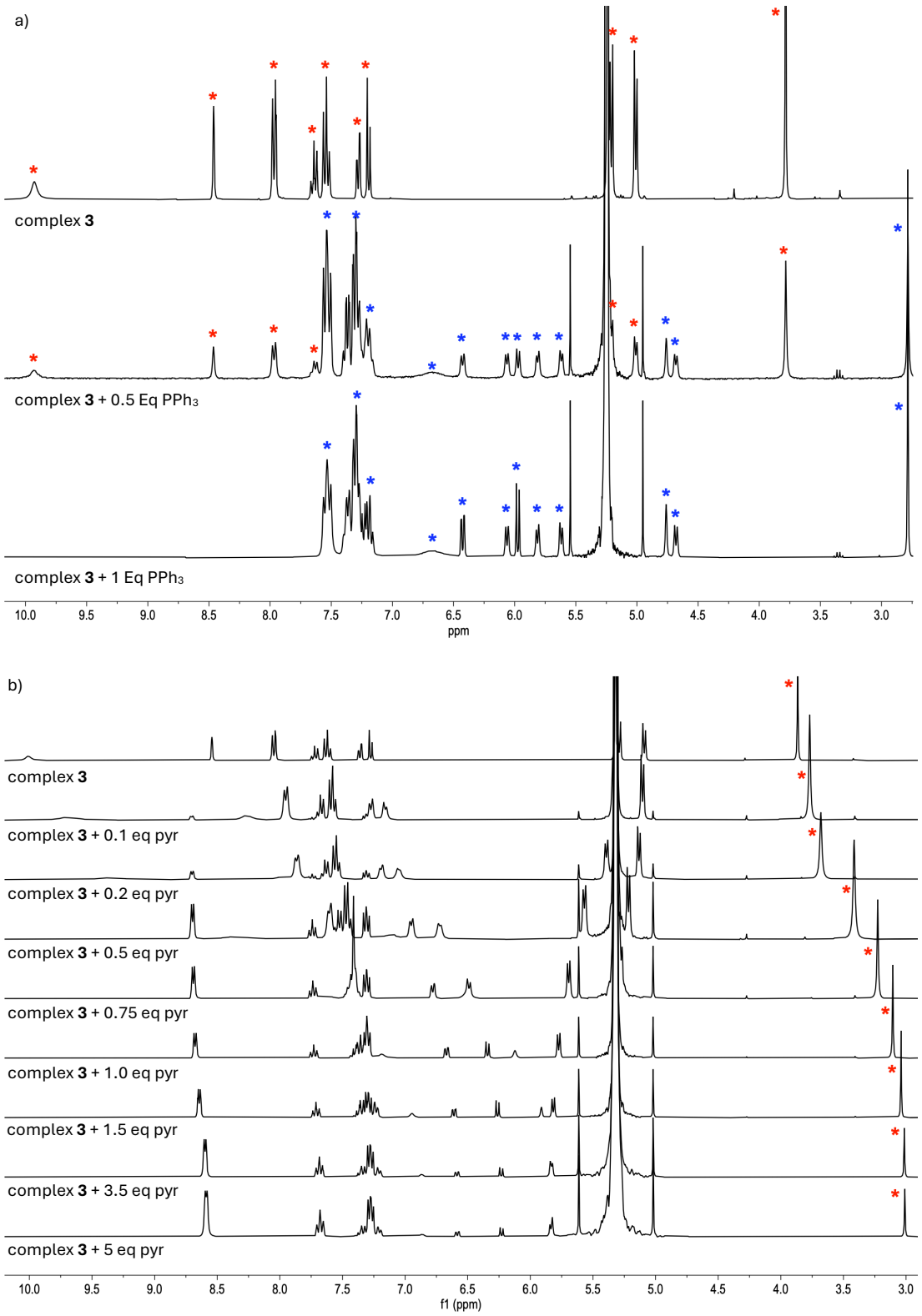

Figure II.2. Stacked solution ^{1}H NMR spectra (CD_2Cl_2, 298K, 300 MHz) of a) complex **3** (red) upon successive addition of PPh_3 forming complex **5** (blue), indicating the presence of two species in the presence of substoichiometric quantities of PPh_3; b) complex **3** upon successive addition of pyridine forming complex **7**, indicative a single average species as exemplified by the N–CH_3 chemical shift (red).

The most diagnostic changes in the NMR spectra pertain to the pyridylidene H_α and H_β protons, which shifted considerably upfield with respect to complex **3** (Table II.1). Moreover, the chemical shift difference between H_α and H_β increased significantly from 0.07 ppm in complex **3** to 0.32 ppm in complex **7** and 0.46 ppm for complexes **4–6**. This larger difference indicates a higher contribution of the neutral quinoidal resonance structure **B** in complexes **7**, and especially **4–6** as compared to the underligated complex **3** (cf. Scheme II.1).[19] Such a change in bonding is in line with less π-donor character of the PYA ligand in the three-legged piano stool geometry as opposed to the two-legged structure in **3**, which features considerable π-bonding through the zwitterionic resonance form.[20] Likewise, the N-CH_3 ^{1}H NMR chemical shift is a useful probe to distinguish quinoidal from zwitterionic PYA resonance structure contributions.[21] Accordingly, the higher field resonance of this group in complexes **4–7** suggests a more pronounced neutral quinoidal PYA structure upon ligand coordination. The shift difference correlates with the donor properties of the added ligand and increases in the sequence pyr (**7**, δ_H = 3.15) < NMI (**6**, δ_H = 3.30) < $P(OMe)_3$ (**4**, δ_H = 3.43). PPh_3 (**5**, δ_H = 2.86) does not follow this trend, presumably because steric factors influence the resonance frequency.

Table II.1. Selected ^{1}H NMR shifts (ppm) of the CH_α, $CH_{\alpha'}$ and CH_β units for complexes **3–7**.

complex	$H_{\alpha'}$	H_α	H_β	$\Delta(H_{\alpha'}–H_\beta)$	$\Delta(H_\alpha–H_\beta)$	N–CH_3
3	8.55	7.35	7.28	1.27	0.07	3.86
4	7.89	6.83	6.37	1.52	0.46	3.43
5	4.84	6.51	6.05	-1.21	0.46	2.86
6	7.25	6.74	6.28	0.97	0.46	3.30
7	6.25	6.72	6.40	-0.15	0.32	3.15

Further evidence for the change in PYA bonding character upon coordination of an exogenous ligand was obtained from X-ray diffraction analysis of phosphine-containing complex **5** and comparison with the data of **3**. The molecular structure of **5** confirmed the three-legged piano-stool geometry of the ruthenium complex (Figure II.3). Phosphine coordination resulted in elongation of both Ru–N bonds by almost 0.1 Å; e.g. the Ru–N1 distance increased from 2.043(2) Å in **3** to 2.126(3) Å in complex **5** (Table II.2). Moreover, the N1–C1 bond is significantly contracted from 1.340(4) in **3** to 1.317(5) Å in **5**, which is indicative of a more pronounced sp^2 character of N1. In line, the C_β–C_γ bonds feature single bond character with 1.421(5) and 1.438(5) Å for C1–C2 and C1–C5 bonds, respectively, while the C_α–C_β bonds are short and suggest localized double bonds (1.338(6) and 1.357(6) Å for C2–C3 and C4–C5 bonds, respectively). Therefore, double bond localization is considerably more pronounced than in complex **3** with average 1.371(10) Å for C_α–C_β bonds and 1.415(6) for the C_β–C_γ bonds.[22] Such heterocyclic double bond localization in complex **5** together with an exocyclic C=N double bond points toward a quinoidal ligand structure and hence neutral ligand properties featuring a π-acidic nitrogen donor site.

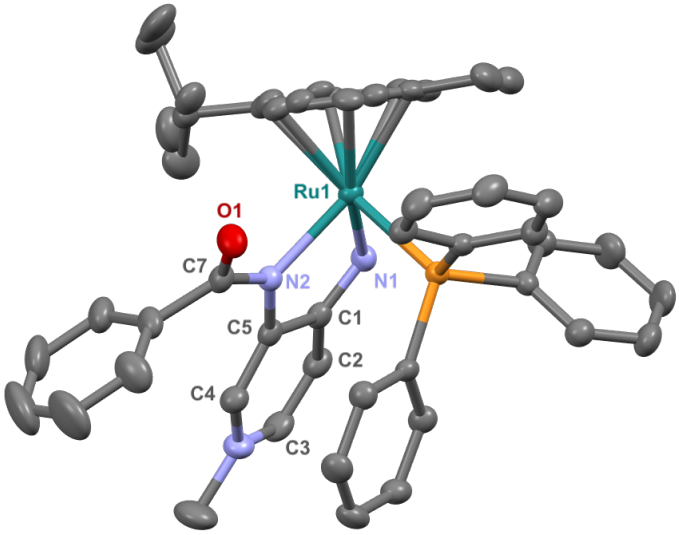

Figure II.3. Molecular structure of ruthenium complex **5** from X-ray diffraction (50% probability ellipsoids; hydrogen atoms and non-coordinating PF_6^- anion omitted for clarity).

Table II.2. Bond lengths and angles in complexes **3** and **5**.

bond (Å) and angle (deg)	compound **3**	compound **5**
Ru1–N1	1.963(2)	2.044(3)
Ru1–N2	2.043(2)	2.126(3)
Ru1–P1	-	2.350(1)
N1–C1	1.340(4)	1.317(5)
Ru1–Cg[a]	1.669	1.722
N2–C7	1.398(3)	1.354(5)
O1–C7	1.216(3)	1.243(5)
N2–C5	1.396(3)	1.421(5)
C_α–C_β[b]	1.371(10)	1.348(12)
C_β–C_γ[c]	1.415(6)	1.430(10)
C1–C2	1.409(3)	1.421(5)
C2–C3	1.361(4)	1.338(6)
C1–C5	1.421(3)	1.438(5)
C4–C5	1.381(4)	1.357(6)
θ(C7O1N2-N1N2Ru1)	39.00	17.02
N1–Ru–N2	78.63(8)	77.26(12)
N1–Ru–P1	-	86.27(10)
N2–Ru–P1	-	87.57(9)

[a]Cg = center of the arene; [b]C_α–C_β is the average bond length of C2–C3 and C4–C5; [c]C_β–C_γ is the average bond length of C1–C2 and C1–C5.

Ligand exchange studies by ^{1}H NMR spectroscopy. To assess the bonding strength of the ligands qualitatively, displacement experiments were performed by exposing complex **3** first to one

equivalent of a given ligand L (L = pyr, NMI, PPh_3 or $P(OMe)_3$) to form complexes **4–7** *in situ*, followed by addition of one equivalent of the competitive ligand L' in CD_2Cl_2 at room temperature. Complex formation was then assessed by ^1H NMR spectroscopy. Thus, addition of one equivalent of $P(OMe)_3$ as ligand L' to *in situ* formed complexes **5–7** resulted in the formation of complex **4** exclusively, accompanied by the release of the previously coordinated ligand L. On the other hand, none of the three ligands pyr, NMI, or PPh_3 was able to displace $P(OMe)_3$ from complex **4.** The reverse reactivity was observed with complex **7**, with immediate replacement of the pyridine ligand by any of the other three ligands to form quantitatively complexes **4–6**. The same experiments were performed with *in situ* formed complexes **5** and **6**. These results indicate increasing bond strength along the sequence pyr < NMI < PPh_3 < $P(OMe)_3$ (Scheme II.3). This sequence suggests that the ligand bonding is governed by a combination of electronic (preference of P- over N-type ligands) as well as steric factors ($P(OMe)_3$ over PPh_3).

UV-Vis spectroscopic determination of binding constant. Quantitative binding constants for the bonding of the different coordinating ligands L (L = pyr, NMI, PPh_3 and $P(OMe)_3$) to complex **3** were determined using UV-Vis spectroscopy through quantitative monitoring of the observed color change from red (λ_{max} at 409 nm) to orange/yellow in complexes **4–7** (λ_{max} in the 340–365 nm range; Table II.3). For these experiments, ligand L was titrated into a 0.05 mM solution of complex **3** in CH_2Cl_2, thus varying the L:**3** ratio from 0.4 to 30 (see Experimental section for details). These titrations resulted in two isosbestic points for each ligand added, characteristic of the presence of two species and a 1:1 binding mode of the ligands L to complex **3** (Figure II.4). For example, upon addition of different amounts of $P(OMe)_3$, two isosbestic points appear at 324 and 381 nm due to the decrease of the absorption at 409 nm and the growth of a new band at 353 nm (Figure II.4.a).

The equilibrium is immediately established between complex **3** and the adduct complex (**4–7**), and the equilibrium constant (K_{eq}) is then represented according to Equations (1) and (2), with M for complex **3**, ML for any of complexes **4–7**, and n equals 1 for the established 1:1 stoichiometry of the reaction.

$$\mathrm{M} + \mathrm{L} \overset{K\mathrm{eq}}{\rightleftarrows} \mathrm{ML} \quad (1)$$

$$K_{\mathrm{eq}} = \frac{[\mathrm{ML}]}{[\mathrm{M}]\,[\mathrm{L}]^{\mathrm{n}}} \quad (2)$$

Table II.3. UV-vis data and equilibrium constants for ligand bonding K_{eq} for all complexes **3–7**.[a]

entry	complex (L)	donor atom	λ_{max} (ε)[b]	K_{eq}[c]	log(K_{eq})
1	**3**	-	409 nm (13×10^3)	-	-
2	**4** ($P(OMe)_3$)	P	353 nm (14×10^3)	4.72 ($\pm$0.07) $\times 10^5$	5.67
3	**5** (PPh_3)	P	365 nm (11×10^3)	1.35 ($\pm$0.14) $\times 10^5$	5.13
4	**6** (NMI)	N	344 nm (12×10^3)	6.54 ($\pm$0.17) $\times 10^4$	4.82
5	**7** (pyr)	N	343 nm (11×10^3)	7.12 ($\pm$0.12) $\times 10^2$	2.85

[a]All measurement in CH_2Cl_2 with [**3**] = 5×10^{-5} M; [b]λ_{max} in nm, ε in $M^{-1}\,cm^{-1}$ assuming 100% conversion of **3** with accuracy $\pm$ 7%; [c]in M^{-1}, determined using Bindfit, see SI for details.

The equilibrium constants K_{eq} were determined using Bindfit[23] (Table II.3) and increase in the order pyr << NMI < PPh_3 < $P(OMe)_3$ (Table II.3). According to these equilibrium constants, PPh_3, $P(OMe)_3$ and NMI are considered as strongly binding ligands with K_{eq} around 1×10^5 M^{-1} or larger. In contrast, pyr is only a weak ligand[24] for complex **3** with less than 50% adduct present at a 1:1 pyr/**3** ratio and $K_{eq} < 10^3$ M^{-1}. These results are in agreement with the qualitative ligand exchange experiments investigated by NMR spectroscopy (*vide supra*).

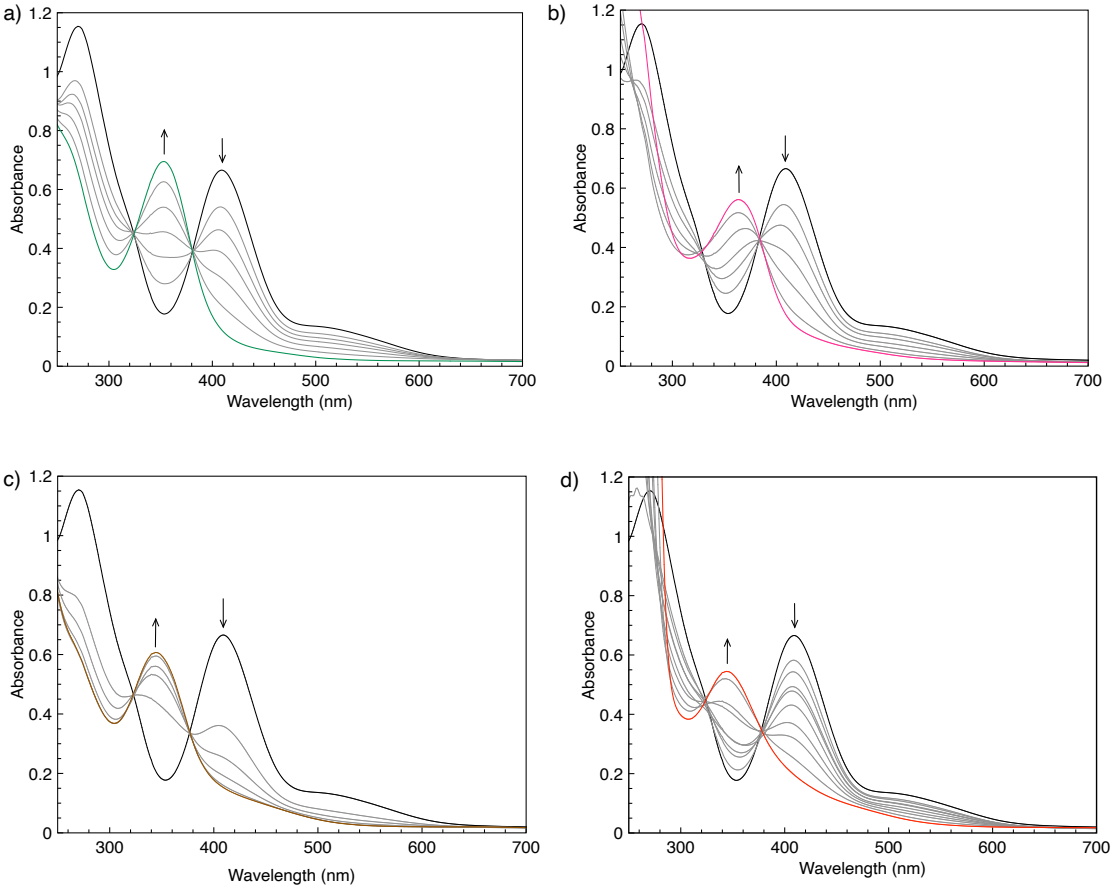

Figure II.4. UV-Vis titration study of the addition of a) $P(OMe)_3$ (0.2 to 4 Eq) to complex **3** (black) to form complex **4** (green); b) PPh_3 (0.2 to 2 Eq) to complex **3** (black) to form complex **5** (pink); c) 1-methylimidazole (1 to 20 Eq) to complex **3** (black) to form complex **6** (brown); d) pyridine (1 to 200 Eq) to complex **3** (black) to form complex **7** (orange).

Reaction of complex 3 with anionic ligand. Reaction of complex **3** with Et_4NCl gave complex **8** after precipitation of Et_4NPF_6 in toluene (Scheme II.4). The formation of **8** was supported by mass spectrometry with a $[M + H]^+$ of 498.0880 corresponding to the coordinated Ru–Cl species (calcd 498.0881) and the disappearance of the PF_6^- signal of **3** by ^{19}F and ^{31}P NMR spectroscopies. In contrast to the effect of neutral two-electron donor ligands, the coordination of chloride induced a deshielding of the pyridylidene H_α protons (δ_H = 9.04 and 8.12 in **8** vs 8.54 and 8.05 for complex **3**) while the H_β proton remained shielded (δ_H = 6.25 vs. δ_H = 7.25 for complex **4**). The larger separation of the H_α and H_β resonances points to a more pronounced quinoidal diene structure in complex **8**, which concurs with the higher electron density at ruthenium due to the bonding of an anionic chloride in complex **8** as compared to the neutral ligand in complexes **4–7**. Chloride bonding is fully reversible,

and complex **3** was readily regenerated upon addition of $NaPF_6$ in acetone. Notably, complex **8** has only limited stability and decomposes upon precipitation, which prevented its analysis by X-ray diffraction or elemental analysis.

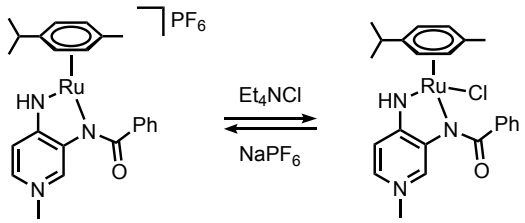

3 **8**

Scheme II.4. Reversible formation of neutral complex **8** via the addition of Et_4NCl.

Application in transfer hydrogenation of ketones. Considering the potential of coordinatively unsaturated ruthenium complex **3** for binding an additional ligand, we sought to exploit this open coordination site for reactivity in hydrogen transfer catalysis. Using acetophenone **9a** as a model substrate and basic *i*PrOH as solvent and hydrogen source, complex **3** (1 mol%) catalyzes the transfer hydrogenation and affords 1-phenethylalcohol **10a** in 99% yield after 4 h (Table II.4, entry 1). Remarkably, transfer hydrogenation also occurs when using EtOH or MeOH instead of *i*PrOH as a hydrogen source, however, yields are lower and reach 66% and 40%, respectively, after 24 h at 80 °C (entries 2-3).

Table II.4. Transfer hydrogenation of acetophenone with **3** using different solvents and hydrogen sources.[a]

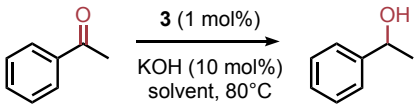

9a **10a**

entry	time (h)	solvent	yield (%)[b]
1	4	iPrOH	99
2	24	MeOH	40
3	24	EtOH	66

[a]General conditions: acetophenone (0.5 mmol), KOH (10 mol%), complex **3** (1 mol%), solvent (2.5 mL); [b]yield determined by ^1H NMR spectroscopy using 1,3,5-trimethoxybenzene as internal standard.

In addition, a small but significant amount of 1-phenylbutanone **11a** was observed using EtOH as hydrogen source, resulting from the α-alkylation of acetophenone (Table II.5, entry 1), which may be due to a transition metal[25–27] or base-only catalyzed reaction.[28–32] Increasing the reaction temperature to 110 °C was deleterious as it reduced the overall conversion and also the selectivity toward the hydrogenation product from about 7:1 to 3:2 (entry 2). Both yield and selectivity increased, however, upon lowering the reaction temperature to 40 °C and afforded the alcohol **10a** in 81% yield (>95% selectivity; entry 3). Replacing KOH as a base with K_2CO_3 further improved the performance at low temperatures (entries 4–7). In particular, at a lower 5 mol% K_2CO_3 loading, hydrogenation proceeded quantitatively and exclusively to product **10a** (entry 6). Changing the base

to Cs_2CO_3 or Na_2CO_3 markedly reduced the reactivity with a maximal yield of less than 75% (entries 8-10). Control experiments indicated that in the absence of either base or complex, no conversion took place (entries 11, 12). The commercial ruthenium complex $[RuCl_2(cym)]_2$ was essentially inactive (entry 13), underpinning the relevance of the PYA ligand for imparting catalytic activity.

Table II.5. Optimization conditions for the transfer hydrogenation of ketones using ethanol source with complex **3**.[a]

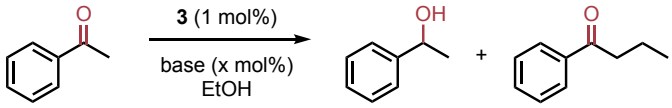

9a **10a** **11a**

entry	base (mol%)	T (°C)	conversion (%)	yield (%)[b]	
				10a	**11a**
1	KOH (10)	80	74	66	9
2	KOH (10)	110	54	32	22
3	KOH (10)	40	85	81	3
4	K_2CO_3 (10)	80	67	61	5
5	K_2CO_3 (10)	40	91	91	<1
6	K_2CO_3 (5)	40	>99	99	<1
7	K_2CO_3 (2)	40	81	80	<1
8	Cs_2CO_3 (10)	80	74	56	17
9	Cs_2CO_3 (10)	40	72	62	8
10[c]	Na_2CO_3 (10)	40	24	24	1
11	–	40	–	<2	<2
12[d]	K_2CO_3 (5)	40	–	<2	<2
13[e]	K_2CO_3 (5)	40	4	<2	<2

[a]General conditions: acetophenone (0.5 mmol), base (mol % as indicated), complex **3** (1 mol %), EtOH (2.5 mL), 24h; [b]yields determined by ^{1}H NMR spectroscopy using 1,3,5-trimethoxybenzene as internal standard; [c]reaction time increased to 48h; [d]without ruthenium source; [e]$[RuCl_2(cym)]_2$ used instead of **3**.

The use of EtOH as hydrogen source complements the more commonly employed isopropanol and formic acid[33–39] and offers major benefits, as it is widely available, environmentally friendly, and a very low-cost hydrogen source. The major reason for the scarce utilization of primary alcohols as hydrogen sources is their unfavorable redox potential. As a consequence, the transfer hydrogenation of acetophenone with *i*PrOH was calculated to be only +4.4 kJ/mol uphill at 40°C, while the equilibrium with EtOH is much more unfavorable (ΔG = +24.4 kJ/mol).[40] In addition, side-products coming aldol condensation often constitute undesired side-products under the basic reaction conditions.[41–44] Nonetheless, Grützmacher and co-workers demonstrated in 2005 the suitability of EtOH in the transfer hydrogenation of ketones and activated olefins with rhodium(I) amide catalysts, even at high substrate/catalyst ratio (S/C = 10,000).[45,46] Even though the use of EtOH as hydrogen source has remained scarce,[47–51] transfer hydrogenation with EtOH has expanded gradually to, for example, asymmetric versions,[52–55] base-free nickel(0)-catalyzed hydrogenation,[47] and to diverse substrates including aldehydes,[40] esters,[56] unactivated alkenes,[57] and the semi-hydrogenation of

alkynes.[58] Moreover, successful transfer hydrogenation with MeOH as hydrogen source was recently reported.[59–67]

Comparison of the different catalysts. Under the optimized conditions developed here, the transfer hydrogenation activity of complex **3** was compared to that of the formal 18e$^-$ complexes **4–7** (Table II.6). The conversion after 24 h provides a good proxy for the overall activity and indicates that the catalytic activity of complexes **4–7** is lower than that of complex **3** (entry 1) and drops along the series **7** > **6** > **5** > **4** (entries 2–5). This trend is inverse to the binding constant for the extraneous ligand and suggests that the availability of a free coordination site at the ruthenium center, ideally directly (complex **3**) or through dissociation of the ligand **L** (complexes **4–7**) is critical for substrate binding and catalytic turnover. Dissociation is obviously easier for ligands with low binding constant such as pyridine in complex **7**, while the tightly bound phosphine and phosphite ligands poison catalytic activity considerably.

Table II.6. Catalytic activity of complexes **3-7** in transfer hydrogenation of acetophenone.[a]

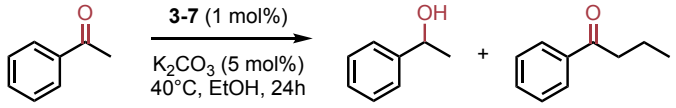

9a **10a** **11a**

entry	catalyst	conversion (%)	yield (%)[b]	
			10a	**11a**
1	**3**	>99	99	1
2	**4**	<2	–	–
3	**5**	38	37	1
4	**6**	60	60	1
5	**7**	88	88	1

[a]General conditions: acetophenone (0.5 mmol), K_2CO_3 (5 mol%), complex **3–7** (1 mol %), ethanol (2.5 mL); [b]yields determined by ^{1}H NMR spectroscopy using 1,3,5-trimethoxybenzene as internal standard.

Catalytic activity of complex 3 in transfer hydrogenation of ketones with ethanol. The transfer hydrogenation catalytic activity of complex **3** was explored with a variety of ketone substrates (Scheme II.5). Modulation of the *para*-substituent in acetophenone revealed excellent conversion in the presence of an electron-withdrawing cyano group and afforded alcohol compound **10b** in 92% yield after just 4 h (cf >90% yield of **10a** required 24 h). However, the nitro analogue **9c** gave only a mediocre yield of 43% after 24 h (66% conversion), and the desired product **10c** was accompanied by unidentified side-products. This poor yield may be associated with partial reduction of the nitro group. Indeed, amino-substituted ketone **9d** largely inhibited catalysis and gave a low 13% yield of **10d** after 24 h. This low transformation is not associated with electronic effects, as the analogous acetophenone containing a similarly electron-donating methoxy substituent is converted to produce alcohol **10e** in 64% yield after 24 h. Complex **3** was also active in the catalytic transfer hydrogenation

of cyclic and acyclic dialkylketones and converted cyclohexanone **9g** to cyclohexanol **10g** in 73% yield (24 h), and similarly 2-hexanone **9h** to the corresponding 2-hexanol **10h**.

Scheme II.5. Catalytic activity of complex **3** in transfer hydrogenation of ketones using ethanol.[a]

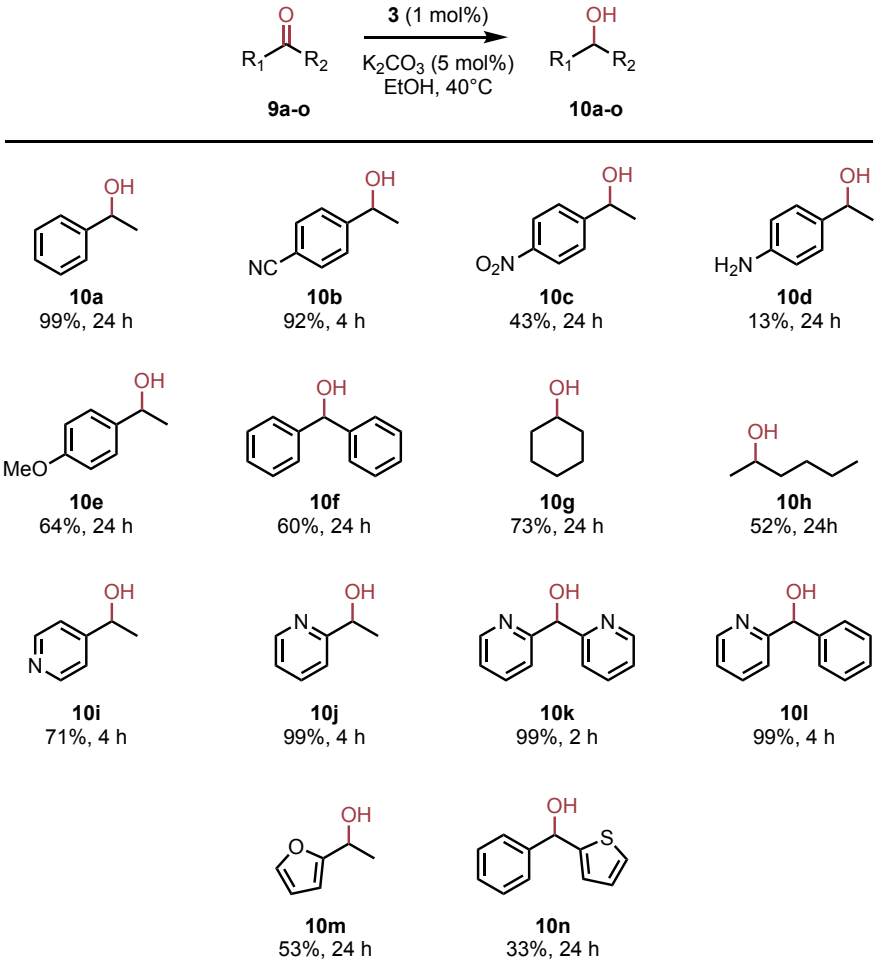

[a]Conditions: substrate (0.5 mmol), K_2CO_3 (5 mol%), complex **3** (1 mol%) in EtOH (2.5 mL). Yields determined by ^{1}H NMR spectroscopy from duplicate runs relative to 1,3,5-trimethoxybenzene as internal standard.

Heteroaromatic ketones are often challenging substrates due to their potentially inhibitive coordination to the metal center.[68] Therefore, they are usually poorly converted to the corresponding alcohol. However, with complex **3**, excellent reactivity toward pyridyl-containing substrates **9i–9l** was observed within 2–4 h.[69] In fact, the introduction of a pyridyl ring is beneficial for catalytic conversion since benzophenone **9f** was converted to diphenylmethanol **10f** in only 60% after 24 h, while the monopyridyl analogue **9l** was fully converted to the alcohol **10l** in 4 h, and incorporation of two pyridyl-rings required even less time (2 h) to quantitatively afford **10k**. These conversion rates are in agreement with the low bond strength of pyridine as evidenced for complex **7** and indicate that the catalytic performance is governed by electronic factors, *i.e.* the electron-withdrawing nature of heterocycles rather than coordinative inhibition, especially for 2-substituted pyridyl substrates. In line, heteroaromatic 2-furyl methyl ketone was converted to the desired alcohol **10m** in 53% yield after 8 h and phenyl(thiophen-2-yl) ketone **9n** was even poorer converted and did not exceed 33%

yield after 24 h. This low activity might also hint at additional catalyst inhibition through thiophene coordination, though addition of 100 equiv of thiophene to complex **3** did not lead to any color change nor ^{1}H NMR chemical shift displacement that would be characteristic for adduct formation. Notably, the addition of thiophene (1 equiv) after 30 min during the catalytic hydrogenation of di(pyridin-2-yl) ketone **9k** reduced the activity of complex **3**. While product **10k** is obtained in 93% yield after 1 h under standard conditions, in the presence of thiophene the yield decreased to 70%, indicating partial catalyst inhibition (Figure II.5). These data indicate that thiophene coordination may be weak yet stronger than that of pyridine and furane.

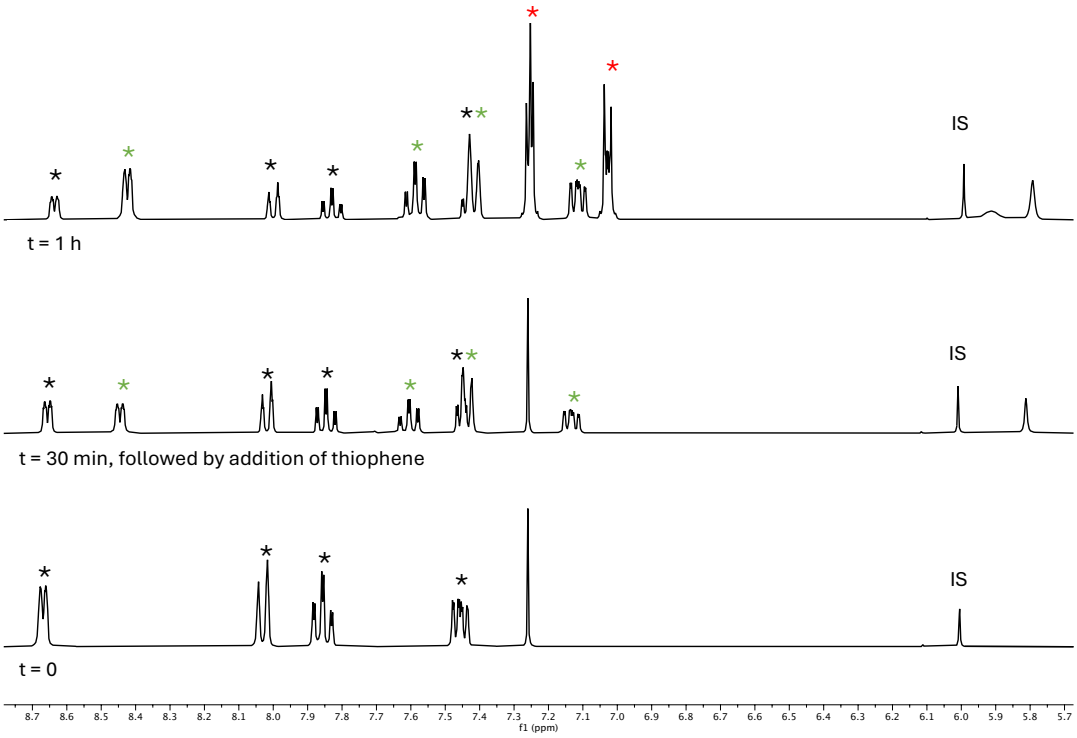

Figure II.5. Stacked solution ^{1}H NMR spectra ($CDCl_3$, 298 K, 300 MHz) of the addition of thiophene (red) to the catalytic hydrogenation of di(pyridin-2-yl)methanone **9k** (black) after 30 min, yielding di(pyridin-2-yl)methanol **10k** (green); IS = internal standard.

While the currently available mechanistic data are not sufficient to propose a detailed catalytic cycle, it should be noted that the ligand in complex **3** contains anionic NH coordination sites that may assist proton transfer.[70] Moreover, the N-heterocycle has been demonstrated to be potentially able to engage in hydride transfer akin to NAD^+.[71] Attempts to intercept a catalytically active species in the transfer hydrogenation catalyzed by complex **3** have failed thus far. Under substoichiometric reaction conditions using EtOH (15 equiv) and NaOEt (5 equiv) in CD_2Cl_2 revealed the formation of a hydride as a minor species, identified by a small resonance at $\delta_H = -5.8$ (Figure II.6). Due to the considerable broadening of all resonances in the 0–10 ppm range, however, it was not possible to correlate this signal with ligand resonances nor to characterize this species in more depth. Similar results were obtained upon changing the base to KOH or KO*t*Bu, or upon reacting complex **3** with 2 eq. superhydride, $NaEt_3BH$. Even though spectroscopic characterization of this hydride and also its role in the catalytic reaction remain inconclusive, we noted that addition of acetophenone as a substrate

to any of these hydride solutions induced hydrogenation. This reactivity may point to an active role of the hydride species in transfer hydrogenation or at least in generating the species active in transfer hydrogenation. Further mechanistic investigations are documented in Chapter III.

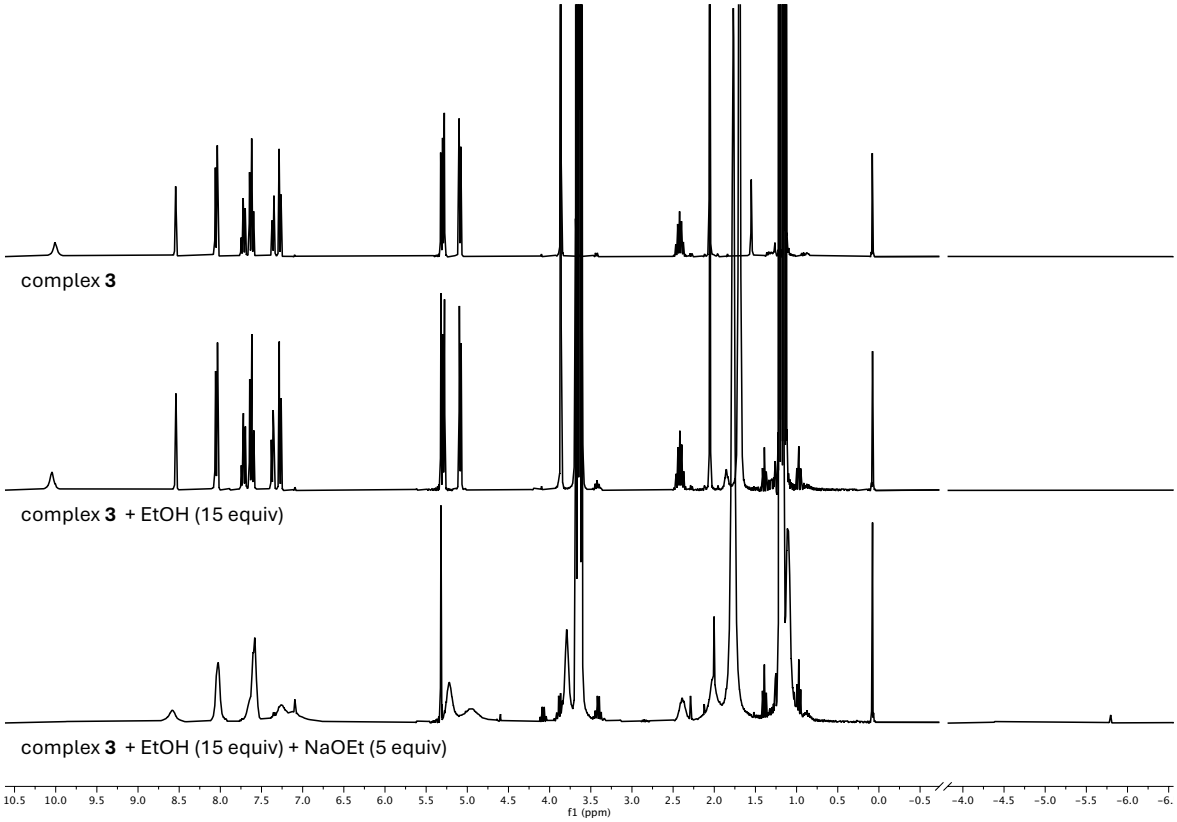

Figure II.6. Stacked solution ^{1}H NMR spectra (CD_2Cl_2, 298K, 300 MHz) of complex **3** (top) after successive addition of EtOH (middle) and NaOEt (bottom).

II.4. Conclusions

We demonstrate here that PYA ligands are well suited to stabilize underligated, operationally unsaturated ruthenium centers. This ability has been attributed to the donor-flexibility of these ligands and their propensity to act as potential $4e^-$ donor site in the zwitterionic π-basic form, while in their π-acidic configuration, they represent a classic $2e^-$ donor systems. Accordingly, the Ru(PYA) complex readily accepts donor ligands to reach coordinative saturation. This ambiguity of the PYA ligand bonding is attractive for catalysis and enabled here the development of an efficient transfer hydrogenation catalyst that allows for EtOH to be used as hydrogen source, which may be enabled by the non-innocent character of the PYA ligand to potentially store protons at its π-basic sites. These bonding principles may also apply to other transition metals and may thus provide a rationale for new catalyst discoveries based on easily accessible ligand scaffolds, especially when considering the straightforward synthesis of pyridinium amides and the flexibility in introducing chelating donor sites.

II.5. Experimental

II.5.1. General. All reactions were performed under air unless stated otherwise. Experiments under inert atmosphere were carried out using standard Schlenk techniques under N_2 atmosphere and dry deoxygenated solvents. Dry solvents were taken from a solvent purification system (SPS), stored over molecular sieves for at least 2 days, and degassed by N_2 gas bubbling for 30 min. All compounds were commercially available and used as received. Nuclear magnetic resonance spectra were recorded on a Bruker Avance Neo spectrometer operating at 300 or 400 MHz for ^{1}H at room temperature unless otherwise noticed. All chemical shifts (d) are quoted in ppm and coupling constants in Hz. Chemical environments have been assigned through COSY, HSQC/HMBC and NOE NMR spectroscopic experiments. Residual protio solvent resonances were used as an internal reference for ^{1}H and ^{13}C{^{1}H} NMR spectra, and externally referenced to $SiMe_4$. ^{31}P{^{1}H} NMR spectra were referenced externally to 85% H_3PO_4 (D_2O). ^{19}F{^{1}H} NMR chemical shifts are externally referenced to $CFCl_3$. The following abbreviations are used: s, singlet; d, doublet; t, triplet; quint, quintet; sept, septet; m, multiplet. Elemental analyses were performed at the DCBP Microanalytic Laboratory using a Thermo Scientific Flash 2000 CHNS-O elemental analyzer. High-resolution mass spectrometry was carried out with a Thermo Scientific LTQ Orbitrap XL (ESI-TOF) by the DCBP mass spectrometry group at the University of Bern. UV-vis spectra were collected on Shimadzu UV 1800 Spectrophotometer, with a silicon photodiode detector ranging from 190 to 1100 nmn. Starna Scientific quartz cuvettes (type 23-N/Q/10) with a path length of 10 mm were used. The spectra were collected at 278K.

II.5.2 Ligand and complex synthesis

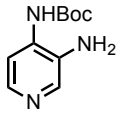

Synthesis of tert-butyl(3-aminopyridin-4-yl)carbamate. The product was synthetized according to a reported procedure.[17] To solution of 3,4-diaminopyridine (1.01 g, 10 mmol, 1 eq) in THF (15 mL) was added di-tert-butyl carbonate (230 µL, 10 mmol, 1 eq) in tetrahydrofuran (5 mL) dropwise, and the mixture was stirred at room temperature for 16 h. After concentration under vacuum, a solution of ethyl acetate/petroleum ether = 1/4 (v/v) was added, and the precipitate formed was collected by filtration. The mother liquor was concentrated, and a solution of ethyl acetate/petroleum ether = 1/4 (v/v) was added which induced the product to precipitate. The combined off-white solids were collected and dried under vacuum (1.70 g, 81%).

^{1}H NMR ($CDCl_3$, 298K, 300 MHz): δ 8.12 (s, 1H, C**H**$_{PYA}$), 8.05 (d, J = 5.4 Hz, 1H, C**H**$_{PYA}$), 7.64 (d, J = 5.4 Hz, 1H, C**H**$_{PYA}$), 7.05 (bs, 1H, N**H**), 3.74 (bs, 2H, N**H**$_2$), 1.51 (s, 9H, C**H**$_{3\text{-}tBu}$).

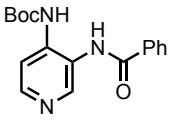

Synthesis of 1. In a round bottom flask, tert-butyl(3-aminopyridin-4-yl)carbamate (500 mg, 2.4 mmol, 1 eq) and triethylamine (370 µL, 2.6 mmol, 1.1 eq) were dissolved in tetrahydrofuran (15 mL) and benzoyl chloride (310 µL, 2.6 mmol, 1.1 eq) was added dropwise under agitation at 0 °C, and then heated at 70 °C for 16 h. The mixture was cooled to room temperature, and all volatiles were removed under reduced pressure. Water (20 mL) was added and the solid was collected by filtration, solubilized in tetrahydrofuran, and dried over Na_2SO_4, filtered and evaporated to dryness to afford 1 as a white solid (673 mg, 90%).

^{1}H NMR (CD_3CN, 298K, 300 MHz): δ 8.80 (bs, 1H, N**H**), 8.48 (s, 1H, C$\mathbf{H}_{PYA}$), 8.35 (d, *J* = 5.6 Hz, 1H, C$\mathbf{H}_{PYA}$), 7.98 (m, 2H, C$\mathbf{H}_{Ph}$), 7.87 (d, *J* = 5.6 Hz, 1H, C$\mathbf{H}_{PYA}$), 7.78 (bs, 1H, N**H**), 7.63 (m, 1H, C$\mathbf{H}_{Ph}$), 7.55 (m, 2H, C$\mathbf{H}_{Ph}$), 1.48 (s, 9H, C$\mathbf{H}_{3\text{-}tBu}$). **^{13}C{^{1}H} NMR ($CD_3CN$, 298 K, 75 MHz):** δ 167.94 (**C**$_{C=O}$), 149.11 (**C**H$_{PYA}$), 148.83 (**C**H$_{PYA}$), 141.99 (**C**$_{Ar}$), 134.66 (**C**$_{Ar}$), 133.23 (**C**H$_{Ph}$), 129.65 (**C**H$_{Ph}$), 128.71 (**C**H$_{Ph}$), 124.51 (**C**$_{Ar}$), 115.57 (**C**H$_{PYA}$), 82.07 (**C**$_{C=O}$), 28.36 (**C**H$_{3\text{-}tBu}$). **ESI-MS (CH_3CN, calc. for [M]$^+$):** 314.1505 (314.1500). **Elemental Analysis (calc. for $C_{17}H_{19}N_3O_3$):** C 65.32 (65.16), H 6.16 (6.11), N 13.22 (13.41).

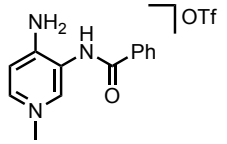

Synthesis of 2a. Under an N_2 atmosphere, compound **1** (1.78 g, 5.7 mmol, 1 eq) and MeOTf (3.2 mL, 28 mmol, 5 eq) were dissolved in dry CH_2Cl_2 (100 mL), and heated at 42 °C in a closed system or at reflux in open vessel for 16 h. After cooling to room temperature, Et_2O (50 mL) was added and the precipitate was collected by filtration and dried thoroughly to yield **2a** as a white solid (1.67 g, 78 %).

^{1}H NMR (CD_3CN, 298K, 300 MHz): δ 8.59 (bs, 1H, N**H**), 8.19 (d, *J* = 1.8 Hz, 1H, C$\mathbf{H}_{PYA}$), 8.01–7.97 (m, 2H, C$\mathbf{H}_{Ph}$), 7.87 (dd, *J* = 7.2, 1.8 Hz, 1H, C$\mathbf{H}_{PYA}$), 7.68–7.62 (m, C$\mathbf{H}_{Ph}$), 7.59-7.53 (m, 2H, C$\mathbf{H}_{Ph}$), 7.01 (d, *J* = 7.2 Hz, 1H, C$\mathbf{H}_{PYA}$), 6.64 (bs, 2H, N**H**), 3.92 (s, 3H, NC$\mathbf{H}_3$). **^{13}C{^{1}H} NMR (CD_3CN, 298 K, 75 MHz):** δ 167.61 (**C**$_{C=O}$), 156.13 (**C**$_{PYA}$), 143.01 (**C**H$_{PYA}$), 142.87 (**C**H$_{PYA}$), 134.12 (**C**$_{Ph}$), 133.51 (**C**H$_{Ph}$), 129.70 (**C**H$_{Ph}$), 128.87 (**C**H$_{Ph}$), 121.12 (**C**$_{PYA}$), 111.36 (**C**H$_{PYA}$), 46.19 (N**C**H$_3$). **^{19}F{^{1}H} NMR** (**CD_3CN, 298 K, 282 MHz**): δ -79.34 (s). **ESI-MS (MeCN, calc. for [M–OTf]$^+$):** 228.1137 (228.1131).

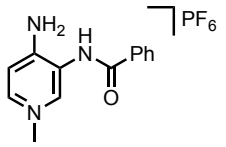

Synthesis of 2b. To a suspension of **2** (290 mg, 0.77 mmol, 1 eq) in MeCN (5 mL) was added a solution of NH_4PF_6 (630 mg, 3.85 mmol, 5 eq) in H_2O (10 mL). The addition of NH_4PF_6 resulted in a clear solution which was stirred for 5 minutes. Then, MeCN was removed in vacuo and the reaction mixture was stored at 4 °C resulting in the formation of an off-white crystalline solid. The solid was filtered and washed with cold water to yield **2b** as a white solid (230 mg, 79%).

^{1}H NMR (CD_3CN, 298K, 300 MHz): δ 8.49 (s, 1H, N**H**), 8.16 (d, *J* = 1.6 Hz, 1H, C$\mathbf{H}_{PYA}$), 7.99–7.95 (m, 2H, C$\mathbf{H}_{Ph}$), 7.86 (dd, *J* = 7.1, 1.6 Hz, C$\mathbf{H}_{PYA}$), 7.69–7.61 (m, 1H, C$\mathbf{H}_{Ph}$), 7.61–7.53 (m, 2H, C$\mathbf{H}_{Ph}$), 6.99 (d, *J* = 7.1 Hz, 1H, C$\mathbf{H}_{PYA}$), 6.59 (s, 2H, N$\mathbf{H}_2$), 3.92 (s, 3H, NC$\mathbf{H}_3$). **^{13}C{^{1}H} NMR (CD_3CN, 298 K, 75 MHz):** δ 167.59 (**C**$_{C=O}$), 156.15 (**C**$_{PYA}$), 143.04 (**C**H$_{PYA}$), 142.93 (**C**H$_{PYA}$), 134.11 (**C**$_{Ph}$), 133.53 (**C**H$_{Ph}$), 129.71 (**C**H$_{Ph}$), 128.83 (**C**H$_{Ph}$), 121.07 (**C**$_{PYA}$), 111.36 (**C**H$_{PYA}$), 46.21 (N**C**H$_3$). **^{19}F{^{1}H} NMR (CD_3CN, 298 K, 282 MHz):** δ -72.96 (d, *J* = 703 Hz, P**F$_6$**). **^{31}P{^{1}H} NMR (CD_3CN, 298 K, 121 MHz):** δ -144.63 (sept, *J* = 703 Hz, **P**F$_6$). **ESI-MS (CH_3CN, calc. for [M–PF_6]$^+$):** 228.1128 (228.1131). **Elemental Analysis (calc. for $C_{13}H_{14}F_6N_3OP$):** C 40.92 (41.83), H 3.66 (3.78), N 11.09 (11.26).

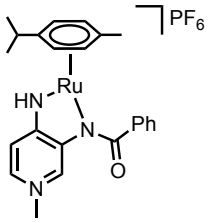

Synthesis of 3. In a round bottom flask, **2b** (500 mg, 1.5 mmol, 1 eq), NaOAc (550 mg, 7.5 mmol, 5 eq) and [Ru(*p*-cym)Cl_2]$_2$ (410 mg, 0.75 mmol, 0.5 eq) were dissolved in CH_2Cl_2 (100 mL). The reaction mixture was refluxed for 18 h, cooled, and filtered through Celite. The filtered solution was washed with saturated $NaHCO_3$ solution (3 x 30 mL). The organic phase was dried over Na_2SO_4, filtered, and evaporated to dryness. The crude product was purified by gradient column chromatography (neutral aluminium oxide, CH_2Cl_2 to CH_2Cl_2/MeOH 99:1) to give **3** as a dark red solid (530 mg, 65%).

^{1}H NMR (CD_2Cl_2, 298K, 300 MHz): δ 9.98 (s, 1H, N**H**), 8.55 (s, 1H, C$\mathbf{H}_{PYA}$), 8.07–8.02 (m, 2H, C$\mathbf{H}_{Ph}$), 7.76–7.68 (m, 1H, C$\mathbf{H}_{Ph}$), 7.65–7.58 (m, 2H, C$\mathbf{H}_{Ph}$), 7.35 (dd, *J* = 6.9, 1.7 Hz, 1H, C$\mathbf{H}_{PYA}$), 7.28 (d, *J* = 6.9 Hz, 1H, C$\mathbf{H}_{PYA}$), 5.28 (d, *J* = 6.4 Hz, 2H, C$\mathbf{H}_{cym}$), 5.08 (d, *J* = 6.4 Hz, 2H, C$\mathbf{H}_{cym}$), 3.86 (s, 3H, NC$\mathbf{H}_3$), 2.42 (sept, *J* = 6.8 Hz, 1H, C**H**(CH$_3$)$_2$), 2.06 (s, 3H, cym-C$\mathbf{H}_3$), 1.14 (d, *J* = 6.8 Hz, 6H, CH(C$\mathbf{H}_3$)$_2$). **^{13}C{^{1}H} NMR (CD_2Cl_2, 298 K, 75 MHz):** δ 182.65 (**C**$_{C=O}$), 160.86 (**C**$_{PYA}$), 140.99 (**C**$_{PYA}$), 140.33 (**C**$_{Ph}$), 133.22 (**C**H$_{PYA}$), 133.02 (**C**H$_{PYA}$), 129.94 (**C**H$_{Ph}$), 129.57 (**C**H$_{PYA}$), 128.87 (**C**H$_{Ph}$), 110.34 (**C**H$_{PYA}$), 91.71 (**C**$_{cym}$), 81.90 (**C**H$_{cym}$), 79.24 (**C**H$_{cym}$), 46.43 (N-**C**H$_3$), 32.04 (**C**H(CH$_3$)$_2$), 23.32 (cym-**C**H$_3$), 19.91 (CH(CH$_3$)$_2$). **^{19}F{^{1}H} NMR (CD_2Cl_2, 298 K, 282 MHz):** δ -72.59 (d, *J* = 712 Hz, P**F$_6$**).

$^{31}P\{^{1}H\}$ NMR (CD_3CN, 298 K, 121 MHz): δ -144.12 (sept, *J* = 703 Hz, **P**F_6). **ESI-MS (CH_2Cl_2, calc. for $[M–PF_6]^+$):** 462.1110 (462.1119). **Elemental Analysis (calc. for $C_{23}H_{26}N_3RuOPF_6$):** C 45.12 (45.55), H 4.50 (4.32), N 6.60 (6.93).

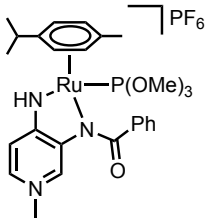

Synthesis of 4. In a round bottom flask, **3** (10.28 mg, 0.017 mmol, 1 eq) was dissolved in CH_2Cl_2 (2 mL) and $P(OMe)_3$ (2.2 μL, 0.019 mmol, 1.1 eq) was added. The reaction mixture was stirred for 5 min, during which the color of the solution changed from dark red to yellow. Pentane (4 mL) was added, and the resulting mixture was kept at –8 °C for 2 h. The yellow precipitate was collected by filtration and dried in vacuo to give complex **4** (11.70 mg, 0.016 mmol, 94%).

^{1}H NMR (CD_2Cl_2, 298K, 300 MHz): δ 7.89 (bs, 1H, C**H**$_{PYA}$), 7.50–7.47 (m, 2H, C**H**$_{Ph}$), 7.39–7.37 (m, 3H, C**H**$_{Ph}$), 6.83 (dd, *J* = 7.1, 1.8 Hz, 1H, C**H**$_{PYA}$), 6.37 (d, *J* = 7.0 Hz, 1H, C**H**$_{PYA}$), 5.54 (d, *J* = 6.1 Hz, 1H, C**H**$_{cym}$), 5.48 (d, *J* = 6.3 Hz, 1H, C**H**$_{cym}$), 5.34 (b, 1H, C**H**$_{cym}$), 4.68 (d, *J* = 6.1 Hz, 1H, C**H**$_{cym}$), 3.68 (d, *J* = 10.9 Hz, 9H, P(OC**H**$_3$)$_3$), 3.43 (m, 3H, NC**H**$_3$), 2.68 (sept, *J* = 6.9 Hz, 1H, C**H**$(CH_3)_2$), 1.99 (s, 3H, cym-C**H**$_3$), 1.16–1.08 (2 × d, J = 7.0, 6.9 Hz, 6H, CH(C**H**$_3$)$_2$). **$^{13}C\{^{1}H\}$ NMR (CD_2Cl_2, 298 K, 75 MHz):** δ 178.54 (**C**$_{C=O}$), 166.13 (**C**$_{PYA}$), 143.09 (**C**$_{Ph}$), 141.40–141.37 (d, *J* = 1.8 Hz, **C**$_{PYA}$), 134.72 (**C**H$_{PYA}$), 132.41 (**C**H$_{PYA}$), 128.96 (**C**H$_{Ph}$), 128.42–127.88 (d, *J* = 40.7 Hz, **C**H$_{Ph}$), 119.32–119.15 (d, *J* = 13.0 Hz, **C**$_{cym}$), 108.57 (**C**H$_{PYA}$), 106.34–106.32 (d, *J* = 2.0 Hz, **C**$_{cym}$), 93.58–93.47 (d, *J* = 8.2 Hz, **C**H$_{cym}$), 91.82 (**C**H$_{cym}$), 89.41–89.36 (d, *J* = 3.8 Hz, **C**H$_{cym}$), 84.91(**C**H$_{cym}$), 54.01–53.91 (d, *J* = 7.5 Hz, P(O**C**H$_3$)$_3$), 44.44 (N**C**H$_3$), 31.14 (**C**H$(CH_3)_2$), 22.96–22.92 (d, *J* = 2.7 Hz, CH(**C**H$_3$)$_2$), 21.49–21.46 (d, *J* = 1.8 Hz, CH(**C**H$_3$)$_2$), 19.00 (cym-**C**H$_3$). **$^{19}F\{^{1}H\}$ NMR** (**CD_2Cl_2, 298 K, 282 MHz):** δ -72.68 (d, *J* = 712 Hz, P**F**$_6$). **$^{31}P\{^{1}H\}$ NMR** (**CD_2Cl_2, 298 K, 121 MHz):** δ 121.06 (s, **P**$(OMe)_3$), -144.31 (sept, *J* = 712 Hz, **P**F_6). **ESI-MS (CH_2Cl_2, calc. for $[M–PF_6]^+$):** 586.1421 (586.1403).

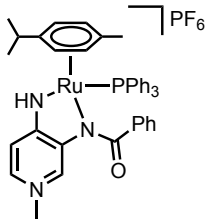

Synthesis of 5. In a round bottom flask, **3** (10.59 mg, 0.017 mmol, 1 eq) was dissolved in CH_2Cl_2 (2 mL) and PPh_3 (5.04 mg, 0.019 mmol, 1.1 eq) was added. The reaction mixture was stirred for 5 min, during which the color of the solution changed from dark red to orange. Pentane (4 mL) was added, and the resulting mixture was kept at -8°C for 2 h. The orange precipitate was collected by filtration and dried in vacuo to give complex **5** (14.52 mg, 0.017 mmol, 96%).

^{1}H NMR (CD_2Cl_2, 298K, 300 MHz): δ 7.67–7.55 (m, 6H, **H_{PPh3}**), 7.50–7.42 (m, 3H, **H_{PPh3}**), 7.41–7.34 (m, 6H, **H_{PPh3}**), 7.34–7.23 (m, 3H, C**H_{Ph}**), 6.73 (s, 1H, N**H**), 6.51 (d, *J* = 7.0 Hz, 1H, C**H_{PYA}**), 6.14 (d, *J* = 6.6 Hz, 1H, C**H_{cym}**), 6.05 (d, *J* = 7.0 Hz, 1H, C**H_{PYA}**), 5.89 (d, *J* = 6.0 Hz, 1H, C**H_{cym}**), 5.70 (d, *J* = 6.0 Hz, 1H, C**H_{cym}**), 4.84 (s, 1H, C**H_{PYA}**), 4.75 (d, *J* = 6.6 Hz, 1H, C**H_{cym}**), 2.86 (s, 3H, NC**H_3**), 2.72 (sept, *J* = 7.0 Hz, 1H, C**H**$(CH_3)_2$), 1.97 (s, 3H, cym-C**H_3**), 1.24 (d, *J* = 7.0 Hz, 3H, CH(C**H_3**)$_2$), 1.15 (d, *J* = 7.0 Hz, 3H, CH(C**H_3**)$_2$). **^{13}C{^{1}H} NMR (CD_2Cl_2, 298 K, 75 MHz):** δ 166.1 (**$C_{C=O}$**), 141.1 (**C_{PYA}**), 139.3 (**C_{Ph}**), 135.4 (d, *J* = 10.4 Hz, **C**H_{PPh3}), 133.7 (**C**H_{PYA}), 132.1 (d, *J* = 45.3 Hz, **C**H_{PPh3}), 131.0 (d, *J* = 2.1 Hz, **C**H_{PPh3}), 129.7 (**C**H_{Ph}), 129.4 (**C**H_{PYA}), 129.2 (**C**H_{Ph}), 128.8 (d, *J* = 9.8 Hz, **C**H_{PPh3}) , 126.9 (**C**H_{Ph}), 108.7 (**C**H_{PYA}), 103.5 (**C_{cym}**), 100.6 (**C_{cym}**), 93.9 (**C**H_{cym}), 93.7 (**C**H_{cym}), 91.6 (**C**H_{cym}), 82.4 (**C**H_{cym}), 43.8 (N**C**H_3), 31.7 (**C**H$(CH_3)_2$), 24.5 (cym-**C**H_3), 21.0 (CH(**C**H_3)$_2$), 18.6 (CH(**C**H_3)$_2$). **^{19}F{^{1}H} NMR** (**CD_2Cl_2, 298 K, 282 MHz**): δ -72.61 (d, *J* = 710 Hz, P**F_6**). **^{31}P{^{1}H} NMR** (**CD_2Cl_2, 298 K, 121 MHz**): δ -44.02 (s, **P**Ph_3), -144.23 (sept, *J* = 710 Hz, **P**F_6). **ESI-MS (CH_2Cl_2, calc. for [M–PF_6]$^+$):** 462.1110 (462.1119).

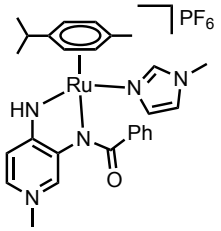

Synthesis of 6. In a round bottom flask, **3** (9.69 mg, 0.016 mmol, 1 eq) was solubilized in CH_2Cl_2 (2 mL) and 1-methylimidazole (6.35 μL, 0.080 mmol, 5 eq) was added. The reaction mixture was stirred for 5 min, during which the color of the solution changed from dark red to orange. Pentane (4 mL) was added, and the resulting mixture was kept at –8 °C for 2 h. The orange precipitate was collected by filtration and dried in vacuo to give complex **6** (8.20 mg, 0.012 mmol, 75%).

^{1}H NMR (CD_2Cl_2, 298K, 300 MHz): δ 7.56 (s, 1H, C**H_{imi}**), 7.43–7.31 (m, 3H, C**H_{Ph}**), 7.27–7.25 (m, 3H, C**H_{Ph}** + C**H_{PYA}**), 6.99 (s, 1H, C**H_{imi}**), 6.86 (s, 1H, C**H_{imi}**), 6.74 (dd, *J* = 7.0, 1.8 Hz, 1H, C**H_{PYA}**), 6.55 (bs, 1H, N**H**), 6.28 (d, *J* = 7.0 Hz, 1H, C**H_{PYA}**), 5.51 (d, *J* = 5.9 Hz, 2H, C**H_{cym}**), 4.88 (bs, 2H, C**H_{cym}**), 3.67 (s, 3H, N_{imi}C**H_3**), 3.30 (s, 3H, NC**H_3**), 2.50 (sept, *J* = 6.9, 1H, C**H**$(CH_3)_2$), 1.78 (s, 3H, cym-C**H_3**), 1.09 (d, *J* = 6.9 Hz, 6H, CH(C**H_3**)$_2$). **^{13}C{^{1}H} NMR (CD_2Cl_2, 298 K, 75 MHz):** δ 164.78, 142.84, 140.55 (**C_{Ph}**), 139.56 (**C**H_{imi}), 134.24 (**C**H_{PYA}), 131.03 (**C_{PYA}**), 130.94 (**C_{PYA}**), 129.36 (**C**H_{imi}), 128.65 (**C**H_{Ph}), 127.80 (**C**H_{Ph}), 121.59 (**C**H_{imi}), 108.12 (**C**H_{PYA}), 99.86 (**C**H_{cym}), 85.41 (**C**H_{cym}), 44.27 (N**C**H_3), 34.93 (N_{imi}**C**H_3), 31.27 (**C**H$(CH_3)_2$), 22.74 (CH(**C**H_3)$_2$), 18.42 (cym-**C**H_3). **^{19}F{^{1}H} NMR** (**CD_2Cl_2, 298 K, 282 MHz**): δ -72.55 (d, *J* = 710 Hz, P**F_6**). **^{31}P{^{1}H} NMR** (**CD_2Cl_2, 298 K, 121 MHz**): δ -144.25 (quint, *J* = 710 Hz, **P**F_6).

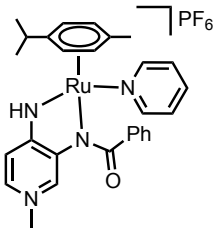

Synthesis of 7. In a round bottom flask, **3** (10.58 mg, 0.017 mmol, 1 eq) was solubilized in CH_2Cl_2 (2 mL) and pyridine (14 μL, 0.174 mmol, 10 eq) was added. The reaction mixture was stirred for 5 min, during which the color of the solution changed from dark red to orange. Pentane (4 mL) was added, and the resulting mixture was kept at –8 °C for 2 h. The orange precipitate was collected by filtration and dried in vacuo to give complex **7** (10.96 mg, 0.016 mmol, 92%).

^{1}H NMR (CD_2Cl_2, 298K, 300 MHz): δ 8.70 (d, *J* = 4.9 Hz, 2H, C**H**$_{pyr}$), 7.74 (t, *J* = 7.5 Hz, 1H, C**H**$_{pyr}$), 7.44-7.29 (m, 8H, C**H**$_{pyr}$, C**H$_{Ph}$**), 6.72 (dd, *J* = 7.0, 1.8 Hz, 1H, C**H$_{PYA}$**), 6.40 (d, *J* = 7.0 Hz, 1H, C**H$_{PYA}$**), 6.25 (bs, 1H, C**H$_{PYA}$**), 5.76 (d, *J* = 5.9 Hz, 2H, C**H$_{cym}$**), 5.31 (d, *J* = 5.9 Hz, 2H, C**H$_{cym}$**), 3.15 (s, 3H, NC**H$_3$**), 2.52 (sept, *J* = 6.9 Hz, 1H, C**H**$(CH_3)_2$), 1.71 (s, 3H, cym-C**H$_3$**), 1.15 (d, *J* = 6.9 Hz, 6H, CH(C**H$_3$**)$_2$). **^{13}C{^{1}H} NMR (CD_2Cl_2, 298 K, 75 MHz):** δ 163.51 (**C**$_{C=O}$), 154.23 (**C**H$_{pyr}$), 140.54, 140.14 (**C**$_{PYA}$), 138.14 (**C**H$_{pyr}$), 133.79 (**C**H$_{PYA}$), 131.07 (**C**H$_{Ph}$), 129.47 (**C**H$_{PYA}$), 128.97 (**C**H$_{Ph}$), 128.75 (**C**H$_{Ph}$), 125.51 (**C**H$_{pyr}$), 108.8 (**C**H$_{PYA}$), 100.26 (**C**$_{cym}$) , 84.03 (**C**H$_{cym}$), 82.29 (**C**H$_{cym}$), 44.96 (N**C**H$_3$), 31.68 (**C**H(**C**H$_3$)$_2$), 23.02 (cym-C**H$_3$**), 18.84 (CH(**C**H$_3$)$_2$). **^{19}F{^{1}H} NMR (CD_2Cl_2, 298 K, 282 MHz):** δ -72.42 (d, *J* = 711. Hz, P**F$_6$**). **^{31}P{^{1}H} NMR (CD_2Cl_2, 298 K, 121 MHz):** δ -144.16 (quint, *J* = 711, **P**F$_6$).

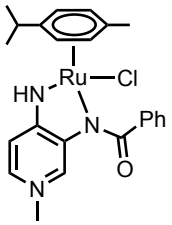

Synthesis of 8. In a round bottom flask, **3** (25 mg, 0.041 mmol, 1 eq) was solubilized in CH_2Cl_2 (5 mL) and Et_4NCl (7.5 mg, 0.045 mmol, 1.1 eq) was added. The solution was stirred for 5 min and concentrated under vacuo. Toluene (5 mL) was added resulting in the precipitation of Et_4NPF_6. The mixture was filtrated through Celite to afford **8** as a red solid (18.17 mg, 0.036 mmol, 88%).

^{1}H NMR (CD_2Cl_2, 298K, 300 MHz): δ 9.03 (s, 1H, C**H$_{PYA}$**), 8.14–8.11 (m, 2H, C**H$_{Ph}$**), 7.44–7.41 (m, 3H, C**H$_{Ph}$**), 6.82 (dd, *J* = 7.0, 1.9 Hz, 1H, C**H$_{PYA}$**), 6.26 (bs, 1H, N**H**), 6.25 (d, *J* = 7.0 Hz, 1H, C**H$_{PYA}$**), 4.96 (d, *J* = 6.2 Hz, C**H$_{cym}$**), 4.08 (bs, 2H, C**H$_{cym}$**), 3.56 (s, 3H, NC**H$_3$**), 2.42 (septet, *J* = 6.9 Hz, 1H, C**H**$(CH_3)_2$), 1.98 (s, 3H, cym-C**H$_3$**), 1.04 (d, *J* = 6.9 Hz, 6H, CH(C**H$_3$**)$_2$). **^{13}C{^{1}H} NMR (CD_2Cl_2, 298 K, 75 MHz):** δ 179.38 (**C**$_{C=O}$), 164.05 (**C**$_{PYA}$), 145.21 (**C**$_{Ph}$), 139.76 (**C**$_{PYA}$), 134.08 (**C**H$_{PYA}$), 131.91 (**C**H$_{PYA}$), 129.57 (**C**H$_{Ph}$), 128.87 (**C**H$_{Ph}$), 127.73 (**C**H$_{Ph}$), 107.66 (**C**H$_{PYA}$), 102.43 (**C**H$_{cym}$), 95.93 (**C**H$_{cym}$), 83.50 (**C**H$_{cym}$), 81.13 (**C**H$_{cym}$), 44.48 (N**C**H$_3$), 31.07 (**C**H$(CH_3)_2$), 22.53 (cym-**C**H$_3$), 18.98 (CH(**C**H$_3$)$_2$). **ESI-MS (CH_2Cl_2, calc. for [M]$^+$):** 498.0880 (498.0881).

II.5.3. Ligand displacement experiments

General procedure for ligand displacement. At room temperature, complex **3** (10 mg, 16 mmol, 1 eq) was charged in an NMR tube and dissolved in CD_2Cl_2 (0.4 mL). Ligand L1 was added (1 eq, from a 0.2 M solution in CD_2Cl_2) and the reaction mixture was analyzed by ^1H NMR spectroscopy. Ligand L2 was added (1 eq, from a 0.2 M solution in CD_2Cl_2) and the resulting mixture was analyzed by ^1H NMR spectroscopy to conclude on the displacement of L1 by L2.

II.5.4. Determination of binding constants by UV-Vis spectroscopy

General procedure for determination of binding constants by UV-Vis spectroscopy. Before each titration, a blank spectrum (of CH_2Cl_2) was collected. A 10 mM stock solution of complex **3** in CH_2Cl_2 was diluted to give samples that were 0.05 mM in complex **3**. The ligands L were titrated to final concentrations varying from 0.02 mM to 1.5 mM as presented in the Tables II.7–II.10.

Table II.7. UV-Vis titration of complex **3** with **L** = $P(OMe)_3$ (CH_2Cl_2, 298 K).

Eq. (**L**)	[**L**]$_0$, mM	[**3**]$_0$, mM
0	0	0.050
0.2	0.010	0.050
0.4	0.020	0.050
0.6	0.030	0.050
0.8	0.040	0.050
1.0	0.050	0.050
2.0	0.100	0.050
4.0	0.200	0.050

Eq. (**L**): number of equivalents of $P(OMe)_3$ added; [**L**]$_0$ and [**3**]$_0$: initial concentrations of $P(OMe)_3$ and complex **3**, respectively.

Table II.8. UV-Vis titration of complex **3** with **L** = PPh_3 (CH_2Cl_2, 298 K).

Eq. (**L**)	[**L**]$_0$, mM	[**3**]$_0$, mM
0	0	0.050
0.2	0.010	0.050
0.4	0.020	0.050
0.6	0.030	0.050
0.8	0.040	0.050
1.0	0.050	0.050
2.0	0.100	0.050

Eq. (**L**): number of equivalents of PPh_3 added; [**L**]$_0$ and [**3**]$_0$: initial concentrations of PPh_3 and complex **3**, respectively.

Table II.9. UV-Vis titration of complex **3** with **L** = 1-methylimidazole (CH_2Cl_2, 298 K).

Eq. (**L**)	$[\mathbf{L}]_0$, mM	$[\mathbf{3}]_0$, mM
0	0	0.050
1	0.050	0.050
2	0.100	0.050
4	0.200	0.050
6	0.300	0.050
10	0.500	0.050
20	1.000	0.050

Eq. **(L)**: number of equivalents of 1-methylimidazole added; $[\mathbf{L}]_0$ and $[\mathbf{3}]_0$: initial concentrations of 1-methylimidazole and complex **3**, respectively**.**

Table II.10. UV-Vis titration of complex **3** with **L** = pyridine (CH_2Cl_2, 298 K).

Eq. (**L**)	$[\mathbf{L}]_0$, mM	$[\mathbf{3}]_0$, mM
0	0	0.050
1	0.050	0.050
2	0.100	0.050
4	0.200	0.050
6	0.300	0.050
8	0.400	0.050
10	0.500	0.050
20	1.000	0.050
30	1.500	0.050
50	2.500	0.050
200	10.00	0.050

Eq. (**L**): number of equivalents of pyridine added; $[\mathbf{L}]_0$ and $[\mathbf{3}]_0$: initial concentrations of pyridine and complex **3**, respectively**.**

General procedure for titration data treatment using Bindfit. The binding constants were obtained from fitting the UV-Vis titration data described in section S.4.1 to the UV 1:1 model (Nelder-Mead method) using Bindfit.[23] The raw input data, calculated fit including mole fractions and other statistical details are available at the following URLs:

UV-Vis titration with $P(OMe)_3$:

http://app.supramolecular.org/bindfit/view/057712ab-1279-48a9-be76-97206d39aed3

UV-Vis titration with PPh_3:

http://app.supramolecular.org/bindfit/view/a1d6f82c-184b-4126-b4eb-96cdfa839ce2

UV-Vis titration with 1-methylimidazole:

http://app.supramolecular.org/bindfit/view/b77a8f91-7185-4e29-ab74-7aab9aebd2ae

UV-Vis titration with pyridine:

http://app.supramolecular.org/bindfit/view/75074d37-6fce-49e5-8b9a-b4ae4a01f176

II.5.5. Catalytic procedures

General catalytic procedure. In a 20 mL pressure tube, the ketone substrate (0.5 mmol), complex **3** (1 mol%) and 1,3,5-trimethoxybenzene (10 mol%) as internal standard were dissolved in EtOH (2.5 mL) and the solution was degassed with N_2 for 10 min. The catalytic run was started with the injection of the base (2 M solution in H_2O) and the tube was placed in a pre-heated oil bath (40–110°C).

Effect of different solvents and hydrogen sources. In a 20 mL pressure tube, the ketone substrate (0.5 mmol), complex **3** (1 mol%) and 1,3,5-trimethoxybenzene (10 mol%) as internal standard were dissolved in the corresponding solvent (2.5 mL; *i*PrOH, MeOH or EtOH) and the solution was degassed with N_2 for 10 min. The catalytic run was started with the injection of KOH (2 M solution in H_2O) and the tube was placed in a pre-heated oil bath (80°C; Table S5).

Addition of thiophene in the catalytic run. Following the general procedure, di(pyridin-2-yl)methanone **9k** (0.5 mmol, 1 eq), complex **3** (1 mol%) and 1,3,5-trimethoxybenzene (10 mol%) as internal standard were dissolved in EtOH (2.5 mL) and the solution was degassed with N_2 for 10 min. The catalytic run was started with the injection of K_2CO_3 (2 M solution in H_2O) and the tube was placed in a pre-heated oil bath (40°C). After 30 min, thiophene (0.5 mmol, 1 eq) was added to the reaction mixture.

II.5.6. Time-conversion profiles of catalytic transfer hydrogenation

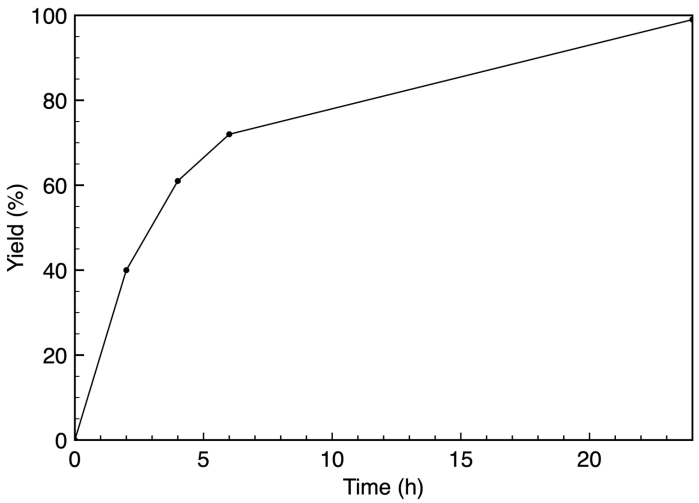

Figure II.7. Time-conversion profile for the catalytic hydrogenation of compound **9a** using the general catalytic procedure.

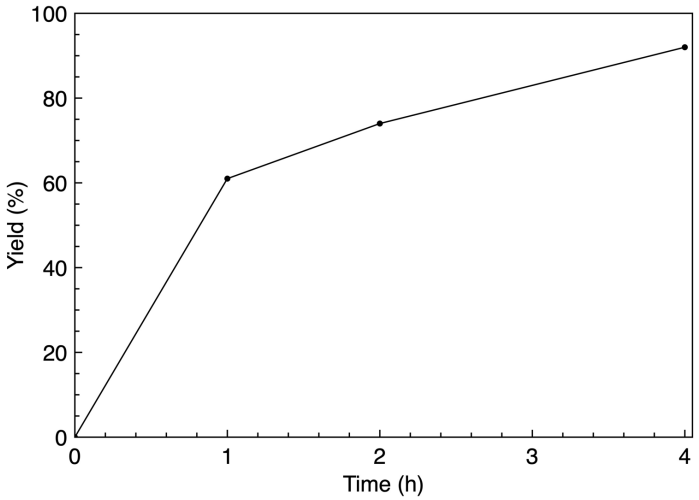

Figure II.8. Time-conversion profile for the catalytic hydrogenation of compound **9b** using the general catalytic procedure.

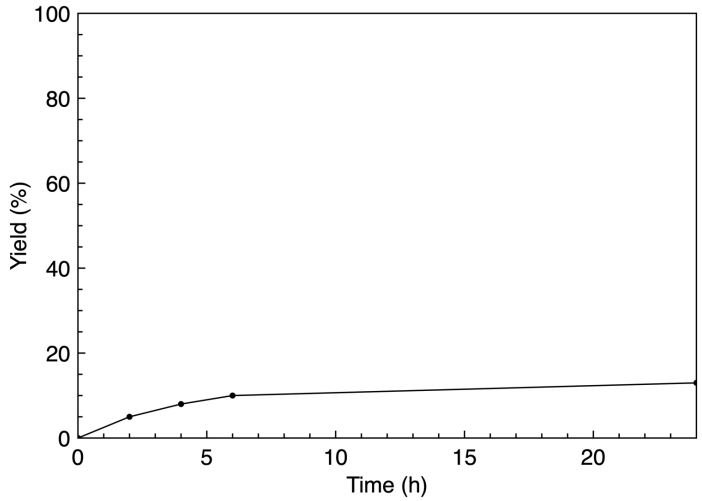

Figure II.9. Time-conversion profile for the catalytic hydrogenation of compound **9c** using the general catalytic procedure.

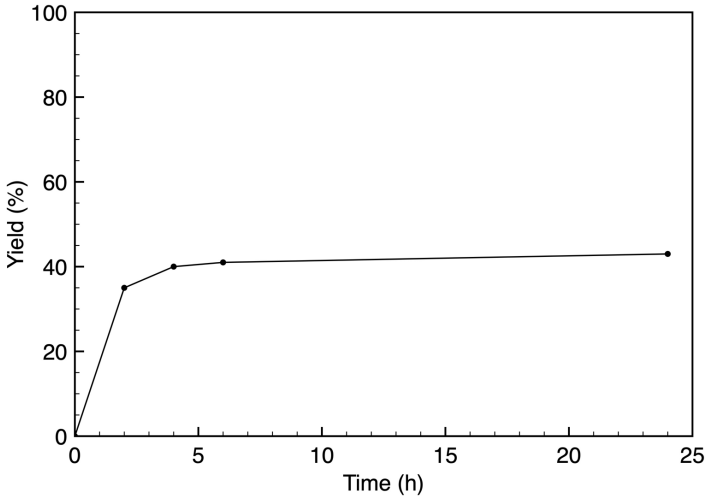

Figure II.10. Time-conversion profile for the catalytic hydrogenation of compound **9d** using the general catalytic procedure.

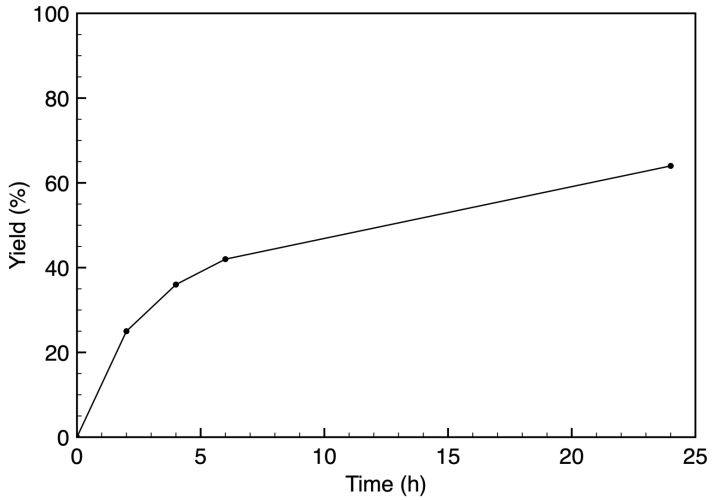

Figure II.11. Time-conversion profile for the catalytic hydrogenation of compound **9e** using the general catalytic procedure.

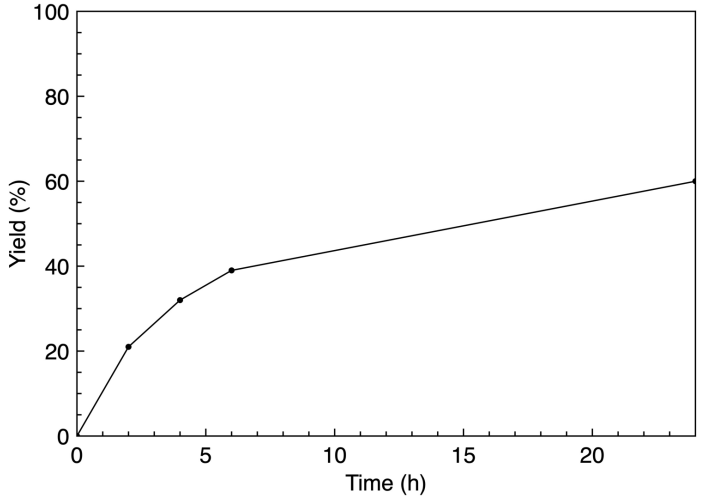

Figure II.12. Time-conversion profile for the catalytic hydrogenation of compound **9f** using the general catalytic procedure.

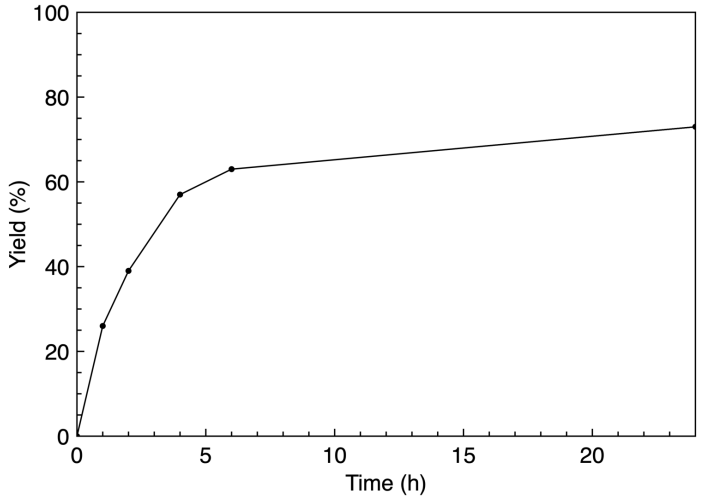

Figure II.13. Time-conversion profile for the catalytic hydrogenation of compound **9g** using the general catalytic procedure.

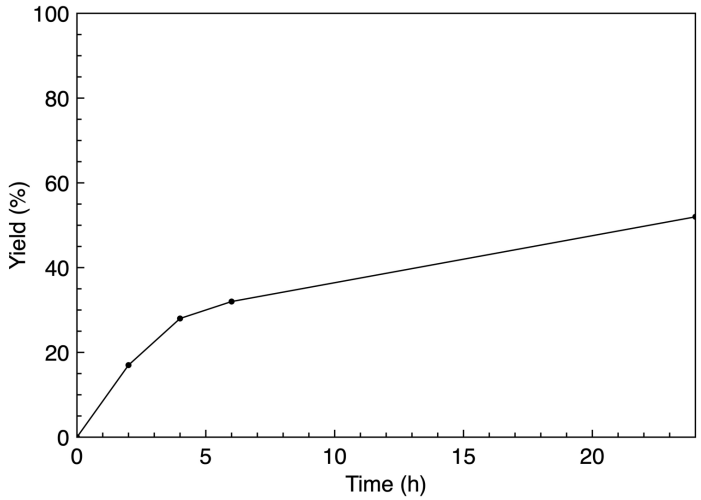

Figure II.14. Time-conversion profile for the catalytic hydrogenation of compound **9h** using the general catalytic procedure.

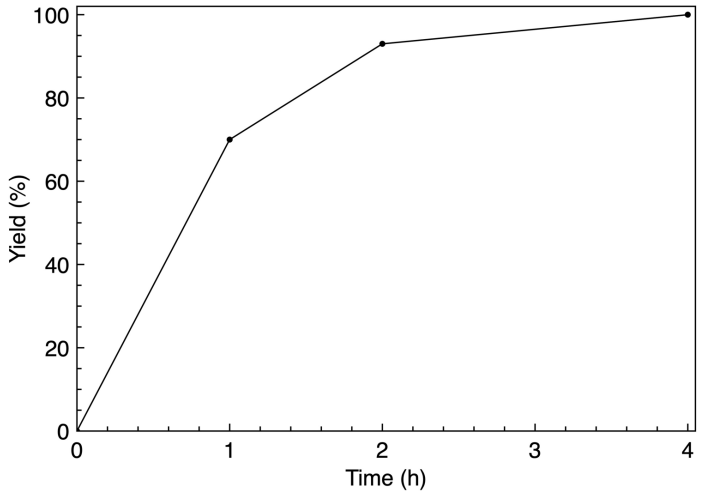

Figure II.15. Time-conversion profile for the catalytic hydrogenation of compound **9i** using the general catalytic procedure.

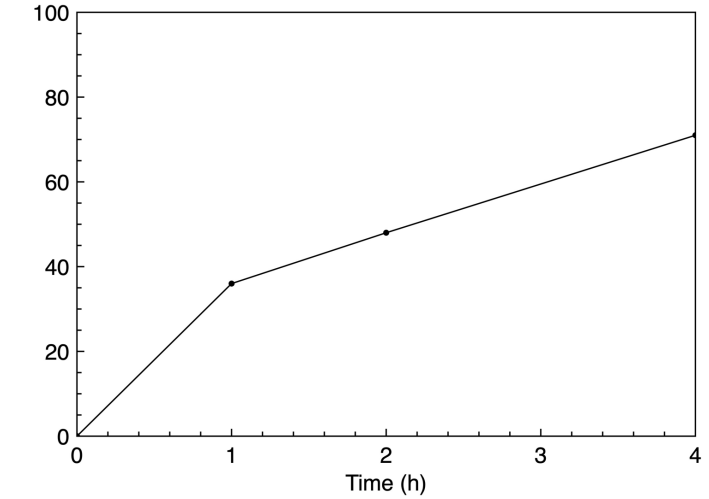

Figure II.16. Time-conversion profile for the catalytic hydrogenation of compound **9j** using the general catalytic procedure.

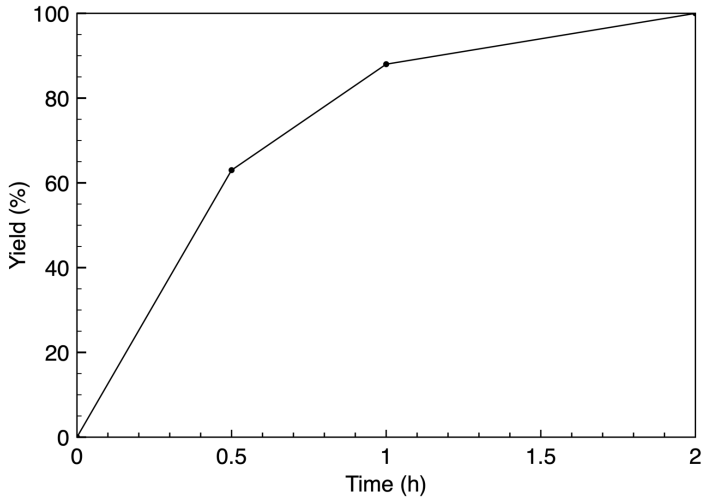

Figure II.17. Time-conversion profile for the catalytic hydrogenation of compound **9k** using the general catalytic procedure.

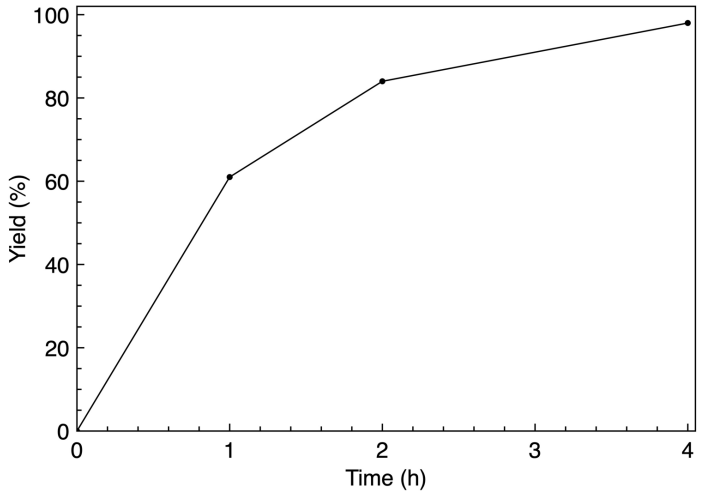

Figure II.18. Time-conversion profile for the catalytic hydrogenation of compound **9l** using the general catalytic procedure.

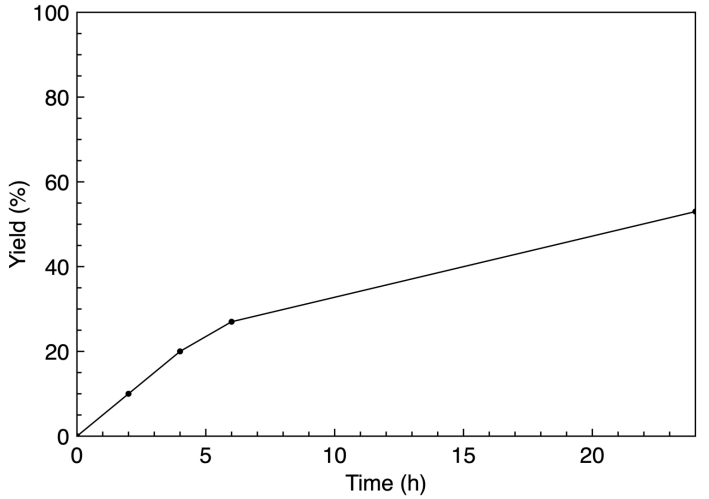

Figure II.19. Time-conversion profile for the catalytic hydrogenation of compound **9m** using the general catalytic procedure.

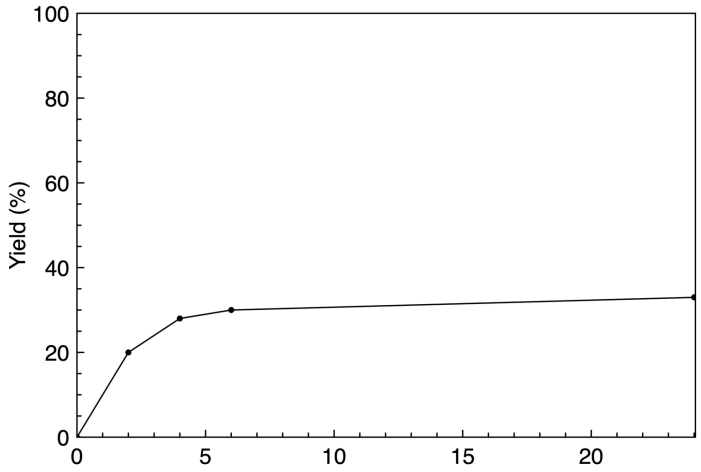

Figure II.20. Time-conversion profile for the catalytic hydrogenation of compound **9n** using the general catalytic procedure.

II.5.7. Characterization of products

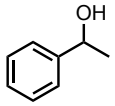

1-Phenylethan-1-ol (10a). Compound **10a** was synthesized according to the general procedure. The crude product was purified by column chromatography (SiO_2, hexane/EtOAc 9:1) to obtain the pure product.[65] **^{1}H NMR (300 MHz, 298K, $CDCl_3$):** δ 7.29-7.21 (m, 4H), 7.19-7.15 (m, 1H), 4.78 (q, *J* = 6.4 Hz, 1H), 1.39 (d, *J* = 6.4 Hz, 3H).

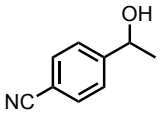

4-(1-Hydroxyethyl)benzonitrile (10b). Compound **10b** was synthesized according to the general procedure. The crude product was purified by column chromatography (SiO_2, hexane/EtOAc 9:1) to obtain the pure product.[65] **^{1}H NMR (300 MHz, 298K, $CDCl_3$):** δ 7.61 (d, *J* = 8.4 Hz, 2H), 7.47 (d, *J* = 8.0 Hz, 2H), 4.94 (q, *J* = 6.5 Hz, 1H), 2.35 (bs, 1H), 1.47 (d, *J* = 6.5 Hz, 3H).

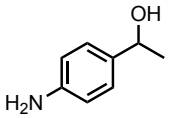

1-(4-aminophenyl)ethan-1-ol (10c). Compound **10c** was synthesized according to the general procedure. The crude product was directly analyzed due to low yield.[70,72] **^{1}H NMR (300 MHz, 298K, $CDCl_3$):** δ 7.10 (d, *J* = 8.1 Hz, 1H), 6.61 (b, 2H), 4.73 (q, *J* = 6.6 Hz, 1H), 1.40 (d, *J* = 6.4 Hz, 4H).

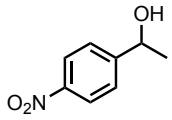

1-(4-Nitrophenyl)ethan-1-ol (10d). Compound **10d** was synthesized according to the general procedure. The crude product was purified by column chromatography (SiO_2, hexane/EtOAc 9:1) to obtain the pure product.[65] **^{1}H NMR (300 MHz, 298K, $CDCl_3$):** δ 8.21 (d, *J* = 8.8 Hz, 2H), 7.55 (d, *J* = 8.3 Hz, 2H), 5.03 (q, *J* = 6.5 Hz, 1H), 1.52 (d, *J* = 6.5 Hz, 3H).

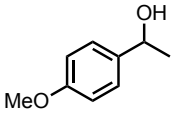

1-(4-Methoxyphenyl)ethan-1-ol (10e). Compound **10e** was synthesized according to the general procedure. The crude product was purified by column chromatography (SiO_2, hexane/EtOAc 9:1) to obtain the pure product.[65] **^{1}H NMR (300 MHz, 298K, $CDCl_3$):** δ 7.29 (d, *J* = 8.4 Hz, 2H), 6.88 (d, *J* = 8.7 Hz, 2H), 4.85 (q, *J* = 6.4 Hz, 1H), 3.80 (s, 3H), 1.78 (bs, 1H), 1.48 (d, *J* = 6.4 Hz, 3H).

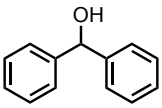

Diphenylmethanol (10f). Compound **10f** was synthesized according to the general procedure. The crude product was purified by column chromatography (SiO_2, hexane/EtOAc 9:1) to obtain the pure product.[65] **^{1}H NMR (300 MHz, 298K, $CDCl_3$):** δ 7.40-7.25 (m, 10H), 5.85 (s, 1H), 2.14 (bs, 1H).

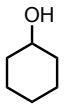

Cyclohexanol (10g). Compound **10g** was synthesized according to the general procedure. The crude product was directly analyzed.[65] **^{1}H NMR (300 MHz, 298K, $CDCl_3$):** δ 3.61 (m, 1H), 1.88 (m, 2H), 1.73 (m, 2H), 1.54 (m, 1H), 1.40 (m, 1H), 1.25 (m, 4H).

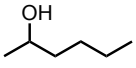

Hexan-2-ol (10h). Compound **10h** was synthesized according to the general procedure. The crude product was directly analyzed.[73] **^{1}H NMR (300 MHz, 298K, $CDCl_3$):** δ 3.73-3.66 (m, 1H), 1.46-1.23 (m, 6H), 1.18 (d, *J* = 6.2 Hz, 3H), 0.90 (t, *J* = 7.5 Hz, 3H).

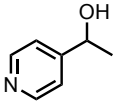

1-(Pyridin-2-yl)ethan-1-ol (10i). Compound **10i** was synthesized according to the general procedure. The crude product was directly analyzed.[65] **^{1}H NMR (300 MHz, 298K, $CDCl_3$):** δ 8.46 (d, *J* = 4.2 Hz, 1H), 7.63 (td, *J* = 7.7, 1.7 Hz, 1H), 7.25 (d, *J* = 8.0 Hz, 1H), 7.14 (ddd, *J* = 7.3, 4.9, 0.6 Hz, 1H), 4.84 (q, *J* = 6.5 Hz, 1H), 1.45 (d, *J* = 6.5 Hz, 3H).

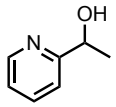

1-(Pyridin-4-yl)ethan-1-ol (10j). Compound **10j** was synthesized according to the general procedure. The crude product was purified by column chromatography (SiO_2, hexane/EtOAc 9:1) to obtain the pure product.[74] **^{1}H NMR (300 MHz, 298K, $CDCl_3$):** δ 8.53 (d, *J* = 5.0 Hz, 2H), 7.33 (d, *J* = 6.3 Hz, 2H), 4.91 (q, *J* = 6.5 Hz, 1H), 1.49 (d, *J* = 6.5 Hz, 3H).

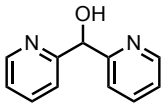

Di(pyridin-2-yl)methanol (10k). Compound **10k** was synthesized according to the general procedure. The crude product was directly analyzed.[75] **^{1}H NMR (300 MHz, 298K, $CDCl_3$):** δ 8.53-8.5 (m, 2H), 7.62 (td, *J* = 7.7, 1.8 Hz, 2H), 7.55-7.48 (m, 2H), 7.16 (ddd, *J* = 7.4, 4.9, 1.2 Hz, 2H), 5.88 (s, 1H).

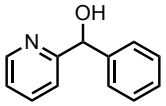

Phenyl(pyridin-2-yl)methanol (10l). Compound **10l** was synthesized according to the general procedure. The crude product was purified by column chromatography (SiO_2, hexane/EtOAc 9:1) to obtain the pure product.[76] **^{1}H NMR (300 MHz, 298K, $CDCl_3$):** δ 8.48 (dt, *J* = 4.9, 1.0 Hz, 1H), 7.53 (td, *J* = 7.7, 1.7 Hz, 1H), 7.34-7.06 (m, 7H), 5.69 (s, 1H), 4.74 (bs, 1H).

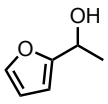

1-(furan-2-yl)ethan-1-ol (10m). Compound **10m** was synthesized according to the general procedure. The crude product was directly analyzed.[77] **^{1}H NMR (300 MHz, 298K, $CDCl_3$):** δ 7.37 (dd, *J* = 1.9, 0.8 Hz, 1H), 6.33 (dd, *J* = 3.2, 1.8 Hz, 1H), 6.23 (dt, *J* = 3.2, 0.8 Hz, 1H), 4.89 (q, *J* = 6.6 Hz, 1H), 1.55 (d, *J* = 6.6 Hz, 3H).

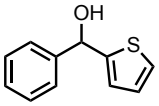

Phenyl(thiophen-2-yl)methanol (10n). Compound **10n** was synthesized according to the general procedure. The crude product was directly analyzed.[78] **^{1}H NMR (300 MHz, 298K, $CDCl_3$):** δ 7.42-7.11 (m, 6H), 6.87-6.75 (m, 2H), 5.95 (s, 1H), 2.37 (bs, 1H).

II.5.7. Crystal structure determination

A crystal of **3** or **5** immersed in parabar oil was mounted at ambient conditions and transferred into the stream of nitrogen (100 K). All measurements were made on a *RIGAKU Synergy S* area-detector diffractometer[4] using mirror optics monochromated Cu $K\alpha$ radiation (λ = 1.54184 Å). The unit cell constants and an orientation matrix for data collection were obtained from a least-squares refinement of the setting angles of reflections in the range 2.789° < θ < 78.282°. A total of 9116 frames were collected using ω scans, with 0.3 second exposure time (2 s for high-angle reflections), a rotation angle of 0.5° per frame, a crystal-detector distance of 32.29 mm, at T = 100(2) K. Data reduction was performed using the *CrysAlisPro*5 program. The intensities were corrected for Lorentz and polarization effects, and an absorption correction based on the multi-scan method using SCALE3 ABSPACK in *CrysAlisPro*5 was applied. Data collection and refinement parameters are given in Table II.11. The structure was solved by intrinsic phasing using *SHELXT*,[79] which revealed the positions of all non-hydrogen atoms of the title compound. All non-hydrogen atoms were refined anisotropically. H-atoms were assigned in geometrically calculated positions and refined using a riding model where each H-atom was assigned a fixed isotropic displacement parameter with a value equal to 1.2Ueq of its parent atom (1.5 Ueq for methyl groups). Refinement of the structure was carried out on *F2* using full-matrix least-squares procedures, which minimized the function $\Sigma w(Fo^2 - Fc^2)^2$. The weighting scheme was based on counting statistics and included a factor to downweight the intense reflections. All calculations were performed using the *SHELXL-2014/7*[80] program in OLEX2.[81] The X-ray crystal structure determination service unit of the Department of Chemistry and Biochemistry of the University of Bern is acknowledged for measuring, solving, refining, and summarizing the structures of compounds **3** and **5**. Crystallographic data for all structures reported in this chapter have been deposited with the Cambridge Crystallographic Data Centre (CCDC) as supplementary publication numbers 2304306 and 2304307.

Table II.11. Selected crystallographic and refinement data.

	Compound **3**	Compound **5**
Identification code	18MA105_PM243	18MA123C3_PM246
Empirical formula	$C_{23}H_{26}F_6N_3OPRu$	$C_{41}H_{41}F_6N_3OP_2Ru$
Formula weight	606.41	868.78
Temperature/K	173.00(10)	173.00(10)
Crystal system	triclinic	orthorhombic
Space group	P-1	$P2_12_12_1$
a/Å	8.8392(2)	9.47318(6)
b/Å	9.1938(2)	18.83614(15)
c/Å	16.5782(5)	21.81942(15)
α/°	74.336(2)	90
β/°	81.139(2)	90
γ/°	72.055(2)	90
Volume/Å^3	1230.41(6)	3893.42(5)
Z	2	4
ρ_{calc}g/cm^3	1.637	1.482
μ/mm^{-1}	0.769	0.550
F(000)	612.0	1776.0
Crystal size/mm^3	0.349 × 0.194 × 0.065	0.282 × 0.095 × 0.051
Radiation	MoKα (λ = 0.71073)	MoKα (λ = 0.71073)
2Θ range for data collection/°	4.794 to 56.364	3.734 to 56.32
Index ranges	-11 ≤ h ≤ 11, -12 ≤ k ≤ 12, -21 ≤ l ≤ 21	-12 ≤ h ≤ 12, -24 ≤ k ≤ 24, -28 ≤ l ≤ 28
Reflections collected	26271	66803
Independent reflections	5605 [R_{int} = 0.0344, R_{sigma} = 0.0301]	9106 [R_{int} = 0.0520, R_{sigma} = 0.0369]
Data/restraints/parameters	5605/388/407	9106/774/623
Goodness-of-fit on F^2	1.056	1.051
Final R indexes [I>=2σ (I)]	R_1 = 0.0286, wR_2 = 0.0656	R_1 = 0.0345, wR_2 = 0.0705
Final R indexes [all data]	R_1 = 0.0353, wR_2 = 0.0693	R_1 = 0.0419, wR_2 = 0.0733
Largest diff. peak/hole / e Å^{-3}	0.56/-0.47	0.44/-0.39
CCDC Number	2304306	2304307

II.5. References

[1] J. Washington, R. McDonald, J. Takats, N. Menashe, D. Reshef, Y. Shvo, *Organometallics* **1995**, *14*, 3996–4003.

[2] M. A. Rankin, R. McDonald, M. J. Ferguson, M. Stradiotto, *Organometallics* **2005**, *24*, 4981–4994.

[3] C. M. Frech, L. J. W. Shimon, D. Milstein, *Organometallics* **2009**, *28*, 1900–1908.

[4] M. Gandelman, L. Konstantinovski, H. Rozenberg, D. Milstein, *Chem. Eur. J.* **2003**, *9*, 2595–2602.

[5] T. Gottschalk-Gaudig, K. Folting, K. G. Caulton, *Inorg. Chem.* **1999**, *38*, 5241–5245.

[6] E. R. Paulson, C. E. Moore, A. L. Rheingold, D. P. Pullman, R. W. Sindewald, A. L. Cooksy, D. B. Grotjahn, *ACS Catal.* **2019**, *9*, 7217–7231.

[7] T. Glöge, K. Jess, T. Bannenberg, P. G. Jones, N. Langenscheidt-Dabringhausen, A. Salzer, M. Tamm, *Dalton Trans.* **2015**, *44*, 11717–11724.

[8] T. A. Peganova, I. S. Sinopalnikova, A. S. Peregudov, I. V. Fedyanin, A. Demonceau, N. A. Ustynyuk, A. M. Kalsin, *Dalton Trans.* **2016**, *45*, 17030–17041.

[9] H. Nagashima, H. Kondo, T. Hayashida, Y. Yamaguchi, M. Gondo, S. Masuda, K. Miyazaki, K. Matsubara, K. Kirchner, *Coord. Chem. Rev.* **2003**, *245*, 177–190.

[10] M. Jiménez-Tenorio, M. C. Puerta, P. Valerga, *Eur. J. Inorg. Chem.* **2004**, *2004*, 17–32.

[11] T. J. Johnson, K. Folting, W. E. Streib, J. D. Martin, J. C. Huffman, S. A. Jackson, O. Eisenstein, K. G. Caulton, *Inorg. Chem.* **1995**, *34*, 488–499.

[12] M. B. Kindervater, V. N. Staroverov, K. M. K. Jackman, A. A. Fogh, L. S. G. Kelley, L. Lim, S. A. Sirohey, P. D. Boyle, J. M. Blacquiere, *Dalton Trans.* **2023**, *52*, 10744–10750.

[13] Q. Shi, R. J. Thatcher, J. Slattery, P. S. Sauari, A. C. Whitwood, P. C. McGowan, R. E. Douthwaite, *Chem. Eur. J.* **2009**, *15*, 11346–11360.

[14] P. D. W. Boyd, L. J. Wright, M. N. Zafar, *Inorg. Chem.* **2011**, *50*, 10522–10524.

[15] J. J. Race, M. Albrecht, *ACS Catal.* **2023**, *13*, 9891–9904.

[16] N. Lentz, M. Albrecht, *ACS Catal.* **2022**, *12*, 12627–12631.

[17] J. C. Wong, G. Tang, X. Wu, C. Liang, Z. Zhang, L. Guo, Z. Peng, W. Zhang, X. Lin, Z. Wang, J. Mei, J. Chen, S. Pan, N. Zhang, Y. Liu, M. Zhou, L. Feng, W. Zhao, S. Li, C. Zhang, M. Zhang, Y. Rong, T.-G. Jin, X. Zhang, S. Ren, Y. Ji, R. Zhao, J. She, Y. Ren, C. Xu, D. Chen, J. Cai, S. Shan, D. Pan, Z. Ning, X. Lu, T. Chen, Y. He, L. Chen, *J. Med. Chem.* **2012**, *55*, 8903–8925.

[18] P. Melle, Y. Manoharan, M. Albrecht, *Inorg. Chem.* **2018**, *57*, 11761–11774.

[19] M. Navarro, C. Segarra, T. Pfister, M. Albrecht, *Organometallics* **2020**, *39*, 2383–2391.

[20] Notably, the chemical shift of $H_{\alpha'}$ varies over a much larger range; in particular, the large upfield shift in the PPh_3 complex **5** to 4.84 ppm suggests considerable stereoelectronic effects beyond simple resonance structure contributions.

[21] N. Lentz, Y. Streit, P. Knörr, M. Albrecht, *Chem. Eur. J.* **2022**, *28*, e202202672.

[22] A. Weilhard, K. Salzmann, M. Navarro, J. Dupont, M. Albrecht, V. Sans, *J. Catal.* **2020**, *385*, 1–9.

[23] D. Brynn Hibbert, P. Thordarson, *Chem. Commun.* **2016**, *52*, 12792–12805.

[24] K. P. Chiang, P. M. Barrett, F. Ding, J. M. Smith, S. Kingsley, W. W. Brennessel, M. M. Clark, R. J. Lachicotte, P. L. Holland, *Inorg. Chem.* **2009**, *48*, 5106–5116.

[25] B. G. Reed-Berendt, D. E. Latham, M. B. Dambatta, L. C. Morrill, *ACS Cent. Sci.* **2021**, *7*, 570–585.

[26] D. Wang, D. Astruc, *Chem. Rev.* **2015**, *115*, 6621–6686.

[27] G. E. Dobereiner, R. H. Crabtree, *Chem. Rev.* **2010**, *110*, 681–703.

[28] H. Shabany, E. Abel, J. P. Evans, I. M. McRobbie, G. W. Gokel, *Tetrahedron Lett.* **2000**, *41*, 6705–6708.

[29] L. J. Allen, R. H. Crabtree, *Green Chem.* **2010**, *12*, 1362–1364.

[30] Q. Xu, J. Chen, H. Tian, X. Yuan, S. Li, C. Zhou, J. Liu, *Angew. Chem. Int. Ed.* **2014**, *53*, 225–229.

[31] B. C. Roy, I. A. Ansari, Sk. A. Samim, S. Kundu, *Chem. Asian J.* **2019**, *14*, 2215–2219.

[32] M. B. Dambatta, J. Santos, R. R. A. Bolt, L. C. Morrill, *Tetrahedron* **2020**, *76*, 131571.

[33] R. Bigler, R. Huber, A. Mezzetti, *Angew. Chem. Int. Ed.* **2015**, *54*, 5171–5174.

[34] S. Huo, Q. Wang, W. Zuo, *Dalton Trans.* **2020**, *49*, 7959–7967.

[35] B. Paul, K. Chakrabarti, S. Kundu, *Dalton Trans.* **2016**, *45*, 11162–11171.

[36] P. Melle, J. Thiede, D. A. Hey, M. Albrecht, *Chem. Eur. J.* **2020**, *26*, 13226–13234.

[37] J. M. Gichumbi, B. Omondi, H. B. Friedrich, *Eur. J. Inorg. Chem.* **2017**, *2017*, 915–924.

[38] Y. Koto, F. Shibahara, T. Murai, *Chem. Lett.* **2016**, *45*, 1327–1329.

[39] R. Wang, Y. Tang, M. Xu, C. Meng, F. Li, *J. Org. Chem.* **2018**, *83*, 2274–2281.

[40] P. Weingart, W. R. Thiel, *ChemCatChem* **2018**, *10*, 4844–4848.

[41] T. Kuwahara, T. Fukuyama, I. Ryu, *Org. Lett.* **2012**, *14*, 4703–4705.

[42] L. K. M. Chan, D. L. Poole, D. Shen, M. P. Healy, T. J. Donohoe, *Angew. Chem. Int. Ed.* **2014**, *53*, 761–765.

[43] H. Xiao, G. Wang, M. J. Krische, *Angew. Chem. Int. Ed.* **2016**, *55*, 16119–16122.

[44] H. Lundberg, H. Adolfsson, *Synthesis* **2016**, *48*, 644–652.

[45] T. Zweifel, J.-V. Naubron, T. Büttner, T. Ott, H. Grützmacher, *Angew. Chem. Int. Ed.* **2008**, *47*, 3245–3249.

[46] P. Maire, F. Breher, H. Schönberg, H. Grützmacher, *Organometallics* **2005**, *24*, 3207–3218.

[47] N. Castellanos-Blanco, A. Arévalo, J. J. García, *Dalton Trans.* **2016**, *45*, 13604–13614.

[48] P. Weingart, Y. Sun, W. R. Thiel, *ChemCatChem* **2020**, *12*, 6223–6233.

[49] K. Wang, J. Heltzel, E. Sandefur, K. Culley, G. Lemcoff, A. Voutchkova-Kostal, *J. Organomet. Chem.* **2020**, *919*, 121310.

[50] R. Ghosh, R. R. Behera, S. Panda, S. K. Behera, N. Ch. Jana, B. Bagh, *ChemCatChem* **2023**, *15*, e202201062.

[51] S. Revathi, T. Ghatak, *J. Catal.* **2024**, *429*, 115207.

[52] H. Lundberg, H. Adolfsson, *Tetrahedron Lett.* **2011**, *52*, 2754–2758.

[53] T. Zweifel, D. Scheschkewitz, T. Ott, M. Vogt, H. Grützmacher, *Eur. J. Inorg. Chem.* **2009**, *2009*, 5561–5576.

[54] W.-P. Liu, M.-L. Yuan, X.-H. Yang, K. Li, J.-H. Xie, Q.-L. Zhou, *Chem. Commun.* **2015**, *51*, 6123–6125.

[55] Y.-M. Zhang, M.-L. Yuan, W.-P. Liu, J.-H. Xie, Q.-L. Zhou, *Org. Lett.* **2018**, *20*, 4486–4489.

[56] A. Dubey, E. Khaskin, *ACS Catal.* **2016**, *6*, 3998–4002.

[57] Y. Wang, Z. Huang, X. Leng, H. Zhu, G. Liu, Z. Huang, *J. Am. Chem. Soc.* **2018**, *140*, 4417–4429.

[58] Y. Wang, Z. Huang, Z. Huang, *Nat. Catal.* **2019**, *2*, 529–536.

[59] N. Castellanos-Blanco, M. Flores-Alamo, J. J. García, *Organometallics* **2012**, *31*, 680–686.

[60] J. Zhang, J. Chen, *ACS Sustain. Chem. Eng.* **2017**, *5*, 5982–5993.

[61] A. H. Aboo, E. L. Bennett, M. Deeprose, C. M. Robertson, J. A. Iggo, J. Xiao, *Chem. Commun.* **2018**, *54*, 11805–11808.

[62] Z. Chen, G. Chen, A. H. Aboo, J. Iggo, J. Xiao, *Asian J. Org. Chem.* **2020**, *9*, 1174–1178.

[63] J. Sklyaruk, V. Zubar, J. C. Borghs, M. Rueping, *Org. Lett.* **2020**, *22*, 6067–6071.

[64] R. Wang, X. Han, J. Xu, P. Liu, F. Li, *J. Org. Chem.* **2020**, *85*, 2242–2249.

[65] R. Ghosh, N. Ch. Jana, S. Panda, B. Bagh, *ACS Sustain. Chem. Eng.* **2021**, *9*, 4903–4914.

[66] L. Zhu, S. Ye, J. Wang, J. Zhu, G. He, X. Liu, *ChemCatChem* **2022**, *14*, e202101794.

[67] N. Garg, H. P. Somasundharam, P. Dahiya, B. Sundararaju, *Chem. Commun.* **2022**, *58*, 9930–9933.

[68] P. Melle, M. Albrecht, *Chimia* **2019**, *73*, 299–303.

[69] Notably, 4-substituted acetylpyridine **9i** was converted to the desired alcohol **10i** only in 71% after 4 h (89% conversion), and different side-products were observed from condensation with EtOH. This lake of selectivity may arise from catalyst inhibition through Ru–N bond formation between the catalytic Ru species and the pyridine nitrogen, which is more favored insterically unshielded pyridine substrates.

[70] R. Noyori, S. Hashiguchi, *Acc. Chem. Res.* **1997**, *30*, 97–102.

[71] N. Lentz, S. Reuge, M. Albrecht, *ACS Catal.* **2023**, *13*, 9839–9844.

[72] E. P. Sánchez-Rodríguez, A. J. Fragoso-Medina, E. Ramírez-Meneses, M. Gouygou, M. C. Ortega-Alfaro, J. G. López-Cortés, *Catal. Comm.* **2018**, *115*, 49–54.

[73] X. Ning, X. Dong, Z. Xiao, C. Yao, Y. Kang, *Asian J. Org. Chem.* **2015**, *4*, 333–336.

[74] K. Kuciński, G. Hreczycho, *Green Chem.* **2019**, *21*, 1912–1915.

[75] P. Comba, H. Rudolf, H. Wadepohl, *Dalton Trans.* **2015**, *44*, 2724–2736.

[76] O. Sugimoto, S. Yamada, K. Tanji, *J. Org. Chem.* **2003**, *68*, 2054–2057.

[77] J. Liu, S. Yang, W. Tang, Z. Yang, J. Xu, *Green Chem.* **2018**, *20*, 2118–2124.

[78] T. Yamamoto, T. Furusawa, A. Zhumagazin, T. Yamakawa, Y. Oe, T. Ohta, *Tetrahedron* **2015**, *71*, 19–26.

[79] Oxford Diffraction. *CrysAlisPro, Version 1.171.40.37a. Oxford Diffraction Ltd., Yarnton, Oxfordshire, UK.* **2018**.

[80] G. M. Sheldrick, *Acta Crystallogr. Sect. A Found. Adv.* **2015**, *71*, 3–8.

[81] G. M. Sheldrick, *Acta Crystallogr. Sect. C Struct. Chem.* **2015**, *71*, 3–8.

Chapter III

Ruthenium-Catalyzed Chemoselective Olefin Transfer Hydrogenation of α,β-Unsaturated Carbonyl Systems By Using EtOH as Hydrogen Source

This chapter has been published and is reproduced from:

A. Beaufils, M. Albrecht

ChemCatChem **2024**, e202401596

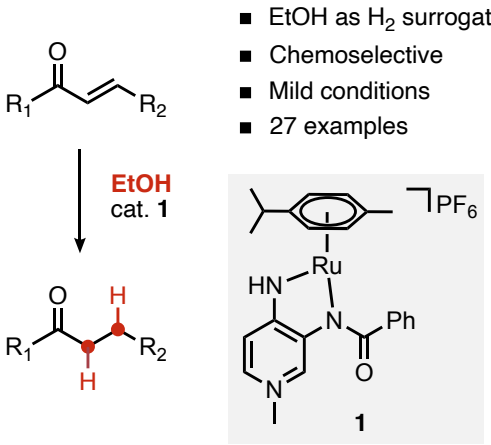

III.1. Abstract

The use of EtOH as hydrogen donor is remarkably underexplored in transfer hydrogenation reactions, even though EtOH represents an appealing hydrogen source. With the cationic ruthenium complex [Ru(PYA)(cymene)]$^+$, **1**, containing a N,N'-bidentate amino-functionalized pyridinium amidate (PYA) ligand as catalyst precursor, we here demonstrate the first example of chemoselective room temperature transfer hydrogenation of the C=C bond in α,β-unsaturated ketones using EtOH as benign hydrogen source to yield a variety of functionalized ketones. The reaction proceeds under mild conditions with K_2CO_3 as base and conveniently at room temperature. A broad substrate scope, including various functionalized α,β-unsaturated carbonyl groups, demonstrates the general applicability of this method. Preliminary mechanistic studies suggest the formation of an alkoxide complex [**1**]–OEt as an initially formed species, and the requirement for EtOH to induce hydride transfer, suggesting a protic activation of the catalyst.

III.2. Introduction

Functionalized ketones are valuable starting materials for chemical synthesis, especially due to the wide variety of transformation methodologies available from carbonyl groups.[1] The selective reduction of the C=C bond in α,β-unsaturated ketones is one of the most atom-economic and efficient approaches to accessing these functionalized ketones (Scheme III.1.a). Conventional hydrogenation methods use metal reductants and proceed via an electron-transfer protocol.[2–8] However, metal leaching, safety issues, and long reaction times have been associated with this methodology and constitute a persistent problem, together with the environmental issues due to stoichiometric amounts of metal hydride waste. While transition metal-catalyzed hydrogenation with H_2 gas offers greater control over reaction conditions and selectivity, this method requires the use of pressurized gas with the hazards related to its handling.[9–20]

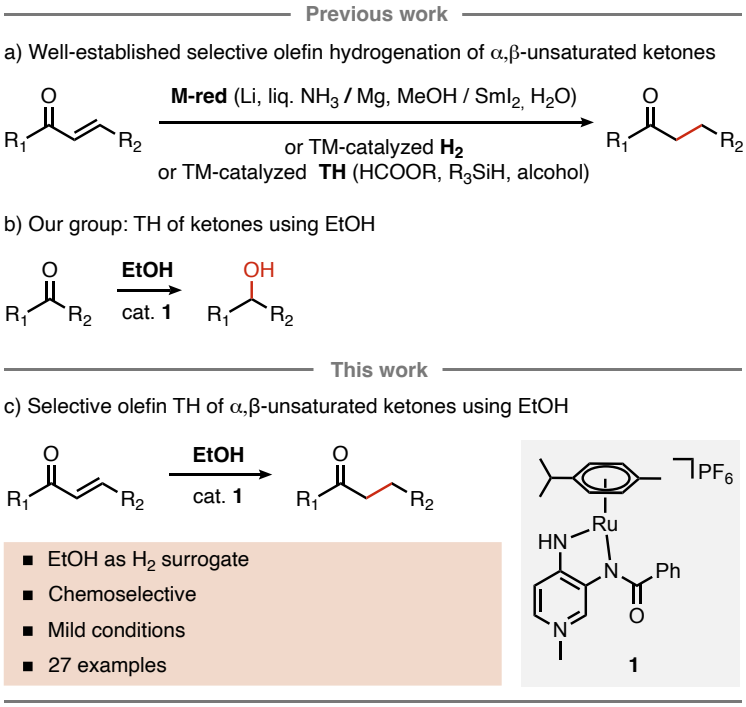

Scheme III.1. Selective reduction of C=C bond of α,β-unsaturated carbonyls.

Over the past years, transfer hydrogenation has emerged as a more environmentally benign alternative to these conventional hydrogenation methods, using formic acid, silane, or *iso*-propanol as the most common H_2 surrogates.[21–30] While selective transfer hydrogenation even of unsaturated carbonyl substrates is a well-established method by now,[31–44] recent focus has been directed toward the use of primary alcohols as H_2 source, in particular methanol.[45–48] However, hydrogen transfer from methanol typically suffers from long reaction times,[45] high reaction temperatures that require pressure equipment,[46,47] or limited substrate scope.[48] In contrast, the use of ethanol in transfer hydrogenation processes has been much less studied, which may be rationalized by its unfavorable redox potential and the generation of reactive intermediates, which have the potential for catalyst poisoning.[49] However, the lower dehydrogenation energy of ethanol compared to methanol (ΔH

(EtOH) = 68 kJ mol^{-1} vs. ΔH (MeOH) = 84 kJ mol^{-1})[50,51] underpins its potential as an appealing hydrogen source in combination with other major benefits, as EtOH is widely abundant, environmentally friendly, and mainly produced from biomass through the refining of renewable fuels.[52,53] Despite these advantages, examples of selective olefin transfer hydrogenation of α,β-unsaturated ketones remain scarce and limited to only a few substrates,[54–58] since typically, carbonyl reduction is competitive.[38,59,60]

We previously reported efficient transfer hydrogenation of ketones using EtOH as a hydrogen source promoted by ruthenium complex **1** containing a N,N'-bidentate pyridinium amidate (PYA) ligand (Scheme III.1.b).[61] During the optimization of the reaction conditions, we noted the presence of α-alkylated products stemming from aldol condensation between the ketone substrate and the acetaldehyde product formed from EtOH dehydrogenation. These results prompted us to further investigate the potential of complex **1** in catalyzing the transfer hydrogenation of related α,β-unsaturated carbonyl substrates. Herein, we describe a practical method to achieve selective olefin transfer hydrogenation of α,β-unsaturated ketones under mild conditions without reducing the carbonyl group (Scheme III.1.c).

III.3. Results and Discussion

Optimization of reaction conditions. Using *trans*-chalcone **2a** as model substrate, we initially evaluated the reactivity of complex **1** in the selective olefin hydrogenation of unsaturated ketones to investigate the influence of commercially available and inexpensive alcohols (Table III.1). When the reaction was performed under standard transfer hydrogenation conditions, that is, KOH and *i*PrOH as solvent and hydrogen source at 110 °C, the fully reduced saturated alcohol **5a** was obtained as the major product after 1 h (entry 1). Transfer hydrogenation also occurred when using primary alcohols as hydrogen source instead of *i*PrOH. Thus, reaction in EtOH yielded the saturated ketone **3a** in 77% yield together with some fully hydrogenated **5a** (23%) after 1 h, while in MeOH, 82% of the saturated ketone **3a** were obtained together with some unreacted starting material (entries 2–3). In contrast, using glycerol as hydrogen source gave only poor conversion (entry 4). Decreasing the temperature to 40 °C was beneficial for selectivity in both *i*PrOH and EtOH, with only 39% and 5%, respectively, of fully hydrogenated alcohol **5a** formed after 1 h (entries 5–7). However, the yield of product **3a** dropped to 26% using MeOH under the same conditions (entry 8). When the reaction temperature was further decreased to 25 °C, remarkably complex **1** catalyzed the transfer hydrogenation in EtOH more efficiently than in *i*PrOH, yielding the desired product **3a** in 80% and 40% yield, respectively (entries 9–10). Increasing the reaction time to 75 min and 2 h was accompanied by an increase of the conversion to 98% and >99%, respectively, with the appearance of just traces (4%) of the fully saturated product **5a** after 2 h (entries 11–12). Note that despite the activity of complex **1** in transfer hydrogenation of ketones,[61] no formation of the allylic alcohol product **4a** was observed, independent of the alcohol as hydrogen source or the reaction temperature.

Table III.1. Transfer hydrogenation catalyzed by **1** with different alcohol solvents at variable temperatures.[a]

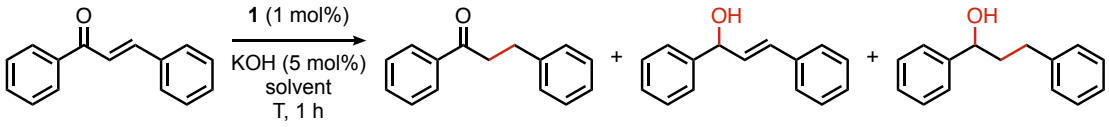

2a **3a** **4a** **5a**

entry	solvent	temperature (°C)	conversion (%)[b]	yield **3a**/**4a**/**5a** (%)[b]
1	iPrOH	110	>99	5:0:95
2	EtOH	110	>99	77:0:23
3	MeOH	110	82	82:0:0
4[c]	glycerol	120	11	11:0:0
5	iPrOH	40	>99	61:0:39
6[d]	iPrOH	40	>99	97:0:0
7	EtOH	40	>99	95:0:5
8	MeOH	40	26	26:0:0
9	iPrOH	25	55	40:0:0
10	EtOH	25	82	80:0:0
11[e]	EtOH	25	98	98:0:0
12[f]	EtOH	25	>99	96:0:4

[a]Reaction conditions: *trans*-chalcone (0.5 mmol), KOH (5 mol%), complex **1** (1 mol%), solvent (2.5 mL), N_2, 1 h, closed system. [b]Conversions and yields determined by ^{1}H NMR spectroscopy relative to an internal standard (1,3,5-trimethoxybenzene) from duplicate runs. [c]6 h reaction time. [d]10 min reaction time. [e]1 h 15 reaction time. [f]2 h reaction time.

We then examine the influence of different bases on the reaction (Table III.2). Replacing KOH with NaOH or LiOH slightly improved the yield from 80% to 82% and 86% respectively (entries 2–3), indicative of a small cation effect. The yield was further increased to 96% using K_2CO_3 as a base (entry 5), while other carbonate bases gave poorer conversion (entries 8–10). This difference in activity within the series of carbonate bases has been attributed to solubility differences of these bases in EtOH. Increasing the amount of K_2CO_3 to 10 mol% was deleterious and lowered the yield of **3a** to only 78% (entry 6), which supports the relevance of mild conditions for selective and efficient hydrogen transfer (see also Table III.1). An increase of the volume of EtOH to 5 mL was also beneficial, and yielded product **5a** in 98% yield after 1 h (entry 7). The use of a stronger base such as NaO*t*Bu and KO*t*Bu gave a similar yield of 95%, however producing also some over-reduced alcohol (4%, entries 11–12). No conversion was observed, however, when using NEt_3 as a mild organic base (entry 13). Noteworthy, a decrease of the catalyst loading of complex **1** to 0.1 mol% yielded quantitative conversion to the desired ketone **3a** within 24 h (entry 14).

Table III.2. Effect of base in the olefin hydrogenation of the unsaturated ketone **2a**.[a]

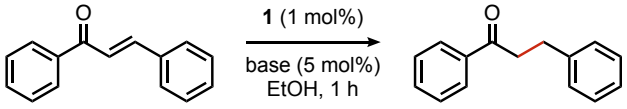

2a **3a**

entry	base (mol %)	yield **3a** (**5a**) (%)[b]
1	KOH (5)	80
2	NaOH (5)	82
3	LiOH (5)	86
4	Li_2CO_3 (5)	< 2
5	K_2CO_3 (5)	96
6	K_2CO_3 (10)	78
7[c]	K_2CO_3 (5)	98
8	Na_2CO_3 (5)	41
9	Cs_2CO_3 (5)	83
10	$(NH_4)_2CO_3$ (5)	< 2
11	*t*BuONa (5)	95
12	*t*BuOK (5)	95 (4)
13	NEt_3 (5)	< 2
14[d]	K_2CO_3 (5)	>98

[a]Reaction conditions: *trans*-chalcone **2a** (0.5 mmol), base (x mol%), complex **1** (1 mol%) in EtOH (2.5 mL), 25 °C, under N_2, 1 h. [b]Yields determined by ^1H NMR spectroscopy relative to 1,3,5-trimethoxybenzene as internal standard, all values average of duplicate runs; yields of **5a** always <2% unless specified in parenthesis. [c]5 mL EtOH used. [d]Catalyst **1** at 0.1 mol%, 24 h.

Control experiments indicated no conversion if the reaction is run either in the absence of a base or without complex **1** (Table III.3, entries 1–2). Similarly, the commercially available $[RuCl_2(p\text{-cymene})]_2$ was inactive under the standard conditions, underpinning the importance of the PYA ligand (entry 3). Interestingly, under harsh conditions (110 °C, 48 h) complex **1** was slightly active under base-free conditions, yielding the desired product **3a** in 28% yield (entry 4). When the transfer hydrogenation was performed under an atmosphere of air instead of N_2, the yield dropped from 96% to 54% and the color of the reaction mixture changed from orange to black, indicative of complex decomposition (entry 5).

Table III.3. Control experiments.[a]

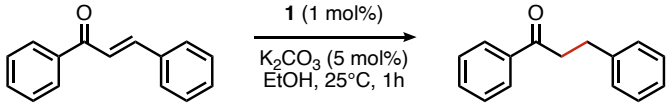

2 **3a**

entry	deviation from standard conditions	yield **3a** (%)[b]
1	No base	<2
2	No ruthenium source	<2
3	[Ru(*p*-cymene)Cl_2]$_2$	<2
4	No base, 110°C, 48h	28
5	Reaction performed under air	54

[a]Standard conditions: *trans*-chalcone (0.5 mmol), K_2CO_3 (5 mol%), complex **1** (1 mol%) in EtOH (2.5 mL), 25°C, under N_2. [b]Yields determined by ^{1}H NMR spectroscopy relative to an internal standard (1,3,5-trimethoxybenzene) from duplicate runs.

Substrate scope and limitations. To demonstrate the general applicability of complex **1**, various α,β-unsaturated ketones were tested using the standard conditions (Scheme III.2). Modulation of the *para*-substituent at the carbonyl (compounds **2a–2d**) and the olefinic end (compounds **2e–2h**) of *trans*-chalcone resulted in excellent yield for both electron-withdrawing and electron-donating groups. Analysis of the initial rates for the conversion of *para*-substituted ketones **2a–2h** revealed a positive linear correlation with the Hammett parameter σ_p ($R^2 > 0.92$, Figures III.1 and III.2). Positive ρ values of +0.95 and +0.25 were deduced for the substitution at the olefinic (**2e–2h**, Table III.4) and ketonic carbonyl side (**2a–2d**, Table III.5), suggesting the build-up of a negative charge in the transition state. This analysis is commensurate with hydride transfer to the substrate as rate-limiting step, as frequently observed in transfer hydrogenation.[49,62,63] The more prominent electronic effect for olefinic *para*-substituted chalcones **2e–2h** is consistent with a direct hydride transfer to the β-carbon of the enone system.

Table III.4. Hammett analysis with *para*-substitution on olefinic scaffold.

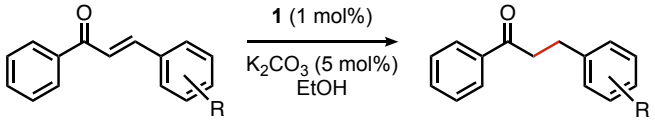

R	$k_X \times 10^{-3}$ (h^{-1})	k_X/k_H	$\log(k_X/k_H)$	σ_p[64]	ρ
Cl	1.04	1.41	0.15	0.23	+0.95 R^2 = 0.97
NHCOMe	0.63	0.85	-0.07	0	
H	0.74	0	0	0	
Ph	0.68	0.92	-0.04	-0.01	
OMe	0.35	0.47	-0.33	-0.27	

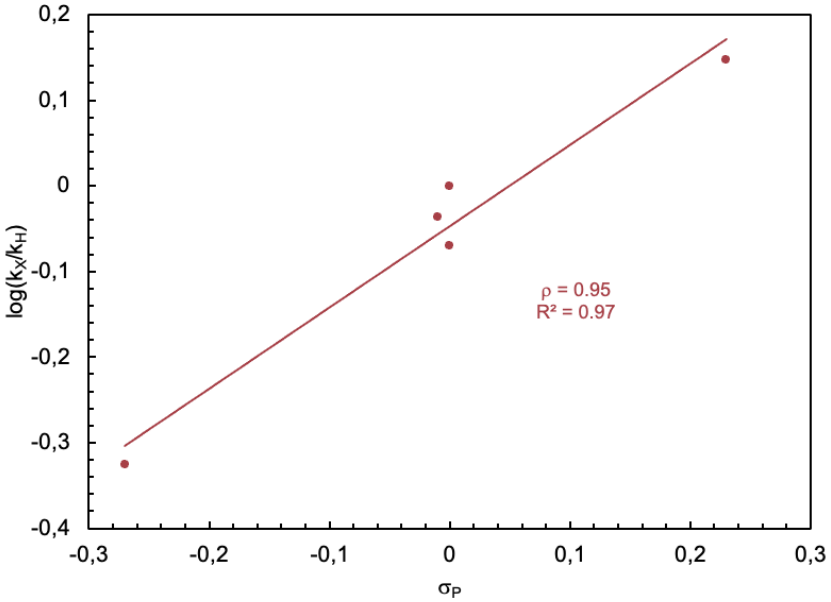

Figure III.1. Hammett plot for the transfer hydrogenation of chalcones **2a, 2e-2h**.

Table III.5. Hammett analysis with *para*-substitution on carbonyl scaffold.

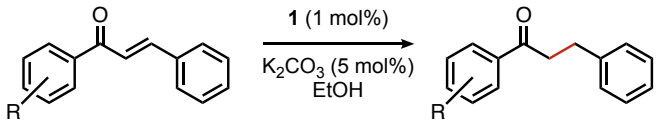

R	$k_X \times 10^{-3}$ (h^{-1})	k_X/k_H	$\log(k_X/k_H)$	σ_p[64]	ρ
CF_3	0.93	1.26	0.10	0.54	
Cl	0.87	1.18	0.07	0.23	+0.25
H	0.74	1	0	0	R^2 = 0.92
OMe	0.58	0.78	-0.11	-0.27	

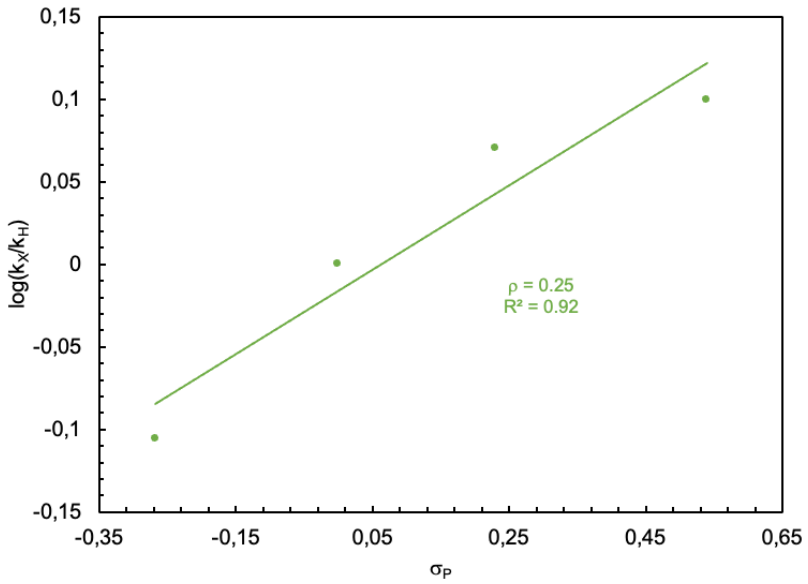

Figure III.2. Hammett plot for the transfer hydrogenation of chalcones **2a-2d**.

High conversion and selectivity was also observed for bulkier substrates such as naphthalene-chalcone **2i** and the biologically active metochalcone **2j**, for substrates containing heteroatoms as furyl-chalcone **2k** or methylenedioxy-chalcone **2l**, and also ferrocene-containing chalcone **2m**, which afforded the corresponding saturated ketones in high yields within 1–6 h. Noteworthy, NH or OH-containing substrates were not tolerated, as exemplified by compounds **2n** and **2o** with no conversion observed after 24 h. This low activity is probably caused by quenching of the base by these acidic substituents. In comparison, compound **2p**, which is identical to **2o** yet lacking -OH functionality, was fully converted within 2 h. Therefore, appropriate protecting group strategies should be applied for substrates containing acidic -OH or -NH groups (see *e.g.* substrate **2j**).

Scheme III.2. Substrate scope and limitation of ruthenium-catalyzed chemoselective transfer hydrogenation of α,β-unsaturated ketones.[a]

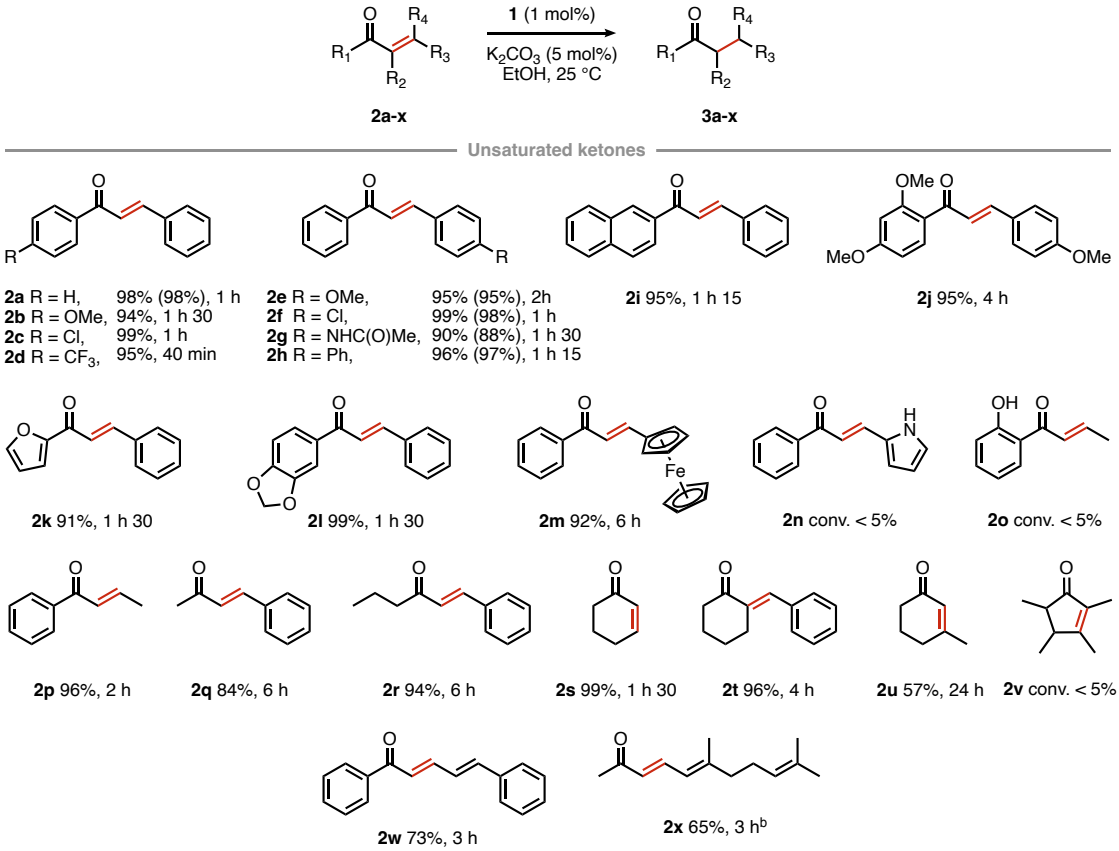

[a]Reaction conditions: substrate (0.5 mmol), K_2CO_3 (5 mol%), complex **1** (1 mol%) in EtOH (5 mL), 25 °C, N_2; yields determined by ^1H NMR spectroscopy relative to an internal standard (1,3,5-trimethoxybenzene or mesitylene) from duplicate runs, isolated yields in parenthesis. [b]Reaction performed at 60 °C.

Introduction of alkyl substituents at the ketone side substantially decreased the rate of the reaction, requiring 6 h reaction time to obtain acceptable yields (compounds **2q–r**). An exception are cyclic substrates such as cyclohexenone **2s**, which is converted within 1 h 30. Benzylidenecyclohexanone **2t**, substituted at the olefinic α-position, was fully converted in 4 h, though introduction of an additional substituent at the olefinic β-position as in **2u** considerably reduced activity, affording the saturated ketone in 57% yield after 24 h. Similarly, fully substituted cyclopentenone **2v** did not undergo any transfer hydrogenation even after 24 h. The conjugated diene **2w** was converted to the desired product in 73% after 3 h, but was accompanied with a mixture of isomerization products.

Similar reactivity was observed using pseudoionone **2x** as substrate, an intermediate in the industrial synthesis of vitamin A, that was hydrogenated to the desired geranylacetone **3x** with an acceptable yield of 65% within 3 h upon increasing the reaction temperature to 60°C. Notably, this site-selective hydrogenation procedure offers an attractive alternative to the direct hydrogenation. For example, a rhodium-xantphos (1 mol%) was recently shown to catalyze this transformation, albeit under highly pressured H_2 at 1000 psi.[11] The hydrogen transfer from EtOH is considerably less hazardous.

Complex **1** is also active in the transfer hydrogenation of olefins when conjugated to electron-withdrawing groups other than ketones, though these substrates generally required an increased reaction temperature of 60 °C (Scheme III.3). Thus, the alkene in diethylfumarate **2y,** which is conjugated to two electron-withdrawing ethyl ester groups, was hydrogenated quantitatively within 15 min. Replacement of one ester group by an alkyl or benzyl substituent drastically reduced the activity and afforded **3z** and **3aa** in only 20% and 52% yield, respectively. Hydrogenation of unsaturated lactones such as coumarin **2ab** was also successful, though it was accompanied by ring opening via trans-esterification and gave ethyl melilotate **3ab** in 93% after 6 h. Similar ring opening was observed previously[57] and represents one of the limitations of transfer hydrogenation of α,β-unsaturated esters under basic conditions. Olefins conjugated to amides were also converted, yielding the corresponding product **3ac** in 50% yield after 24 h (*cf.* the corresponding ketone **2p** is converted essentially quantitatively in 2 h at 25°C). Noteworthy, selective hydrogenation of the aldehyde rather than the olefinic C=C bond was observed for cinnamaldehyde **2ad.**[65]

Non-activated olefins such as styrene (**2ae**) were, however, not hydrogenated under these reaction conditions (Scheme 3, bottom). Moreover, olefins conjugated to electron-withdrawing cyano- or nitro-groups (**2af, 2ag**) also did not react, suggesting that the carbonyl group is required for the reaction to proceed. Even though α,β-unsaturated carboxylic acids such as **2ah** are not hydrogenated, presumably because the base required for transfer hydrogenation is neutralized by the acidic substrate, hydrogenation of the ester analogue such as **2y** followed by hydrolysis is possible.

Scheme III.3. Substrate scope and limitation of ruthenium-catalyzed transfer hydrogenation of olefins conjugated to electron-withdrawing groups other than a ketone.[a]

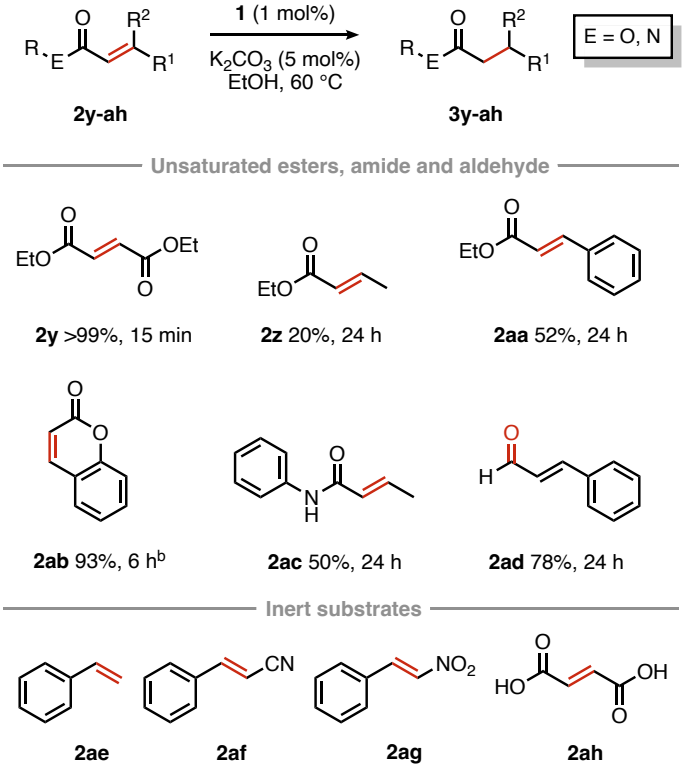

[a]Reaction conditions: substrate (0.5 mmol), K_2CO_3 (5 mol%), complex **1** (1 mol%) in EtOH (5 mL), 60 °C, N_2; yields determined by ^1H NMR spectroscopy relative to 1,3,5-trimethoxybenzene as internal standard, averaged from duplicate runs. [b]Olefin transfer hydrogenation with ring opening to form the ethyl ester.

Sequential reduction of α,β-unsaturated ketones. The selectivity of complex **1** towards olefin hydrogenation without affecting the carbonyl functionality is obviously dependent on several factors, including the reaction conditions, the hydrogen source, and the substrate reactivity. High temperatures tend to lead to over-reduction, while room temperature (RT) or only slightly elevated temperatures produce the saturated ketone in high selectivity. Likewise, readily dehydrogenated *i*PrOH as hydrogen source leads to fast hydrogenation and produces considerable amounts of fully hydrogenated alcohol, while MeOH, which is more difficult to dehydrogenate, leads to incomplete reactions (Table III.1). In contrast, EtOH offers an advantageous compromise to keep both reactivity and selectivity of complex **1** high. Such a model was supported by performing the transfer hydrogenation of *trans*-chalcone **2a** over an extended period of time. These experiments revealed a sequential hydrogenation involving first the olefinic π-bond to yield **3a**, and after full conversion also the carbonyl π-bond to produce the saturated alcohol **5a** (Figure III.3.a). The reaction rates for the reduction of the C=C and C=O double bonds are drastically different, with quantitative conversion of the *trans*-chalcone to the desired ketone in 1 h at RT, while ketone reduction reached only 59% after an overall reaction time of 24 h (Figure III.3.b). Using directly the saturated ketone **3a** as substrate yielded compound **5a** in only 11% after 1 h, confirming the much slower rate of ketone *vs* olefin hydrogenation (Figure III.3.c). An increase of the reaction temperature to 60 °C yielded the fully

saturated product **5a** in 87% after 24 h, demonstrating that forcing conditions allow for complete hydrogenation. This marked difference in rate is a rather unique characteristic of complex **1**, as many other catalysts display a higher affinity for ketone reduction,[54] or feature similar rates for both C=C and C=O bond hydrogenation and lead to mixtures of products.[38,59,60] The rate difference was also observed in intermolecular competition experiments. Under standard conditions, transfer hydrogenation with equimolar quantities of acetophenone and *trans*-chalcone as substrates resulted in the selective olefin hydrogenation of the *trans*-chalcone and gave compound **3a** in 95% yield after 2 h, with full recovery of acetophenone (Figure III.3.d). The reaction was slightly slower than in the absence of acetophenone, but fully selective towards olefin hydrogenation, demonstrating the preference of the catalyst derived from complex **1** to reduce C=C bonds over carbonyl hydrogenation.

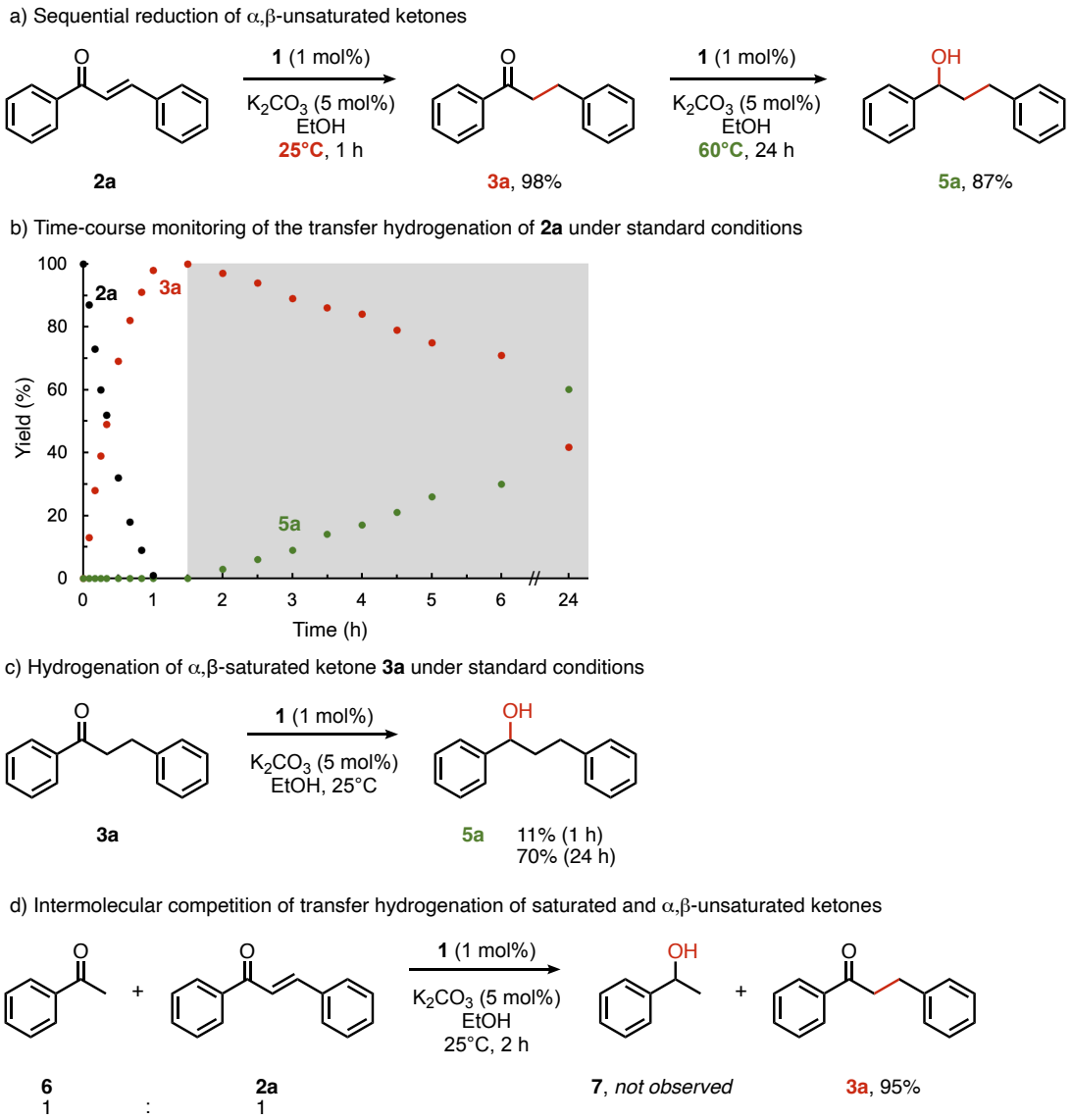

Figure III.3. Time-dependent and chemo-selective transfer hydrogenation of α,β-unsaturated ketones using EtOH. Reaction conditions: substrate (0.5 mmol), K_2CO_3 (5 mol%), complex **1** (1 mol%) in EtOH (5 mL), N_2; yields determined by ^1H NMR spectroscopy relative to 1,3,5-trimethoxybenzene as internal standard from duplicate runs.

Even though allylic alcohol **4a** was not observed by ^{1}H NMR spectroscopy under the standard conditions, such species are often described as reaction intermediate in the transfer hydrogenation of unsaturated ketones.[59,60,66] We tested this hypothesis by using allylic alcohol **4a** directly as substrate under the standard conditions (Scheme III.4). Only 5% of isomerized ketone **3a** was obtained after 1 h, while *trans*-chalcone yielded **3a** in 98% under the same conditions. These conversions therefore do not support the formation of allylic alcohol as an initial, short-lived product that then rapidly isomerizes to **3a**, corroborating direct hydride attack at the enone β-carbon as deduced from the Hammett analysis (*vide supra*). Upon extending the reaction time to 24 h, slow isomerization was noted (29%), together with some hydrogenation to the saturated alcohol **5a** (28%).

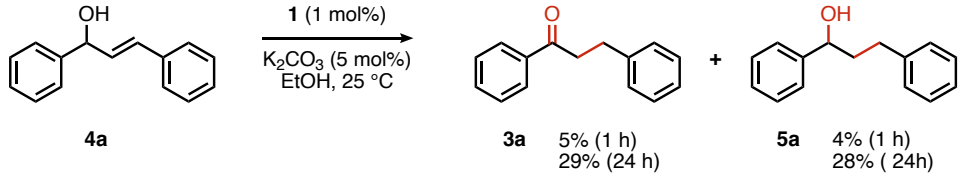

Scheme III.4. Isomerization of allylic alcohol **4a** catalyzed by complex **1**.

Similar double bond migration was catalyzed by complex **1** under transfer hydrogenation conditions also with simple alkenes. For example, 1-hexene isomerized to a mixture of 2- and 3-hexenes upon heating to 60 °C for 48 h, without any hydrogenation of the double bond (Scheme III.5).

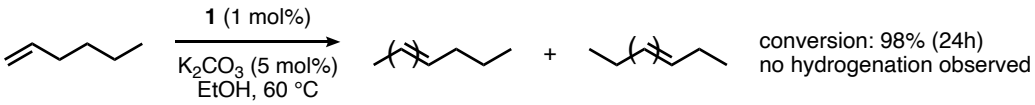

Scheme III.5. Isomerization of hex-1-ene catalyzed by complex **1**.

Migration over several bonds is slow, however. For example, the homoallylic alcohol **8** was converted only in 11% to the corresponding propyl phenyl ketone **9** at 60 °C and after 24 h (Scheme III.6).

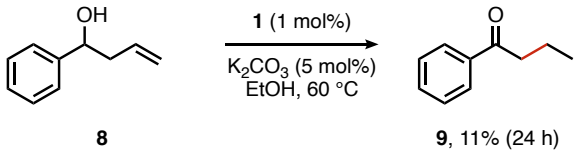

Scheme III.6. Double bond migration catalyzed by complex **1**.

Further mechanistic investigations aimed at probing dehydrogenation of EtOH to form H_2 as the effective reducing agent. While complex **1** as the pre-catalyst is unreactive towards H_2 (Scheme III.7.a),[61] the active catalyst may show distinct reactivity. Thus, transfer hydrogenation of **3a** was performed under standard conditions, though after 15 min (ca. 25% conversion), the reaction mixture was saturated with H_2 (Scheme III.7.b). No changes in the conversion rates were noted, and final yields were identical, indicating that H_2 exerts neither a beneficial nor inhibiting effect and that the active catalyst derived from **1** is inert towards H_2. These results indicate that the mechanism does

not involve sequential hydrogenation of EtOH followed by hydrogenation of the substrate with the putative formed dihydrogen.

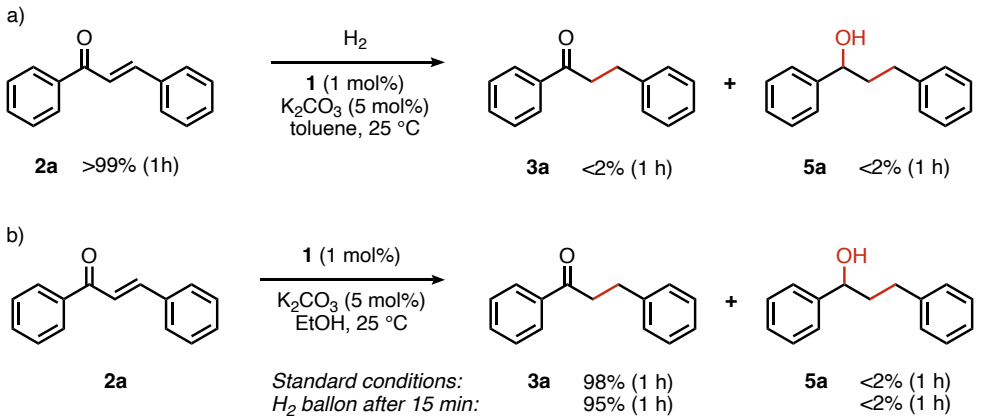

Scheme III.7. a) Hydrogenation of **2a** in the presence of H_2 catalyzed by complex **1**. b) Transfer hydrogenation of **2a** in the presence of H_2 catalyzed by complex **1**.

Stoichiometric reactions to identify the catalytically active species. In an attempt to identify the catalytically active species, a reaction of complex **1** with a large excess of EtOH (1000 eq) and KOH (5 eq) was monitored by NMR spectroscopy in CD_2Cl_2 (Figure III.4). This reaction gave a white precipitate and a new ruthenium species in solution that was silent in the ^{19}F NMR spectrum, suggesting precipitation of a PF_6^- salt.[67]

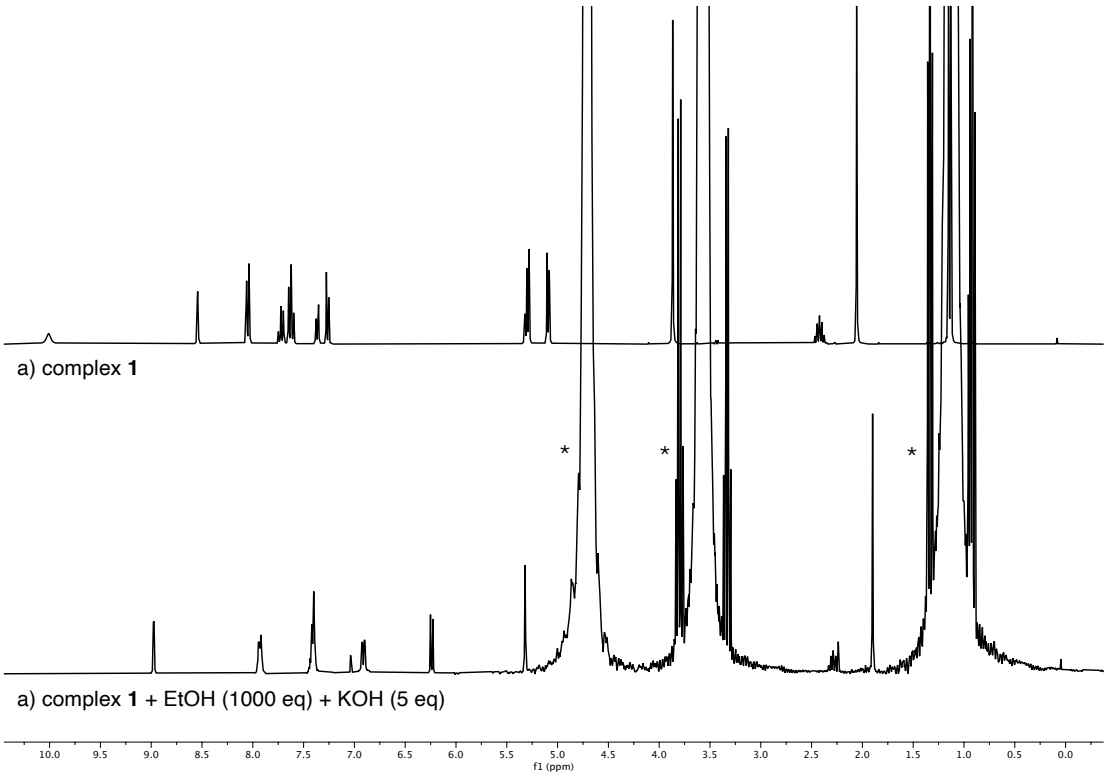

Figure III.4. Stacked solution ^1H NMR spectra (CD_2Cl_2, 298 K, 300 MHz) of a) complex **1** and b) after addition of EtOH (1000 eq) and KOH (5 eq) (* = EtOH), showing quantitative formation of [**1**]–OEt.

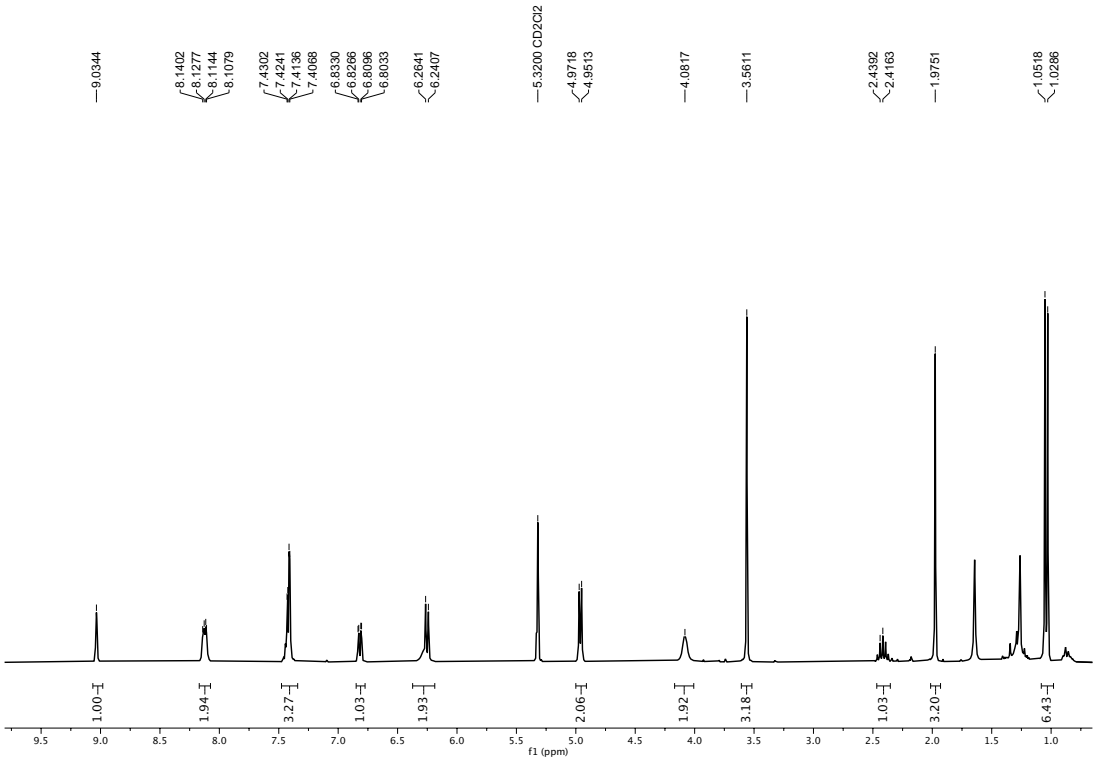

Figure III.5. Solution ^{1}H NMR spectra (CD_2Cl_2, 298 K, 300 MHz) of [**1**]–Cl complex.

The new species in solution featured chemical shifts of the PYA and the cymene ligands that are very similar to those observed in the chloride salt of **1** (Figure III.5),[61] thus suggesting the presence of a coordinated anion at the ruthenium center. As no resonance was observed in the hydridic region, this new species was tentatively attributed to the neutral complex [**1**]–OEt, even though the OEt resonances were not detectable due to the presence of a large excess of EtOH.[68] In support of this assignment, reaction of complex **1** directly with NaOEt in CD_3OD gave the same species, although the resonances were slightly shifted due to the change of solvent, or due to the formation of the methoxide analogue [**1**]–OMe (Figure III.6). Further analysis of the species was prevented by the lability of the complex. For example, concentration of the mixture afforded the cationic complex **1** again. Likewise, MS analysis only gave signals that were consistent with the starting material.

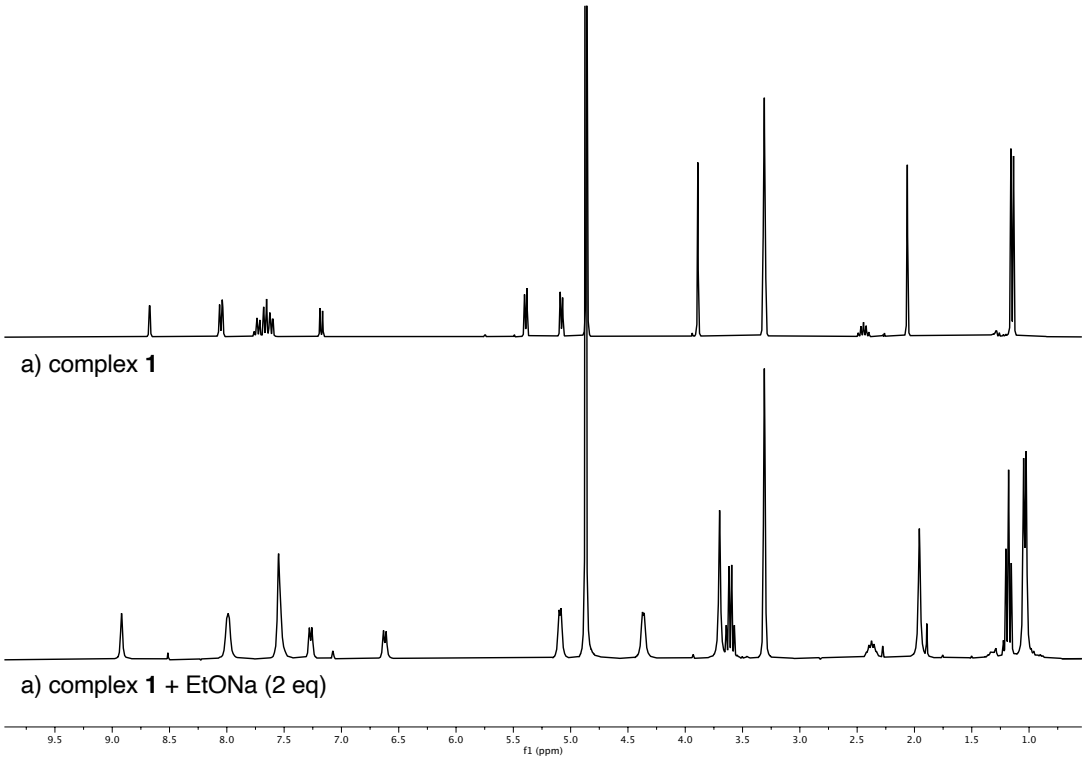

Figure III.6. Stacked solution ^{1}H NMR spectra (MeOD, 298 K, 300 MHz) of a) complex **1** followed by the addition of EtONa (2 eq) at rt.

Addition of the *trans*-chalcone **2a** to the alkoxide complex [**1**]–OEt did not lead to any reaction according to NMR spectroscopy, which only showed the superimposed signals of both species (Figure III.7). These observations suggest that the ethoxy group cannot undergo β-hydrogen elimination in [**1**]–OEt, and further activation is needed. Indeed, addition of EtOH induced immediate transfer hydrogenation, indicating a protic activation of the catalyst (Figure III.8). Such behaviour is consistent with the beneficial catalytic effect observed when increasing the volume of EtOH (*cf* Table III.2). Speculatively, such activation may be rationalized by PYA ligand protonation, which reduces its donor strength and may either lead to transient decoordination or to a breakdown of π-bonding. Either of these events is supposed to facilitate β-hydrogen elimination and formation of the putative hydride as reactive species that induces the reduction of the C=C bond. Attempts to induce a similar activation with $(NH_4)I$ instead of EtOH induced a color change of the solution from red to green, however, the NMR spectra only revealed signals characteristic for [**1**]–OEt, and no *trans*-chalcone hydrogenation was detected. Speculatively, formation of the reactive hydride species is quenched by the presence of acidic NH_4^+ faster than reaction with the substrate. The appearance of a Ru–H species was observed previously in small quantities when reacting **1** with NaOEt in the presence of 15 eq. EtOH, though it is unclear whether this species corresponds to a short-lived intermediate that rapidly reacts with the substrate, or if this metal hydride is an off-cycle species resulting from decomposition or deactivation. With EtOH in large quantities as used here, no hydride species was detected at any time point of the reaction.

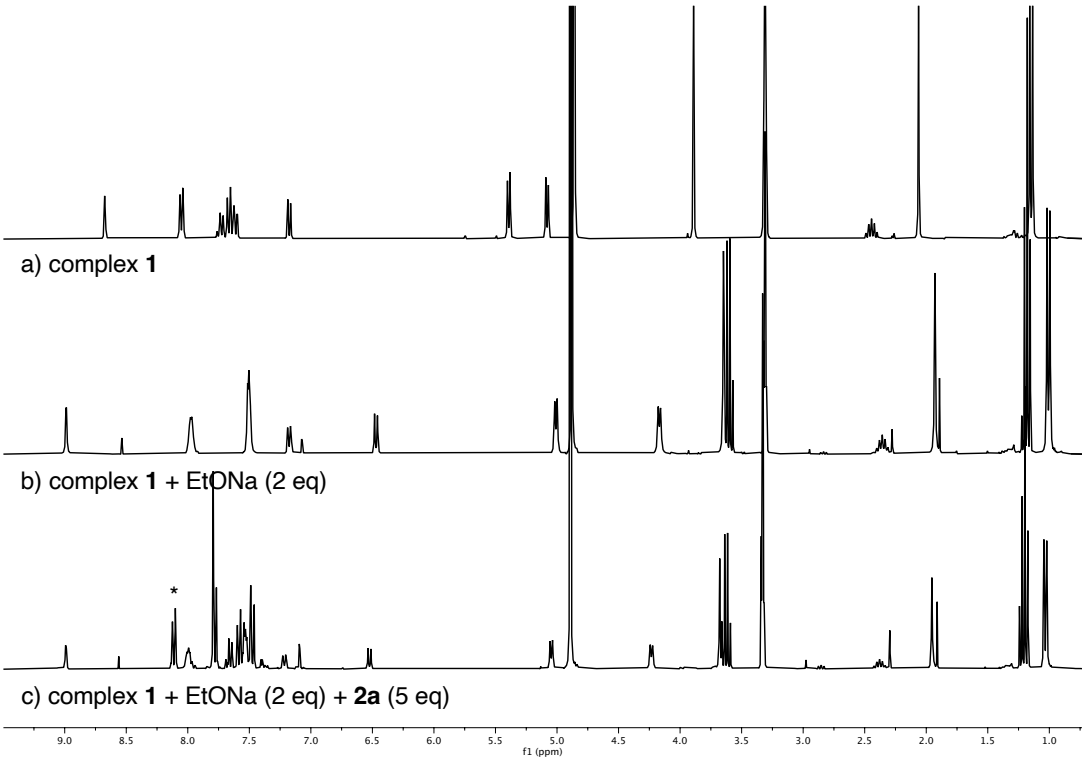

Figure III.7. Stacked solution ^{1}H NMR spectra (MeOD, 298 K, 300 MHz) of a) complex **1** followed by successive addition of b) EtONa; c) *trans*-chalcone **2a** (* = **2a**) showing no hydrogenated product.

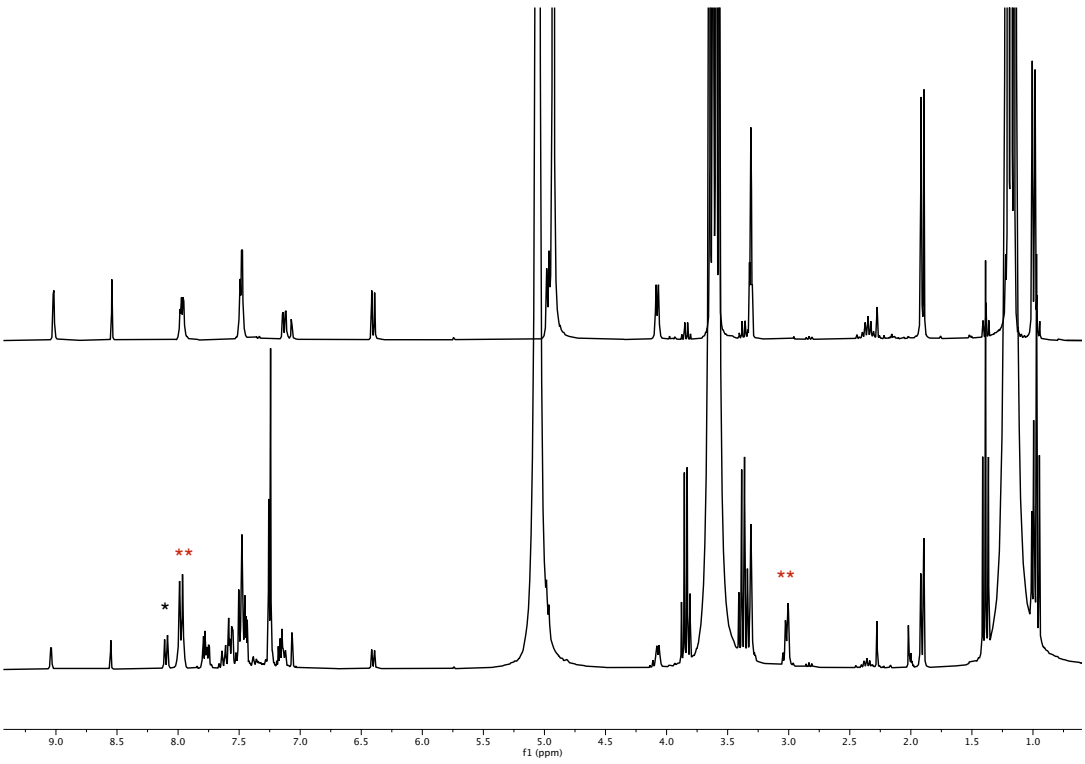

Figure III.8. Stacked solution ^{1}H NMR spectra (MeOD, 298 K, 300 MHz) of a) complex [**1**]–OEt formed *in situ* followed by addition of b) *trans*-chalcone **2a** (5 eq, * = **2a**) and EtOH (500 eq), resulting in the formation of the corresponding product **3a** (**= **3a**).

III.4. Conclusions

This work presents a highly effective and environmentally friendly method for the chemoselective olefin transfer hydrogenation of α,β-unsaturated carbonyl compounds using ethanol as a hydrogen source. The use of a N,N'-bidentate pyridinium amidate (PYA) ruthenium(II) complex demonstrated excellent activity for a wide range of functionalized α,β-unsaturated carbonyl substrates, operating at low temperature (25-60°C) in the presence of catalytic amount of common laboratory base. Further efforts are underway to elucidate the implication of the ligand system and achieve higher activity and selectivity.

III.5. Experimental

III.5.1. General. All reactions were performed under air unless stated otherwise. Experiments under inert atmosphere were carried out using standard Schlenk techniques under an N_2 atmosphere and dry deoxygenated solvents. Dry solvents were taken from a solvent purification system (SPS), stored over molecular sieves for at least 2 days, and degassed by N_2 gas bubbling for 30 min. Absolute-grade solvents were used for the catalytic runs without further purification. The synthesis of complex one has been previously described.[61] All other reagents were purchased from commercial suppliers and used without further purification unless stated otherwise.

III.5.2. Synthesis of starting α,β-unsaturated carbonyls

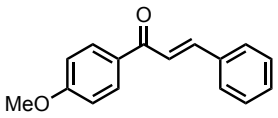

1-(4-methoxyphenyl)-3-phenylprop-2-en-1-one (2b).[69] To benzaldehyde (0.51 mL, 5 mmol, 1 eq) and 1-(4-methoxyphenyl)ethan-1-one (0.69 mL, 5 mmol, 1 eq) dissolved in EtOH (25 mL) was added dropwise a NaOH aqueous solution (1.5 M, 5 mL) at room temperature. After 16 h, the resulting mixture was neutralized with 2M HCl solution. The resulting precipitate was filtered and recrystallized from EtOH to afford the desired compound **2b** (1.12 g, 4.7 mmol, 94%).

^{1}H NMR (300 MHz, 298 K, $CDCl_3$) δ 8.07 (dt, *J* = 9.0, 2.8 Hz, 2H), 7.83 (d, *J* = 15.7 Hz, 1H), 7.70–7.63 (m, 2H), 7.57 (d, *J* = 15.6 Hz, 1H), 7.47–7.40 (m, 3H), 7.01 (dt, *J* = 8.9, 2.0 Hz, 2H), 3.91 (s, 3H). **^{13}C{^{1}H} NMR ($CDCl_3$, 298 K, 75 MHz):** δ 188.79, 163.54, 144.04, 135.20, 131.21, 130.92, 130.43, 129.03, 128.47, 122.00, 113.96, 55.60.

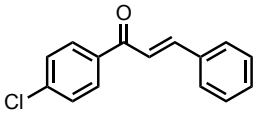

1-(4-chlorophenyl)-3-phenylprop-2-en-1-one (2c).[69] To benzaldehyde (0.51 mL, 5 mmol, 1 eq) and 1-(4-chlorophenyl)ethan-1-one (0.65 mL, 5 mmol, 1 eq) dissolved in EtOH (25 mL) was added

dropwise a NaOH aqueous solution (1.5 M, 5 mL) at room temperature. After 16 h, the resulting mixture was neutralized with 2M HCl solution. The resulting precipitate was filtered and recrystallized from EtOH to afford the desired compound **2c** (1.03 g, 4.2 mmol, 85%).

^{1}H NMR (300 MHz, 298 K, $CDCl_3$) δ 7.97 (dt, *J* = 8.6, 2.4 Hz, 2H), 7.82 (d, *J* = 15.7 Hz, 1H), 7.71–7.59 (m, 2H), 7.5 –7.39 (m, 6H). **^{13}C{^{1}H} NMR ($CDCl_3$, 298 K, 75 MHz):** δ 189.19, 145.36, 139.24, 136.53, 134.72, 130.76, 129.93, 129.03, 128.97, 128.53, 121.53.

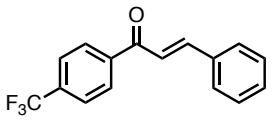

3-phenyl-1-(4-(trifluoromethyl)phenyl)prop-2-en-1-one (2d).[70] NaOH (220 mg, 5.5 mmol, 1.0 eq) was dissolved in H_2O (10 mL) and added at 0°C to a stirred solution of 4-trifluoromethyl-acetophenone (941 mg, 5.0 mmol, 1.0 eq) in EtOH (20 mL). Benzaldehyde (0.51 mL, 5.0 mmol, 1.0 eq) was added dropwise after 5 min and the reaction mixture was stirred for 16 h at room temperature. The resulting precipitate was collected by filtration and washed with water to afford the desired compound **2d** (1.21 g, 4.4 mmol, 87%).

^{1}H NMR (300 MHz, 298 K, $CDCl_3$) δ 8.11 (d, *J* = 7.9 Hz, 2H), 7.84 (d, *J* = 15.8 Hz, 1H), 7.78 (d, *J* = 8.2 Hz, 1H), 7.71–7.63 (m, 2H), 7.54–7.41 (m, 4H). **^{13}C{^{1}H} NMR ($CDCl_3$, 298 K, 75 MHz):** δ 189.83, 146.27, 141.22, 134.67, 134.40 (d, $^2J_{C,F}$ = 32.7 Hz), 131.12, 129.21, 128.92, 128.75, 125.83 (q, $^3J_{C,F}$ = 3.8 Hz), 123.82 (d, $^1J_{C,F}$ = 272.3 Hz), 121.76.

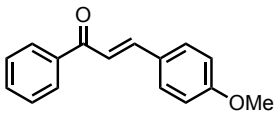

3-(4-methoxyphenyl)-1-phenylprop-2-en-1-one (2e).[69] To 4-methoxybenzaldehyde (0.61 mL, 5 mmol, 1 eq) and acetophenone (0.58 mL, 5 mmol, 1 eq) dissolved in EtOH (25 mL) was added dropwise a NaOH aqueous solution (1.5 M, 5 mL) at room temperature. After 16 h, the resulting mixture was neutralized with 2M HCl solution. The resulting precipitate was filtered and recrystallized from EtOH to afford the desired compound **2e** (1.11 g, 4.7 mmol, 93%).

^{1}H NMR (300 MHz, 298 K, $CDCl_3$) δ 8.03–8.00 (m, 2H), 7.79 (d, *J* = 15.7 Hz, 1H), 7.62–7.55 (m, 3H), 7.52–7.44 (m, 2H), 7.42 (d, *J* = 15.6 Hz, 1H), 6.95–6.92 (m, 2H), 3.85 (s, 3H). **^{13}C{^{1}H} NMR ($CDCl_3$, 298 K, 75 MHz):** δ 190.69, 161.81, 144.81, 138.64, 132.67, 130.35, 128.68, 128.53, 127.75, 119.92, 114.55, 55.53.

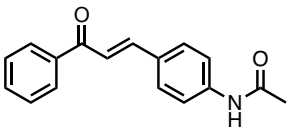

***N*-(4-(3-oxo-3-phenylprop-1-en-1-yl)phenyl)acetamide (2g).**[71] To acetophenone (0.58 mL, 5 mmol, 1 eq) and N-(4-formylphenyl)acetamide (0.82 g, 5 mmol, 1 eq) dissolved in EtOH (25 mL) was added dropwise a NaOH aqueous solution (1.5 M, 5 mL) at room temperature and the reaction mixture was stirred for 16 h at room temperature. The resulting precipitate was collected by filtration and washed with H_2O before being purified by flash column chromatography (silica gel, EtOAc/petroleum ether 1:30) to afford the desired compound **2g** (1.00 g, 3.7 mmol, 75%).

^{1}H NMR (300 MHz, 298 K, $CDCl_3$) δ 8.03–8.00 (m, 2H), 7.77 (d, *J* = 15.7 Hz, 1H), 7.63–7.56 (m, 5H), 7.53–7.42 (m, 4H), 2.21 (s, 3H). **^{13}C{^{1}H} NMR ($CDCl_3$, 298 K, 75 MHz):** δ 190.73, 168.47, 144.35, 140.18, 138.45, 132.89, 130.87, 129.63, 128.77, 128.61, 121.18, 119.81, 24.91.

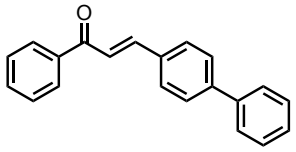

3-([1,1'-biphenyl]-4-yl)-1-phenylprop-2-en-1-one (2h).[71] To acetophenone (0.58 mL, 5 mmol, 1 eq) and [1,1'-biphenyl]-4-carbaldehyde (0.91 g, 5 mmol, 1 eq) dissolved in EtOH (25 mL) was added dropwise a NaOH aqueous solution (1.5 M, 5 mL) at room temperature and the reaction mixture was stirred for 16 h at room temperature. The resulting precipitate was collected by filtration and washed with H_2O before being purified by flash column chromatography (silica gel, EtOAc/petroleum ether 1:30) to afford the desired compound **2h** (1.10 g, 3.8 mmol, 77%).

^{1}H NMR (300 MHz, 298 K, $CDCl_3$) δ 8.06–8.03 (m, 2H), 7.87 (d, *J* = 15.7 Hz, 1H), 7.75–7.36 (m, 13H). **^{13}C{^{1}H} NMR ($CDCl_3$, 298 K, 75 MHz):** δ 190.66, 144.55, 143.48, 140.28, 138.44, 134.01, 132.93, 129.13, 129.07, 128.79, 128.66, 128.06, 127.76, 127.21, 122.08.

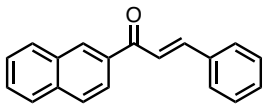

1-(naphthalen-2-yl)-3-phenylprop-2-en-1-one (2i).[72] To 1-(naphthalen-2-yl)ethan-1-one (0.85 g, 5 mmol, 1 eq) and benzaldehyde (0.66 mL, 6.5 mmol, 1.3 eq) dissolved in EtOH (2.5 mL) was added a saturated ethanolic NaOH solution (20 mL) at room temperature and the reaction mixture was stirred for 16 h at room temperature. H_2O (50 mL) was added, and the resulting precipitate was collected by filtration and recrystallized from EtOH to afford the desired compound **2i** (0.85 g, 3.3 mmol, 66%).

^{1}H NMR (300 MHz, 298 K, $CDCl_3$) δ 8.55 (s, 1H), 8.12 (d, *J* = 8.6 Hz, 1H), 8.02–7.87 (m, 4H), 7.73–7.68 (m, 3H), 7.60 (m, 2H), 7.47–7.43 (m, 3H). **^{13}C{^{1}H} NMR ($CDCl_3$, 298 K, 75 MHz):** δ 190.32, 144.81, 135.59, 135.52, 135.00, 132.60, 130.58, 129.97, 129.56, 129.01, 128.62, 128.53, 128.42, 127.87, 126.82, 124.53, 122.14.

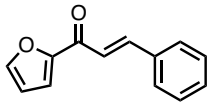

1-(furan-2-yl)-3-phenylprop-2-en-1-one (2k).[73] 1-(furan-2-yl)ethan-1-one (0.55 g, 5 mmol, 1 eq) and benzaldehyde (0.51 mL, 5 mmol, 1 e) were dissolved in a NaOH aqueous solution (1M, 5 mL) and the reaction mixture was stirred for 16 h at room temperature. The resulting mixture was extracted with CH_2Cl_2 (3 × 5 mL), dried over Na_2SO_4, filtered and concentrated under vacuum to afford the desired compound **2k** (0.92 g, 4.6 mmol, 93%).

^{1}H NMR (300 MHz, 298 K, $CDCl_3$) δ 7.89 (d, *J* = 15.8 Hz, 1H), 7.70 – 7.62 (m, 3H), 7.46 (d, *J* = 15.8 Hz, 1H), 7.45–7.41 (m, 3H), 7.34 (dd, *J* = 3.6, 0.8 Hz, 1H), 6.60 (dd, *J* = 3.6, 1.7 Hz, 1H). **^{13}C{^{1}H} NMR ($CDCl_3$, 298 K, 75 MHz):** δ 178.15, 153.85, 146.66, 144.12, 134.87, 130.75, 129.08, 128.67, 121.30, 117.64, 112.68.

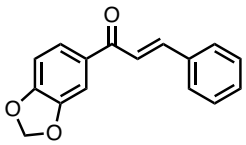

1-(benzo[*d*][1,3]dioxol-5-yl)-3-phenylprop-2-en-1-one (2l).[47] To 1-(benzo[d][1,3]dioxol-5-yl)ethan-1-one (0.33 g, 2 mmol, 1 eq) and benzaldehyde (0.21 mL, 2 mmol, 1 eq) dissolved in EtOH (10 mL) was added dropwise a 10% aqueous solution of NaOH (1.2 mL) at 0°C. The reaction mixture was stirred for 8 h at room temperature before being placed in the fridge overnight. The obtained precipitate was collected by filtration and rinsed with H_2O/ EtOH mixture (1:1) until the pH of the filtration became 7 before being purified by flash column chromatography (silica gel, EtOAc/hexane 1:9) to afford the desired compound **2l** (0.33 g, 1.3 mmol, 65%).

^{1}H NMR (300 MHz, 298 K, $CDCl_3$) δ 7.80 (d, *J* = 15.6 Hz, 1H), 7.71–7.58 (m, 3H), 7.57–7.44 (m, 2H), 7.47–7.36 (m, 3H), 6.90 (d, *J* = 8.2 Hz, 1H), 6.07 (s, 2H). **^{13}C{^{1}H} NMR ($CDCl_3$, 298 K, 75 MHz):** δ 188.42, 151.87, 148.47, 144.40, 135.16, 133.15, 130.56, 129.09, 128.53, 124.83, 121.89, 108.61, 108.08, 102.02.

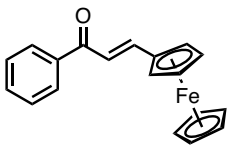

3-Ferrocenyl-1-phenyl-2-propen-1-one (2m).[47] To acetophenone (0.58 mL, 5 mmol, 1 eq) and ferrocenecarboxaldehyde (1.06 g, 5 mmol, 1 eq) dissolved in EtOH (25 mL) was added dropwise a 10% aqueous solution of NaOH (3 mL) at 0°C. The reaction mixture was stirred for 5 h at room temperature before being placed in the fridge overnight. The obtained precipitate was collected by filtration and rinsed with H_2O/ EtOH mixture (1:1) until the pH of the filtration became 7 before being

purified by flash column chromatography (silica gel, EtOAc/hexane 1:9) to afford the desired compound **2m** (0.98 g, 3.12 mmol, 62%).

^{1}H NMR (300 MHz, 298 K, $CDCl_3$) δ 8.00–7.97 (m, 2H), 7.76 (d, *J* = 15.4 Hz, 1H), 7.57 (tt, *J* = 7.1, 1.4 Hz, 1H), 7.49 (tt, *J* = 7.3, 1.2 Hz, 2H), 7.13 (d, *J* = 15.4 Hz, 1H), 4.60 (t, *J* = 1.9 Hz, 2H), 4.49 (t, *J* = 1.9 Hz, 2H), 4.19 (s, 4H). **^{13}C{^{1}H} NMR ($CDCl_3$, 298 K, 75 MHz):** δ 190.02, 146.97, 138.79, 132.49, 128.66, 128.48, 119.32, 79.33, 71.52, 69.95, 69.16.

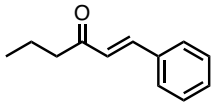

1-phenylhex-1-en-3-one (2r).[74] Pentan-2-one (0.53 mL, 5.0 mmol, 1 eq) and benzaldehyde (0.51 mL, 5 mmol, 1 eq) were dissolved in 10 mL solvent mixture of EtOH and 10% NaOH aqueous solution (3:5, V/V) and stirred at room temperature for 24 h. The resulting mixture was extracted with CH_2Cl_2 (3 × 10 mL) and the combined organic layer was washed with H2O (15 mL), dried over Na_2SO_4 and filtrated before being concentrated under vacuo. The residue was purified by flash column chromatography (silica gel, EtOAc/petroleum ether 5:95) to afford the desired compound **2r** (0.61 g, 3.5 mmol, 70%).

^{1}H NMR (300 MHz, 298 K, $CDCl_3$) δ 7.60–7.51 (m, 3H), 7.43–7.37 (m, 3H), 6.74 (d, *J* = 16.2 Hz, 1H), 2.65 (t, *J* = 7.3 Hz, 2H), 1.72 (h, *J* = 7.4 Hz, 2H), 0.98 (t, *J* = 7.4 Hz, 3H). **^{13}C{^{1}H} NMR ($CDCl_3$, 298 K, 75 MHz):** δ 200.69, 142.45, 134.77, 130.51, 129.08, 128.38, 126.47, 42.97, 17.96, 14.01.

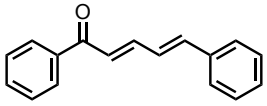

1,5-diphenylpenta-2,4-dien-1-one (2s).[69] To cinnamaldehyde (0.63 mL, 5 mmol, 1 eq) and acetophenone (0.58 mL, 5 mmol, 1 eq) dissolved in EtOH (25 mL) was added dropwise a NaOH aqueous solution (1.5 M, 5 mL) at room temperature. After 16 h, the resulting mixture was neutralized with 2M HCl solution. The resulting precipitate was filtered and recrystallized from EtOH to afford the desired compound **2s** (0.91 g, 3.9 mmol, 78%).

^{1}H NMR (300 MHz, 298 K, $CDCl_3$) δ 8.00–7.97 (m, 2H), 7.65–7.55 (m, 2H), 7.52–7.47 (m, 4H), 7.40–7.32 (m, 3H), 7.10 (d, *J* = 15.1 Hz, 1H), 7.06–7.01 (m, 2H). **^{13}C{^{1}H} NMR ($CDCl_3$, 298 K, 75 MHz):** δ 190.66, 144.99, 142.06, 138.39, 136.26, 132.80, 129.38, 129.01, 128.73, 128.54, 127.44, 127.10, 125.60.

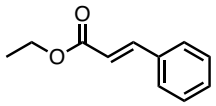

Ethyl cinnamate (2aa).[74] Cinnamoyl chloride (0.83 g, 5 mmol, 1 eq) was dissolved in dry CH_2Cl_2 (30 mL) and the solution was cooled to 0°C. EtOH (0.29 mL, 5 mmol, 1 eq) was added dropwise. The reaction mixture was stirred for 1h at 0°C. The resulting solution was washed with H_2O (3 × 15 mL) and 5% Na_2CO_3 solution (15 mL), before being dried over Na_2SO_4, filtered, and concentrated under vacuo. The crude product was purified by flash column chromatography (silica gel, EtOAc/petroleum ether 1:10) to afford the desired compound **2aa** (0.82 g, 4.6 mmol, 93%).

^{1}H NMR (300 MHz, 298 K, $CDCl_3$) δ 7.69 (d, *J* = 16.0 Hz, 1H), 7.55–7.51 (m, 2H), 7.39–7.37 (m, 3H), 6.44 (d, *J* = 16.0 Hz, 1H), 4.27 (q, *J* = 7.1 Hz, 2H), 1.34 (t, *J* = 7.1 Hz, 3H). **^{13}C{^{1}H} NMR ($CDCl_3$, 298 K, 75 MHz):** δ 167.15, 144.73, 134.63, 130.36, 129.02, 128.19, 118.44, 60.65, 14.47.

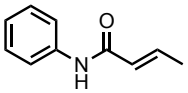

N-phenylbut-2-enamide (2ac).[75] Aniline (0.82 mL, 9 mmol, 1.8 eq) was dissolved in dry CH_2Cl_2 (10 mL) and the solution was cooled to 0°C. 2-butenoyl chloride (0.48 mL, 5 mmol, 1 eq) in CH_2Cl_2 (5 mL) was added dropwise. The reaction mixture was stirred for 2h at room temperature before being concentrated under vacuo. The residue was dissolved in EtOAc (10 mL) and filtered. The resulting solution was washed with 5% HCl solution (3 × 10 mL), saturated $NaHCO_3$ solution (10 mL) and brine (10 mL), before being dried over Na_2SO_4, filtered, and concentrated under vacuo. The crude product was recrystallized in a hexane/EtOAc mixture to afford the desired compound **2ac** (0.38 g, 2.3 mmol, 47%).

^{1}H NMR (300 MHz, 298 K, $CDCl_3$) δ 7.56 (d, *J* = 7.9 Hz, 2H), 7.39 (bs, 1H), 7.31 (tt, *J* = 8.4, 2.2 Hz, 2H), 7.10 (t, *J* = 7.3 Hz, 1H), 6.98 (dq, *J* = 15.1, 6.9 Hz, 1H), 5.96 (dq, *J* = 15.1, 1.7 Hz, 1H), 1.89 (dd, *J* = 6.9, 1.7 Hz, 3H). **^{13}C{^{1}H} NMR ($CDCl_3$, 298 K, 75 MHz):** δ 164.22, 141.70, 138.17, 129.12, 125.56, 124.40, 120.12, 17.97.

III.5.3 Catalytic procedures

General catalytic procedure A (screening of solvent and temperature, base optimization, and control experiments). In a 20 mL pressure tube, *trans*-chalcone (0.5 mmol), complex **1** (1 mol%) and 1,3,5-trimethoxybenzene (10 mol%) as internal standard were dissolved in the corresponding solvent (2.5 mL; *i*PrOH, MeOH, EtOH or glycerol) and the solution was degassed with N_2 for 10 min. The catalytic run was started with the injection of the base (2 M solution in H_2O) and the tube was placed in a pre-heated oil bath (25–110°C). The reaction was monitored by ^{1}H NMR spectroscopy (300 MHz, 298K), with reaction aliquots (ca. 0.1 mL) taken at set times under N_2 and dissolved in $CDCl_3$ (0.5 mL) to determine the spectroscopic conversion and yields relative to the internal standard.

General catalytic procedure B (substrate scope). In a 10 mL round bottom flask, the substrate (0.5 mmol), complex **1** (1 mol%), 1,3,5-trimethoxybenzene or mesitylene (10 mol%) as internal

standards were dissolved in EtOH (5 mL) and the solution was degassed with N_2 for 10 min. The catalytic run was started with the injection of K_2CO_3 (5 mol%, 2 M solution in H_2O) and the tube was placed in a pre-heated oil bath (25 or 60°C). The reaction was monitored by ^1H NMR spectroscopy (300 MHz, 298K), with reaction aliquots (ca. 0.1 mL) taken at set times under N_2 and dissolved in $CDCl_3$ (0.5 mL) to determine the spectroscopic conversion and yields relative to the internal standard. For isolated yield, the reaction was performed in the absence of internal standard and the crude mixture was purified by column chromatography (silica, Hexane/EtOAc).

III.5.4.Time-conversion profiles of catalytic transfer hydrogenation

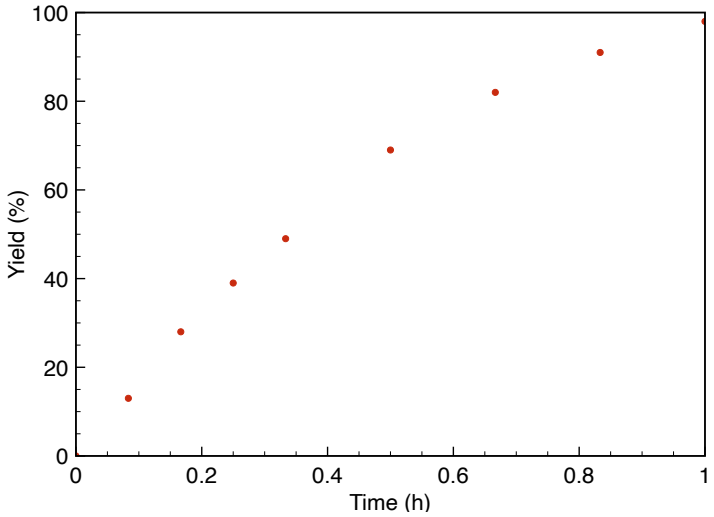

Figure III.8. Time-conversion profile for the catalytic transfer hydrogenation of compound **2a** using the general catalytic procedure B.

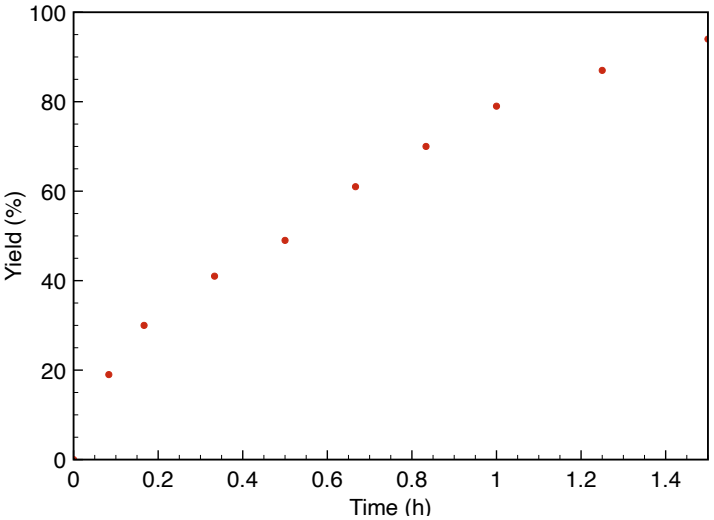

Figure III.9. Time-conversion profile for the catalytic transfer hydrogenation of compound **2b** using the general catalytic procedure B.

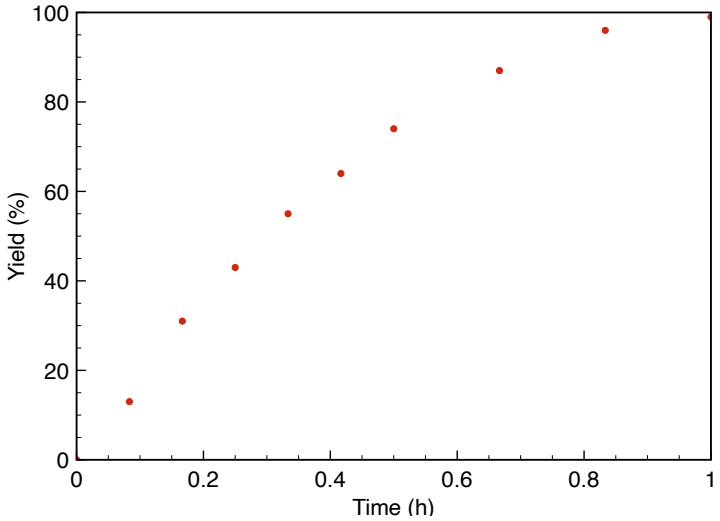

Figure III.10. Time-conversion profile for the catalytic transfer hydrogenation of compound **2c** using the general catalytic procedure B.

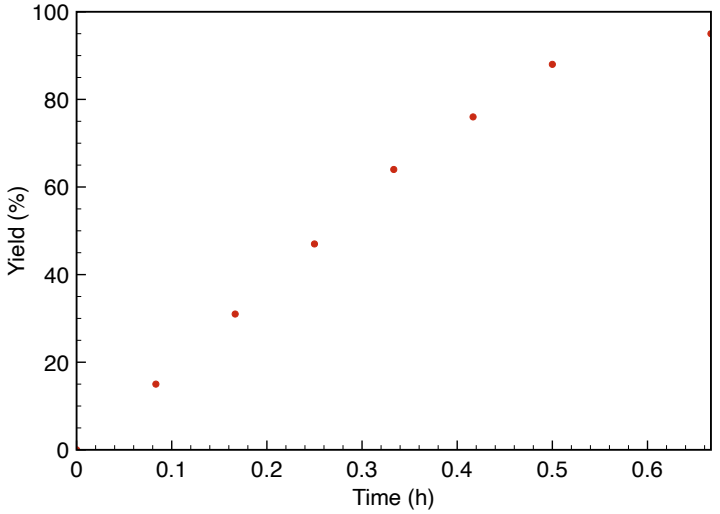

Figure III.11. Time-conversion profile for the catalytic transfer hydrogenation of compound **2d** using the general catalytic procedure B.

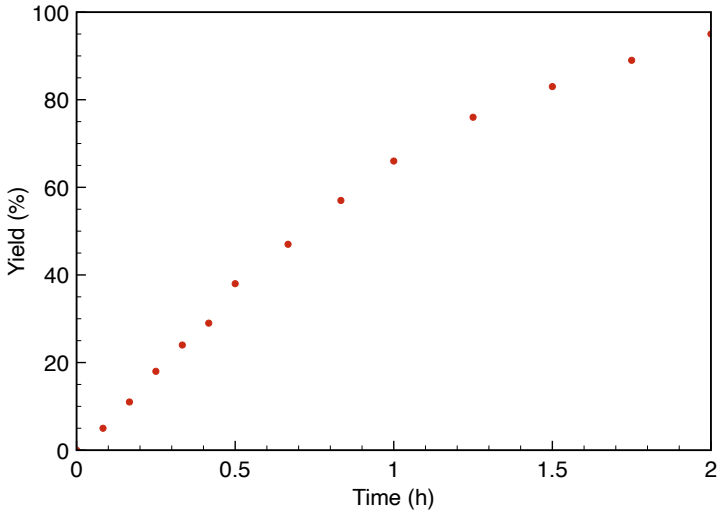

Figure III.12. Time-conversion profile for the catalytic transfer hydrogenation of compound **2e** using the general catalytic procedure B.

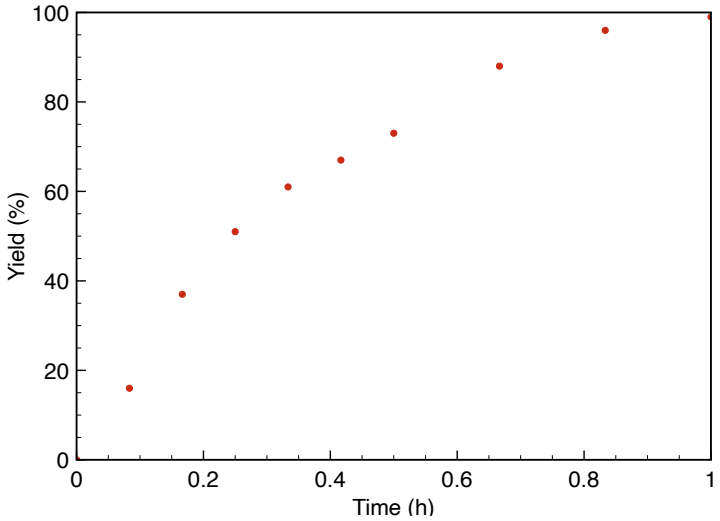

Figure III.13. Time-conversion profile for the catalytic transfer hydrogenation of compound **2f** using the general catalytic procedure B.

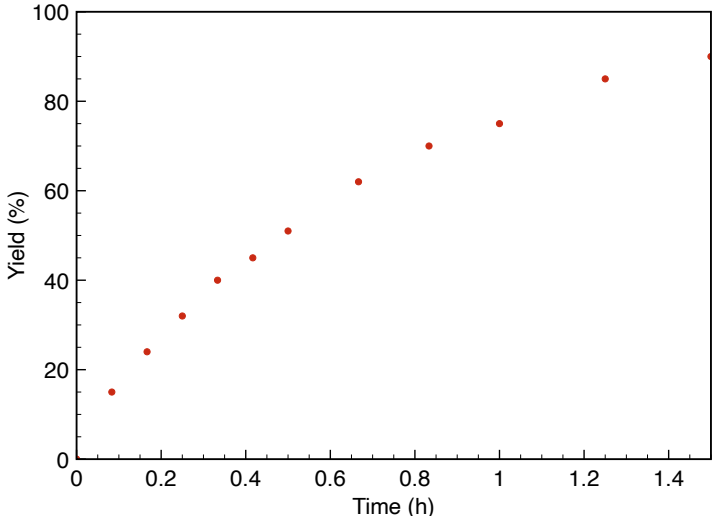

Figure III.14. Time-conversion profile for the catalytic transfer hydrogenation of compound **2g** using the general catalytic procedure B.

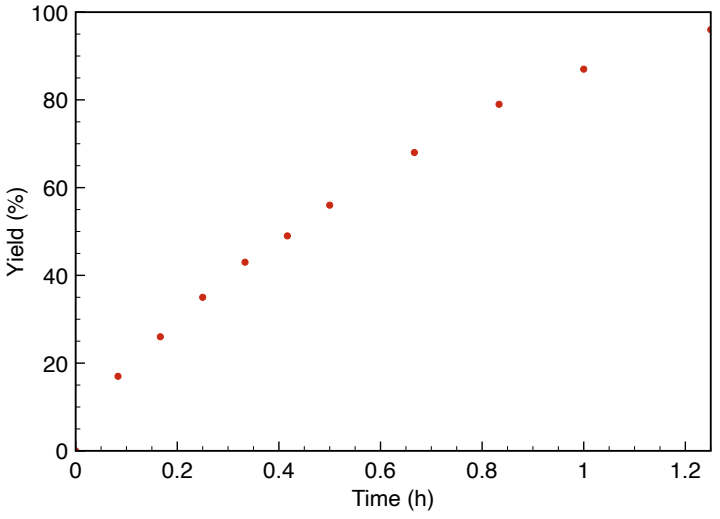

Figure III.15. Time-conversion profile for the catalytic transfer hydrogenation of compound **2h** using the general catalytic procedure B.

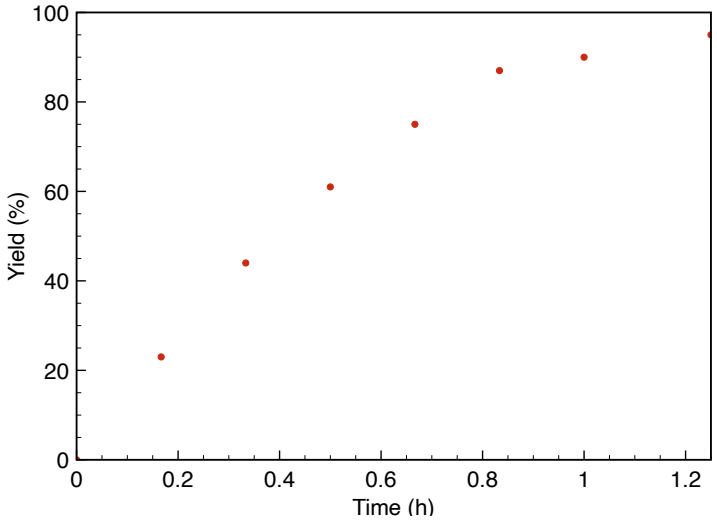

Figure III.16. Time-conversion profile for the catalytic transfer hydrogenation of compound **2i** using the general catalytic procedure B.

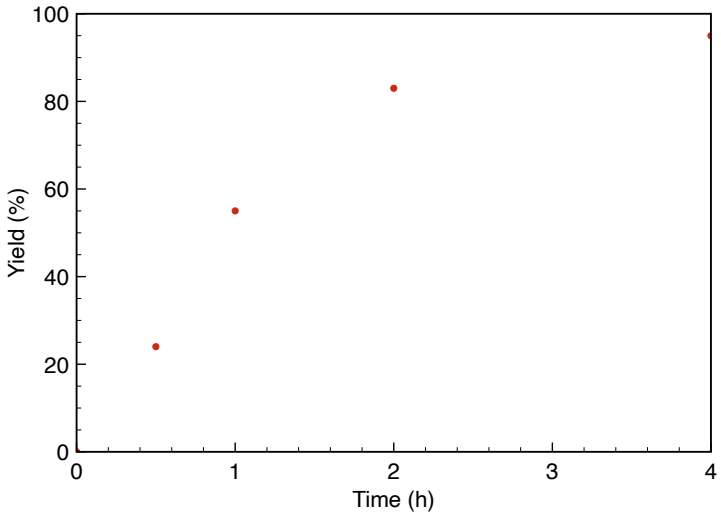

Figure III.17. Time-conversion profile for the catalytic transfer hydrogenation of compound **2j** using the general catalytic procedure B.

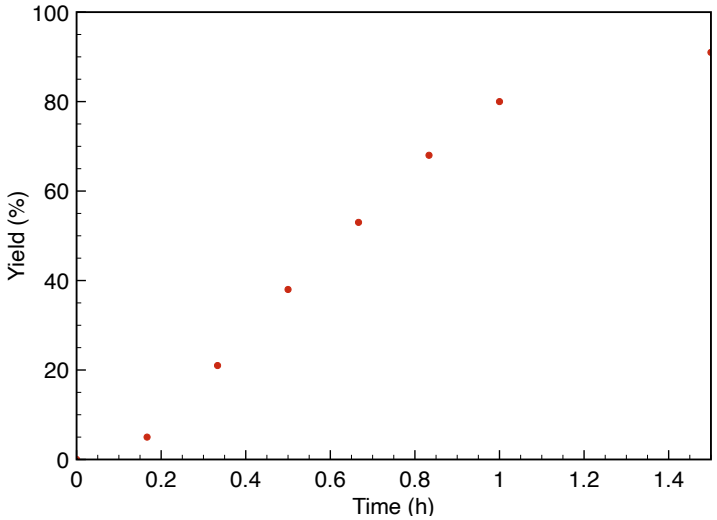

Figure III.18. Time-conversion profile for the catalytic transfer hydrogenation of compound **2k** using the general catalytic procedure B.

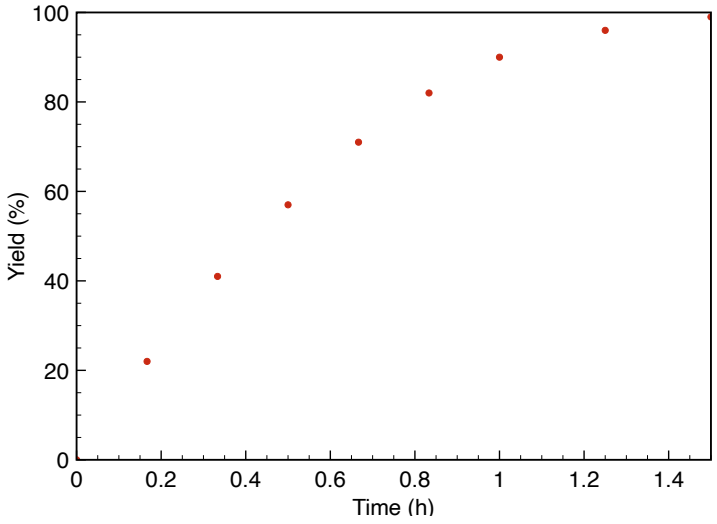

Figure III.19. Time-conversion profile for the catalytic transfer hydrogenation of compound **2l** using the general catalytic procedure B.

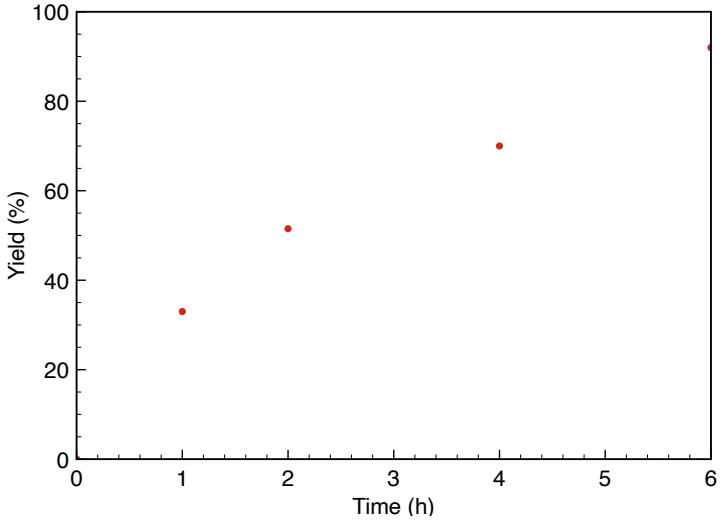

Figure III.20. Time-conversion profile for the catalytic transfer hydrogenation of compound **2m** using the general catalytic procedure B.

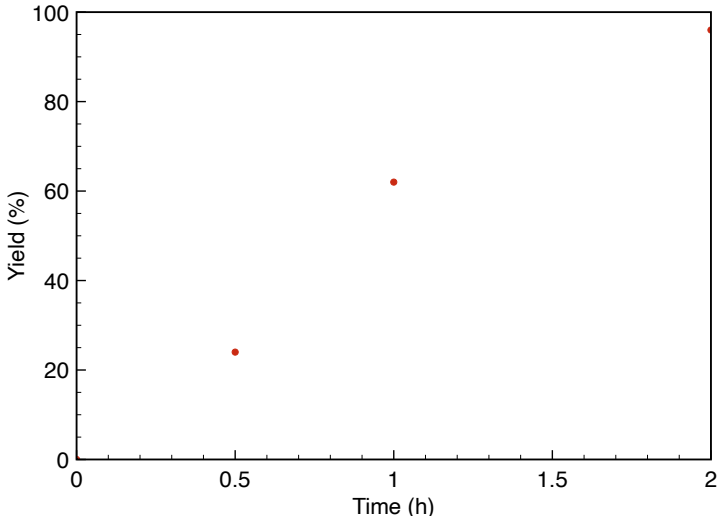

Figure III.21. Time-conversion profile for the catalytic transfer hydrogenation of compound **2p** using the general catalytic procedure B.

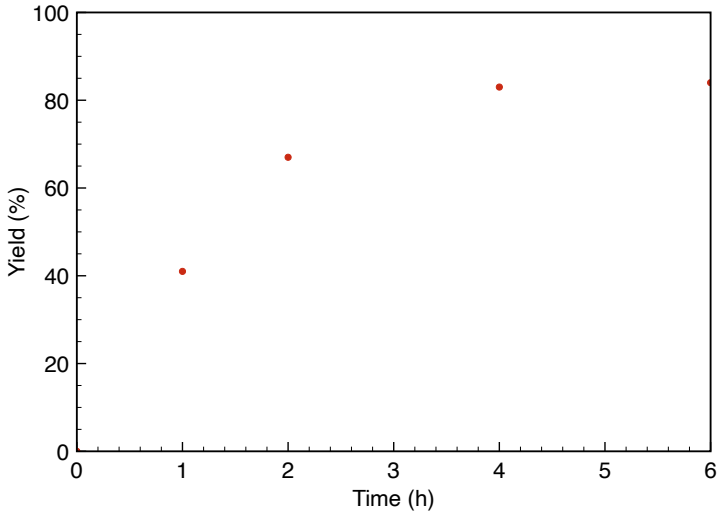

Figure III.22. Time-conversion profile for the catalytic transfer hydrogenation of compound **2q** using the general catalytic procedure B.

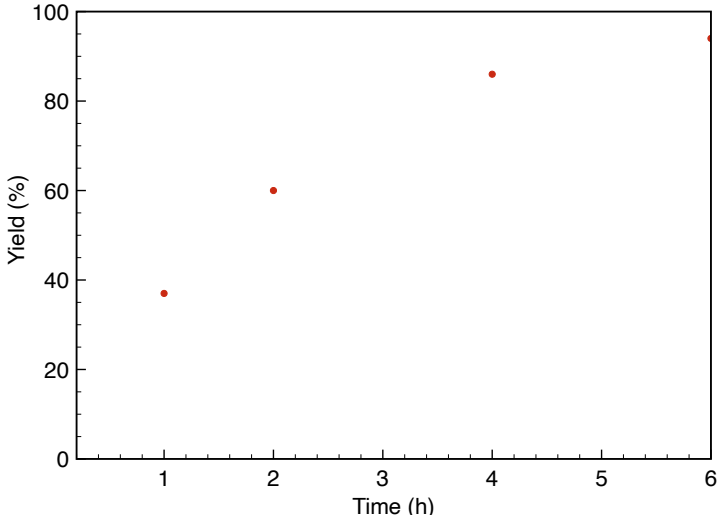

Figure III.23. Time-conversion profile for the catalytic transfer hydrogenation of compound **2r** using the general catalytic procedure B.

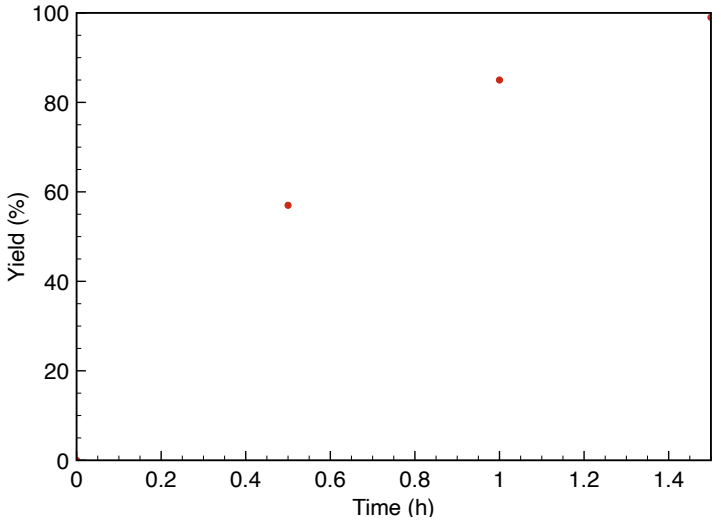

Figure III.24. Time-conversion profile for the catalytic transfer hydrogenation of compound **2s** using the general catalytic procedure B.

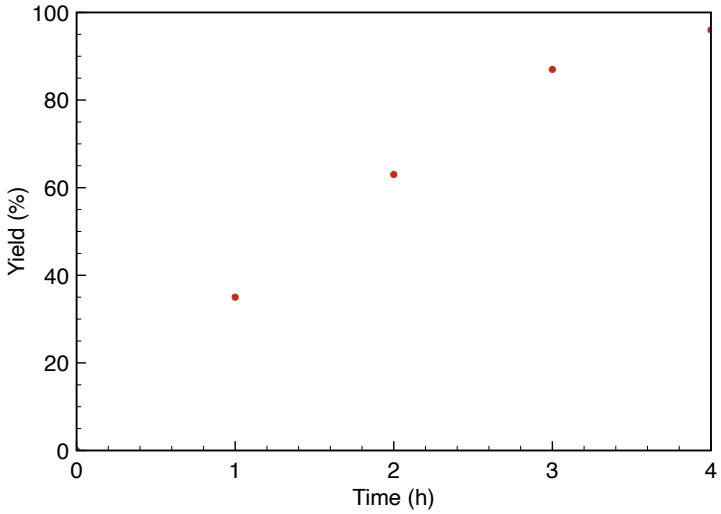

Figure III.25. Time-conversion profile for the catalytic transfer hydrogenation of compound **2t** using the general catalytic procedure B.

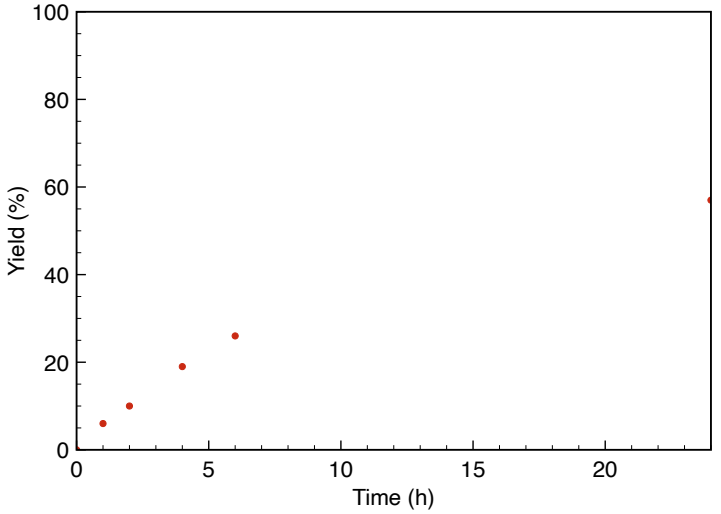

Figure III.26. Time-conversion profile for the catalytic transfer hydrogenation of compound **2u** using the general catalytic procedure B.

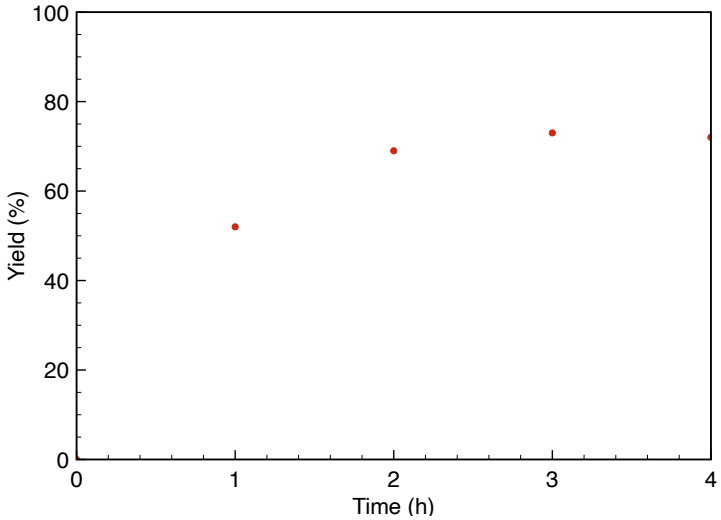

Figure III.27. Time-conversion profile for the catalytic transfer hydrogenation of compound **2w** using the general catalytic procedure B.

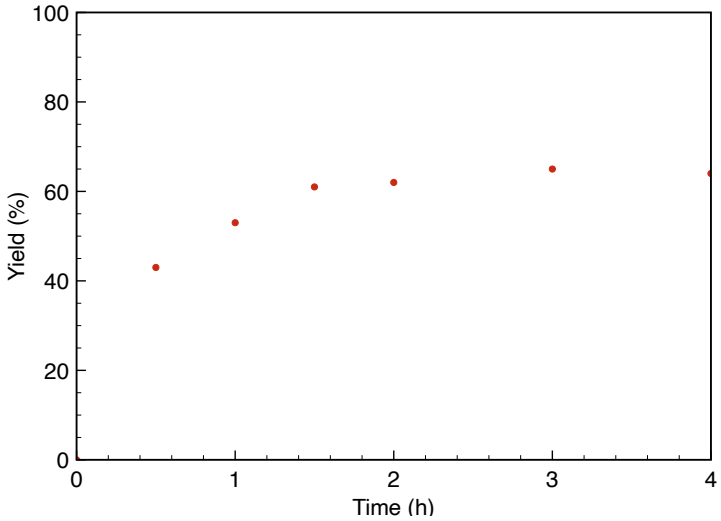

Figure III.28. Time-conversion profile for the catalytic transfer hydrogenation of compound **2x** using the general catalytic procedure B.

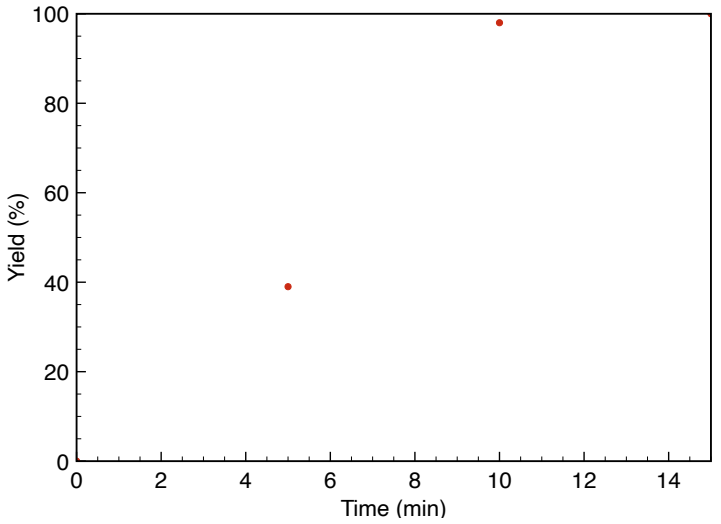

Figure III.29. Time-conversion profile for the catalytic transfer hydrogenation of compound **2y** using the general catalytic procedure B.

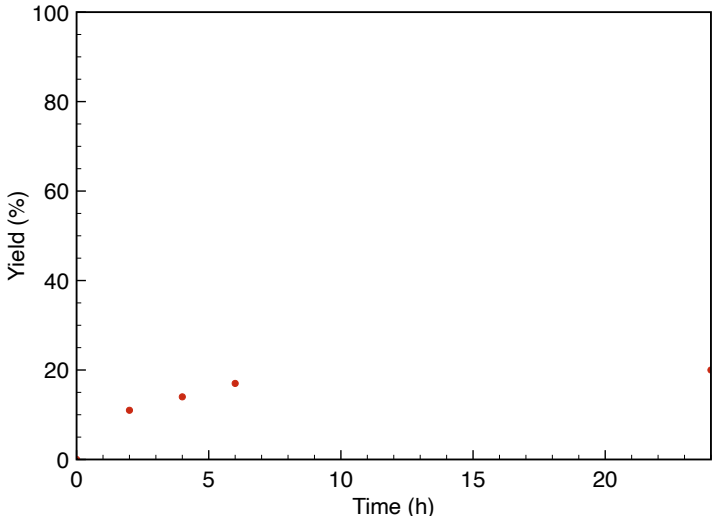

Figure III.30. Time-conversion profile for the catalytic transfer hydrogenation of compound **2z** using the general catalytic procedure B.

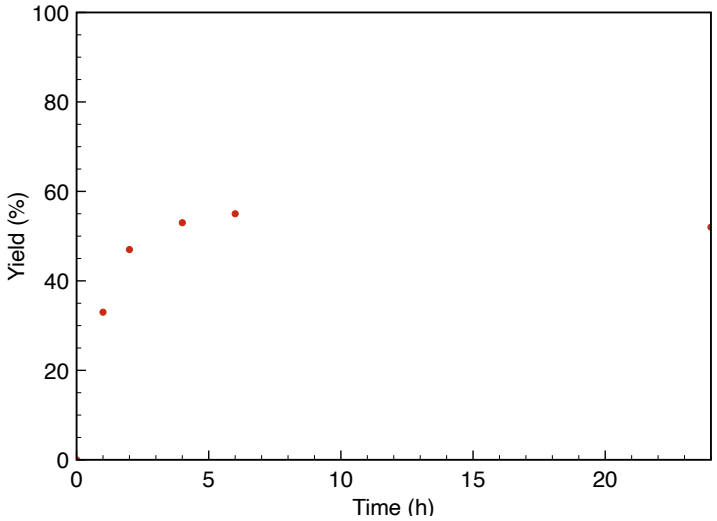

Figure III.31. Time-conversion profile for the catalytic transfer hydrogenation of compound **2aa** using the general catalytic procedure B.

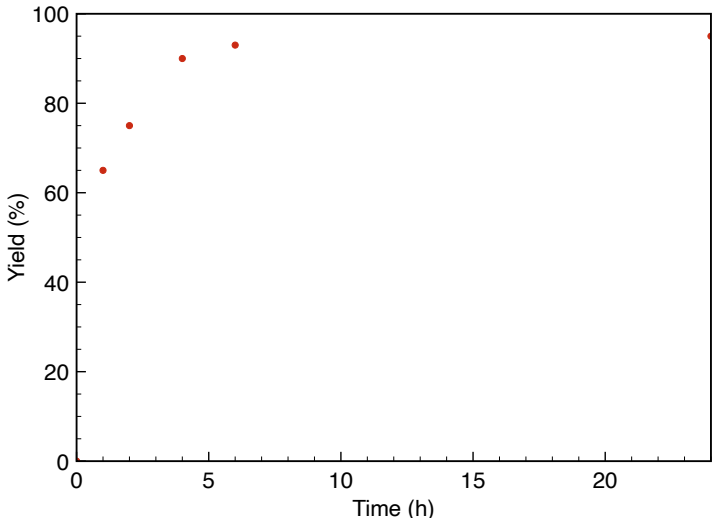

Figure III.32. Time-conversion profile for the catalytic transfer hydrogenation of compound **2ab** using the general catalytic procedure B.

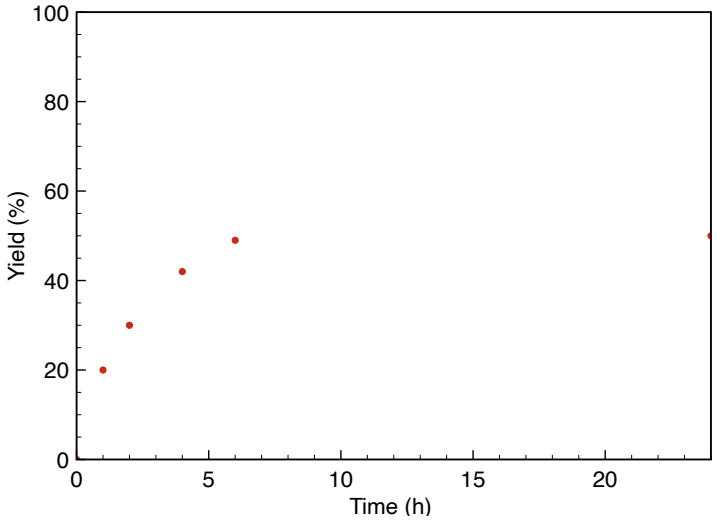

Figure III.33. Time-conversion profile for the catalytic transfer hydrogenation of compound **2ac** using the general catalytic procedure B.

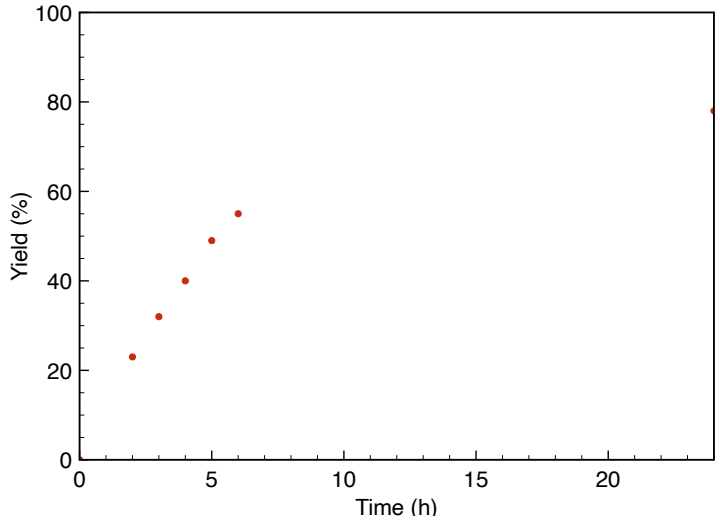

Figure III.34. Time-conversion profile for the catalytic transfer hydrogenation of compound **2ad** using the general catalytic procedure B.

III.5.5. Hammett plots

The initial rate constants k_X for the catalytic transfer hydrogenation of *para*-substituted chalcones **2a-2h** were determined using the general catalytic procedure B. The corresponding time-conversion profiles are represented in Figures III.8–III.15. Reactivity towards chalcones **2a-2d** substituted at the ketonic part followed the sequence: *p*-CF_3 > *p*-Cl > *p*-H > *p*-OMe, and reactivity towards chalcones **2a,2e-2h** substituted at the ketonic part followed the sequence: *p*-Cl > *p*-NHCOMe > *p*-H > *p*-Ph > *p*-OMe.

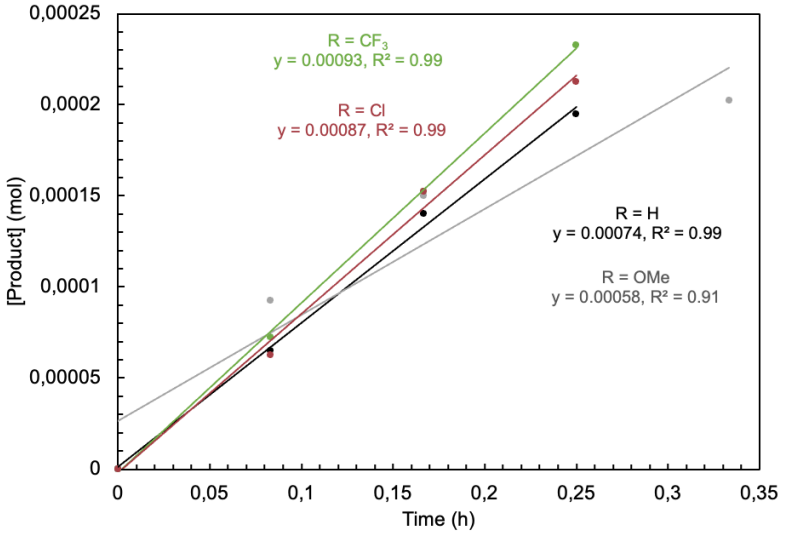

Figure III.35. Determination of initial rate constants (k_X) for the transfer hydrogenation of chalcones **2a-2d** with *para*-substitution at the ketonic scaffold.

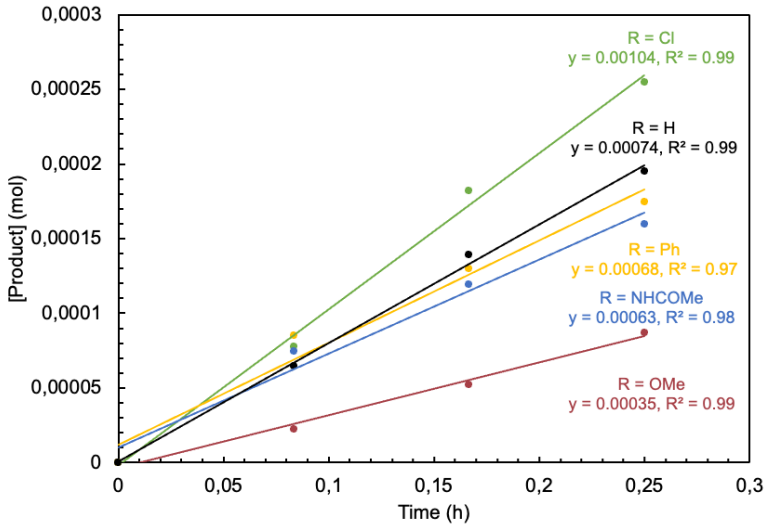

Figure III.36. Determination of initial rate constants (k_X) for the transfer hydrogenation of chalcones **2a, 2e-2h** with *para*-substitution at the olefinic scaffold.

III.5.6. Characterization of products

General procedure for product characterization: Either after substrate consumption or after a maximum of 24 h, the reaction mixture was cooled down to room temperature if necessary and concentrated under reduced pressure. All products were isolated before characterization unless stated otherwise. Product isolation was performed by concentration of the crude mixture followed by flash column chromatography (SiO_2, hexane/EtOAc) using Isolera One Flash Chromatography Instrument.

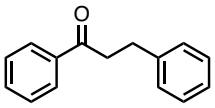

1,3-diphenylpropan-1-one (3a). Compound **3a** was prepared according to General Procedure B from compound **2a**. The crude product was purified by flash column chromatography (SiO_2, hexane/EtOAc 95:5) to obtain the corresponding product. The NMR data are consistent with the literature.[76]

^{1}H NMR (300 MHz, 298K, $CDCl_3$): δ 7.96 (m, 2H), 7.55 (t, *J* = 7.3, 1H), 7.45 (t, *J* = 7.2, 2H), 7.37–7.14 (m, 4H), 3.31 (t, *J* = 7.7 Hz, 2H), 3.07 (t, *J* = 8.0 Hz, 2H). **^{13}C{^{1}H} NMR ($CDCl_3$, 298 K, 75 MHz):** δ 199.37, 141.44, 137.02, 133.20, 128.75, 128.68, 128.57, 128.19, 126.28, 40.60, 30.29.

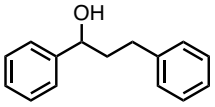

1,3-diphenylpropan-1-ol (5a). Compound **5a** was prepared according to General Procedure B from compound **2a**. The crude product was purified by flash column chromatography (SiO_2,

hexane/EtOAc 95:5) to obtain the corresponding product. The NMR data are consistent with the literature.[77]

^{1}H NMR (300 MHz, 298K, $CDCl_3$): δ 7.31–7.05 (m, 10H), 4.66–4.55 (m, 1H), 2.74–2.53 (m, 2H), 2.14–1.87 (m, 2H). **$^{13}C\{^1H\}$ NMR ($CDCl_3$, 298 K, 75 MHz):** δ 144.70, 141.91, 128.66, 128.58, 128.53, 127.78, 126.06, 125.99, 74.03, 40.60, 32.20.

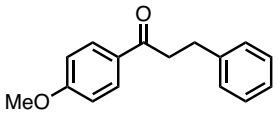

1-(4-methoxyphenyl)-3-phenylpropan-1-one (3b). Compound **3b** was prepared according to General Procedure B from compound **2b**. The crude product was purified by flash column chromatography (SiO_2, hexane/EtOAc 9:1) to obtain the corresponding product. The NMR data are consistent with the literature.[76]

^{1}H NMR (300 MHz, 298K, $CDCl_3$): δ 7.95 (d, *J* = 8.9, 2H), 7.35–7.17 (m, 5H), 6.92 (d, *J* = 9.0 Hz, 2H), 3.87 (s, 3H), 3.25 (t, *J* = 8.1 Hz, 2H), 3.06 (t, *J* = 7.2 Hz, 2H). **$^{13}C\{^1H\}$ NMR ($CDCl_3$, 298 K, 75 MHz):** δ 197.89, 163.55, 141.58, 130.40, 130.08, 128.61, 128.53, 126.18, 113.83, 55.55, 40.20, 30.44.

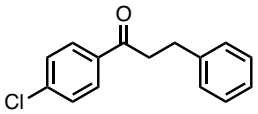

1-(4-chlorophenyl)-3-phenylpropan-1-one (3c). Compound **3c** was prepared according to General Procedure B from compound **2c**. The crude product was purified by flash column chromatography (SiO_2, hexane/EtOAc 9:1) to obtain the corresponding product. The NMR data are consistent with the literature.[76]

^{1}H NMR (300 MHz, 298K, $CDCl_3$): δ 7.87 (d, *J* = 8.6 Hz, 2H), 7.40 (d, *J* = 8.6 Hz, 2H), 7.31–7.16 (m, 5H), 3.24 (t, *J* = 7.7 Hz, 2H), 3.04 (t, *J* = 8.0 Hz, 2H). **$^{13}C\{^1H\}$ NMR ($CDCl_3$, 298 K, 75 MHz):** δ 198.08, 141.18, 139.62, 135.30, 129.58, 129.04, 128.69, 128.53, 126.35, 40.54, 30.18.

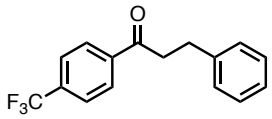

3-phenyl-1-(4-(trifluoromethyl)phenyl)propan-1-one (3d). Compound **3d** was prepared according to General Procedure B from compound **2d**. The crude product was purified by flash column chromatography (SiO_2, hexane/EtOAc 95:5) to obtain the corresponding product. The NMR data are consistent with the literature.[47]

^{1}H NMR (300 MHz, 298K, $CDCl_3$): δ 8.04 (d, *J* = 8.1 Hz, 1H), 7.72 (d, *J* = 8.1 Hz, 1H), 7.33–7.19 (m, 5H), 3.33 (t, *J* = 7.0 Hz, 1H), 3.09 (t, *J* = 7.9 Hz, 1H). **^{13}C{^{1}H} NMR ($CDCl_3$, 298 K, 75 MHz):** δ 198.34, 141.00, 139.64, 134.53 (d, *J* = 32.6 Hz), 128.75, 128.55, 128.50, 126.45, 125.84 (q, *J* = 3.8 Hz), 40.89, 30.08.

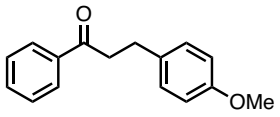

3-(4-methoxyphenyl)-1-phenylpropan-1-one (3e). Compound **3e** was prepared according to General Procedure B from compound **2e**. The crude product was purified by flash column chromatography (SiO_2, hexane/EtOAc 9:1) to obtain the corresponding product. The NMR data are consistent with the literature.[76]

^{1}H NMR (300 MHz, 298K, $CDCl_3$): δ 7.97–7.94 (m, 2H), 7.56 (t, *J* = 7.3 Hz, 1H), 7.45 (t, *J* = 7.2 Hz, 2H), 7.18 (d, *J* = 8.6 Hz, 2H), 6.85 (d, *J* = 8.8 Hz, 2H), 3.79 (s, 3H), 3.27 (t, *J* = 8.1 Hz, 2H), 3.02 (t, *J* = 8.0 Hz, 2H). **^{13}C{^{1}H} NMR ($CDCl_3$, 298 K, 75 MHz):** δ 199.52, 158.14, 137.06, 133.46, 133.16, 129.49, 128.73, 128.18, 114.09, 55.41, 40.85, 29.43.

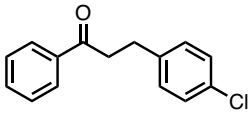

3-(4-chlorophenyl)-1-phenylpropan-1-one (3f). Compound **3f** was prepared according to General Procedure B from compound **2f**. The crude product was purified by flash column chromatography (SiO_2, hexane/EtOAc 9:1) to obtain the corresponding product. The NMR data are consistent with the literature.[76]

^{1}H NMR (300 MHz, 298K, $CDCl_3$): δ 7.97–7.94 (m, 2H), 7.56 (t, *J* = 7.5 Hz, 1H), 7.46 (t, *J* = 7.1 Hz, 2H), 7.25 (d, *J* = 8.6 Hz, 2H), 7.15 (d, *J* = 8.6 Hz, 2H), 3.29 (t, *J* = 7.6 Hz, 2H), 3.05 (t, *J* = 7.5 Hz, 2H). **^{13}C{^{1}H} NMR ($CDCl_3$, 298 K, 75 MHz):** δ 198.91, 139.85, 136.86, 133.26, 131.96, 129.93, 128.74, 128.69, 128.10, 40.21, 29.47.

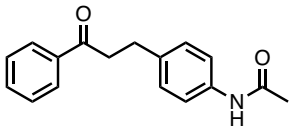

***N*-(4-(3-oxo-3-phenylpropyl)phenyl)acetamide (3g).** Compound **3g** was prepared according to General Procedure B from compound **2g**. The crude product was directly analyzed. The NMR data are consistent with the literature.[45]

^{1}H NMR (300 MHz, 298K, $CDCl_3$): δ 7.95 (d, *J* = 7.1 Hz, 2H), 7.56 (t, *J* = 7.4 Hz, 1H), 7.47–7.40 (m, 4H), 7.31 (bs, 1H), 7.19 (d, *J* = 8.2 Hz, 2H), 3.27 (t, *J* = 7.5 Hz, 2H), 3.03 (t, *J* = 7.6 Hz, 2H), 2.15 (s,

3H). **$^{13}C\{^1H\}$ NMR ($CDCl_3$, 298 K, 75 MHz):** δ 199.39, 168.40, 137.45, 136.97, 136.13, 133.23, 129.06, 128.76, 128.16, 120.36, 40.52, 29.67, 24.66.

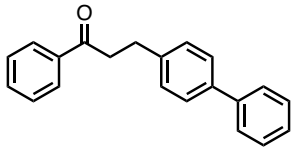

3-([1,1'-biphenyl]-4-yl)-1-phenylpropan-1-one (3h). Compound **3h** was prepared according to General Procedure B from compound **2h**. The crude product was purified by flash column chromatography (SiO_2, hexane/EtOAc 9:1) to obtain the corresponding product. The NMR data are consistent with the literature.[78]

^1H NMR (300 MHz, 298K, $CDCl_3$): δ 8.05–7.96 (m, 2H), 7.65–7.53 (m, 5H), 7.52–7.41 (m, 4H), 7.39–7.32 (m, 3H), 3.36 (t, *J* = 7.3 Hz, 2H), 3.14 (t, *J* = 7.3 Hz, 2H). **$^{13}C\{^1H\}$ NMR ($CDCl_3$, 298 K, 75 MHz):** δ 199.26, 141.10, 140.52, 139.25, 136.98, 133.20, 128.98, 128.85, 128.74, 128.17, 127.38, 127.22, 127.12, 40.48, 29.85.

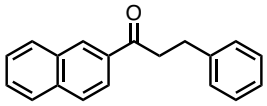

1-(naphthalen-2-yl)-3-phenylpropan-1-one (3i). Compound **3i** was prepared according to General Procedure B from compound **2i**. The crude product was purified by flash column chromatography (SiO_2, hexane/EtOAc 9:1) to obtain the corresponding product. The NMR data are consistent with the literature.[76]

^1H NMR (300 MHz, 298K, $CDCl_3$): δ 8.40 (s, 1H), 7.99 (d, *J* = 8.6, 1H), 7.89–7.79 (m, 3H), 7.56–7.46 (m, 2H), 7.31–7.24 (m, 4H), 7.21–7.15 (m, 1H), 3.38 (t, *J* = 8.1 Hz, 2H), 3.09 (td, *J* = 8.2, 4.9 Hz, 2H). **$^{13}C\{^1H\}$ NMR ($CDCl_3$, 298 K, 75 MHz):** δ 199.19, 141.45, 135.66, 134.27, 132.61, 129.77, 129.63, 128.65, 128.57, 128.54, 128.52, 127.86, 126.85, 126.26, 123.93, 40.62, 30.36.

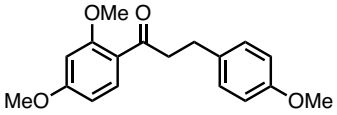

1-(2,4-dimethoxyphenyl)-3-(4-methoxyphenyl)propan-1-one (3j). Compound **3j** was prepared according to General Procedure B from compound **2j**. The crude product was purified by flash column chromatography (silica gel, hexane/EtOAc 9:1) to obtain the corresponding product. The NMR data are consistent with the literature.[79]

^1H NMR (300 MHz, 298K, $CDCl_3$): δ 7.81 (d, *J* = 8.7 Hz, 1H), 7.15 (d, *J* = 8.5 Hz, 2H), 6.83 (d, *J* = 8.6 Hz, 2H), 6.53 (dd, *J* = 8.7, 2.3 Hz, 1H), 6.45 (d, *J* = 2.3 Hz, 1H), 3.87 (s, 3H), 3.85 (s, 3H), 3.79 (s, 3H), 3.24 (t, *J* = 8.2 Hz, 2H), 2.95 (t, *J* = 7.3 Hz, 2H). **$^{13}C\{^1H\}$ NMR ($CDCl_3$, 298 K, 75 MHz):** δ

199.70, 164.49, 160.87, 157.91, 134.19, 132.89, 129.48, 121.26, 113.92, 105.24, 98.48, 55.65, 55.59, 55.38, 45.73, 29.91.

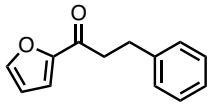

1-(furan-2-yl)-3-phenylpropan-1-one (2k). Compound **3k** was prepared according to General Procedure B from compound **2k**. The crude product was purified by flash column chromatography (SiO_2, hexane/EtOAc 9:1) to obtain the corresponding product. The NMR data are consistent with the literature.[80]

^{1}H NMR (300 MHz, 298K, $CDCl_3$): δ 7.57 (dd, *J* = 1.7, 0.8 Hz, 1H), 7.36–7.12 (m, 5H), 7.17 (dd, *J* = 3.6, 0.7 Hz, 1H), 6.52 (dd, *J* = 3.6, 1.7 Hz, 1H), 3.22–3.11 (m, 2H), 3.11–2.99 (m, 2H). **^{13}C{^{1}H} NMR ($CDCl_3$, 298 K, 75 MHz):** δ 188.52, 152.74, 146.39, 141.04, 128.58, 128.48, 126.24, 117.08, 112.28, 40.22, 30.02.

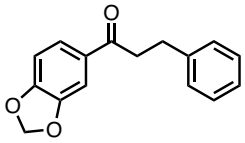

1-(benzo[*d*][1,3]dioxol-5-yl)-3-phenylpropan-1-one (3l). Compound **3l** was prepared according to General Procedure B from compound **2l**. The crude product was purified by flash column chromatography (SiO_2, hexane/EtOAc 9:1) to obtain the corresponding product. The NMR data are consistent with the literature.[45]

^{1}H NMR (300 MHz, 298K, $CDCl_3$): δ 7.56 (dd, *J* = 8.2, 1.7 Hz, 1H), 7.44 (d, *J* = 1.7 Hz, 1H), 7.34–7.17 (m, 5H), 6.83 (d, *J* = 8.1 Hz, 1H), 6.04 (s, 2H), 3.22 (t, *J* = 7.8 Hz, 2H), 3.05 (t, *J* = 7.4 Hz, 2H). **^{13}C{^{1}H} NMR ($CDCl_3$, 298 K, 75 MHz):** δ 197.42, 151.85, 148.33, 141.47, 131.91, 128.65, 128.55, 126.25, 124.38, 108.01, 108.00, 101.96, 40.35, 30.49.

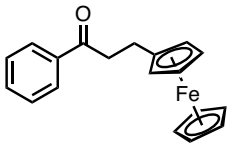

3-phenyl-1-(ferrocynyl)propan-1-one (3m). Compound **3m** was prepared according to General Procedure B from compound **2m**. The crude product was purified by flash column chromatography (SiO_2, hexane/EtOAc 9:1) to obtain the corresponding product. The NMR data are consistent with the literature.[47]

^{1}H NMR (300 MHz, 298K, $CDCl_3$): δ 7.99–7.95 (m, 2H), 7.57 (tt, *J* = 7.5, 1.1 Hz, 1H), 7.47 (tt, *J* = 7.2, 1.2 Hz, 2H), 4.14 (s, 5H), 4.10 (dt, *J* = 14.1, 1.8 Hz, 4H), 3.21 (t, *J* = 7.9 Hz, 2H), 2.80 (t, *J* = 7.2

Hz, 2H). **$^{13}C\{^{1}H\}$ NMR ($CDCl_3$, 298 K, 75 MHz):** δ 199.62, 137.06, 133.13, 128.72, 128.16, 88.15, 68.68, 68.26, 67.49, 40.47, 24.23.

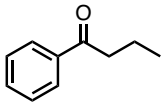

1-phenylbutan-1-one (3p). Compound **3p** was prepared according to General Procedure B from compound **2p**. The crude product was purified by flash column chromatography (SiO_2, hexane/EtOAc 9:1) to obtain the corresponding product. The NMR data are consistent with the literature.[81]

^{1}H NMR (300 MHz, 298K, $CDCl_3$): δ 7.96 (d, *J* = 7.1 Hz, 2H), 7.55 (tt, *J* = 7.1, 1.3 Hz, 1H), 7.46 (tt, *J* = 7.5, 1.6 Hz, 2H), 2.95 (t, *J* = 7.3 Hz, 2H), 1.84–1.71 (m, 2H), 1.01 (t, *J* = 7.4 Hz, 3H). **$^{13}C\{^{1}H\}$ NMR ($CDCl_3$, 298 K, 75 MHz):** δ 200.59, 137.28, 133.00, 128.68, 128.18, 40.67, 17.93, 14.03.

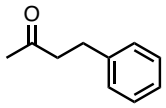

4-phenylbutan-2-one (3q). Compound **3q** was prepared according to General Procedure B from compound **2q**. The crude product was purified by flash column chromatography (SiO_2, hexane/EtOAc 9:1) to obtain the corresponding product. The NMR data are consistent with the literature.[45]

^{1}H NMR (300 MHz, 298K, $CDCl_3$): δ 7.26–7.21 (m, 2H), 7.16–7.12 (m, 3H), 2.85 (t, *J* = 7.5 Hz, 2H), 2.71 (t, *J* = 7.2 Hz, 2H), 2.09 (s, 3H). **$^{13}C\{^{1}H\}$ NMR ($CDCl_3$, 298 K, 75 MHz):** δ 207.98, 141.08, 128.57, 128.37, 126.19, 45.23, 30.13, 29.81.

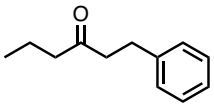

1-phenylhexan-3-one (3r). Compound **3r** was prepared according to General Procedure B from compound **2r**. The crude product was purified by flash column chromatography (SiO_2, hexane/EtOAc 9:1) to obtain the corresponding product. The NMR data are consistent with the literature.[82]

^{1}H NMR (300 MHz, 298K, $CDCl_3$): δ 7.27–7.21 (m, 2H), 7.17–7.09 (m, 3H), 2.87 (t, *J* = 7.8 Hz, 2H), 2.68 (t, *J* = 7.8 Hz, 2H), 2.32 (t, *J* = 7.3 Hz, 2H), 1.56 (h, *J* = 7.4 Hz, 2H), 0.86 (t, *J* = 7.4 Hz, 3H). **$^{13}C\{^{1}H\}$ NMR ($CDCl_3$, 298 K, 75 MHz):** δ 210.08, 141.21, 128.47, 128.33, 126.06, 44.91, 44.25, 29.78, 17.24, 13.74.

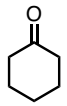

Cyclohexanone (3s). Compound **3s** was prepared according to General Procedure B from compound **2s**. The crude product was purified by flash column chromatography (silica gel, hexane/EtOAc 9:1) to obtain the corresponding product. The NMR data are consistent with the literature.[83]

^{1}H NMR (300 MHz, 298K, $CDCl_3$): δ 2.31 (t, *J* = 6.7 Hz, 4H), 1.87–1.79 (m, 4H), 1.73–1.65 (m, 2H). **^{13}C{^{1}H} NMR ($CDCl_3$, 298 K, 75 MHz):** δ 212.30, 42.05, 27.10, 25.07.

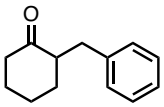

2-benzylcyclohexan-1-one (3t). Compound **3t** was prepared according to General Procedure B from compound **2t**. The crude product was purified by flash column chromatography (SiO_2, hexane/EtOAc 9:1) to obtain the corresponding product. The NMR data are consistent with the literature.[84]

^{1}H NMR (300 MHz, 298K, $CDCl_3$): δ 7.31–7.24 (m, 2H), 7.23–7.11 (m, 3H), 3.24 (dd, *J* = 13.7, 4.6 Hz, 1H), 2.63–2.49 (m, 1H), 2.49–2.26 (m, 3H), 2.12–1.97 (m, 2H), 1.88–1.78 (m, 1H), 1.75–1.50 (m, 2H), 1.43–1.25 (m, 1H). **^{13}C{^{1}H} NMR ($CDCl_3$, 298 K, 75 MHz):** δ 212.66, 140.53, 129.27, 128.43, 126.09, 52.63, 42.31, 35.61, 33.55, 28.19, 25.21.

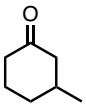

3-methylcyclohexan-1-one (3u). Compound **3u** was prepared according to General Procedure B from compound **2u**. The crude product was purified by flash column chromatography (silica gel, hexane/EtOAc 9:1) to obtain the corresponding product. The NMR data are consistent with the literature.[85]

^{1}H NMR (300 MHz, 298K, $CDCl_3$): δ 2.40–2.29 (m, 2H), 2.28–17 (m, 1H), 2.08–1.83 (m, 4H), 1.73–1.61 (m, 1H), 1.39–1.26 (m, 1H), 1.02 (d, *J* = 6.2 Hz, 3H). **^{13}C{^{1}H} NMR ($CDCl_3$, 298 K, 75 MHz):** δ 212.14, 50.15, 41.28, 34.34, 33.45, 25.45, 22.21.

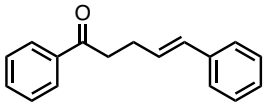

1,5-diphenylpent-4-en-1-one (3w). Compound **3w** was prepared according to General Procedure B from compound **2w**. The crude product was purified by flash column chromatography (silica gel,

hexane/EtOAc 9:1) to obtain the corresponding product. The NMR data are consistent with the literature.[76]

^{1}H NMR (300 MHz, 298K, $CDCl_3$): δ 8.00–7.97 (m, 2H), 7.57 (t, *J* = 7.4, 1H), 7.47 (t, *J* = 7.0 Hz, 2H), 7.37–7.26 (m, 4H), 7.20 (t, *J* = 7.4 Hz, 1H), 6.48 (d, *J* = 15.9 Hz, 1H), 6.30 (dt, *J* = 15.8, 6.8 Hz, 1H), 3.17 (t, *J* = 7.5 Hz, 2H), 2.67 (q, *J* = 6.7 Hz, 2H). **^{13}C{^{1}H} NMR ($CDCl_3$, 298 K, 75 MHz):** δ 199.48, 137.62, 137.09, 133.20, 130.96, 129.28, 128.77, 128.64, 128.20, 127.22, 126.18, 38.43, 27.66.

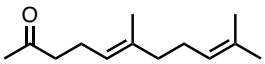

5,9-dimethyl-1-phenyldec-8-en-1-one (3x). Compound **3x** was prepared according to General Procedure B from compound **2x**. The crude product was purified by flash column chromatography (silica gel, hexane/EtOAc 9:1) to obtain the corresponding product. The NMR data are consistent with the literature.[11]

^{1}H NMR (300 MHz, 298K, $CDCl_3$): δ 5.10–5.04 (m, 2H), 2.47–2.39 (m, 2H), 2.29–2.22 (m, 2H), 2.13 (s, 3H), 2.06–1.93 (m, 4H), 1,67 (s, 3H), 1.60 (s, 3H), 1,59 (s, 3H). **^{13}C{^{1}H} NMR ($CDCl_3$, 298 K, 75 MHz, major, *E*-product):** δ 209.00, 136.51, 131.54, 124.32, 122.67, 43.90, 39.77, 30.06, 26.75, 25.81, 22.62, 17.80, 16.10. **^{13}C{^{1}H} NMR ($CDCl_3$, 298 K, 75 MHz, minor, *Z*-product):** δ 208.89, 136.63, 131.80, 124.30, 123.47, 44.15, 32.00, 30.03, 26.63, 25.83, 23.48, 22.42, 17.76. **ESI-MS** (calc. for [$C_{13}H_{22}O]^+$): *m/z* 194.1670 (194.1671).

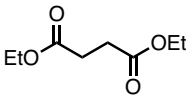

Diethyl succinate (3y). Compound **3y** was prepared according to General Procedure B from compound **2y**. The crude product was directly characterized after concentration. The NMR data are consistent with the literature.[86]

^{1}H NMR (300 MHz, 298K, $CDCl_3$): δ 4.12 (q, *J* = 7.1 Hz, 4H), 2.59 (s, 4H), 1.23 (t, *J* = 7.1 Hz, 6H). **^{13}C{^{1}H} NMR ($CDCl_3$, 298 K, 75 MHz):** δ 172.40, 60.73, 29.28, 14.25.

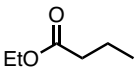

Ethyl butyrate (3z). Compound **3z** was prepared according to General Procedure B from compound **2z**. Due to its high volatility, compound **3z** could not be isolated and was directly analyzed from the reaction mixture. The NMR data are consistent with the literature.[87]

^{1}H NMR (300 MHz, 298K, $CDCl_3$): δ 3.98 (q, overlapping with EtOH), 2.15 (t, *J* = 7.4 Hz, 2H), 1.52 (s, *J* = 7.4 Hz, 2H), 0.82 (t, *J* = 7.3 Hz, 3H).

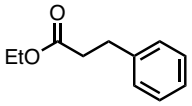

Ethyl 3-phenylpropanoate (3aa). Compound **3aa** was prepared according to General Procedure B from compound **2aa**. The crude product was purified by flash column chromatography (silica gel, hexane/EtOAc 9:1) to obtain the corresponding product. The NMR data are consistent with the literature.[88]

^{1}H NMR (300 MHz, 298K, $CDCl_3$): δ 7.32–7.27 (m, 2H), 7.22–7.18 (m, 3H), 4.13 (q, *J* = 7.1 Hz, 2H), 2.96 (t, *J* = 7.8 Hz, 2H), 2.62 (t, *J* = 7.5 Hz, 2H), 1.24 (t, *J* = 7.2 Hz, 4H). **^{13}C{^{1}H} NMR ($CDCl_3$, 298 K, 75 MHz):** δ 173.05, 140.72, 128.60, 128.43, 126.35, 60.54, 36.08, 31.12, 14.33.

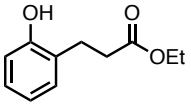

Ethyl 3-(2-hydroxyphenyl)propanoate (3ab). Compound **3ab** was prepared according to General Procedure B from compound **2ab**. The crude product was purified by flash column chromatography (silica gel, hexane/EtOAc 9:1) to obtain the corresponding product. The NMR data are consistent with the literature.[57]

^{1}H NMR (300 MHz, 298K, $CDCl_3$): δ 7.23 (bs, 1H), 7.16 – 7.04 (m, 2H), 6.87 (t, *J* = 8.4 Hz, 2H), 4.15 (q, *J* = 7.2 Hz, 2H), 2.95 (t, *J* = 6.2 Hz, 2H), 2.71 (t, *J* = 6.8 Hz, 2H), 1.24 (t, *J* = 7.2 Hz, 3H). **^{13}C{^{1}H} NMR ($CDCl_3$, 298 K, 75 MHz):** δ 175.78, 154.46, 130.68, 128.11, 127.48, 120.91, 117.33, 61.44, 35.37, 24.78, 14.21.

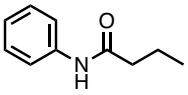

***N*-phenylbutyramide (3ac).** Compound **3ac** was prepared according to General Procedure B from compound **2ac.** The crude product was purified by flash column chromatography (silica gel, hexane/EtOAc 9:1) to obtain the corresponding product. The NMR data are consistent with the literature.[86]

^{1}H NMR (300 MHz, 298K, $CDCl_3$): δ 7.52 (d, *J* = 8.1 Hz, 2H), 7.38 (bs, 1H), 7.30 (t, *J* = 7.9 Hz, 2H), 7.09 (t, *J* = 7.4 Hz, 1H), 2.33 (t, *J* = 7.5 Hz, 2H), 1.75 (h, *J* = 7.4 Hz, 2H), 1.00 (t, *J* = 7.4 Hz, 3H). **^{13}C{^{1}H} NMR ($CDCl_3$, 298 K, 75 MHz):** δ 171.51, 138.12, 129.09, 124.29, 119.97, 39.80, 19.20, 13.87.

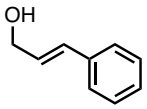

3-phenylprop-2-en-1-ol (3ad). Compound **3ad** was prepared according to General Procedure B from compound **2ad**. The crude product was purified by flash column chromatography (silica gel, hexane/EtOAc 9:1) to obtain the corresponding product. The NMR data are consistent with the literature.[89]

^{1}H NMR (300 MHz, 298K, $CDCl_3$): δ 7.41–7.38 (m, 2H), 7.35–7.30 (m, 2H), 7.25–7.19 (m, 1H), 6.63 (dt, *J* = 15.9, 1.6 Hz, 1H), 6.37 (dt, *J* = 15.9, 5.7 Hz, 1H), 4.33 (td, *J* = 5.7, 1.5 Hz, 2H). **^{13}C{^{1}H} NMR ($CDCl_3$, 298 K, 75 MHz):** δ 136.82, 131.33, 128.74, 128.65, 127.86, 126.62, 63.91.

III.5.7. Intermolecular competitive transfer hydrogenation

Procedure: In a 5 mL round bottom flask, acetophenone **6** (0.5 mmol), *trans*-chalcone **2a** (0.5 mmol), complex **1** (1 mol%) and 1,3,5-trimethoxybenzene (10 mol%) as internal standard were dissolved in EtOH (5 mL) and the solution was degassed with N_2 for 10 min. The catalytic run was started with the injection of K_2CO_3 (5 mol%, 2 M solution in H_2O), and the flask was placed in a pre-heated oil bath (25°C). Under N_2, aliquots (ca. 0.1 mL) were taken as set times and dissolved in $CDCl_3$ (0.5 mL) to determine the spectroscopic conversion and yields relative to the internal standard.

III.5.8. Transfer hydrogenation of α,β-saturated ketone

Procedure: In a 5 mL round bottom flask, 1,3-diphenylpropan-1-one **3a** (0.5 mmol), complex **1** (1 mol%) and 1,3,5-trimethoxybenzene (10 mol%) as internal standard were dissolved in EtOH (5 mL) and the solution was degassed with N_2 for 10 min. The catalytic run was started with the injection of K_2CO_3 (5 mol%, 2 M solution in H_2O), and the flask was placed in a pre-heated oil bath (25°C). Under N_2, aliquots (ca. 0.1 mL) were taken as set times and dissolved in $CDCl_3$ (0.5 mL) to determine the spectroscopic conversion and yields relative to the internal standard.

III.5.9. Use of allylic alcohol as model substrate

Procedure: In a 5 mL round bottom flask, trans-1,3-diphenyl-2-propen-1-ol **4a** (0.5 mmol), complex **1** (1 mol%) and 1,3,5-trimethoxybenzene (10 mol%) as internal standard were dissolved in EtOH (5 mL) and the solution was degassed with N_2 for 10 min. The catalytic run was started with the injection of K_2CO_3 (2 M solution in H_2O), and the flask was placed in a pre-heated oil bath (25°C). Under N_2, aliquots (ca. 0.1 mL) were taken as set times and dissolved in $CDCl_3$ (0.5 mL) to determine the spectroscopic conversion and yields relative to the internal standard.

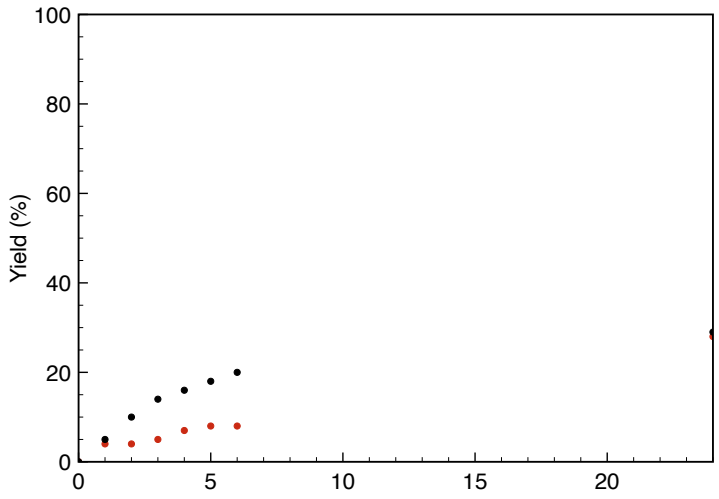

Figure III.37. Time-conversion profile for the catalytic hydrogenation of allylic alcohol **4a** to compound **3a** (black) and compound **5a** (red).

III.5.10. Isomerization of hex-1-ene

Procedure: The reaction was performed according to general procedure C (see section S.3.1). In a 5 mL round bottom flask, hex-1-ene (0.5 mmol), complex **1** (1 mol%) and 1,3,5-trimethoxybenzene (10 mol%) as internal standard were dissolved in EtOH (5 mL) and the solution was degassed with N_2 for 10 min. The catalytic run was started with the injection of K_2CO_3 (2 M solution in H_2O), and the flask was placed in a pre-heated oil bath (60°C).

Remarks: After 24 h (conversion 98 %), a mixture of isomerization products is obtained without the formation of any hydrogenated product. The absence of acetaldehyde or ethyl acetate, formed during the transfer hydrogenation in EtOH, is also indicative of the absence of hydrogenation.

III.5.11. Isomerization and transfer hydrogenation of 1-phenylbut-3-en-1-ol

Procedure: The reaction was performed according to general procedure C (see section S.3.1). In a 5 mL round bottom flask, 1-phenylbut-3-en-1-ol (0.5 mmol), complex **1** (1 mol%) and 1,3,5-trimethoxybenzene (10 mol%) as internal standard were dissolved in EtOH (5 mL) and the solution was degassed with N_2 for 10 min. The catalytic run was started with the injection of K_2CO_3 (2 M solution in H_2O), and the flask was placed in a pre-heated oil bath (60°C).

III.5.12. H_2 as hydrogen source

Procedure: In a 5 mL round bottom flask, *trans*-chalcone (0.5 mmol), complex **1** (1 mol%) and 1,3,5-trimethoxybenzene (10 mol%) as internal standard were dissolved in toluene (5 mL) and the solution was degassed with H_2 for 10 min. The catalytic run was started with the injection of K_2CO_3 (2 M solution in H_2O), and the flask was placed in a pre-heated oil bath (25°C).

III.5.13. Test of the activation of H_2 under transfer hydrogenation conditions

Procedure: In a 5 mL round bottom flask, *trans*-chalcone (0.5 mmol), complex **1** (1 mol%) and 1,3,5-trimethoxybenzene (10 mol%) as internal standard were dissolved in EtOH (5 mL) and the solution was degassed with N_2 for 10 min. The catalytic run was started with the injection of K_2CO_3 (2 M solution in H_2O), and the flask was placed in a pre-heated oil bath (25°C). After 15 min, the reaction atmosphere was replaced by bubbling H_2 for 5 min using a balloon. Under N_2 (before t = 15 min) or under H_2 (after t = 15 min), aliquots (ca. 0.1 mL) were taken as set times and dissolved in $CDCl_3$ (0.5 mL) to determine the spectroscopic conversion and yields relative to the internal standard.

Remarks: The data were compared to the standard conditions (Table III.2). Similar time-conversion profiles were obtained, suggesting that both complex **1** and the active species are inert towards H_2 activation. These results are in accordance with section III.5.12, showing that complex **1** in the presence of H_2 gas in toluene is not yielding to any hydrogenation after 1 h.

III.5.14. Reactions of complex 1 with a base in the presence of an excess of EtOH

Procedure: Compound **1** (8.4 mg, 13.7 μmol, 1 eq) was suspended in CD_2Cl_2 (0.5 mL) and KOH dissolved in H_2O (173 μL, 70 μmol, 2M, 5 eq) and EtOH (810 μL, 13.7 mmol, 1000 eq) were added at rt before being filtrated. The filtrate was directly analyzed in CD_2Cl_2, and the resulting precipitate was filtrated and dissolved in D_2O before being analyzed by ^{19}F NMR spectroscopy.

Remarks: To reproduce more closely the reaction conditions, a large excess of EtOH (1000 eq) was added in the presence of the base. Upon addition of KOH and EtOH, the reaction mixture immediately changes color from red to orange and is accompanied by the formation of precipitate. After 5 min, we observed by ^1H NMR spectroscopy that complex **1** has been fully consumed together with the formation of a new species, without hydride formation. Filtration of the reaction mixture indicated that the new compound is ^{19}F NMR spectroscopy silent, while the ^{19}F NMR analysis of the precipitate in D_2O suggested a PF_6^- salt. We assigned this new species to neutral complex [**1**]–OEt, in which the OEt^- is coordinating to the ruthenium center, with very similar chemical shifts to [**1**]–Cl complex previously reported.[61]

III.5.15. Preparation of [1]–OEt

Procedure: In a NMR tube, compound **1** (5 mg, 8.2 μmol, 1 eq) was suspended in MeOD (0.5 mL) and EtONa (1.1 mg, 16.5 μmol, 2 eq) was added at rt. The reaction was analyzed by ^1H NMR spectroscopy.

Remarks: Due to the lack of solubility of EtONa in CD_2Cl_2, the reaction was performed in MeOD. It is noteworthy to specify that no transfer hydrogenation is observed in MeOD at rt. After addition of EtONa, the reaction mixture immediately changes color from red to orange upon stirring. After 10 min, we observed by ^1H NMR spectroscopy that complex **1** has been fully consumed together with the formation of a new species, without hydride formation (up to -20 ppm). The chemical shift

similarities to the compound formed in the presence of an excess of EtOH and KOH suggest the formation of [**1**]–OEt under these two conditions. Concentration under vacuo of the reaction mixture yielded the starting compound **1**, indicating reversible coordination of EtO^- to the ruthenium center. Difficulties to isolate [**1**]–OEt, together with poor stability over time through *p*-cymene dissociation, did not allow further analysis.

III.5.16. Reactivity of [1]–OEt with *trans*-chalcone in the presence of EtOH

Procedure: In a NMR tube, compound **1** (8.3 mg, 13.7 μmol, 1 eq) was suspended in MeOD (0.5 mL) and EtONa (1.9 mg, 27.4 μmol, 2 eq) was added at rt to form compound **6** in situ. *Trans*-chalcone **2a** (14.6 mg, 68.4 μmol, 5 eq) and EtOH (400 μL, 6.9 mmol, 500 eq) were added to the reaction mixture. The reaction was analyzed by ^{1}H NMR spectroscopy.

Remarks: *In situ* reactivity tests were performed directly after the addition of EtONa. Surprisingly, upon the addition of *trans*-chalcone **2a** no hydrogenation was observed after 10 min by ^{1}H NMR spectroscopy. A large excess of EtOH (500 eq) was required to observe the corresponding hydrogenated product **3a**. These observations suggest that [**1**]–OEt is stable in the presence of the substrate and requires an excess of EtOH to either push the equilibrium towards the formation of an active Ru-H (less likely - not observed by ^{1}H NMR spectroscopy), or enable concomitant hydrogenation with EtO^- and EtOH.

III.6. References

[1] D. J. Foley, H. Waldmann, *Chem. Soc. Rev.* **2022**, *51*, 4094–4120.

[2] G. E. Keck, M. D. McLaws, *Tetrahedron Lett.* **2005**, *46*, 4911–4914.

[3] S. G. Davies, H. Rodríguez-Solla, J. A. Tamayo, A. C. Garner, A. D. Smith, *Chem. Commun.* **2004**, 2502–2503.

[4] A. Dahlén, G. Hilmersson, *Chem. Eur. J.* **2003**, *9*, 1123–1128.

[5] T. Ling, C. Chowdhury, B. A. Kramer, B. G. Vong, M. A. Palladino, E. A. Theodorakis, *J. Org. Chem.* **2001**, *66*, 8843–8853.

[6] Z.-Y. Wei, E. E. Knaus, *Tetrahedron Lett.* **1993**, *34*, 4439–4442.

[7] T. Hudlicky, G. Sinai-Zingde, M. G. Natchus, *Tetrahedron Lett.* **1987**, *28*, 5287–5290.

[8] M. J. Taschner, A. Shahripour, *J. Am. Chem. Soc.* **1985**, *107*, 5570–5572.

[9] K. Dey, G. De Ruiter, *Org. Lett.* **2024**, *26*, 4173–4177.

[10] B. B. C. Peters, J. Zheng, N. Birke, T. Singh, P. G. Andersson, *Nat. Commun.* **2022**, *13*, 361.

[11] D. Kong, Q. Qiqige, W. McNutt, R. Paciello, A. Schäfer, M. Schelwies, R. J. Lundgren, *Angew. Chem. Int. Ed.* **2022**, *61*, e202210601.

[12] I. Kisets, S. Zabelinskaya, D. Gelman, *Organometallics* **2022**, *41*, 76–82.

[13] Y. Gu, J. R. Norton, F. Salahi, V. G. Lisnyak, Z. Zhou, S. A. Snyder, *J. Am. Chem. Soc.* **2021**, *143*, 9657–9663.

[14] X. Du, Y. Xiao, J.-M. Huang, Y. Zhang, Y.-N. Duan, H. Wang, C. Shi, G.-Q. Chen, X. Zhang, *Nat. Commun.* **2020**, *11*, 3239.

[15] H. A. Patel, M. Rawat, A. L. Patel, A. V. Bedekar, *Appl. Organomet. Chem.* **2019**, *33*, e4767.

[16] J. Mendes-Burak, B. Ghaffari, C. Copéret, *Chem. Commun.* **2019**, *55*, 179–181.

[17] Y. Lin, D.-P. Zhu, Y.-R. Du, R. Zhang, S.-J. Zhang, B.-H. Xu, *Org. Lett.* **2019**, *21*, 2693–2698.

[18] W. Li, Y. Wang, P. Chen, M. Zeng, J. Jiang, Z. Jin, *Catal. Sci. Technol.* **2016**, *6*, 7386–7390.

[19] L. S. Bennie, C. J. Fraser, S. Irvine, W. J. Kerr, S. Andersson, G. N. Nilsson, *Chem. Commun.* **2011**, *47*, 11653–11655.

[20] M. D. Bhor, A. G. Panda, S. R. Jagtap, B. M. Bhanage, *Catal. Lett.* **2008**, *124*, 157–164.

[21] G. Brieger, T. J. Nestrick, *Chem. Rev.* **1974**, *74*, 567–580.

[22] R. Noyori, S. Hashiguchi, *Acc. Chem. Res.* **1997**, *30*, 97–102.

[23] M. J. Palmer, M. Wills, *Tetrahedron: Asymmetry* **1999**, *10*, 2045–2061.

[24] S. E. Clapham, A. Hadzovic, R. H. Morris, *Coord. Chem. Rev.* **2004**, *248*, 2201–2237.

[25] S. Gladiali, E. Alberico, *Chem. Soc. Rev.* **2006**, *35*, 226–236.

[26] C. Wang, X. Wu, J. Xiao, *Chem. Asian J.* **2008**, *3*, 1750–1770.

[27] D. Wang, D. Astruc, *Chem. Rev.* **2015**, *115*, 6621–6686.

[28] A. Corma, J. Navas, M. J. Sabater, *Chem. Rev.* **2018**, *118*, 1410–1459.

[29] L. Alig, M. Fritz, S. Schneider, *Chem. Rev.* **2019**, *119*, 2681–2751.

[30] D. Baidilov, D. Hayrapetyan, A. Y. Khalimon, *Tetrahedron* **2021**, *98*, 132435.

[31] M. F. Ansari, Anshika, J. Sortais, S. Elangovan, *Eur. J. Org. Chem.* **2024**, *27*, e202301278.

[32] Y. Xia, L. Ouyang, J. Liao, X. Yang, R. Luo, *SynOpen* **2021**, *05*, 36–42.

[33] D. Zhang, T. Iwai, M. Sawamura, *Org. Lett.* **2019**, *21*, 5867–5872.

[34] M.-J. Zhang, D.-W. Tan, H.-X. Li, D. J. Young, H.-F. Wang, H.-Y. Li, J.-P. Lang, *J. Org. Chem.* **2018**, *83*, 1204–1215.

[35] S. Chen, G. Lu, C. Cai, *RSC Adv.* **2015**, *5*, 13208–13211.

[36] B. Ding, Z. Zhang, Y. Liu, M. Sugiya, T. Imamoto, W. Zhang, *Org. Lett.* **2013**, *15*, 3690–3693.

[37] J. Broggi, V. Jurčík, O. Songis, A. Poater, L. Cavallo, A. M. Z. Slawin, C. S. J. Cazin, *J. Am. Chem. Soc.* **2013**, *135*, 4588–4591.

[38] X. Li, L. Li, Y. Tang, L. Zhong, L. Cun, J. Zhu, J. Liao, J. Deng, *J. Org. Chem.* **2010**, *75*, 2981–2988.

[39] Z. Baán, Z. Finta, G. Keglevich, I. Hermecz, *Green Chem.* **2009**, *11*, 1937.

[40] C.-H. Doi, T. Fukuyama, J. Horiguchi, T. Okamura, I. Ryu, *Synlett* **2006**, *5*, 0721–0724.

[41] S. Sakaguchi, T. Yamaga, Y. Ishii, *J. Org. Chem.* **2001**, *66*, 4710–4712.

[42] D. H. Appella, Y. Moritani, R. Shintani, E. M. Ferreira, S. L. Buchwald, *J. Am. Chem. Soc.* **1999**, *121*, 9473–9474.

[43] Y. Sasson, J. Blum, *J. Org. Chem.* **1975**, *40*, 1887–1896.

[44] X. Yu, S. Wan, W. Zhou, *Synlett* **2023**, *34*, 1399–1402.

[45] N. Garg, H. P. Somasundharam, P. Dahiya, B. Sundararaju, *Chem. Commun.* **2022**, *58*, 9930–9933.

[46] A. Mandal, K. Ganguli, M. Pradhan, A. Gorai, S. Kundu, *ChemSusChem* **2023**, *16*, e202300683.

[47] A. Sau, D. Mahapatra, S. Dey, D. Panja, S. Saha, S. Kundu, *Org. Chem. Front.* **2023**, *10*, 2274–2286.

[48] N. Castellanos-Blanco, M. Flores-Alamo, J. J. García, *Organometallics* **2012**, *31*, 680–686.

[49] P. Weingart, W. R. Thiel, *ChemCatChem* **2018**, *10*, 4844–4848.

[50] A. C. Papes Filho, R. Maciel Filho, in *Blucher Chemical Engineering Proceedings*, **2018**, 2478–2481.

[51] W.-H. Lin, H.-F. Chang, *Catal. Today* **2004**, *97*, 181–188.

[52] C. S. Gong, N. J. Cao, J. Du, G. T. Tsao, in *Recent Progress in Bioconversion of Lignocellulosics* (Eds.: G.T. Tsao, A.P. Brainard, H.R. Bungay, N.J. Cao, P. Cen, Z. Chen, J. Du, B. Foody, C.S. Gong, P. Hall, N.W.Y. Ho, D.C. Irwin, P. Iyer, T.W. Jeffries, C.M. Ladisch, M.R. Ladisch, Y.Y. Lee, N.S. Mosier, H.M. Mühlemann, M. Sedlak, N.-Q. Shi, G.T. Tsao, J.S. Tolan, R.W. Torget, D.B. Wilson, L. Xia), **1999**, 207–241.

[53] C. C. Geddes, I. U. Nieves, L. O. Ingram, *Curr. Opin. Biotechnol.* **2011**, *22*, 312–319.

[54] R. A. Farrar-Tobar, Z. Wei, H. Jiao, S. Hinze, J. G. de Vries, *Chem. Eur. J.* **2018**, *24*, 2725–2734.

[55] R. D. Patil, A. R. Shelte, A. V. Biradar, S. Pratihar, *Appl. Organomet. Chem.* **2023**, *37*, e7221.

[56] T. Zweifel, J.-V. Naubron, T. Büttner, T. Ott, H. Grützmacher, *Angew. Chem. Int. Ed.* **2008**, *47*, 3245–3249.

[57] Y. Wang, Z. Huang, X. Leng, H. Zhu, G. Liu, Z. Huang, *J. Am. Chem. Soc.* **2018**, *140*, 4417–4429.

[58] R. D. Patil, S. Pratihar, *J. Org. Chem.* **2024**, *89*, 1361–1378.

[59] V. Vigneswaran, S. N. MacMillan, D. C. Lacy, *Organometallics* **2019**, *38*, 4387–4391.

[60] S. Horn, C. Gandolfi, M. Albrecht, *Eur. J. Inorg. Chem.* **2011**, *2011*, 2863–2868.

[61] A. Beaufils, P. Melle, N. Lentz, M. Albrecht, *Inorg. Chem.* **2024**, *63*, 2072–2081.

[62] P. Weingart, Y. Sun, W. R. Thiel, *ChemCatChem* **2020**, *12*, 6223–6233.

[63] M. Delgado-Rebollo, D. Canseco-Gonzalez, M. Hollering, H. Mueller-Bunz, M. Albrecht, *Dalton Trans.* **2014**, *43*, 4462–4473.

[64] Corwin. Hansch, A. Leo, R. W. Taft, *Chem. Rev.* **1991**, *91*, 165–195.

[65] H. Wang, B. Liu, F. Liu, Y. Wang, X. Lan, S. Wang, B. Ali, T. Wang, *ACS Sustain. Chem. Eng.* **2020**, *8*, 8195–8205.

[66] M. Ito, S. Kitahara, T. Ikariya, *J. Am. Chem. Soc.* **2005**, *127*, 6172–6173.

[67] Separation of the precipitate by filtration and analysis of a D_2O solution by ^{19}F NMR spectroscopy revealed a doublet at $\delta_F = -72.10$ ($J_{PF} = 709$ Hz), in agreement with the presence of a PF_6^- salt, see for example R. R. Golwankar, T. D. Curry II, C. J. Paranjothi, J. D. Blakemore, *Inorg. Chem.* **2023**, *62*, 9765–9780.

[68] Another hypothesis involves the deprotonation of the ligand NH site, though experiments using 1 and KOtBu in CD_2Cl_2 did not give any compelling evidence for ligand deprotonation and only minor shifts of the ligand resonances were observed. Therefore this hypothesis has not been pursued any further. Moreover, reaction of **1** with KOtBu in CD_3OD gave [**1**]–OtBu, though this complex showed only very poor reactivity in chalcone hydrogenation even in the presence of a large excess of EtOH. This distinct reactivity has been attributed to stronger bonding of the alkoxide in [**1**]–OtBu vs [**1**]–OEt and thus inhibition of β-hydrogen elimination to form the putative hydride required for hydrogen transfer.

[69] W. Xu, Y. Zhou, R. Wang, G. Wu, P. Chen, *Org. Biomol. Chem.* **2012**, *10*, 367–371.

[70] A. Seitz, P. J. Kohlpaintner, T. Van Lingen, M. Dyga, F. Sprang, M. Zirbes, S. R. Waldvogel, L. J. Gooßen, *Angew. Chem. Int. Ed.* **2022**, *61*, e202117563.

[71] M. Zheng, C. Huang, J.-Z. Yan, S.-L. Xie, S.-J. Ke, H.-D. Xia, Y.-N. Duan, *J. Org. Chem.* **2023**, *88*, 1504–1514.

[72] A. E. Lubaev, M. D. Rathnayake, F. Eze, L. Bayeh-Romero, *J. Am. Chem. Soc.* **2022**, *144*, 13294–13301.

[73] X. Jiang, H. Jin, T. Wang, H. Yoo, S. Koo, *Synthesis* **2019**, *51*, 3259–3268.

[74] D.-D. Chen, B.-Y. Zhang, X.-X. Liu, X.-Q. Li, X.-J. Yang, L. Zhou, *Bioorg. Med. Chem. Let.* **2018**, *28*, 1149–1153.

[75] J. Ji, Z. Yang, R. Liu, Y. Ni, S. Lin, Q. Pan, *Tetrahedron Let.* **2016**, *57*, 2723–2726.

[76] G. Zhang, J. Wu, H. Zeng, S. Zhang, Z. Yin, S. Zheng, *Org. Lett.* **2017**, *19*, 1080–1083.

[77] A. S. Nayak, S. Jaiswal, M. K. Sahu, C. Gunanathan, *J. Chem. Sci.* **2024**, *136*, 5.

[78] Y. Saga, Y. Nakayama, T. Watanabe, M. Kondo, S. Masaoka, *Org. Lett.* **2023**, *25*, 1136–1141.

[79] A. Naderi, A. Akıncıoğlu, A. Çağan, H. Çelikkaleli, H. Akıncıoğlu, S. Göksu, *Bioorg. Chem.* **2024**, *144*, 107146.

[80] E. K. Nielsen, K. El-Chami, C. M. De Lichtenberg, R. Madsen, *Eur. J. Org. Chem.* **2024**, *27*, e202400109.

[81] X. Yang, Y. Guo, H. Tong, H. Guo, R. Liu, R. Zhou, *Org. Lett.* **2023**, *25*, 5486–5491.

[82] D. D. Youmans, H. N. Tran, L. M. Stanley, *Org. Lett.* **2023**, *25*, 3559–3563.

[83] Y. Zhu, B. Zhao, Y. Shi, *Org. Lett.* **2013**, *15*, 992–995.

[84] M. Yang, Z. Xing, B. Fang, X. Xie, X. She, *Org. Biomol. Chem.* **2020**, *18*, 288–291.

[85] Z. Ding, C. Li, J. Chen, J. Zeng, H. Tang, Y. Ding, Z. Zhan, *Adv. Synth. Catal.* **2017**, *359*, 2280–2287.

[86] L. Li, X. Wang, N. Fu, *Angew. Chem. Int. Ed.* **2024**, *63*, e202403475.

[87] Q. Ji, O. Š. Miljanić, *J. Org. Chem.* **2013**, *78*, 12710–12716.

[88] Z. Deng, S. Han, M. Ke, Y. Ning, F.-E. Chen, *Chem. Commun.* **2022**, *58*, 3921–3924.

[89] E. Klumbys, Z. Zebec, N. J. Weise, N. J. Turner, N. S. Scrutton, *Green Chem.* **2018**, *20*, 658–663.

Chapter IV

Ligand Modification for the Tuning of Activity and Selectivity in Chemoselective Transfer Hydrogenation of α,β-Unsaturated Carbonyls using EtOH as Hydrogen Source

IV.1. Abstract

The selective olefin reduction of α,β-unsaturated ketones is an attractive method, particularly using environmentally friendly ethanol as hydrogen source. Recently, we reported a coordinatively unsaturated N,N'-bidentate pyridinium amidate (PYA) ruthenium **3a** as an efficient catalyst for ethanol-based transfer hydrogenation of α,β-unsaturated ketones, however with a decrease in the selectivity towards olefin hydrogenation over an extended period of time. Using the facile modification of PYA ligands, we synthesized a series of PYA ruthenium complexes **3b–e** derived from the **3a** with modifications on the acyl unit. ^{1}H NMR spectroscopy of these complexes in CD_2Cl_2 and CD_3OD suggests a higher contribution of the neutral quinoidal structure in the PYA unit in donor solvent, particularly interesting in the stabilization of catalytically relevant alkoxide intermediate **4**. Application of complexes **3a–3e** in transfer hydrogenation of *trans*-chalcone indicates a good selectivity towards olefin hydrogenation, particularly for complex **3c** providing almost exclusively the desired ketone product with only traces of the saturated alcohol after 24h.

IV.2. Introduction

We previously demonstrated the ability of a ruthenium complex bearing a N,N-bidentate pyridinium amidate (PYA) ligand to efficiently catalyze the transfer hydrogenation of α,β-unsaturated ketones under mild conditions using ethanol as a renewable and attractive hydrogen source.[1] Despite their high efficiency, the hydrogen transfer led to over-reduction of the C=O bond after complete transformation of the olefinic C=C bond, thus limiting its applicability since quenching of the reaction at full conversion is necessary to maintain high selectivity. This limitation prompted us to investigate the implication of the ligand system in order to suppress the undesired carbonyl reduction reactivity.

Among the PYA ligands reported over the years, one influential variation on the ligand scaffold pertains to the acyl unit. For example, carbonyl substituents incorporating donor motifs, as pyridine, NHC, or phenyl, as chelating ligands have been developed.[2–5] Taking advantage of the specific N,N'-coordination of the ligand and the easy modification of PYAs,[6] in this chapter, we describe the synthesis and characterization of a series of N,N'-bidentate PYA ruthenium complexes with modified acyl units. In addition to the flexible N-donation of the PYA unit,[6] either coordinating as a π-acidic nitrogen **A** or a neutral π-basic structure **B** (Figure IV.1), thus facilitating the stabilization of the metal center, we envisioned that the acyl substituents **R** can also affect the electronic properties of the metal center. Another limiting resonance structure **A'** can be proposed, with the introduction of a neutral nitrogen within the acyl unit (Figure IV.1). Such electronic modulation in the acyl unit was previously observed with first-row pincer-type PYA complexes, though with a change in the acyl coordination from nitrogen to oxygen.[7] Furthermore, steric effects at this position may influence the accessibility of the metal center by the substrate, thus impacting both activity and selectivity, a common challenge for transfer hydrogenation of α,β-unsaturated ketones. [8,9]

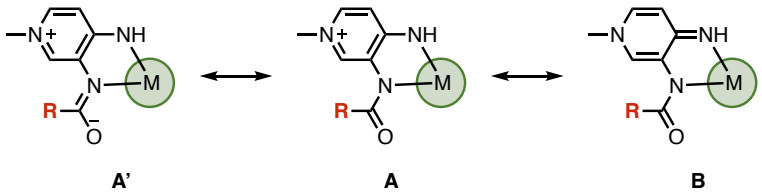

Figure IV.1. Schematic representation of the limiting resonance structures in N,N'-bidentate PYA complexes.

We further explore the impact of these systematic acyl modifications with the catalytic application of this series of N,N'-bidentate PYA ruthenium complexes in transfer hydrogenation using ethanol as hydrogen source. Our study discloses how variations of the acyl unit can enhance the selectivity towards olefin reduction over extended reaction times.

IV.3. Results and discussion

Synthesis and characterization of second-generation of *N,N'*-bidentate PYA ruthenium complexes. The ligand precursor pyridinium salts were synthesized according to previously reported procedures,[10] starting from *tert*-butyl(3-amino-pyridin-4-yl)carbamate and substituted acyl chlorides (Scheme IV.1.a). The acyl chlorides were commercially available except for 4-methoxy-1-naphthoyl chloride, which was synthesized in quantitative yield from the corresponding carboxylic acid in the presence of an excess of $SOCl_2$. Amidation of these acyl chlorides under basic conditions yielded compounds **1a–e** in acceptable 54–90% yields. In the presence of 5 eq of MeOTf, selective methylation of the pyridine nitrogen accompanied with Boc-deprotection of the 4-amino sites yielded the corresponding pyridinium salts **2a–e**. Direct anion exchange from OTf^- to PF_6^- was performed for complexes 2a and 2b and was accomplished with an excess of NH_4PF_6 in a $MeCN/H_2O$ mixture. While the triflate salt of **2b** was isolated as an oil, the PF_6^- analogue was obtained as a solid, which facilitated purification considerably. An attempt to expand the aryl substituent to anthracyl groups failed because methylation of **1f** gave only decomposition products irrespective of the methylating agent (MeOTf or MeI), or the reaction conditions (25–40°C, CH_3CN or CH_2Cl_2 as solvent, 1–5 eq MeX) and yielded the starting compound pyridine-3,4-diamine as the major product (Scheme IV.1.b). Salts **2a–b** were ruthenated in the presence of $[RuCl_2(cym)]_2$ (cym = p-cymene) and NaOAc in CH_2Cl_2 under reflux conditions, and with the addition of $NaPF_6$ for salts **2c–e** to afford the corresponding air- and moisture-stable complexes **3a–e** in 66–92% yield. Successful formation of the ruthenium complexes **3a–e** was indicated macroscopically by a change of color of the reaction mixture from light to dark red and was confirmed by mass spectrometry and elemental analysis. Evidence for the formation of complexes **3a–e** was obtained by ^1H NMR spectroscopy, with loss of the amide proton resonance and strong deshielding of the NH singlet integrating for one proton only. Moreover, while the pyridylidene protons $H_{\alpha'}$ and H_β shifted downfield upon ruthenation, the pyridylidene protons H_α noticeably shifted downfield for all complexes **3a–e**. Complexation of ligand **2g** with an alkyl rather than an aryl substituent, led to a mixture of products and was not pursued further (Scheme IV.1.b).

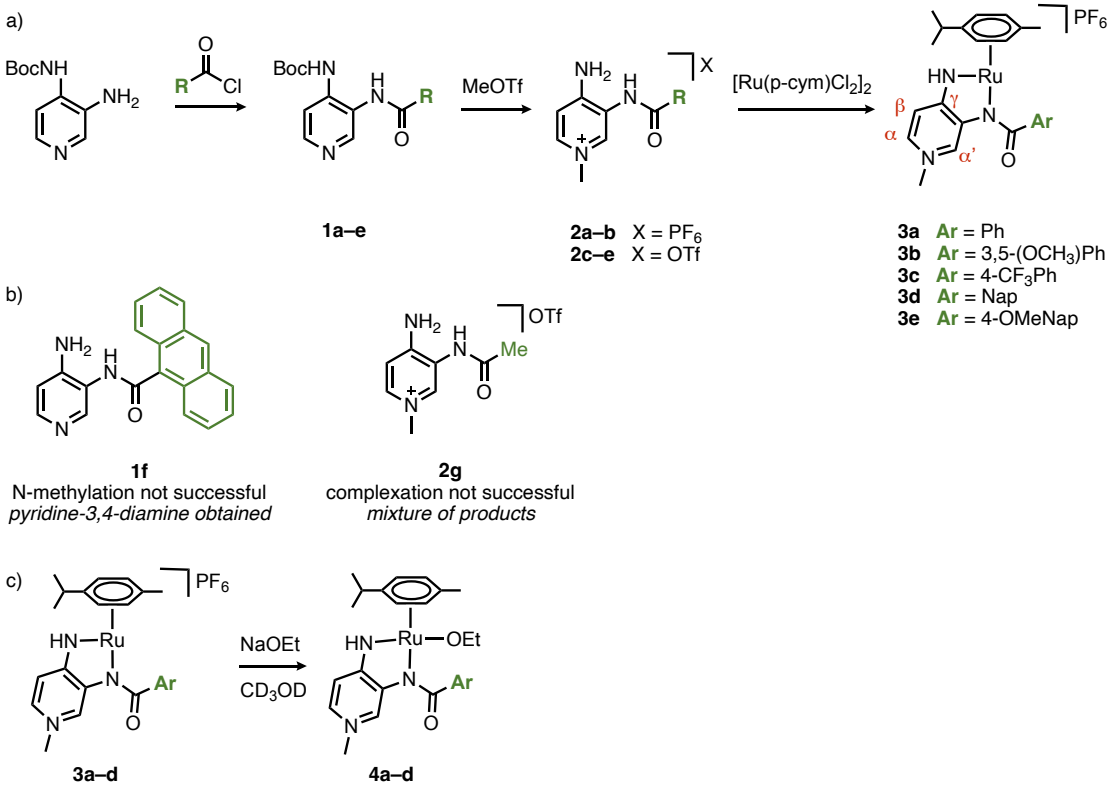

Scheme IV.1. a) General synthesis of complexes **3a–e**; b) Unsuccessful synthesis; c) Synthesis of alkoxides complexes **4a–d**.

Spectroscopic and structural analysis of complexes 3a–e.

We previously described the flexible character of the PYA ligand in complex **3a**, which either stabilizes the formally underligated complex through π-donation (neutral quinoidal structure **B**, Figure IV.1) or facilitates through π-acidic bonding properties the coordination of another ligand L to the ruthenium center (through resonance form **A**).[10] The chemical shift difference between pyridylidene protons H_α and H_β (cf. Scheme IV.1) is a diagnostic probe to evaluate the electronic structure of the ligand, with larger values indicating higher contribution of the neutral quinoidal form **B**. Comparison of chemical shifts of pyridylidene H_α, $H_{\alpha'}$ and H_β protons of complexes **3a–e** in CD_2Cl_2, a non-coordinating solvent, gave no compelling evidence of a change in the ligand electronic structure upon variation of the acyl substituents (Table IV.1, entries 1–5). Most notably, $H_{\alpha'}$ is considerably deshielded in complexes **3d** and **3e** (δ_H = 9.22 and 8.94, respectively) in comparison to the frequencies observed for complexes **3a–c**, δ_H = 8.56(1), which has been tentatively attributed to a more defined orientation of the naphthyl substituents compared to the phenyl analogues and ensuing hydrogen bonding of the carbonyl oxygen with $H_{\alpha'}$. However, $\Delta(H_\alpha–H_\beta)$ is very similar in all complexes around 0.10(3) ppm. When the ^{1}H NMR analyses were performed in CD_3OD instead of CD_2Cl_2, a significant increase of the chemical shift differences of these pyridylidene protons to $\Delta(H_\alpha–H_\beta)$ = 0.46(3) ppm was observed (entries 6–10). A shift, though smaller, is also observed in the aromatic *p*-cym protons (Table IV.7, supporting information). This larger shift difference in CD_3OD for complexes **3a–e** suggests a higher contribution of the quinoidal form **B** in CD_3OD. Although opposed to what is generally observed,[2,11,12] this behavior is similar to recently reported

coordinatively unsaturated iridium PYE complexes manifesting more relevant contribution of the L-type ligand in polar solvents.[13] In both cases, reversible solvent coordination leading to a higher electron density at the metal center may induce the higher predominance of the neutral quinoidal structure.

Table IV.1. Selected ^{1}H NMR shifts (ppm) of the CH_α, $CH_{\alpha'}$, CH_β units for complexes **3a–e** and **4a–d**.

entry	complex	solvent	$H_{\alpha'}$	H_α	H_β	$\Delta(H_{\alpha'}–H_\beta)$	$\Delta(H_\alpha–H_\beta)$
1	**3a**	CD_2Cl_2	8.55	7.35	7.28	1.27	0.07
2	**3b**	CD_2Cl_2	8.55	7.34	7.25	1.30	0.09
3	**3c**	CD_2Cl_2	8.57	7.38	7.30	1.27	0.08
4	**3d**	CD_2Cl_2	9.22	7.42	7.29	1.93	0.13
5	**3e**	CD_2Cl_2	8.94	7.38	7.28	1.66	0.10
6	**3a**	CD_3OD	8.67	7.61	7.18	1.49	0.43
7	**3b**	CD_3OD	8.70	7.58	7.15	1.55	0.43
8	**3c**	CD_3OD	8.76	7.58	7.09	1.67	0.49
9	**3d**	CD_3OD	9.28	7.98	7.12	2.16	0.86
10	**3e**	CD_3OD	9.03	7.66	7.20	1.83	0.46
11	**4a**	CD_3OD	8.91	7.28	6.63	2.28	0.65
12	**4b**	CD_3OD	8.96	7.12	6.38	2.58	0.74
13	**4c**	CD_3OD	9.07	7.14	6.40	2.67	0.74
14	**4d**	CD_3OD	9.26	7.17	6.42	2.84	0.75

Preliminary mechanistic studies of the catalytic transfer hydrogenation with complex **3a** using EtOH as hydrogen source suggest the formation of the alkoxide complexes **4** as an initially formed species. Alkoxide coordination to complexes **3a–d** was accomplished with NaOEt in CD_3OD (Scheme IV.1.c) and induced an even larger separation of H_α and H_β protons $\Delta(H_\alpha–H_\beta)$ = 0.70(5) ppm (Table IV.1, entries 11–14), with $\Delta(H_\alpha–H_\beta)$ indicating a more pronounced quinoidal form upon coordination of an anionic ligand. Such a modification of the PYA properties towards a more π-acidic bonding mode is in accordance with a higher electron density at the ruthenium center.[10] These NMR spectroscopic data therefore underscore the electronically dynamic character of the PYA system (Figure IV.2), with a higher contribution of the neutral resonance form **B** in donor solvents, which is particularly useful to generate and stabilize the catalytically relevant intermediate **4**.

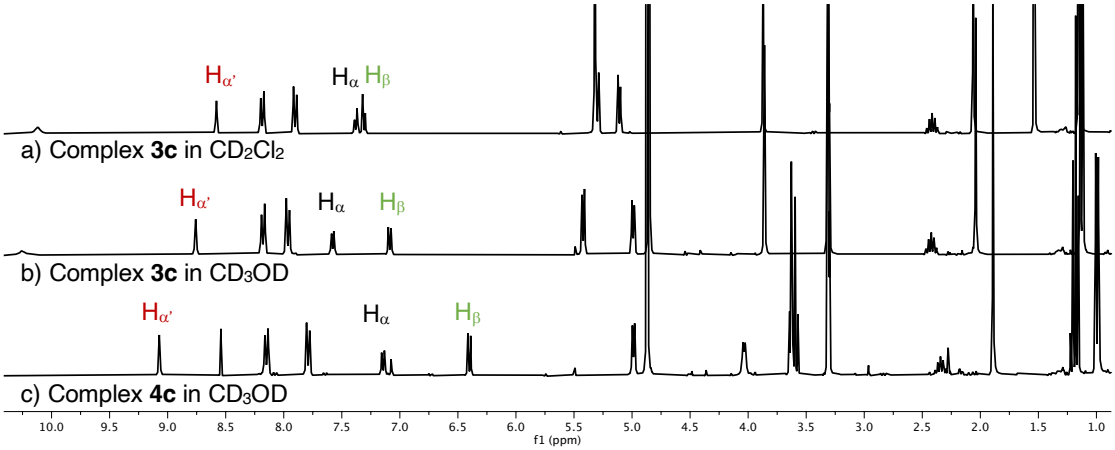

Figure IV.2. Stacked ^{1}H NMR spectra (298K, 300 MHz) of a) complex **3c** in CD_2Cl_2, b) **3c** in CD_3OD, and c) **4c** in CD_3OD, showing the chemical shift of pyridylidene protons H_α, $H_{\alpha'}$, and H_β.

UV-Vis spectroscopy has been used to probe the donor strength of the ligand system (Table IV.2).[14] The MLCT bands in the visible region are useful indicators of the electronic impact of the ligand. Figure IV.3.a shows the UV-Vis absorption spectra of complexes **3a–e** measured in CH_2Cl_2. Very similar absorption bands were observed, with λ_{max} = 410±1 nm for all complexes **3a–e**. This similarity is in alignment with the similar shifts of pyridylidene protons for complexes **3a–e** in non-coordinating solvent, suggesting no impact of the acyl modification on the ligand donor properties under these conditions. Very little or no bath- or hypsochromic shift of the band was observed upon changing the solvent to CH_3OH, but only a hypochromic effect for complexes **3a–e** (Figure IV.3.b). It should be mentioned that a change in the molar absorptivity cannot be interpreted in an easy qualitative manner as for bath- or hypsochromic effects.[15] As underlined by Schulz,[16] the rationalization of solvatochromism, determined by the metal-ligand bond polarities in the ground and MLCT excited state of the complex, is not simple and can be associated with ligand basicity, loss of aromaticity, and usually need further support from calculated Hückel MO coefficients c^2 and ESR coupling constants from the ligand coordination centers, and redox potentials of the coordinated metal fragments.

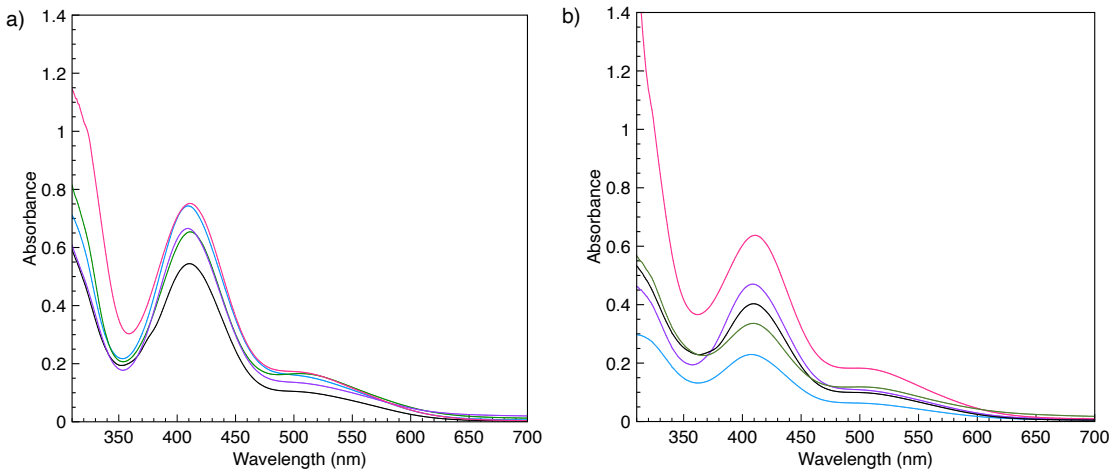

Figure IV.3. UV-Vis absorption spectra of Ru(II) PYA complexes with various acyl substituents in CH_2Cl_2 (a) and in CH_3OH (b); color key: **3a** (violet), **3b** (black), **3c** (blue), **3d** (green), and **3e** (pink).

Table IV.2. Absorption maxima λ_{max} (nm) and extinction coefficients ε ($M^{-1}cm^{-1}$) for complexes **3a–e** in CH_2Cl_2 and CH_3OH.

entry	complex	solvent	λ_{max} (nm)[a]	ε ($M^{-1}.cm^{-1}$)[b]
1	**3a**	CH_2Cl_2	409	13×10^3
2	**3a**	CH_3OH	409	9×10^3
3	**3b**	CH_2Cl_2	410	11×10^3
4	**3b**	CH_3OH	409	8×10^3
5	**3c**	CH_2Cl_2	409	15×10^3
6	**3c**	CH_3OH	407	5×10^3
7	**3d**	CH_2Cl_2	411	13×10^3
8	**3d**	CH_3OH	409	7×10^3
9	**3e**	CH_2Cl_2	411	15×10^3
10	**3e**	CH_3OH	411	13×10^3

[a]0.1 nm wavelength accuracy; [b]<10% esd.

Electrochemical measurement is another technique to probe the ligand-based electronic properties by evaluating the electron density at the metal center. However, cyclic voltammetry measurement of complex **3a** revealed four reversible processes: $E_{1/2}$ = +0.24, +0.72, + 1.18, and + 1.51 V, presumably a combination of 2e ligand- and 1e metal-centered oxidation (Figure IV.4). The difficulty in attributing and thus rationalizing the different processes does not allow further use of this technique to probe the donor strength of the ligand.

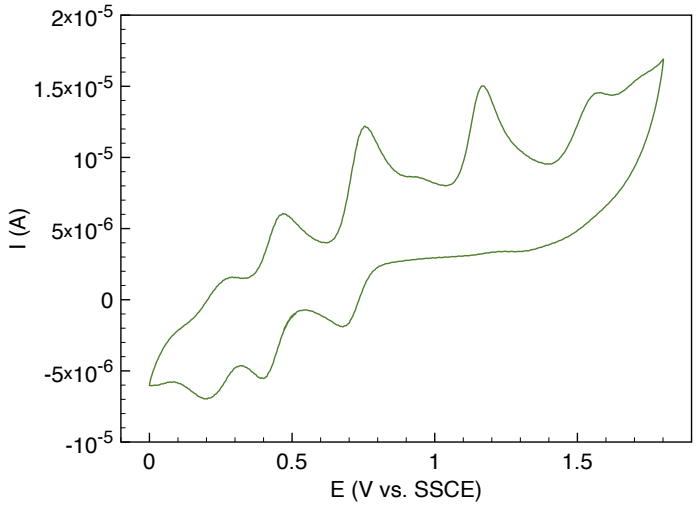

Figure IV.4. Cyclic voltammetry measurement of complex **3a**. Potential vs. Fc^+/Fc couple in CH_3CN, $(Bu_4N)PF_6$ as supporting electrolyte.

Suitable crystals of complex **3b** for X-ray diffraction analysis were obtained from a CH_2Cl_2/Et_2O mixture. The structure of complex **3b** revealed a two-legged piano-stool geometry in the solid state (Figure IV.5). The pyramidalization angle α, representing the angle between the centroid of the N–Ru–N moiety, the Ru center, and the centroid of the capping *p*-cymene, is a good indicator of the coordinative unsaturation of complexes.[17] Complexes **3a** and **3b** present a pyramidalization angle α of 176°, confirming the absence

of agostic interactions between the ligand and the metal center and a monomeric structure in the solid-state (Table IV.3). Comparison of the bond lengths with complex **3a**, bearing a phenyl group instead of 3,5-triomethoxyphenyl, revealed a highly similar structure within the PYA system. While single crystals of complexes **3c** and **3e** were also grown, they did not diffract enough for a full measurement. Nonetheless, the preliminary structure of complex **3c** revealed the same two-legged piano stool structure as confirmed for **3b**.

Table IV.3. Selected bond lengths (Å) and angles (deg) in complexes **1** and **2**.

	complex **3a**	complex **3b**
Ru1–N1	1.963(2)	1.968(2)
Ru1–N2	2.043(2)	2.044(2)
N1–C1	1.340(4)	1.338(3)
N2–C5	1.396(3)	1.396(3)
N2–C7	1.398(3)	1.399(2)
C7–O1	1.216(3)	1.216(2)
C7–C8	1.493(3)	1.500(3)
C_α–C_β[a]	1.371(8)	1.367(7)
C_β–C_γ[b]	1.415(6)	1.415(5)
N3–C_α[c]	1.352(6)	1.354(6)
N1–Ru–N2	78.63(8)	78.52
α[d]	176.55	176.75

[a]C_α–C_β is the average bond length of C2–C3 and C4–C5. [b]C_β–C_γ is the average bond length of C1–C2 and C1–C5. [c]N3–C_α is the average bond length of N3–C3 and N3–C4. [d]Pyramidalization angle α is the angle between the centroid of N–Ru–N moiety, Ru, and the centroid of *p*-cym.

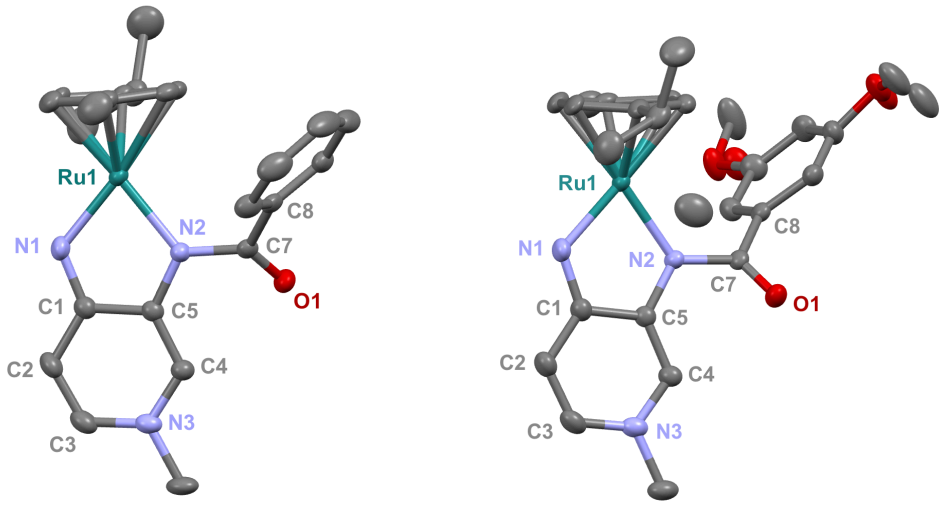

Figure IV.5. Molecular structure of complexes **3a** (left)[9] and **3b** (right) from X-ray diffraction (50% probability ellipsoids; hydrogen atoms and non-coordinating PF_6^- anions omitted for clarity).

Chemoselective transfer hydrogenation of α,β-unsaturated ketones. Based on the activity of **3a** in the chemoselective transfer hydrogenation of unsaturated ketones,[1] complexes **3a–e** were investigated in this reaction using *trans*-chalcone **5a** as model substrate (Table IV.4). Under optimized conditions, *i.e.* 1 mol% complex and 5 mol% K_2CO_3 in 5 mL EtOH at 25 °C under a N_2 atmosphere, complex **3a** achieved 98% yield of the desired saturated ketone **6a** within 1 h. Time-dependent monitoring of the conversion revealed a maximum turnover frequency $TOF_{C=C}$ = 170 h^{-1} (entry 1). The reaction rates were slower when using complexes **3b** or **3c**, which required 3 and 2 h, respectively, to reach similar yields (entries 2–3). The most active complex of this series was the naphthalene-based complex **3d**, with a $TOF_{C=C}$ = 200 h^{-1} and achieving 97% yield of ketone **6a** in 50 min (entry 4). Similarly, 96% yield of **6a** was obtained with complex **3e** after a slightly longer reaction time of 1 h (entry 5). Further monitoring of the reaction revealed that upon full consumption of the substrate, hydrogenation of the carbonyl bond was initiated to eventually afford the fully saturated alcohol **7a**. This second hydrogenation was slower for all catalysts tested here, as seen from the $TOF_{C=O}$ equal or inferior to 11 h^{-1} (see Experimental section for details). For example, complex **3a** accomplished 59% ketone hydrogenation in 24 h to give the alcohol **7a** (Figure IV.6.a). Complex **3b**, which is less active in olefin hydrogenation, is also less active in carbonyl hydrogenation, yielding a modest 11% of the fully saturated product **7a** after 24 h (Figure IV.6.b). Complex **3c** is even slower in this second hydrogenation, and the ketone was recovered in 98% after 24 h (Figure IV.6.c). In sharp contrast, the fastest olefin hydrogenation complex **3d** ($k_{C=C}$ = 101 10^{-5} h^{-1}) also showed high activity towards C=O bond hydrogenation and reached 85% yield of alcohol **6a** in 24 h ($k_{C=O}$ = 5.5 10^{-5} h^{-1}, Figure IV.6.d). Similarly, a lack of selectivity was observed with complex **3e**, with 61% of the fully hydrogenated product **7a** present after 24 h (Figure IV.6.e). While these data indicate good general selectivity towards olefin hydrogenation of all complexes **3a–e**, the specificity of complex **3c** stands out as it provides exclusively the ketone product with only traces of the saturated alcohol even after extended reaction times.

Table IV.4. Comparison of catalytic data for transfer hydrogenation of *trans*-chalcone using complexes **3a–e**.[a]

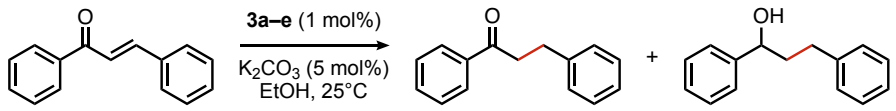

	5a		**6a**		**7a**		
entry	complex	$yield_{max}$ **5a** (time)	**5a** : **6a** (%) (24 h)	$k_{C=C}$ (10^{-5} h^{-1})	$k_{C=O}$ (10^{-5} h^{-1})	$TOF_{C=C}$ (h^{-1})	$TOF_{C=O}$ (h^{-1})
1	**3a**	98% (1 h)	41 : 59	74	3.9	170	7
2	**3b**	98% (3 h)	90 : 11	38	~1.5[b]	100	2
3	**3c**	98% (2 h)	98 : 2	56	0.5	130	1
4	**3d**	97% (0.83 h)	15 : 85	101	5.5	200	11
5	**3e**	96% (1 h)	39 : 61	76	5.1	160	9

[a]Reaction conditions: *trans*-chalcone (0.5 mmol), K_2CO_3 (5 mol%), complex **3a–e** (1 mol%) in EtOH (5 mL), 25 °C, N_2; yields determined by ^1H NMR spectroscopy relative to 1,3,5-trimethoxybenzene from duplicate runs. R^2 for rates > 0.98. [b]Not enough data points for an accurate determination.

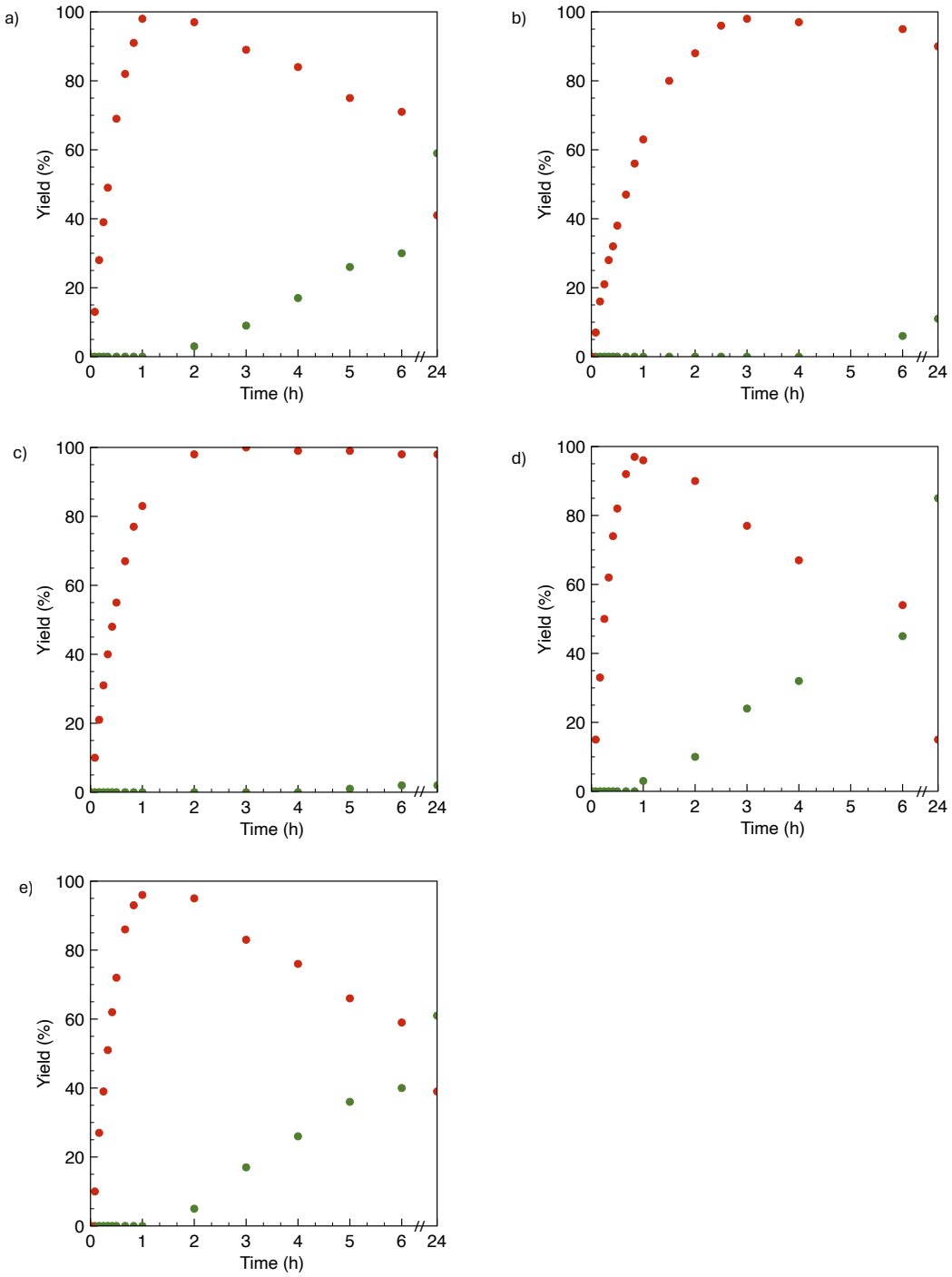

Figure IV.6. Time-conversion profiles of transfer hydrogenation of *trans*-chalcone **5a** to form subsequently 1,3-diphenylpropan-1-one (red) and 1,3-diphenylpropan-1-ol (green) using EtOH as hydrogen source under the standard conditions catalyzed by a) complex **3a**; b) complex **3b**; c) complex **3c**; d) complex **3d**, e) complex **3e**.

Transfer hydrogenation of α,β-saturated ketones. This trend in ketone hydrogenation activity of complexes **3a–e** was further confirmed when using pure 1,3-diphenylpropan-1-one **6a** directly as substrate under the optimized catalytic conditions (Figure IV.7). In this reaction, complex **3d** provided again the most active catalyst, with 91% of alcohol **7a** after 24 h *vs* 85% starting from *trans*-chalcone (Table IV.5, entry 4). Moderate yields of 70% and 62% were obtained for complexes **3a** and **3e**,

respectively (entries 1 and 5), and **3b** achieved only 41% yield within 24 h. Complex **3c** gave the lowest activity towards C=O bond hydrogenation, with 14% yield of alcohol product **6a** after 24 h.[18]

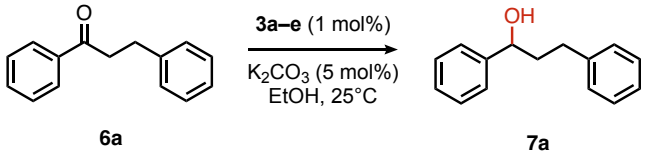

6a **7a**

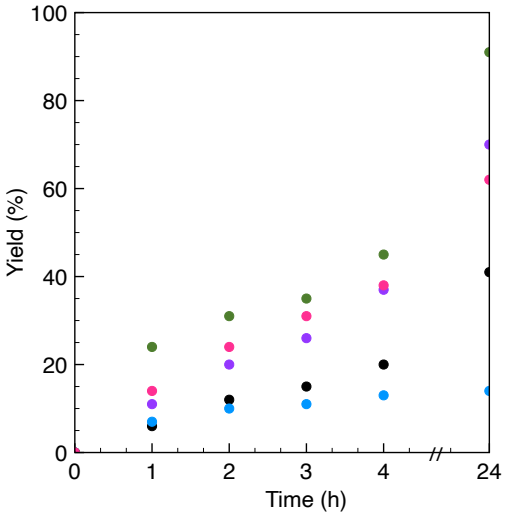

Figure IV.7. Time-conversion profiles of transfer hydrogenation of 1,3-diphenylpropan-1-one **6a** using EtOH as hydrogen source under the standard conditions, catalyzed by complexes **3a** (violet), **3b** (black), **3c** (blue), **3d** (green), and **3e** (pink).

Table IV.5. Comparison of catalytic data for the transfer hydrogenation of 1,3-diphenylpropan-1-one **6a** using complexes **3a–e**.

entry	complex	TON
1	**3a**	70
2	**3b**	41
3	**3c**	14
4	**3d**	91
5	**3e**	62

Reaction conditions: **6a** (0.5 mmol), K_2CO_3 (5 mol%), complex **3a–e** (1 mol%) in EtOH (5 mL), 25 °C, N_2; yields determined by ^1H NMR spectroscopy relative to 1,3,5-trimethoxybenzene from duplicate runs.

Application of complex 3c for other substrates. Similarly, high selectivity for olefin transfer hydrogenation of α,β-unsaturated ketones was observed when using complex **3c** with the bulkier substrate **5b**. Within 4 h complete and selective hydrogenation of the olefinic C=C bond was observed with full retention of the C=O bond. After 24 h, the selectivity was 93% and thus still very high (Table IV.6, entry 2). However, when using the conjugated diene **5c** as a substrate, conversion was considerably reduced and only reached 48% after 4 h, with a maximum yield of 40% of compound **6c** together with a mixture of isomerized products (entry 3). Longer reaction times did not improve the yield but instead only led to an increase of isomerized products. Similar isomerization side reactions were observed with complex **3a**, however conversion was almost complete and 73% yield of compound **6c** were obtained already after 3 h (entry 3). Even though complex **3c** is highly selective towards hydrogenation of the olefin bond in α,β-unsaturated ketones, with good retention of selectivity over time (entries 1–2), complex **3a** is preferred for the conjugated dienone substrate **5c**.

Table IV.6. Application of complex **3c** in transfer hydrogenation of unsaturated ketones **5a–c**.[a]

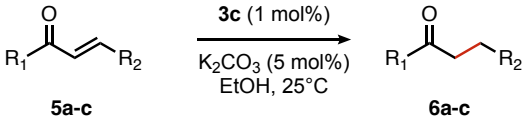

5a-c 6a-c

entry	substrate	product	conversion (%)	yield (%)
1	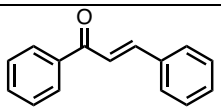 5a	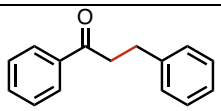 6a	98%, 2 h >99% 24 h	98%, 2 h 98% 24 h
2	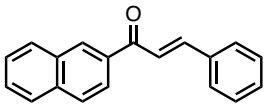 5b	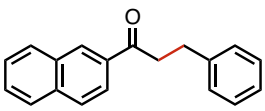 6b	>99%, 4 h >99%, 24 h	99%, 4 h 93%, 24 h
3	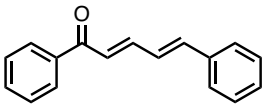 5c	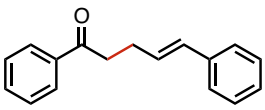 6c	52%, 4 h 59%, 24 h 94%, 3 h[b]	40%, 4 h 39%, 24 h 73%, 3 h[b]

[a]Reaction conditions: substrate (0.5 mmol), K_2CO_3 (5 mol%), complex **3c** (1 mol%) in EtOH (5 mL), 25 °C, N_2; yields determined by ^1H NMR spectroscopy relative to 1,3,5-trimethoxybenzene and average of duplicate runs; [b]using complex **3a**.

IV.4. Conclusions

In this work, we presented a series of N,N'-bidentate PYA ruthenium complexes as efficient catalysts for the selective olefin transfer hydrogenation of α,β-unsaturated ketones using ethanol as hydrogen source. Particularly, the introduction of a *para*-CF_3 group in the ligand acyl unit drastically improved the selectivity toward olefin hydrogenation, providing almost exclusively the desired ketone product with only traces of the saturated alcohol after 24 h. The general adaptability of these complexes, with stabilization through the ligand neutral quinoidal form upon solubilization in donor solvent, constitutes an exciting platform for further catalytic applications.

IV.5. Experimental

IV.5.1. General. All reactions were performed under air unless stated otherwise. Experiments under inert atmosphere were carried out using standard Schlenk techniques under N_2 atmosphere and dry deoxygenated solvents. Dry solvents were taken from a solvent purification system (SPS), stored over molecular sieves for at least 2 days, and degassed by N_2 gas bubbling for 30 min. All compounds were commercially available and used as received. Nuclear magnetic resonance spectra were recorded on a Bruker Avance Neo spectrometer operating at 300 or 400 MHz for ^1H at room temperature unless otherwise noticed. All chemical shifts (d) are quoted in ppm and coupling constants in Hz. Chemical environments have been assigned through COSY, HSQC/HMBC or NOE NMR spectroscopic experiments. Residual protio solvent resonances were used as an internal reference for ^1H and $^{13}C\{^1H\}$ NMR spectra, and externally referenced to $SiMe_4$. $^{31}P\{^1H\}$ NMR spectra were referenced externally to 85% H_3PO_4 (D_2O). $^{19}F\{^1H\}$ NMR chemical shifts are externally referenced to $CFCl_3$. The following abbreviations are used: s, singlet; d, doublet; t, triplet; sept,

septet; m, multiplet. Elemental analyses were performed at the DCBP Microanalytic Laboratory using a Thermo Scientific Flash 2000 CHNS-O elemental analyzer. High-resolution mass spectrometry was carried out with a Thermo Scientific LTQ Orbitrap XL (ESI-TOF) by the DCBP mass spectrometry group at the University of Bern. UV-vis spectra were collected on Shimadzu UV 1800 Spectrophotometer, with a silicon photodiode detector ranging from 190 to 1100 nm. Starna Scientific quartz cuvettes (type 23-N/Q/10) with a path length of 10 mm were used. The spectra were collected at 298 K. The synthesis of complex **3a** and substrates **5a–c** have been previously reported.[1]

IV.5.2. Synthesis of *tert*-butyl (3-aminopyridin-4-yl)carbamate[19]

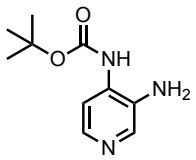

^{1}H NMR ($CDCl_3$, 298K, 300 MHz): δ 8.12 (s, 1H, C**H**$_{PYA}$), 8.05 (d, *J* = 5.4 Hz, 1H, C**H**$_{PYA}$), 7.64 (d, *J* = 5.4 Hz, 1H, C**H**$_{PYA}$), 7.05 (bs, 1H, N**H**), 3.74 (bs, 2H, N**H**), 1.51 (s, 9H, C**H**$_{3\text{-}t\text{Bu}}$).

IV.5.3. Synthesis of amides 1b–e

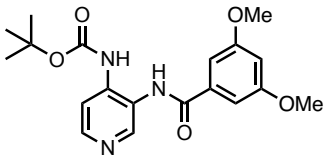

***Tert*-butyl(3-(3,5-dimethoxybenzamido)pyridin-4-yl)carbamate (1b).** *Tert*-butyl(3-aminopyridin-4-yl)carbamate (500 mg, 2.4 mmol, 1 eq) and Et_3N (355 μL, 2.63 mmol, 1.1 eq) were dissolved in THF (15 mL) and 3,5-dimethoxybenzoyl chloride (527 mg, 2.6 mmol, 1.1 eq) was added dropwise under agitation at 0 °C, and then stirred for 16 h at 70 °C. The reaction mixture was cooled to room temperature, and all volatiles were removed under reduced pressure. Water was added and the solid was collected by filtration and solubilized in THF. The solution was dried over Na_2SO_4, filtered, and evaporated to dryness. The crude product was purified by column chromatography (SiO_2; hexane/ethyl acetate 9:1 to 1:1) to afford **1b** as a white solid (622 mg, 70%).

^{1}H NMR (CD_3CN, 298K, 300 MHz): δ 8.74 (bs, 1H, N**H**), 8.46 (s, 1H, C**H**$_{PYA}$), 8.35 (d, *J* = 5.6 Hz, 1H, C**H**$_{PYA}$), 7.89 (d, *J* = 5.6 Hz, 1H, C**H**$_{PYA}$), 7.74 (bs, 1H, N**H**), 7.11 (d, *J* = 2.3 Hz, 2H, C**H**$_{Ar}$), 6.72 (t, *J* = 2.3 Hz, 1H, C**H**$_{Ar}$), 3.85 (s, 6H, C**H**$_{3\text{-}OMe}$), 1.48 (s, 9H, C**H**$_{3\text{-}t\text{Bu}}$). **^{13}C{^{1}H} NMR (CD_3CN, 298 K, 75 MHz):** δ 167.62 (**C**$_{C=O}$), 162.06 (**C**$_{Ar}$), 153.56 (**C**$_{C=O}$), 149.23 (**C**H$_{PYA}$), 149.08 (**C**H$_{PYA}$), 141.98 (**C**$_{PYA}$), 136.80 (**C**$_{Ar}$), 124.34 (**C**$_{PYA}$), 115.53 (**C**H$_{PYA}$), 106.63 (**C**H$_{Ar}$), 105.05 (**C**H$_{Ar}$), 82.08 (**C**$_{t\text{Bu}}$), 56.40 (**C**H$_{3\text{-}OMe}$), 28.37 (**C**H$_{3\text{-}t\text{Bu}}$). **ESI-MS (MeCN, calc. for [$C_{19}H_{23}N_3O_5$]$^+$):** 374.1709 (374.1710).

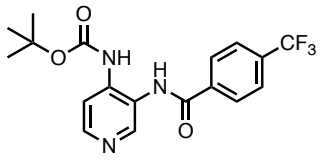

***Tert*-butyl(3-(4-(trifluoromethyl)benzamido)pyridin-4-yl)carbamate (1c**). Using the procedure described for **1b**, compound **1c** was obtained from *tert*-butyl(3-aminopyridin-4-yl)carbamate (250 mg, 2.4 mmol, 1 eq) and 4-(trifluoromethyl)benzoyl chloride (160 µL, 2.6 mmol, 1.1 eq) as a white solid (302 mg, 66%).

^{1}H NMR (CD_3CN, 298K, 300 MHz): δ 8.91 (bs, 1H, N**H**), 8.49 (s, 1H, C$\mathbf{H}_{PYA}$), 8.36 (d, *J* = 5.6 Hz, 1H, C$\mathbf{H}_{PYA}$), 8.13 (d, *J* = 8.3 Hz, 2H, C$\mathbf{H}_{Ar}$), 7.90 (d, *J* = 5.6 Hz, 1H, C$\mathbf{H}_{PYA}$), 7.86 (d, *J* = 8.2 Hz, 2H, C$\mathbf{H}_{Ar}$), 7.78 (bs, 1H, N**H**), 1.48 (s, 9H, C$\mathbf{H}_{3\text{-}t\text{Bu}}$). **^{13}C{^{1}H} NMR ($CD_3CN$, 298 K, 75 MHz):** δ 166.74 (**C**$_{C=O}$), 153.62 (**C**$_{C=O}$), 149.37 (**C**H$_{PYA}$), 149.20 (**C**H$_{PYA}$), 142.20 (**C**$_{PYA}$), 138.46 (**C**$_{Ar}$), 133.59 (**C**$_{Ar}$), 129.52 (**C**H$_{Ar}$), 129.29 (**C**$_{Ar}$), 126.56 (q, *J* = 3.9 Hz, **C**H$_{Ar}$), 123.23 (**C**$_{PYA}$), 115.45 (**C**H$_{PYA}$), 82.16 (**C**$_{t\text{Bu}}$), 28.35 (**C**H$_{3\text{-}t\text{Bu}}$). **ESI-MS (MeCN, calc. for [$C_{18}H_{18}F_3N_3O_3$]$^+$):** 382.1371 (382.1373).

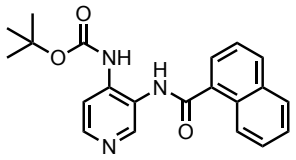

***Tert*-butyl(3-(1-naphthamido)pyridin-4-yl)carbamate (1d).** Using the procedure described for **1b**, compound **1d** was prepared from *tert*-butyl(3-aminopyridin-4-yl)carbamate (500 mg, 2.4 mmol, 1 eq) and 1-naphthoyl chloride (310 µL, 2.6 mmol, 1.1 eq) and was obtained as a white solid (612 mg, 70%).

^{1}H NMR (CD_3CN, 298K, 300 MHz): δ 8.77 (bs, 1H, N**H**), 8.59 (s, 1H, C$\mathbf{H}_{PYA}$), 8.40–8.37 (m, 2H, C$\mathbf{H}_{PYA}$, C$\mathbf{H}_{Ar}$), 8.09 (d, *J* = 8.3 Hz, 1H, C$\mathbf{H}_{Ar}$), 8.01–7.99 (m, 1H, C$\mathbf{H}_{Ar}$), 7.93–7.89 (m, 2H, C$\mathbf{H}_{PYA}$, C$\mathbf{H}_{Ar}$), 7.86 (bs, 1H, N**H**), 7.65–7.59 (m, 3H, C$\mathbf{H}_{Ar}$), 1.48 (s, 9H, C$\mathbf{H}_{3\text{-}t\text{Bu}}$). **^{13}C{^{1}H} NMR ($CD_3CN$, 298 K, 75 MHz):** δ 169.94 (**C**$_{C=O}$), 153.56 (**C**$_{C=O}$), 149.06 (**C**H$_{PYA}$), 148.96 (**C**H$_{PYA}$), 141.61 (**C**$_{PYA}$), 134.78 (**C**$_{Ar}$), 134.13 (**C**$_{Ar}$), 132.31 (**C**H$_{Ar}$), 131.15 (**C**$_{Ar}$), 129.46 (**C**H$_{Ar}$), 128.26 (**C**H$_{Ar}$), 127.60 (**C**H$_{Ar}$), 127.12 (**C**H$_{Ar}$), 126.37 (**C**H$_{Ar}$), 125.85 (**C**H$_{Ar}$), 124.58 (**C**$_{PYA}$), 115.83 (**C**H$_{PYA}$), 82.06 (**C**$_{t\text{Bu}}$), 28.39 (**C**H$_{3\text{-}t\text{Bu}}$). **ESI-MS (MeCN, calc. for [$C_{21}H_{21}N_3O_3$]$^+$):** 364.1649 (364.1656).

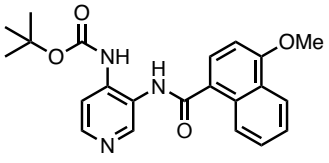

***Tert*-butyl(3-(4-methoxy-1-naphthamido)pyridin-4-yl)carbamate (1e).** Adapted from a reported procedure,[20] 4-methoxy-1-naphthoic acid (250 mg, 1.24 mmol, 1 eq), $SOCl_2$ (180 µL, 2.48 mmol, 2 eq) and few drops of DMF were dissolved in CH_2Cl_2 (10 mL) and the mixture was stirred for 6 h

under reflux. The reaction mixture was cooled to room temperature, and all volatiles were removed under reduced pressure, and the precipitate was washed thoroughly with Et_2O and used without further purification. The obtained 4-methoxy-1-naphthoic chloride was dissolved in THF and added dropwise under agitation at 0 °C to a solution of *tert*-butyl(3-aminopyridin-4-yl)carbamate (258 mg, 1.24 mmol, 1 eq) and Et_3N (183 μL, 1.36 mmol, 1.1 eq) in THF. The reaction mixture was cooled to room temperature, and all volatiles were removed under reduced pressure. The crude product was purified by column chromatography (SiO_2; hexane/ethyl acetate 8:2 to 1:1) to afford the corresponding product as an off-white solid (262 mg, 54%).

^{1}H NMR (CD_3CN, 298K, 300 MHz): δ 8.69 (bs, 1H, N**H**), 8.55 (s, 1H, C$\mathbf{H}_{PYA}$), 8.47 (d, *J* = 7.9 Hz, 1H, C$\mathbf{H}_{Ar}$), 8.37–8.30 (m, 2H, C$\mathbf{H}_{PYA}$, C$\mathbf{H}_{Ar}$), 7.94–7.89 (m, 3H, N**H**, C$\mathbf{H}_{PYA}$, C$\mathbf{H}_{Ar}$), 7.66–7.55 (m, 2H, C$\mathbf{H}_{Ar}$), 7.00 (d, *J* = 8.1 Hz, 1H, C$\mathbf{H}_{Ar}$), 4.08 (s, 3H, OC$\mathbf{H}_3$), 1.48 (s, 9H, C$\mathbf{H}_{3\text{-}t\mathrm{Bu}}$). **^{13}C{^{1}H} NMR ($CD_3CN$, 298 K, 75 MHz):** δ 169.93 (**C**$_{C=O}$), 158.80 (**C**$_{Ar}$), 153.53 (**C**$_{C=O}$), 148.82 (2×**C**H$_{PYA}$), 141.71 (**C**$_{PYA}$), 132.60 (**C**$_{Ar}$), 128.89 (**C**H$_{Ar}$), 128.67 (**C**H$_{Ar}$), 126.90 (**C**H$_{Ar}$), 126.55 (**C**$_{Ar}$), 126.41 (**C**H$_{Ar}$), 125.83 (**C**$_{Ar}$), 124.85 (**C**$_{PYA}$), 123.01 (**C**H$_{Ar}$), 115.73 (**C**H$_{PYA}$), 103.79 (**C**H$_{Ar}$), 81.99 (**C**$_{t\mathrm{Bu}}$), 56.70 (O**C**H$_3$), 28.38 (**C**H$_{3\text{-}t\mathrm{Bu}}$). **ESI-MS (MeCN, calc. for [$C_{22}H_{23}N_3O_4$]$^+$):** 394.1751 (394.1761).

IV.5.4. Synthesis of pyridinium salts 2b–e

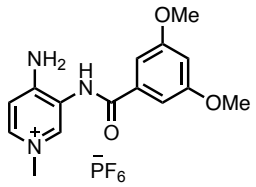

4-amino-3-(3,5-dimethoxybenzamido)-1-methylpyridin-1-ium trifluoromethanesulfonate (2b). Under an N_2 atmosphere, compound **1b** (100 mg, 0.27 mmol, 1 eq) and MeOTf (147 μL, 1.3 mmol, 5 eq) were dissolved in dry CH_2Cl_2 (5 mL) and heated at 42 °C in a closed system for 16 h. After cooling to room temperature, the reaction mixture was concentrated to few mL and MeCN was added until all material was solubilized (ca. 1 mL). Then, a solution of NH_4PF_6 (218 mg, 1.3 mmol, 5 eq) in H_2O (5 mL) was added. After stirring the mixture at rt for 30 min, MeCN was removed under reduced pressure, resulting in the precipitation of a white solid. The mixture was stored at 4 °C for 16 h, then the precipitate was collected by filtration and dried in vacuo to yield the corresponding product as a white solid (65 mg, 43%).

^{1}H NMR (CD_3CN, 298K, 300 MHz): δ 8.44 (bs, 1H, N**H**), 8.17 (d, *J* = 1.8 Hz, 1H, C$\mathbf{H}_{PYA}$), 7.87 (dd, *J* = 7.1, 1.8 Hz, 1H, C$\mathbf{H}_{PYA}$), 7.09 (d, *J* = 2.3 Hz, 2H, C$\mathbf{H}_{Ar}$), 6.99 (d, *J* = 7.1 Hz, 1H, C$\mathbf{H}_{PYA}$), 6.74 (t, *J* = 2.3 Hz, 1H, C$\mathbf{H}_{Ar}$), 6.58 (bs, 2H, N$\mathbf{H}_2$), 3.92 (s, 3H, NC$\mathbf{H}_3$), 3.85 (s, 6H, 2×OC$\mathbf{H}_3$). **^{13}C{^{1}H} NMR (CD_3CN, 298 K, 75 MHz):** δ 167.20 (**C**$_{C=O}$), 162.08 (**C**$_{Ar}$), 156.06 (**C**$_{PYA}$), 143.03 (**C**H$_{PYA}$), 142.94 (**C**H$_{PYA}$), 136.21 (**C**$_{Ar}$), 120.93 (**C**$_{PYA}$), 111.40 (**C**H$_{PYA}$), 106.77 (**C**H$_{Ar}$), 105.11 (**C**H$_{Ar}$), 56.45 (O**C**H$_3$), 46.22 (N**C**H$_3$). **^{19}F{^{1}H} NMR** (**CD_3CN, 298 K, 282 MHz**): δ -72.88 (d, *J* = 707 Hz, P$\mathbf{F}_6$). **^{31}P{^{1}H} NMR (CD_3CN, 298 K, 121 MHz):** δ -144.62 (sept, *J* = 707 Hz, **P**F_6). **ESI-MS (MeCN, calc. for [M–PF_6]$^+$):** 288.1342 (288.1343).

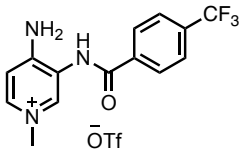

4-amino-1-methyl-3-(4-(trifluoromethyl)benzamido)pyridin-1-ium trifluoromethanesulfonate (2c). Under an N_2 atmosphere, compound **1c** (100 mg, 0.26 mmol, 1 eq) and MeOTf (143 μL, 1.3 mmol, 5 eq) were dissolved in dry CH_2Cl_2 (5 mL) and heated at 42 °C in a closed system for 16 h. After cooling to room temperature, Et_2O (50 mL) was added, and the precipitate was collected by filtration and dried thoroughly to yield **2c** as a white solid (94 mg, 80%).

^{1}H NMR (CD$_3$CN, 298K, 300 MHz): δ 8.71 (bs, 1H, N**H**), 8.19–8.12 (m, 3H, C**H**$_{PYA}$, 2×C**H**$_{Ar}$), 7.90–7.87 (m, 3H, C**H**$_{PYA}$, 2×C**H**$_{Ar}$), 7.01 (d, *J* = 7.2 Hz, 1H, C**H**$_{PYA}$), 6.66 (bs, 2H, N**H$_2$**), 3.92 (s, 3H, NC**H$_3$**). **^{13}C{^{1}H} NMR (CD$_3$CN, 298 K, 75 MHz):** δ 166.12 (**C**$_{C=O}$), 155.70 (**C**$_{PYA}$), 142.74 (**C**H$_{PYA}$), 142.67 (**C**H$_{PYA}$), 137.38 (**C**$_{Ar}$), 133.44 (**C**$_{Ar}$), 129.36 (**C**$_{Ar}$), 129.27 (**C**H$_{Ar}$), 126.25 (q, *J* = 3.9 Hz, **C**H$_{Ar}$), 120.23 (**C**$_{PYA}$), 111.04 (**C**H$_{PYA}$), 45.80 (N**C**H$_3$). **^{19}F{^{1}H} NMR** (**CD$_3$CN, 298 K, 282 MHz**): δ -63.57 (s), -79.35 (s). **ESI-MS (MeCN, calc. for [M–PF$_6$]$^+$):** 288.1342 (288.1343).

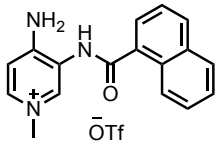

4-amino-3-(3,5-dimethoxybenzamido)-1-methylpyridin-1-ium trifluoromethanesulfonate (2d). Using the procedure described for **2c**, compound **2d** was prepared from **1d** (130 mg, 0.36 mmol, 1 eq) and MeOTf (196 μL, 1.8 mmol, 5 eq) and was isolated as a white solid (135 mg, 88%).

^{1}H NMR (CD$_3$CN, 298K, 300 MHz): δ 8.51 (bs, 1H, N**H**), 8.44 (s, 1H, C**H**$_{PYA}$), 8.41–8.38 (m, 1H, C**H**$_{Ar}$), 8.11 (d, *J* = 8.4 Hz, 1H, C**H**$_{Ar}$), 8.02–7.99 (m, 1H, C**H**$_{Ar}$), 7.95 (dd, *J* = 7.1, 1.2 Hz, 1H, C**H**$_{Ar}$), 7.89 (dd, *J* = 7.1, 1.8 Hz, 1H, C**H**$_{PYA}$), 7.66–7.59 (m, 3H, 3×C**H**$_{Ar}$), 7.04 (d, *J* = 7.1 Hz, 1H, C**H**$_{PYA}$), 6.63 (bs, 2H, N**H$_2$**), 3.96 (s, 3H, NC**H$_3$**). **^{13}C{^{1}H} NMR (CD$_3$CN, 298 K, 75 MHz):** δ 169.48 (**C**$_{C=O}$), 155.36 (**C**$_{PYA}$), 142.68 (**C**H$_{PYA}$), 142.37 (**C**H$_{PYA}$), 134.75 (**C**$_{Ar}$), 133.24 (**C**$_{Ar}$), 132.71 (**C**H$_{Ar}$), 131.13 (**C**$_{Ar}$), 129.48 (**C**H$_{Ar}$), 128.37 (**C**H$_{Ar}$), 127.68 (**C**H$_{Ar}$), 127.61 (**C**H$_{Ar}$), 126.36 (**C**H$_{Ar}$), 125.81 (**C**H$_{Ar}$), 121.08 (**C**$_{PYA}$), 111.51 (**C**H$_{PYA}$), 46.32 (N**C**H$_3$). **^{19}F{^{1}H} NMR** (**CD$_3$CN, 298 K, 282 MHz**): δ -79.35 (s). **ESI-MS (MeCN, calc. for [C$_{17}$H$_{16}$N$_3$O]$^+$):** 278.1280 (278.1288).

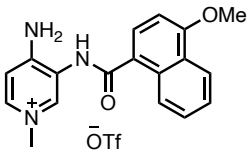

4-amino-3-(4-methoxy-1-naphthamido)-1-methylpyridin-1-ium trifluoromethanesulfonate (2e) Using the procedure described for **2c**, compound **2e** was obtained from **1e** (100 mg, 0.25 mmol, 1 eq) and MeOTf (140 μL, 1.3 mmol, 5 eq) as a white solid (85 mg, 73%).

^{1}H NMR (CD_3CN, 298K, 300 MHz): δ 8.49 (d, *J* = 8.2 Hz, 1H, C**H**$_{Ar}$), 8.41 (bs, 1H, N**H**), 8.38 (s, 1H, C**H**$_{PYA}$), 8.32 (d, *J* = 8.2 Hz, 1H, C**H**$_{Ar}$), 7.97 (d, *J* = 8.1 Hz, 1H, C**H**$_{Ar}$), 7.88 (d, *J* = 7.2 Hz, 1H, C**H**$_{PYA}$), 7.61 (m, C**H**$_{Ar}$), 7.02 (dd, *J* = 7.6, 4.5 Hz, 2H, C**H**$_{PYA}$, C**H**$_{Ar}$), 6.62 (bs, 2H, N**H$_2$**), 4.09 (s, 3H, OC**H$_3$**), 3.95 (s, 3H, NC**H$_3$**). **^{13}C{^{1}H} NMR (CD_3CN, 298 K, 75 MHz):** δ 169.31 (**C**$_{C=O}$), 159.12 (**C**$_{Ar}$), 155.50 (**C**$_{PYA}$), 142.57 (**C**H$_{PYA}$), 142.33 (**C**H$_{PYA}$), 132.65 (**C**$_{Ar}$), 129.48 (**C**H$_{Ar}$), 128.80 (**C**H$_{Ar}$), 126.99 (**C**H$_{Ar}$), 126.54 (**C**$_{Ar}$), 126.42 (**C**H$_{Ar}$), 124.96 (**C**$_{Ar}$), 123.04 (**C**H$_{Ar}$), 121.42 (**C**$_{PYA}$), 111.41 (**C**H$_{PYA}$), 103.75 (**C**H$_{Ar}$), 56.77 (O**C**H$_3$), 46.29 (N**C**H$_3$). **^{19}F{^{1}H} NMR** (**CD_3CN, 298 K, 282 MHz**): δ -79.34 (s). **ESI-MS (MeCN, calc. for $C_{18}H_{18}N_3O_2$ [M]$^+$):** 308.1385 (308.1394).

IV.5.6. Synthesis of complexes 3b–e

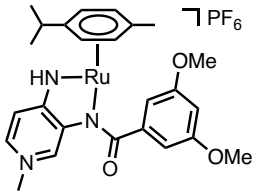

Complex 3b. In a round bottom flask, compound **2b** (107 mg, 0.25 mmol, 1 eq), NaOAc (101 mg, 1.23 mmol, 5 eq) and [Ru(*p*-cym)Cl_2]$_2$ (75 mg, 0.13 mmol, 0.5 eq) were dissolved in CH_2Cl_2 (10 mL). The reaction mixture was refluxed for 16 h, cooled, and filtered through Celite. The filtered solution was washed with saturated $NaHCO_3$ solution (3 x 10 mL). The organic phase was dried over Na_2SO_4, filtered, and evaporated to dryness. The crude product was purified by gradient column chromatography (neutral Al_2O_3; CH_2Cl_2 to CH_2Cl_2/MeOH 99:1) to give the pure compound as a red solid (128 mg, 78%).

^{1}H NMR (CD_2Cl_2, 298K, 300 MHz): δ 9.90 (bs, 1H, N**H**), 8.55 (s, 1H, C**H$_{PYA}$**), 7.34 (dd, *J* = 6.9, 1.7 Hz, 1H, C**H$_{PYA}$**), 7.25 (d, *J* = 6.8 Hz, 1H, C**H$_{PYA}$**), 7.17 (d, *J* = 2.4 Hz, 2H, C**H$_{Ar}$**), 6.78 (t, *J* = 2.3 Hz, 1H, C**H$_{Ar}$**), 5.36 (d, *J* = 6.2 Hz, 2H, C**H$_{cym}$**), 5.14 (d, *J* = 6.1 Hz, 2H, C**H$_{cym}$**), 3.90 (s, 6H, 2×OC**H$_3$**), 3.86 (s, 3H, NC**H$_3$**), 2.43 (septet, *J* = 6.9 Hz, 1H, C**H**(CH$_3$)$_2$), 2.06 (s, 3H, cym-C**H$_3$**), 1.15 (d, *J* = 6.9 Hz, 6H, CH(C**H$_3$**)$_2$). **^{13}C{^{1}H} NMR (CD_2Cl_2, 298 K, 75 MHz):** δ 182.12 (**C**=O), 161.24 (**C**$_{Ar}$), 160.99 (**C**$_{PYA}$), 142.34 (**C**$_{Ar}$), 140.94 (**C**$_{PYA}$), 133.29 (**C**H$_{PYA}$), 129.65 (**C**H$_{PYA}$), 110.34 (**C**H$_{PYA}$), 108.24 (**C**H$_{Ar}$), 104.29 (**C**H$_{Ar}$), 100.90 (**C**$_{cym}$), 92.10 (**C**$_{cym}$), 82.09 (**C**H$_{cym}$), 79.41 (**C**H$_{cym}$), 56.24 (O**C**H$_3$), 46.42 (N**C**H$_3$), 32.09 (**C**H(CH$_3$)$_2$), 23.36 (CH(**C**H$_3$)$_2$), 19.96 (cym-**C**H$_3$). **^{19}F{^{1}H} NMR** (**CD_2Cl_2, 298 K, 282 MHz**): δ -72.44 (d, J = 711 Hz, P**F$_6$**). **^{31}P{^{1}H} NMR (CD_3CN, 298 K, 121 MHz):** -144.17 (septet, *J* = 711 Hz, **P**F$_6$). **ESI-MS (calc. for [2–PF_6]$^+$):** 522.1313 (522.1325). **Elemental Analysis found (calcd.) for $C_{25}H_{30}F_6N_3O_3PRu$:** C 45.82 (45.05), H 4.52 (4.54), N 6.19 (6.30).

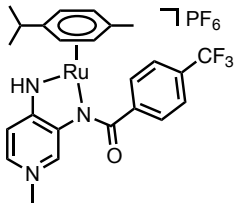

Complex 3c. In a round bottom flask, compound **2c** (67 mg, 0.15 mmol, 1 eq), NaOAc (61 mg, 0.75 mmol, 5 eq), [Ru(*p*-cym)Cl_2]$_2$ (46 mg, 0.07 mmol, 0.5 eq) and $NaPF_6$ (63 mg, 0.37 mmol, 2.5 eq) were dissolved in CH_2Cl_2 (10 mL). The reaction mixture was refluxed for 16 h, cooled, and filtered through Celite. The filtrate was washed with saturated $NaHCO_3$ solution (3 x 5 mL). The organic phase was dried over Na_2SO_4, filtered, and evaporated to dryness. The crude product was purified by gradient column chromatography (neutral Al_2O_3; CH_2Cl_2 to CH_2Cl_2/MeOH 99:1) to give the pure compound as a red solid (71 mg, 70%).

^{1}H NMR (CD_2Cl_2, 298K, 300 MHz): δ 10.13 (bs, 1H, N**H**), 8.57 (s, 1H, C**H$_{PYA}$**), 8.18 (d, *J* = 8.0 Hz, 2H, C**H$_{Ar}$**), 7.90 (d, *J* = 8.1 Hz, 2H, C**H$_{Ar}$**), 7.38 (dd, *J* = 6.9, 1.7 Hz, 1H, C**H$_{PYA}$**), 7.30 (d, *J* = 6.9 Hz, 1H, C**H$_{PYA}$**), 5.30 (d, *J* = 6.3 Hz, 2H, C**H$_{cym}$**), 5.11 (d, *J* = 6.2 Hz, 2H, C**H$_{cym}$**), 3.87 (s, 3H, NC**H$_3$**), 2.42 (septet, *J* = 6.9 Hz, 1H, C**H**$(CH_3)_2$), 2.06 (s, 3H, cym-C**H$_3$**), 1.15 (d, *J* = 6.9 Hz, 6H, CH(C**H$_3$**)$_2$). **^{13}C{^{1}H} NMR (CD_2Cl_2, 298 K, 75 MHz):** δ 181.11 (**C**=O), 161.13 (**C**$_{PYA}$), 143.90 (**C**$_{Ar}$), 140.70 (**C**$_{PYA}$), 133.74 (**C**H$_{PYA}$), 130.35 (**C**H$_{Ar}$), 130.10 (**C**H$_{PYA}$), 125.94 (q, *J* = 4.0 Hz, **C**H$_{Ar}$), 110.60 (**C**H$_{PYA}$), 101.13 (**C**$_{cym}$), 91.84 (**C**$_{cym}$), 81.99 (**C**H$_{cym}$), 79.33 (**C**H$_{cym}$), 46.51 (N**C**H$_3$), 32.12 (**C**H$(CH_3)_2$), 23.33 CH(**C**H$_3$)$_2$, 20.00 (cym-**C**H$_3$). **^{19}F{^{1}H} NMR** (**CD_2Cl_2, 298 K, 282 MHz**): δ -63.14 (s, C**F$_3$**), -72.13 (d, *J* = 711 Hz, P**F$_6$**). **^{31}P{^{1}H} NMR (CD_3CN, 298 K, 121 MHz):** δ -144.11 (septet, *J* = 711 Hz, **P**F_6). **ESI-MS (calc. for [3–PF$_6$]):** 530.0976 (530.0988). **Elemental Analysis found (calcd.) for $C_{24}H_{25}F_9N_3OPRu$:** C 44.06 (42.74), H 3.91 (3.74), N 5.97 (6.23).

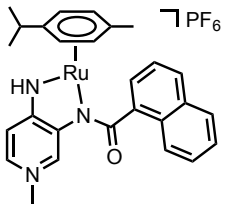

Complex 3d. Using the procedure described for **3c**, complex **3d** was prepared from compound **2d** (144 mg, 0.33 mmol, 1 eq), NaOAc (138 mg, 1.68 mmol, 5 eq), [Ru(*p*-cym)Cl_2]$_2$ (103 mg, 0.17 mmol, 0.5 eq) and $NaPF_6$ (141 mg, 0.84 mmol, 2.5 eq). The product was obtained as a red solid (152 mg, 68%).

^{1}H NMR (CD_2Cl_2, 298K, 300 MHz): δ 10.11 (bs, 1H, N**H**), 9.22 (s, 1H, C**H**$_{PYA}$), 8.18 (dd, *J* = 13.5, 8.2 Hz, 2H, C**H**$_{Ar}$), 8.12–8.03 (m, 1H, C**H**$_{Ar}$), 7.97 (dd, *J* = 7.1, 1.3 Hz, 1H, C**H**$_{Ar}$), 7.77–7.55 (m, 3H, C**H**$_{Ar}$), 7.42 (dd, *J* = 6.8, 1.8 Hz, 1H, C**H**$_{PYA}$), 7.29 (d, *J* = 6.8 Hz, 1H, C**H**$_{PYA}$), 5.07 (s, 1H, C**H**$_{cym}$), 4.89 (s, 1H, C**H**$_{cym}$),4.60 (s, 2H, C**H**$_{cym}$), 3.92 (s, 3H, NC**H$_3$**), 2.11 (septet, *J* = 6.9 Hz, 1H, C**H**$(CH_3)_2$), 1.71 (s, 3H, cym-C**H$_3$**), 1.04 (d, *J* = 6.9 Hz, 6H, CH(C**H$_3$**)$_2$). **^{13}C{^{1}H} NMR (CD_2Cl_2, 298 K, 75 MHz):**

δ 182.85 (**C**=O), 161.44 (**C**$_{PYA}$), 140.03 (**C**$_{Ar}$), 139.82 (**C**$_{PYA}$), 134.08 (**C**H$_{PYA}$), 133.97 (**C**$_{Ar}$), 131.69 (**C**H$_{PYA}$), 131.57 (**C**H$_{Ar}$), 131.50 (**C**$_{Ar}$), 129.24 (**C**H$_{Ar}$), 127.99 (**C**H$_{Ar}$), 127.50 (**C**H$_{Ar}$), 127.33 (**C**H$_{Ar}$), 126.14 (**C**H$_{Ar}$), 125.31 (**C**H$_{Ar}$), 110.38 (**C**H$_{PYA}$), 100.19 (**C**$_{cym}$), 91.30 (**C**$_{cym}$), 82.03 (**C**H$_{cym}$), 79.24 (**C**H$_{cym}$), 46.58 (N**C**H$_3$), 31.83 (**C**H(CH$_3$)$_2$), 23.32 (CH(**C**H$_3$)$_{2)}$, 19.71 (cym-**C**H$_3$). **^{19}F{^{1}H} NMR** (**CD$_2$Cl$_2$, 298 K, 282 MHz**): δ -72.17 (d, *J* = 712 Hz, P**F$_6$**). **^{31}P{^{1}H} NMR (CD$_3$CN, 298 K, 121 MHz):** δ -144.10 (septet, *J* = 712 Hz, **P**F$_6$). **ESI-MS (calc. for [4–PF$_6$]):** 512.1260 (512.1270). **Elemental Analysis found (calcd.) for C$_{27}$H$_{28}$F$_6$N$_3$OPRu:** C 49.34 (49.39), H 4.19 (4.30), N 6.21 (6.40).

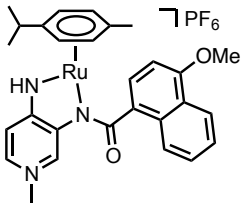

Complex 3e. Using the procedure described for **3c**, complex **3e** was prepared from compound **2e** (47 mg, 0.10 mmol, 1 eq), NaOAc (43 mg, 0.51 mmol, 5 eq), [Ru(*p*-cym)Cl$_2$]$_2$ (32 mg, 0.05 mmol, 0.5 eq) and NaPF$_6$ (44 mg, 0.25 mmol, 2.5 eq). The product was obtained as a red solid (66 mg, 92%).

^{1}H NMR (CD$_2$Cl$_2$, 298K, 300 MHz): δ 10.02 (bs, 1H, N**H**), 8.94 (s, 1H, C**H**$_{PYA}$), 8.46 (dt, *J* = 6.9, 3.5 Hz, 1H, C**H**$_{Ar}$), 8.35 (dt, *J* = 6.4, 3.6 Hz, 1H, C**H**$_{Ar}$), 7.97 (d, *J* = 8.0 Hz, 1H, C**H**$_{Ar}$), 7.64 (dt, *J* = 6.5, 3.4 Hz, 2H, C**H**$_{Ar}$), 7.38 (dd, *J* = 6.9, 1.7 Hz, 1H, C**H**$_{PYA}$), 7.28 (d, *J* = 6.9 Hz, 1H, C**H**$_{PYA}$), 7.00 (d, *J* = 8.0 Hz, 1H, C**H**$_{Ar}$), 5.15 (s, 1H, C**H**$_{cym}$), 5.01 (s, 1H, C**H**$_{cym}$), 4.77 (s, 2H, C**H**$_{cym}$), 4.16 (s, 3H, OC**H$_3$**), 3.90 (s, 3H, NC**H$_3$**), 2.23 (septet, *J* = 6.7 Hz, 1H, C**H**(CH$_3$)$_2$), 1.81 (s, 3H, cym-C**H$_3$**), 1.07 (d, *J* = 6.9 Hz, 6H, CH(C**H$_3$**)$_2$). **^{13}C{^{1}H} NMR (CD$_2$Cl$_2$, 298 K, 75 MHz):** δ 182.91 (**C**=O), 161.21 (**C**$_{PYA}$), 158.87 (**C**$_{Ar}$), 140.44 (**C**$_{PYA}$), 133.51 (**C**H$_{PYA}$), 132.93 (**C**$_{Ar}$), 131.04 (**C**$_{Ar}$), 130.53 (**C**H$_{Ar}$), 130.16 (**C**H$_{PYA}$), 128.59 (**C**H$_{Ar}$), 126.58 (**C**H$_{Ar}$), 126.09 (**C**H$_{Ar}$), 125.98 (**C**$_{Ar}$), 123.16 (**C**H$_{Ar}$), 110.34 (**C**H$_{PYA}$), 102.94 (**C**H$_{Ar}$), 100.52 (**C**$_{cym}$), 91.43 (**C**$_{cym}$), 81.87 (**C**H$_{cym}$), 79.20 (**C**H$_{cym}$), 56.47 (O**C**H$_3$), 46.50 (N**C**H$_3$), 31.94 (**C**H(CH$_3$)$_2$), 23.38 CH(**C**H$_3$)$_2$, 19.86 (cym-**C**H$_3$). **^{19}F{^{1}H} NMR** (**CD$_2$Cl$_2$, 298 K, 282 MHz**): δ -72.37 (d, *J* = 711 Hz, P**F$_6$**). **^{31}P{^{1}H} NMR (CD$_3$CN, 298 K, 121 MHz):** δ -144.14 (septet, *J* = 709 Hz, **P**F$_6$). **ESI-MS (calc. for [5–PF$_6$]):** 542.1366 (542.1376). **Elemental Analysis found (calcd.) for C$_{28}$H$_{30}$F$_6$N$_3$O$_2$PRu:** C 48.87 (48.98), H 4.44 (4.40), N 5.61 (6.12).

Table IV.7. Comparison of ^{1}H NMR shifts (ppm) of the aromatic *p*-cymene protons depending on the solvent for complexes **3a–e**.

entry	complex	$\delta_{H,cym}$ (CD_2Cl_2)	$\delta_{H,cym}$ (CD_3OD)
1	**3a**	5.28 (d, 2H), 5.08 (d, 2H)	5.39 (d, 2H), 5.08 (d, 2H)
2	**3b**	5.36 (d, 2H), 5.14 (d, 2H)	5.46 (d, 2H), 5.10 (d, 2H)
3	**3c**	5.30 (d, 2H), 5.11 (d, 2H)	5.42 (d, 2H), 4.99 (d, 2H)
4	**3d**	5.07 (s, 1H), 4.89 (s, 1H), 4.60 (s, 2H)	5.28 (s, 1H), 4.55 (s, 2H)[a]
5	**3e**	5.15 (s, 1H), 5.01 (s, 1H), 4.77 (s, 2H)	5.33 (s, 1H), 4.97 (s, 1H), 4.77 (d, 2H)

[a]Overlap with the solvent signal at 4.85 ppm.

IV.5.7. Synthesis of complex 4a–d

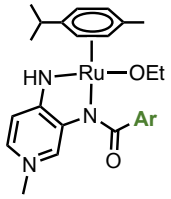

In a NMR tube, compound **3a–d** (1 eq) was suspended in MeOD (0.5 mL) and EtONa (2 eq) was added at rt. The reaction was analyzed by ^{1}H NMR spectroscopy.

Complex 4a – ^{1}H NMR (CD_3OD, 298K, 300 MHz): δ 8.91 (s, 1H, C**H**$_{PYA}$), 7.99 (bs, 2H, C**H**$_{Ar}$), 7.60–7.48 (m, 3H, C**H**$_{PYA}$, C**H**$_{Ar}$), 7.28 (d, *J* = 6.7 Hz, 1H, C**H**$_{Ar}$), 6.63 (d, *J* = 7.0 Hz, 1H, C**H**$_{PYA}$), 5.10 (d, *J* = 5.7 Hz, 2H, C**H**$_{cym}$), 4.38 (d, *J* = 5.6 Hz, 2H, C**H**$_{cym}$), 3.70 (s, 3H, NC**H$_3$**), 3.61 (q, *J* = 7.0 Hz, 4H, OC**H$_2$**CH_3), 2.38 (septet, *J* = 6.9 Hz, 1H, C**H**$(CH_3)_2$), 1.96 (s, 3H, cym-C**H$_3$**), 1.18 (t, *J* = 7.0 Hz, 6H, OCH_2C**H$_3$**), 1.04 (d, *J* = 6.6 Hz, 6H, $CH(CH_3)_2$).

Complex 4b – ^{1}H NMR (CD_3OD, 298K, 300 MHz): δ 8.96 (s, 1H, C**H**$_{PYA}$), 7.16 (d, *J* = 2.3 Hz, 1H, C**H**$_{Ar}$), 7.12 (m, 1H, C**H**$_{PYA,}$), 6.59 (t, *J* = 2.3 Hz, 1H, C**H**$_{Ar}$), 6.38 (d, *J* = 7.1 Hz, 1H, C**H**$_{PYA}$), 5.14 (d, *J* = 5.8 Hz, 2H, C**H**$_{cym}$), 4.04 (d, *J* = 5.6 Hz, 2H, C**H**$_{cym}$), 3.89 (s, 3H, NC**H$_3$**), 3.62 (q, *J* = 7.0 Hz, 4H, OC**H$_2$**CH_3), 2.39–2.28 (m, 1H, C**H**$(CH_3)_2$), 1.88 (s, 3H, cym-C**H$_3$**), 1.18 (t, *J* = 7.0 Hz, 6H, OCH_2C**H$_3$**), 1.00 (d, *J* = 6.9 Hz, 6H, $CH(CH_3)_2$).

Complex 4c – ^{1}H NMR (CD_3OD, 298K, 300 MHz): δ 9.07 (s, 1H, C**H**$_{PYA}$), 8.15 (d, *J* = 8.0 Hz, 2H, C**H**$_{Ar}$), 7.79 (d, *J* = 8.0 Hz, 2H, C**H**$_{Ar}$), 7.14 (dd, *J* = 7.1, 1.9 Hz, 1H, C**H**$_{PYA}$), 6.40 (d, *J* = 7.1 Hz, 1H, C**H**$_{PYA}$), 4.99 (d, *J* = 5.7 Hz, 2H, C**H**$_{cym}$), 4.03 (d, *J* = 5.6 Hz, 2H, C**H**$_{cym}$), 3.63 (s, 3H, NC**H$_3$**), 3.61 (q, *J* = 7.1 Hz, 4H, OC**H$_2$**CH_3), 2.34 (septet, *J* = 6.9 Hz, 1H, C**H**$(CH_3)_2$), 1.89 (s, 3H, cym-C**H$_3$**), 1.18 (t, *J* = 7.0 Hz, 6H, OCH_2C**H$_3$**), 0.99 (d, *J* = 6.9 Hz, 6H, $CH(CH_3)_2$).

Complex 4d – ^{1}H NMR (CD_3OD, 298K, 300 MHz): δ 9.26 (s, 1H, C**H**$_{PYA}$), 8.35–8.24 (m, 1H, C**H**$_{Ar}$), 7.98 (dd, *J* = 8.2, 5.7 Hz, 2H, C**H**$_{Ar}$), 7.87–7.78 (m, 1H, C**H**$_{Ar}$), 7.70–7.53 (m, 3H, C**H**$_{Ar}$), 7.17 (dd, *J*

= 7.1, 1.9 Hz, 1H, C**H**$_{PYA}$), 6.42 (d, *J* = 7.1 Hz, 1H, C**H**$_{PYA}$), 5.28 (s, 1H, C**H**$_{cym}$), 4.60 (s, 1H, C**H**$_{cym}$), 4.37 (s, 1H, C**H**$_{cym}$), 3.66 (s, 3H, NC**H**$_3$), 3.61 (q, *J* = 7.1 Hz, 4H, OC**H**$_2$CH$_3$), 2.27 (m, 1H, C**H**(CH$_3$)$_2$), 1.89 (s, 3H, cym-C**H**$_3$), 1.18 (t, *J* = 7.0 Hz, 6H, OCH$_2$C**H**$_3$), 0.95 (bs, 6H, CH(C**H**$_3$)$_2$).

IV.5.8. Catalytic data

General catalytic procedure for catalytic transfer hydrogenation: In a 10 mL round bottom flask, the substrate (0.5 mmol), complex **3a–e** (1 mol%), and 1,3,5-trimethoxybenzene (10 mol%) as internal standards were dissolved in EtOH (5 mL) and the solution was degassed with N_2 for 10 min. The catalytic run was started with the injection of K_2CO_3 (5 mol%, 2 M solution in H_2O) and the tube was placed in a pre-heated oil bath (25 °C). The reaction was monitored by ^{1}H NMR spectroscopy (300 MHz, 298K), with reaction aliquots (ca. 0.1 mL) taken at set times under N_2 and dissolved in $CDCl_3$ (0.5 mL) to determine the spectroscopic conversion and yields relative to the internal standard.

Rate constant determination: Under the general catalytic procedure, the rate constants $k_{C=C}$ and $k_{C=O}$ for the successive C=C and C=O bond catalytic transfer hydrogenation of *trans*-chalcone for complexes **3a–e** were extracted from the linear regimes (Tables IV.8–17, 1,3-diphenylpropan-1-one in red, 1,3-diphenylpropan-1-ol in green). For the C=O bond transfer hydrogenation, the initial time t = 0 was set at >97% conversion of *trans*-chalcone to 1,3-diphenylpropan-1-one, *i.e.* after 50 min for complex **3d**, after 1h for complexes **3a** and **3e**, after 2h for complex **3c**, and after 3h for complex **3b**.

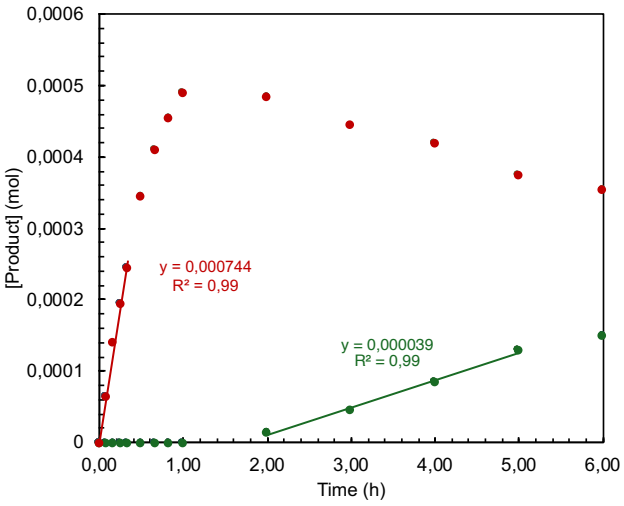

Figure IV.8. Determination of rate constants $k_{C=C}$ and $k_{C=O}$ for the consecutive C=C and C=O transfer hydrogenation of *trans*-chalcone catalyzed by complex **3a**.

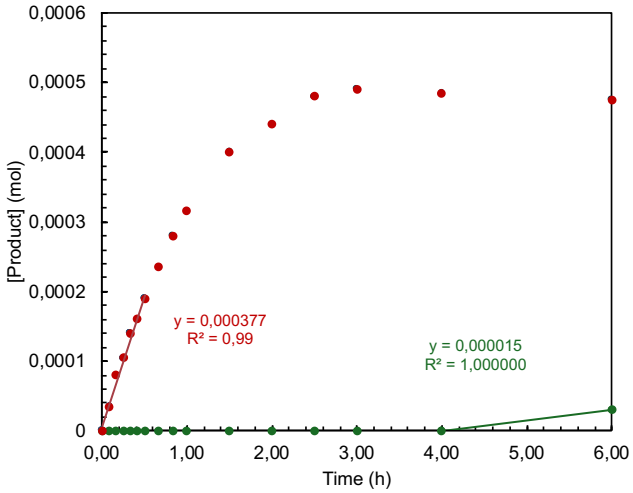

Figure IV.9. Determination of rate constants $k_{C=C}$ and $k_{C=O}$ for the consecutive C=C and C=O transfer hydrogenation of *trans*-chalcone catalyzed by complex **3b**.

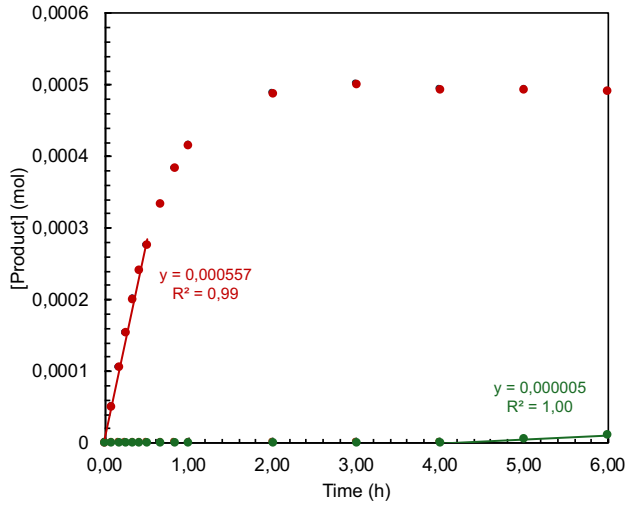

Figure IV.10. Determination of rate constants $k_{C=C}$ and $k_{C=O}$ for the consecutive C=C and C=O transfer hydrogenation of *trans*-chalcone catalyzed by complex **3c**.

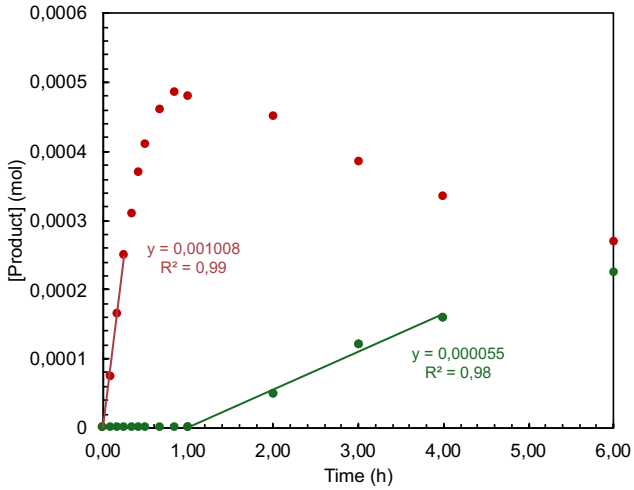

Figure IV.11. Determination of rate constants $k_{C=C}$ and $k_{C=O}$ for the consecutive C=C and C=O transfer hydrogenation of *trans*-chalcone catalyzed by complex **3d**.

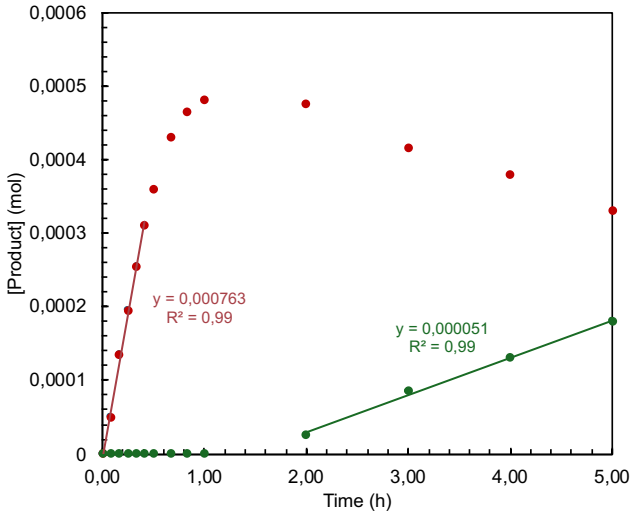

Figure IV.12. Determination of rate constants $k_{C=C}$ and $k_{C=O}$ for the consecutive C=C and C=O transfer hydrogenation of *trans*-chalcone catalyzed by complex **3e**.

Table IV.8. Data for the determination of $k_{C=C}$ and max $TOF_{C=C}$ of the C=C transfer hydrogenation of *trans*-chalcone catalyzed by complex **3a**.

Time (h)	[Product]	$k_{C=C}$ (h^{-1})	max $TOF_{C=C}$ (h^{-1})
0.00	0		
0.08	0.000065	74×10^{-5}	170
0.17	0.000140	$R^2 = 0.99$	(at 28% conversion,
0.25	0.000195		t = 0.17 h)
0.33	0.000245		

Table IV.9. Data for the determination of $k_{C=C}$ and max $TOF_{C=C}$ of the C=C transfer hydrogenation of *trans*-chalcone catalyzed by complex **3b**.

Time (h)	[Product]	$k_{C=C}$ (h^{-1})	max $TOF_{C=C}$ (h^{-1})
0.00	0		
0.08	0.000035		
0.17	0.000080	38×10^{-5}	100
0.25	0.000105	$R^2 = 0.99$	(at 17% conversion,
0.33	0.000140		t = 0.17 h)
0.42	0.000160		
0.50	0.000190		

Table IV.10. Data for the determination of $k_{C=C}$ and max $TOF_{C=C}$ of the C=C transfer hydrogenation of *trans*-chalcone catalyzed by complex **3c**.

Time (h)	[Product]	$k_{C=C}$ (h^{-1})	max $TOF_{C=C}$ (h^{-1})
0.00	0		
0.08	0.000050		
0.17	0.000105	56×10^{-5}	130
0.25	0.000153	$R^2 = 0.99$	(at 21% conversion,
0.33	0.000200		t = 0.17 h)
0.42	0.000240		
0.50	0.000275		

Table IV.11. Data for the determination of $k_{C=C}$ and max $TOF_{C=C}$ of the C=C transfer hydrogenation of *trans*-chalcone catalyzed by complex **3d**.

Time (h)	[Product]	$k_{C=C}$ (h^{-1})	max $TOF_{C=C}$ (h^{-1})
0.00	0		
0.08	0.000075	101×10^{-5}	200
0.17	0.000165	$R^2 = 0.99$	(at 50% conversion,
0.25	0.000250		t = 0.25 h)

Table IV.12. Data for the determination of $k_{C=C}$ and max $TOF_{C=C}$ of the C=C transfer hydrogenation of *trans*-chalcone catalyzed by complex **3e**.

Time (h)	[Product]	$k_{C=C}$ (h^{-1})	max $TOF_{C=C}$ (h^{-1})
0.00	0		
0.08	0.000050		
0.17	0.000135	76×10^{-5}	160
0.25	0.000195	$R^2 = 0.99$	(at 27% conversion,
0.33	0.000255		t = 0.17 h)
0.42	0.000310		

Table IV.13. Data for the determination of $k_{C=O}$ and max $TOF_{C=O}$ of the *in situ* C=O transfer hydrogenation of 1,3-diphenylpropan-1-one catalyzed by complex **3a**.

Time (h)	[Product]	$k_{C=O}$ (h^{-1})	max $TOF_{C=O}$ (h^{-1})
0	0	3.9×10^{-5} $R^2 = 0.99$	7 (at 26% conversion, t = 4 h)
1	0.000015		
2	0.000045		
3	0.000085		
4	0.000130		

Table IV.14. Data for the determination of $k_{C=O}$ and max $TOF_{C=O}$ of the *in situ* C=O transfer hydrogenation of 1,3-diphenylpropan-1-one catalyzed by complex **3b**.

Time (h)	[Product]	$k_{C=O}$ (h^{-1})	max $TOF_{C=O}$ (h^{-1})
0	0	1.5×10^{-5} [a]	2 (at 6% conversion, t = 3 h)
1	0		
3	0.000030		

[a]Not enough data points for an accurate determination.

Table IV.15. Data for the determination of $k_{C=O}$ and max $TOF_{C=O}$ of the *in situ* C=O transfer hydrogenation of 1,3-diphenylpropan-1-one catalyzed by complex **3c**.

Time (h)	[Product]	$k_{C=O}$ (h^{-1})	max $TOF_{C=O}$ (h^{-1})
0	0	0.5×10^{-5} $R^2 = 1.00$	1 (at 2% conversion, t = 4 h)
1	0		
2	0		
3	0.000005		
4	0.000010		

Table IV.16. Data for the determination of $k_{C=O}$ and max $TOF_{C=O}$ of the *in situ* C=O transfer hydrogenation of 1,3-diphenylpropan-1-one catalyzed by complex **3d**.

Time (h)	[Product]	$k_{C=O}$ (h^{-1})	max $TOF_{C=O}$ (h^{-1})
0	0	5.5×10^{-5} $R^2 = 0.99$	11 (at 24% conversion, t = 2.17 h)
1.17	0.000050		
2.17	0.000120		
3.17	0.000160		

Table IV.17. Data for the determination of $k_{C=O}$ and max $TOF_{C=O}$ of the *in situ* C=O transfer hydrogenation of 1,3-diphenylpropan-1-one catalyzed by complex **3e**.

Time (h)	[Product]	$k_{C=O}$ (h^{-1})	max $TOF_{C=O}$ (h^{-1})
0	0	5.1×10^{-5} $R^2 = 0.99$	9 (at 17% conversion, t = 2 h)
1	0,000025		
2	0,000085		
3	0,00013		
4	0,00018		

IV.5.9. UV-Vis spectroscopy

General procedure: Before each measurement, a blank spectrum (of CH_2Cl_2) was collected. A 10 mM stock solution of complex **3a–e** in CH_2Cl_2 was diluted to give samples that were 0.05 mM in complex **3a–e**.

IV.5.10. Crystal structure determination

A crystal of **3b** immersed in parabar oil was mounted at ambient conditions and transferred into the stream of nitrogen (100 K). All measurements were made on a *RIGAKU Synergy S* area-detector diffractometer using mirror optics monochromated Cu *K*a radiation (λ = 1.54184 Å). The unit cell constants and an orientation matrix for data collection were obtained from a least-squares refinement of the setting angles of reflections in the range 2.789° < θ < 78.282°. A total of 9116 frames were collected using ω scans, with 0.3 second exposure time (2 s for high-angle reflections), a rotation angle of 0.5° per frame, a crystal-detector distance of 31.0 mm, at T = 173.00(10) K. Data reduction was performed using the *CrysAlisPro*5 program. The intensities were corrected for Lorentz and polarization effects, and an absorption correction based on the multi-scan method using SCALE3 ABSPACK in *CrysAlisPro*5 was applied. Data collection and refinement parameters are given in Table IV.18. The structure was solved by intrinsic phasing using *SHELXT*, which revealed the positions of all non-hydrogen atoms of the title compound. All non-hydrogen atoms were refined anisotropically. H-atoms were assigned in geometrically calculated positions and refined using a riding model where each H-atom was assigned a fixed isotropic displacement parameter with a value equal to 1.2Ueq of its parent atom (1.5Ueq for methyl groups), except for that attached to N1, where the H atom was located from the difference density map and had its position and isotropic displacement parameter refined freely. Refinement of the structure was carried out on F^2 using full-matrix least-squares procedures, which minimized the function $\Sigma w(Fo^2–Fc^2)^2$. The weighting scheme was based on counting statistics and included a factor to downweight the intense reflections. All calculations were performed using the *SHELXL-2014/7*[21] program in OLEX2.[22] Disorder model was used for parts of the structure where the occupancies of each disorder component was refined through the use of a free variable. The sum of equivalent components was constrained to 1, i.e. 100%. The X-ray crystal structure determination service unit of the Department of Chemistry and

Biochemistry of the University of Bern is acknowledged for measuring, solving, refining, and summarizing the structures of compound **3b**.

Table IV.18. Selected crystallographic and refinement data.

	Compound **3b**
Identification code	24MA093_AB-3-169
Empirical formula	$C_{25}H_{30}F_6N_3O_3PRu$
Formula weight	666.56
Temperature/K	173.00(10)
Crystal system	triclinic
Space group	P-1
a/Å	8.77993(9)
b/Å	9.12402(11)
c/Å	18.0299(2)
α/°	81.6256(10)
β/°	80.8187(9)
γ/°	73.6818(9)
Volume/Å^3	1360.63(3)
Z	2
ρ_{calc}g/cm^3	1.627
μ/mm^{-1}	5.889
F(000)	676.0
Crystal size/mm^3	0.243 × 0.152 × 0.076
Radiation	Cu Kα (λ = 1.54184)
2Θ range for data collection/°	4.994 to 149
Index ranges	-10 ≤ h ≤ 10, -11 ≤ k ≤ 11, -22 ≤ l ≤ 22
Reflections collected	48200
Independent reflections	5503 [R_{int} = 0.0294, R_{sigma} = 0.0135]
Data/restraints/parameters	5503/120/455
Goodness-of-fit on F^2	1.108
Final R indexes [I>=2σ (I)]	R_1 = 0.0254, wR_2 = 0.0609
Final R indexes [all data]	R_1 = 0.0257, wR_2 = 0.0611
Largest diff. peak/hole / e Å^{-3}	0.58/-0.63

IV.6. References

[1] M. Albrecht, A. Beaufils, *ChemCatChem* **2024**, e202401596.

[2] V. Leigh, D. J. Carleton, J. Olguin, H. Mueller-Bunz, L. J. Wright, M. Albrecht, *Inorg. Chem.* **2014**, *53*, 8054–8060.

[3] M. Navarro, M. Li, H. Müller-Bunz, S. Bernhard, M. Albrecht, *Chemistry. A European. J.* **2016**, *22*, 6740–6745.

[4] M. Navarro, C. A. Smith, M. Albrecht, *Inorg. Chem.* **2017**, *56*, 11688–11701.

[5] P. D. W. Boyd, L. J. Wright, M. N. Zafar, *Inorg. Chem.* **2011**, *50*, 10522–10524.

[6] J. J. Race, M. Albrecht, *ACS Catal.* **2023**, *13*, 9891–9904.

[7] P. Melle, N. Ségaud, M. Albrecht, *Dalton Trans.* **2020**, *49*, 12662

[8] V. Vigneswaran, S. N. MacMillan, D. C. Lacy, *Organometallics* **2019**, *38*, 4387–4391.

[9] S. Horn, C. Gandolfi, M. Albrecht, *Eur. J. Inorg. Chem.* **2011**, *2011*, 2863–2868.

[10] A. Beaufils, P. Melle, N. Lentz, M. Albrecht, *Inorg. Chem.* **2024**, *63*, 2072–2081.

[11] A. Abbotto, S. Bradamante, G. A. Pagani, *J. Org. Chem.* **2001**, *66*, 8883–8892.

[12] K. Salzmann, C. Segarra, M. Albrecht, *Angew Chem Int Ed* **2020**, *59*, 8932–8936.

[13] N. Lentz, S. Reuge, A. Beaufils, M. Albrecht, *Organometallics* **2024**, *43*, 1536–1546.

[14] V. Leigh, D.J. Carleton, J. Olguin, H. Mueller-Bunz, L.J. Wright, M. Albrecht, *Inorg. Chem.* **2014**, *53*, 8054–8060.

[15] C. Reichardt, T. Welton, *Solvents and Solvent Effects in Organic Chemistry*, Wiley, **2010**.

[16] W. Kaim, S. Kohlmann, S. Ernst, B. Olbrich-Deussner, C. Bessenbacher, A. Schulz, *Journal of Organometallic Chemistry* **1987**, *321*, 215–226.

[17] M. Jiménez-Tenorio, M. C. Puerta, P. Valerga, *Eur. J. Inorg. Chem.* **2004**, *2004*, 17–32.

[18] 14% of alcohol product is considerably higher than the 2% obtained when starting from *trans*-chalcone, indicating some product inhibition when ketone **5a** is generated in situ. This has been observed previously with a pincer PYA Ru complex for the selective transfer hydrogenation of methyl cinnamylketone using iPrOH (cf. P. Melle, Y. Manoharan, M. Albrecht, *Inorg. Chem.* **2018**, *57*, 11761–11774). In the latter, deactivation of the catalytically active species was confirmed upon addition of acetophenone after full consumption of the substrate, resulting in negligeable 5% conversion after 6 h while full conversion is obtained in 0.5 h in a separate run.

[19] J. C. Wong, G. Tang, X. Wu, C. Liang, Z. Zhang, L. Guo, Z. Peng, W. Zhang, X. Lin, Z. Wang, J. Mei, J. Chen, S. Pan, N. Zhang, Y. Liu, M. Zhou, L. Feng, W. Zhao, S. Li, C. Zhang, M. Zhang, Y. Rong, T.-G. Jin, X. Zhang, S. Ren, Y. Ji, R. Zhao, J. She, Y. Ren, C. Xu, D. Chen, J. Cai, S. Shan, D. Pan, Z. Ning, X. Lu, T. Chen, Y. He, L. Chen, *J. Med. Chem.* **2012**, *55*, 8903–8925.

[20] Y. Zuo, X. He, Q. Tang, W. Hu, T. Zhou, W. Hu, Y. Shang, *Adv Synth Catal* **2021**, *363*, 2117–2123.

[21] G. M. Sheldrick, *Acta Crystallogr. Sect. A Found. Adv.* **2015**, *71*, 3–8.

[22] G. M. Sheldrick, *Acta Crystallogr. Sect. C Struct. Chem.* **2015**, *71*, 3–8.

Chapter V

Conclusions

This thesis highlights the application of coordinatively unsaturated PYA ruthenium complexes in transfer hydrogenation using ethanol as a benign hydrogen source. In addition to good activities in transfer hydrogenation of ketones, particularly with pyridyl-containing substrates, here we demonstrate the first examples of room-temperature chemoselective olefin transfer hydrogenation of α,β-unsaturated carbonyl compounds using EtOH. The general applicability of this catalytic system was demonstrated on a broad substrate scope, including various functionalized α,β-unsaturated carbonyl compounds. Further improvement on the selectivity was enabled by modification on the acyl unit of the PYA ligand, which eliminates a time-dependent variation of selectivity and suppresses gradual over-reduction of the carbonyl bond. Particularly, the introduction of a *para*-CF_3 aryl unit in the ligand unlocked a highly selective reduction of exclusively the C=C bond, with only traces of the fully saturated alcohol after 24 h.

Different suggestions could be investigated to further improve this catalytic system, in order of sustainability but also for potential industrial application. The transition to first-row transition metals, as iron, would enhance the economic efficiency of the system and align with the green chemistry principles. The operation under base-free conditions is also highly interesting, as many substrates are sensitive to basic conditions. The firstly described ruthenium complex was slightly active under base-free conditions using EtOH, however under harsh conditions (110°C, 48 h). A more promising alternative would be the direct use of ruthenium alkoxides that we suggested as initially formed species during the reaction. Deeper mechanistic studies using computational techniques could at the same time elucidate the role of the different intermediates and help to understand the overall selectivity of the system.

In a more general aspect, the use of coordinatively unsaturated complexes, particularly using PYA and PYE ligands, is still largely underexplored. Apart from this work, the only coordinatively unsaturated complexes bearing PYE or PYA ligands are the series of O,N-bidentate PYE iridium complexes presented in the introduction. Because these complexes display remarkable activity and longevity in formic acid dehydrogenation, the investigation of these coordinatively unsaturated systems is promising for application in (de)hydrogenation reactions and beyond. Particularly, the use of exocyclic heteroatoms may be necessary in order to stabilize such coordinatively unsaturated species.

Declaration of Consent

on the basis of Article 28 para. 2 of the RSL05 phil.-nat.

Name/First Name: Alicia Beaufils

Matriculation Number: 20-131-702

Study program: PhD-program in Chemistry and Molecular Sciences

Bachelor ☐ Master ☐ Dissertation ☑

Title of the thesis: Synthesis and Catalytic Application of Complexes with Pyridylidene Amide Ligands in Transfer Hydrogenation

Supervisor: Prof. Martin Albrecht

I declare herewith that this thesis is my own work and that I have not used any sources other than those stated. I have indicated the adoption of quotations as well as thoughts taken from other authors as such in the thesis. I am aware that the Senate pursuant to Article 36 para. 1 lit. r of the University Act of 5 September, 1996 is authorised to revoke the title awarded on the basis of this thesis. I allow herewith inspection in this thesis.

Signature 

Curriculum Vitae

Alicia Beaufils was born on June 27, 1996 in Ambilly, France. She started her undergraduate studies in Chemistry at Grenoble Alpes University in 2015. She joined the group of Prof. Vallée for her Bachelor thesis, which specialized in prebiotic chemistry, with a particular focus on the role of Sulphur amino acids could have played in the primitive ocean. Afterward, she joined the group of Dr. Wong, who worked on the synthesis of cyclopeptides coupled to a fluorescent probe and acting as transmembrane carrier. In 2020, she joined Dr. Kochem for her Master thesis in a multidisciplinary project for the development of multi-catalytic reactions for the synthesis of products of pharmacological interest using graphene-functionalized iron complexes.

In October 2020, she started her Ph.D. studies under the supervision of Prof. Albrecht on the synthesis, characterization, and catalytic application of ruthenium complexes bearing flexible N-donor ligands. Her project focused particularly on the synthesis and characterization of coordinatively unsaturated ruthenium complexes and their catalytic application in transfer hydrogenation using ethanol as hydrogen source. She supervised different undergraduate laboratory courses and mentored one bachelor student. She presented her Ph.D results at various national and international conferences, including contributed talks at the BeNeFri Student Spring Symposium 2023 and SCS Fall Meeting 2023.

List of Publications

Air-Stable Coordinatively Unsaturated Ruthenium(II) Complex for Ligand Binding and Catalytic Transfer Hydrogenation of Ketones from Ethanol

A. Beaufils, P. Melle, N. Lentz, M. Albrecht, *Inorg. Chem.* **2024**, *63*, 2072–2081

Modulation of Phenolate-Functionalized Donor-Flexible PYE Ligands for Iridium-Catalyzed Formic Acid Dehydrogenation

N. Lentz, S. Reuge, A. Beaufils, M. Albrecht, *Organometallics* **2024**, *43*, 1536–1546

Ruthenium-Catalyzed Chemoselective Olefin Transfer Hydrogenation of alpha,beta-Unsaturated Carbonyl Systems By Using EtOH as Hydrogen Source

A. Beaufils, M. Albrecht, *ChemCatChem* **2025**, e202401596